

*Doctoral thesis submitted for the degree of Doctor of Philosophy in  
Telecommunication Engineering*

*Postgraduate programme: TECOMBER*

---

# **Analysis, Characterization and Modeling of Interference Sources on Wireless Communication Systems in Complex Indoor Scenarios**

*Presented by:*

**Peio Lopez-Iturri**

*Supervised by:*

**Dr. Francisco Falcone Lanas**

**Iruña-Pamplona, February 2017**



*“A flower does not think of competing to the flower next to it. It just  
blooms.”*

— from Zen Shin Talks





# Contents

<b>Abstract .....</b>	<b>VII</b>
<b>Acknowledgments .....</b>	<b>IX</b>
<b>Chapter 1: Introduction.....</b>	<b>1</b>
<b>1.1 Motivation .....</b>	<b>1</b>
<b>1.2 Objectives .....</b>	<b>3</b>
<b>1.3 Structure of the thesis.....</b>	<b>5</b>
<b>Chapter 2: Wireless Communications.....</b>	<b>9</b>
<b>2.1 Historic Review .....</b>	<b>10</b>
<b>2.2 Radio Propagation .....</b>	<b>11</b>
2.2.1 Propagation Losses .....	12
2.2.2 Absorption .....	13
2.2.3 Reflection, Scattering and Diffraction .....	14
2.2.4 Multipath Propagation .....	15
<b>2.3 Wireless Communication Systems .....</b>	<b>19</b>
2.3.1 ZigBee .....	20
<b>2.4 Wireless Interferences .....</b>	<b>31</b>
<b>2.5 Radio Propagation Models .....</b>	<b>32</b>
2.5.1 Theoretical models .....	33
2.5.2 Empirical models .....	33
2.5.3 Deterministic models.....	34
<b>Chapter 3: 3D Ray Launching.....</b>	<b>36</b>
<b>3.1 The 3D Ray Launching simulation tool .....</b>	<b>36</b>

<b>3.2</b>	<b>Modeling of complex environments and validation of the 3D Ray Launching method .....</b>	<b>44</b>
3.2.1	Office environments .....	44
3.2.2	Home environments .....	63
3.2.3	Vehicular environments.....	74
3.2.4	Sport environments .....	107
3.2.5	Commercial area environments.....	137
3.2.6	Smart City environments .....	156
<b>3.3</b>	<b>Main Contributions .....</b>	<b>176</b>
<b>Chapter 4: Deterministic Interference Analysis .....</b>		<b>179</b>
<b>4.1</b>	<b>Interference Analysis Results .....</b>	<b>180</b>
4.1.1	Human Body Effect .....	214
4.1.2	Acceleration Technique .....	248
<b>4.2</b>	<b>Main Contributions .....</b>	<b>265</b>
<b>Chapter 5: Modeling of Wireless Interference Sources. 267</b>		
<b>5.1</b>	<b>Microwave Oven Interference on WSNs.....</b>	<b>268</b>
<b>5.2</b>	<b>Deterministic Estimation of Radiated Emissions of Electric Appliances: The Microwave Oven .....</b>	<b>276</b>
<b>5.3</b>	<b>Application on Dosimetric Studies .....</b>	<b>304</b>
<b>5.4</b>	<b>Main Contributions .....</b>	<b>316</b>
<b>Chapter 6: Conclusions and Future Work .....</b>		<b>318</b>
<b>6.1</b>	<b>Conclusions .....</b>	<b>318</b>
<b>6.2</b>	<b>Future Work.....</b>	<b>322</b>
<b>Bibliography.....</b>		<b>325</b>
<b>List of Publications .....</b>		<b>350</b>
	International Indexed Journals .....	350
	Book Chapters.....	353

International Conference Contributions.....	353
National Conference Contributions .....	358
Other Merits and Awards .....	360



# Abstract

This research work presents a novel methodology of assessing wireless interferences on Wireless Sensor Networks (WSN) by the aid of an in-house developed 3D Ray Launching method, which is a novel deterministic approach for radio propagation prediction in complex environments. Firstly, the 3D Ray Launching simulation procedure has been validated by means of comparing the simulation results with radio propagation measurements within different complex scenarios. Afterwards, a novel point of view regarding the traditional use of radio propagation models is presented: its use for assessing wireless interferences between different deployed wireless networks and WSNs, instead of only predicting the radio propagation of the transceivers belonging to a wireless communication system. The obtained results show that the assessment of potential wireless interferences will be a major issue in order to deploy optimally WSNs, even more taking into account that in a future framed by the Smart City concept and the so called Internet of Things (IoT) along the appearance of 5G systems, the quantity of wireless transceivers is expected to be huge.

Once the methodology for the assessment of the interferences between wireless communication systems has been performed, a further step has been taken in order to analyze the interferences created by electrical devices which do not belong to wireless communication systems. For that purpose, a novel hybrid simulation method based on the 3D Ray Launching algorithm and Equivalent Sources has been developed in order to obtain computational models for the estimation of radiated emissions of potential wireless interference sources. Specifically, a common domestic microwave oven has been chosen as the interference source under analysis.

Finally, in addition to the original aim of analyzing interferences on wireless networks, the microwave oven computational model obtained by the proposed hybrid method has been successfully applied to dosimetric assessment studies.

# Acknowledgments

First of all, I would like to thank sincerely my supervisor Dr. Francisco Falcone for his guidance, advisory, teachings and dedication over all these years. But above all, I truly appreciate his ever-present support.

My teammates Leire and Erik, with whom I have worked for all these years. Thanks for making the work more bearable and entertaining.

I would also like to thank all the people of the Public University of Navarre (UPNA) and all the people from other Institutions I have collaborate with and who have helped me developing this work.

Last but not least, my parents Cristobal and Pili, Sandra and Eihar, for giving me a happy life and the needed support to develop this research work successfully.





# Chapter 1

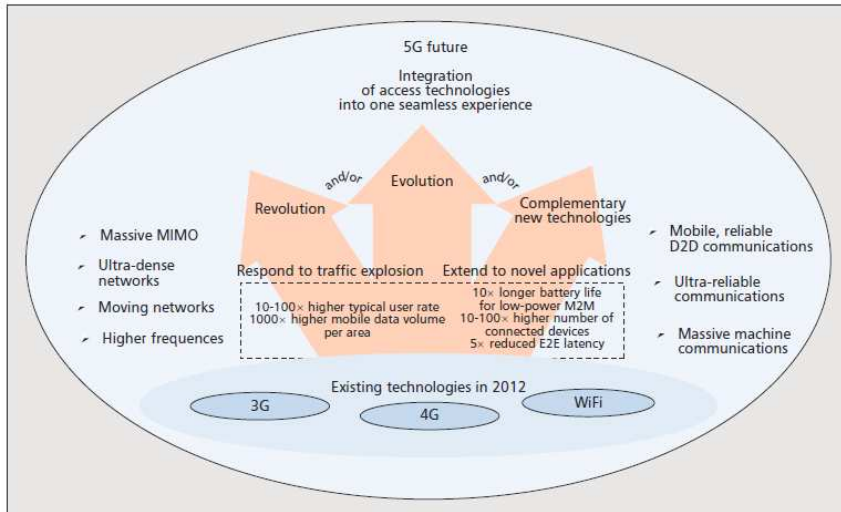
## Introduction

**T**HE aim of this introductory chapter is to present the framework of the thesis. Section 1.1 is focused on the motivation of the thesis. General objectives of the thesis are covered in Section 1.2 and, finally, a summary of the structure of the work is provided in Section 1.3.

### 1.1 Motivation

Advances in information technology and the continued miniaturization of mobile communication devices have increased the use of wireless communications exponentially. Due to this great growth, wireless networks have experienced rapid changes and the development of new applications. Recently, wireless networks have come into prominence, and the impact of wireless networks has been and will continue to be profound because they hold the potential to revolutionize many segments of economy and life, such as environmental monitoring and conservation, manufacturing and business management, automation in the transportation systems and

health care industries. This adoption of wireless communications leads nowadays to concepts such as Internet of Things (IoT), Context Aware scenarios, Smart Cities and Smart Health (s-Health), which will be boosted by the developing 5G wireless communication systems.



The 5G roadmap: revolution, evolution, and complementary new technologies.

\*Figure obtained from <http://trends-in-telecoms.blogspot.com.es/>

In this scenario, several wireless communication systems can be operating simultaneously, with different requirements in terms of coverage as well as capacity. Even more, dense wireless networks are expected to be deployed, contributing to 5G small-cell technology, machine-to-machine (M2M) communications, vehicular communications and Wireless Sensor Networks (WSNs). However, the deployment of dense wireless networks in environments where different wireless technologies coexist entails key technical issues which are necessary to be solved. One of the most important of these issues is the interference management due to its direct negative effect in the quality of the communication and the performance of the wireless networks, but paradoxically, it is usually an overlooked aspect when a deployment of mentioned wireless networks is being designed.

Although the concern about interferences in wireless

communications is an old issue [Tay11][Agg40], the advent of IoT, Smart Cities and 5G systems have made the researchers again be aware about the interference problem, as can be seen in very recent works [Laz16][Mar16][AIK17], where the neediness of further research and in-depth radio analysis taking into account intra-system and inter-system interferences is highlighted. Same idea is concluded specifically for 2.4 GHz band wireless communication systems [Azm14], which is the main frequency band studied in this thesis.

Taking into account this framework, next subsection presents the main objectives of this thesis work.

## 1.2 Objectives

The main objectives of this thesis are listed as follows:

- To validate an in-house developed 3D Ray Launching radio propagation model for its use in complex environments where WSNs, Context Aware scenarios, IoT and 5G wireless communication systems will potentially be deployed.
- The radio propagation models have been traditionally used to obtain received RF power estimations of a transmitting wireless communication device. Another objective of this thesis is to employ the 3D Ray Launching tool for the assessment of interferences within complex scenarios in terms of radio propagation, giving a novel point of view regarding the use of radio propagation models.
- Additionally, due to the computational cost that requires the simulation of big complex scenarios with dense wireless networks, another objective is the development of acceleration techniques for the 3D Ray Launching algorithm in order to minimize the needed computational time.

- Since wireless communication systems are not the only sources of interference, another objective of this thesis is to analyze how electronic devices and appliances can cause destructive interferences on wireless communication systems.
- To assess the presence of human beings and their effect on the performance of wireless communication systems by means of the 3D Ray Launching algorithm.
- Finally, one of the most important goals of this thesis is to develop a method for modeling electromagnetic noise sources in order to implement them in the 3D Ray Launching algorithm. Thus, the radiated power distribution of these sources could be determined within the complete volume of different environments.

Fulfilling these objectives, this thesis tries to contribute to understand the importance that the interference analysis will have when it comes to conduct radio planning tasks for the deployment of WSNs, new 5G communications networks and IoT devices. Besides, an accurate and efficient tool is provided for carrying out these tasks, which will optimize the performance of the wireless networks in terms of throughput and energy consumption: the in-house developed 3D Ray Launching algorithm. Finally, the development of a novel method for modeling electromagnetic noise sources provides a very valuable tool for radio planning task within harsh environments in terms of electromagnetic noise such as industrial, transportation or hospital scenarios.

### 1.3 Structure of the thesis

This thesis consists of six main chapters followed by the bibliography and the list of publications derived from the presented work.

Chapter 1 is this introductory chapter, which is focused on explaining the motivation, the structure and objectives of the thesis. Figure 1.1 shows schematically the summary of the work carried out within the frame of this thesis.

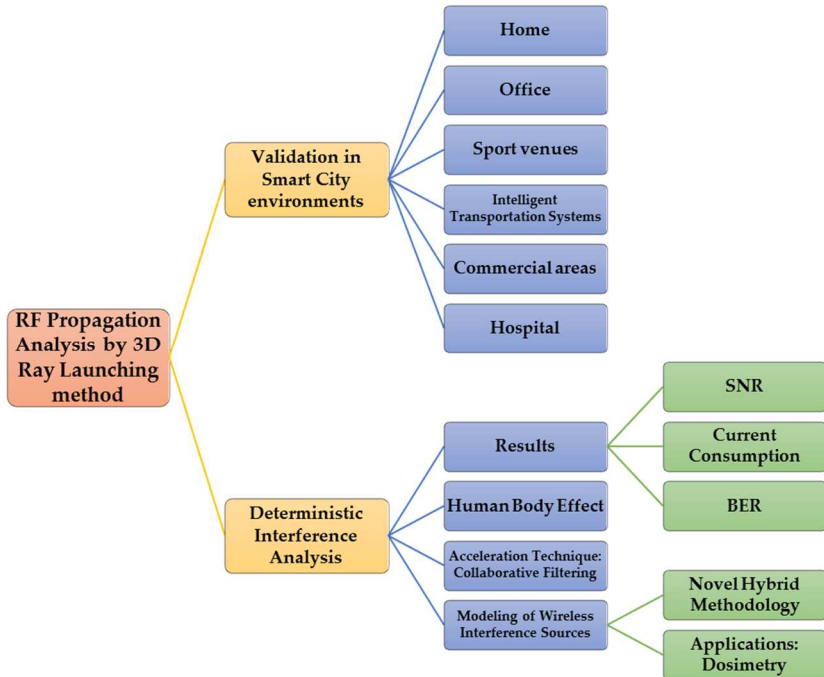


**Figure 1.1.** Summary of the work presented in this thesis.

Chapter 2 starts with a brief historic review about wireless communications. Then, the main radio propagation phenomena that occur within the scenarios analyzed in this thesis are presented. Following, the current wireless communication systems are presented, emphasizing ZigBee since it is the technology on which the devices used in this thesis are based. A section dedicated to wireless interferences has been included since interference management is expected to be a major issue in the deployment of future wireless networks such as 5G and IoT networks. Finally, a classification of existing radio propagation models is presented.

In Chapter 3 the in-house developed 3D Ray Launching method is presented, which is a deterministic radio propagation model. In contrast to other deterministic methods, it provides a good trade-off between results accuracy and required computational time. Once the 3D Ray Launching tool is described, its use in different scenarios within the frame of Smart City environment is analyzed. The results validate the estimations obtained by this method. Figure 1.2 shows the types of scenarios where the 3D Ray Launching tool has been validated.

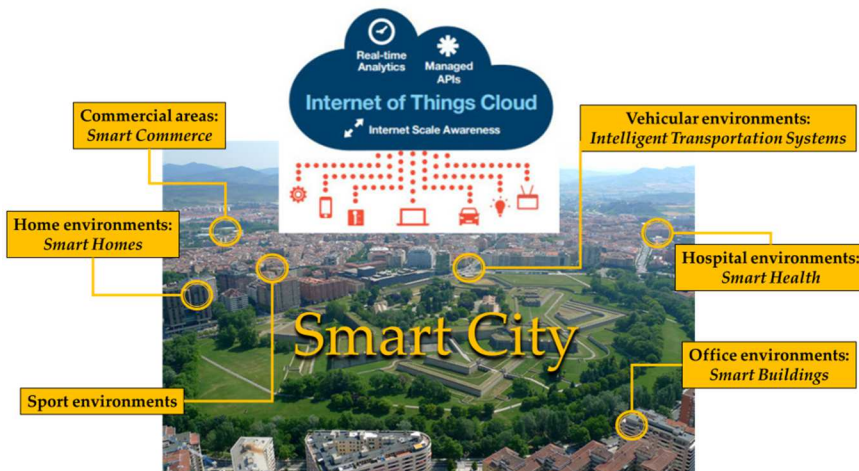


Figure 1.2. Overview of the analyzed environments.

Chapter 4 presents a novel point of view on the use of deterministic radio propagation models: the interference analysis. Traditionally, radio propagation models are used to estimate the received signal level in a potential location of a receiver device within the scenario where wireless communication systems are going to be deployed. Thus, knowing the sensitivity of the receiver, coverage estimations can be inferred. But in real environments, this is not usually enough to ensure the good performance of many wireless networks. For an optimized radio planning, the influence of interferences has to be taken into account, much more in scenarios where dense wireless networks will coexist (IoT, 5G). Therefore, in this chapter interference analysis are carried out by means of the 3D Ray Launching simulation tool, obtaining estimations of SNR, current consumption and BER. Besides, the Human Body Effect is also studied since the presence of human beings can drastically affect the expected performance of a wireless link. Finally, in order to carry out this kind of analysis in scenarios where dense wireless networks are deployed, a novel acceleration technique has been developed during this thesis work, with the aim of reducing drastically the computational time required by the 3D Ray Launching algorithm.

Chapter 5 presents a step further in the analysis of wireless interferences. It is well known that electric devices and appliances radiate RF power. This radiated power could interfere, acting as noise, a communications between wireless devices. In this chapter, a very common appliance (the domestic microwave oven) has been chosen to assess its potential interferences on WSNs. Once the negative impact that an operating microwave oven can have on the performance of WSNs is empirically demonstrated, a novel hybrid *Equivalent Source – 3D Ray Launching* simulation technique for deterministic estimation of radiated emissions of electric appliances is developed, particularized to a microwave oven. Finally, the obtained microwave oven model for 3D Ray Launching simulations is successfully used for dosimetric studies.

Finally, in Chapter 6 the conclusions of the results obtained during this thesis work are presented. In the same way, future research lines are proposed.



# Chapter 2

## Wireless Communications

**I**N this chapter, an introduction to wireless communications is presented. First, in Section 2.1, a historic review of wireless communications is presented. Then, in Section 2.2 a brief description of the main electromagnetic wave propagation phenomena is made, focusing on the most relevant propagation phenomenon that occurs within indoor complex environments: the multipath propagation. Afterwards, Section 2.3 describes the most significant characteristics of the ZigBee standard, which is the standard on which the wireless devices used during this thesis are based, as it is specifically developed for the deployment of WSNs. Then, in Section 2.4 a commonly overlooked topic regarding WSN deployment is presented, but which has a great importance in this thesis work: Wireless interferences. Finally, Section 2.5 presents the existing radio propagation model types.

## 2.1 Historic Review

The first successful utilization of radio waves for communications purposes happened in 1895, when the Italian Guglielmo Marconi introduced the first wireless transmission of telegraph signals through the Earth's atmosphere. This experiment was exceptional as it was conducted without the support of the traditional wire guiding line. Instead, Marconi used a spark-gap as a transmitting source for the electromagnetic radiation and a coherer as a reception device. Almost at the same time (1896) but independently, the Russian physicist Alexander S. Popov carried out successfully a similar demonstration.

The importance of such invention and the impact that wireless communications have had in the development of human society is irrefutable. However, it is mandatory to name other scientists which their previous works were indispensable: In 1864, the Scottish mathematician and theoretical physicist James C. Maxwell developed theoretical hypotheses of the existence of free propagating electromagnetic waves based on the experimental investigations of Michael Faraday and the André-Marie Ampère. His greatest merit was a theoretical prediction of the displacement currents in dielectrics and vacuum, which generalized the concept of current continuity in Ampere's law. The fundamental equations of electromagnetism (known as Maxwell's equations) were later updated to achieve complete and symmetric form by the introduction of magnetic currents, making possible the comprehension of the nature of electromagnetic waves capable of propagating for long distances without the neediness of physical guides such as wires and waveguides.

The experimental verification of the existence of electromagnetic waves was made by the German physicist Heinrich R. Hertz in 1880s, when he demonstrated a propagation of the spark from a transmitting Leyden jar to the terminals of a remote receiving antenna. Figure 2.1 shows graphically the chronology of the electromagnetic wave theory and practice history.

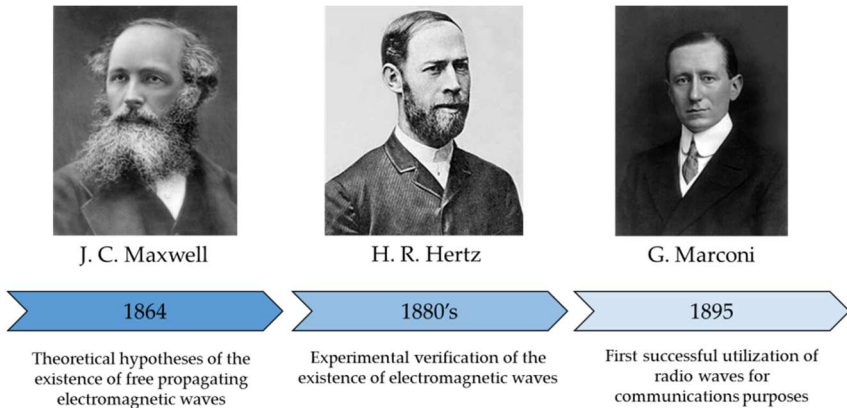


**Figure 2.1.** Chronology of the beginnings of the electromagnetic wave theory and practice.

Soon after Marconi's and Popov's experiments with the transmission of telegraph signals over the distance of several miles, in 1901 Marconi greatly extended the propagation range sending an electromagnetic signal from the United Kingdom to Canada over the Atlantic Ocean. For this accomplishment, a sinusoidal carrier, a resonant LC filter at the receiver's input and a vertical grounded radiator (operating as antenna) were used. This great success of Marconi's long-range signal transmission motivated engineers and research scientists to study propagation mechanisms. This interest in radio propagation phenomena and wireless communication systems arrives to our days, with many researchers, enterprises and governments around the world investing money and time with the aim of developing new and better ways to transmit electromagnetic waves wirelessly.

## 2.2 Radio Propagation

Wireless communications have an unavoidable characteristic that makes the communication unreliable. This characteristic is the channel, the atmosphere, which has not the physical boundaries provided by cable communications.

Several factors affect the wireless communications channel, such as the radiofrequency noise produced by machines, physical changes in

the environment, the presence of people, metals, changes in the atmosphere, etc. Furthermore, in the ISM frequency band of 2.4 GHz, the band in which this work focuses, there can be a greater amount of interference due to the wireless communication systems that operate at that frequency band. All these effects could cause a failure in data transmission.

Because of that, telecommunication systems are designed so that the received signal complies with a minimum SNR to ensure the correct reception of the transmitted message. In the case of wireless communications, electromagnetic waves are exposed to different phenomena that can alter its propagation, influencing the received power, and therefore the SNR.

Therefore, for a correct planning of a wireless communication system, such as ZigBee-based WSNs, it is essential to know the factors that can affect electromagnetic propagation in the corresponding frequency band. Therefore, understanding the propagation characteristics of an environment is essential to avoid problems and to make a correct implementation and deployment of the network.

In this section, the different phenomena that occur in the propagation process of electromagnetic waves are briefly explained.

### 2.2.1 Propagation Losses

Like all transmission channels, air also attenuates the signal. This attenuation will vary mainly due to the transmission frequency and the physical distance between the transmitter and receiver. This attenuation is a loss, and it can be approximated by the formula of Friis, which gives a relation between the transmitted and the received power:

$$\frac{Pr}{Pt} = \frac{1}{4 \cdot \pi \cdot r^2} \cdot D_T \cdot A_{efR} = \left( \frac{\lambda}{4 \cdot \pi \cdot r} \right)^2 \cdot D_T \cdot D_R = \left( \frac{1}{\lambda \cdot r} \right)^2 \cdot A_{efT} \cdot A_{efR}$$

The most important inference to be drawn from this formula is that the transmitted power will decrease with the square of the distance between the transmitter and the receiver 'r'. Therefore, the distance is a

key parameter for the calculation of propagation losses, and therefore, for the received power level.

### 2.2.2 Absorption

The electromagnetic waves, when they pass from one physical medium to another, suffer a deviation in their path. This phenomenon is called refraction, and appears whenever an electromagnetic wave passes from a physical medium with a particular refractive index to another medium with a different refractive index. The refractive index ( $n$ ) is the ratio between the wave propagation velocity in a reference medium, which in the case of electromagnetic waves is the vacuum, and the propagation velocity of the wave in the particular medium itself.

The relationship between the incident wave and the refracted wave is given by Snell's law. The formula and a diagram are shown in Figure 2.2.

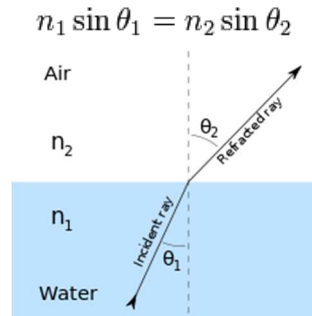


Figure 2.2. Snell's law and refraction phenomenon.

When a transmitted signal, i.e. electromagnetic wave, penetrates an object, the signal suffers attenuation. This attenuation will be higher or lower depending on the absorption characteristics of the object, its temperature and the frequency of the signal. Each material has associated an attenuation constant,  $\alpha$  (dB/m). For example, the attenuation constant for water at ambient temperature for a frequency of 2.4 GHz is approximately 330 dB/m. The human body is water in a high percentage, so it attenuates electromagnetic signals significantly

(known as shadow effect). Therefore, the deployment of a wireless sensor network in a scenario in which the presence of persons will be usual is an important issue to take into account.

The effect that the frequency of the signal has on the penetration depends on the material. Usually, considering the common materials that can be found in a home or within an office building, the higher the frequency, the greater the attenuation suffered by the signal is.

### 2.2.3 Reflection, Scattering and Diffraction

The phenomena of reflection, scattering and diffraction are very important in wireless communications, especially in indoor scenarios since the presence of objects and walls produces these three phenomena very often. Reflection will occur when the radiated electromagnetic wave reached a surface. The percentage of the reflected power will depend on the material of the object hit by the propagating wave. Figure 2.3 shows schematically the reflection phenomenon, where the incident angle ( $\theta_i$ ) and the reflected angle ( $\theta_r$ ) are equal.

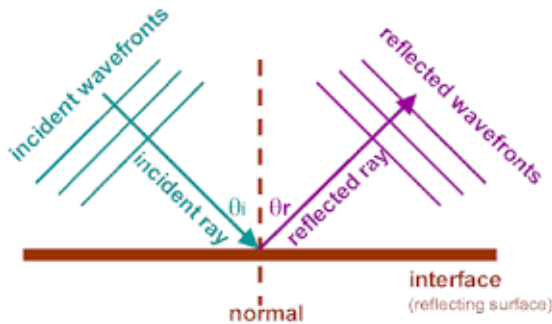


Figure 2.3. Reflection phenomenon representation.

The scattering occurs when electromagnetic waves reach a rough surface, which depends on the wavelength ( $\lambda$ ) of the incident wave. Generally, if the variation of the surface is larger than  $\lambda/8$ , the surface is considered rough and signal will be scattered in various directions (see Figure 2.4).

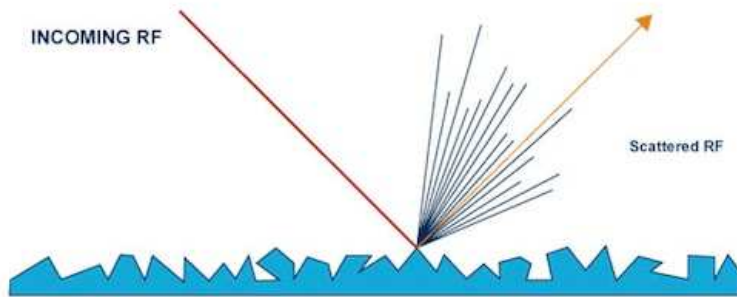


Figure 2.4. Scattering phenomenon representation.

Finally, the diffraction phenomenon occurs when an electromagnetic wave reaches an edge or a very narrow object. In that case, the object acts as a new source for the wave, radiating again part of the received energy, enabling in some cases the reception in places that previously was not possible due to lack of direct vision between the transmitter and the receiver (see Figure 2.5).

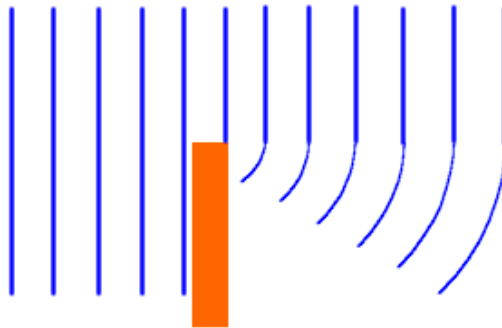


Figure 2.5. Diffraction phenomenon representation.

### 2.2.4 Multipath Propagation

The multipath propagation is the most influential phenomenon in radio propagation within complex indoor scenarios. Due to the multiple objects that are present in this kind of scenarios, the transmitted signal usually reaches the receiver following different

paths, generated by the electromagnetic phenomena mentioned previously, i.e. refraction, reflection, diffraction and scattering. Thus, the receiver device receives a signal that will be the sum of the different signals propagated through different paths.

Each of the different propagation paths of the received wave will arrive with different power level and different delay because each path has different distance between the transmitter and the receiver. Or what is the same, each received wave will have a particular phase, which when added to the others could create reception problems. The simplest case of multipath propagation is shown in Figure 2.6.

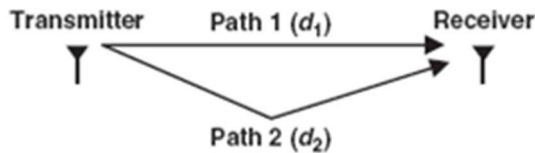


**Figure 2.6.** Multipath propagation representation. Figure obtained from [Far08].

The phase difference (in radians) between the two received signals for the case represented in Figure 2.6 can be calculated with the following formula:

$$\Delta\theta = \frac{2\pi f}{C} (d_1 - d_2) = \frac{2\pi f}{C} \Delta d$$

being 'C' the speed of light in vacuum ( $3 \times 10^8$  m/s),  $d_1$  and  $d_2$  the distances (in meters) of each path and 'f' the frequency of the signal (in Hz).

In a multipath propagation environment, multiple versions of the same signal with different phases and attenuation will reach the receiver due mainly to multiple reflections and diffractions. These versions of the signal are added in the received, resulting in a distorted signal, which depends on the phase of each received signal. This sum of phases can take a value between  $-180^\circ$  and  $+180^\circ$ , and can increase the power of the original signal, but may also cause a poor reception quality, even cutting the communication. The two extreme cases are:



- a- Signals arrive in phase (phase difference =  $0^\circ$ ), so the signals are added constructively.
- b- Signals arrive in counter-phase (phase difference =  $180^\circ$ ), so the signals are added destructively.

Therefore, the possibility for a partial or complete cancelation of the received signal exists, which will lead to an incorrect data transmission. In static scenarios, such as those studied in this work, the impact of this phenomenon will be less than for scenarios where the transmitter or receiver is moving. This is because in a static scenario the sum of the arrival phases will give a constant value, whereas in a dynamic one the value will be random. This is not entirely true, though. The environments are never completely static, and the change in the position of an object or the presence of people could generate new paths for the signal, changing the contribution to the sum of the received phase.

### Multipath fading

As already mentioned, the propagation of electromagnetic waves through a medium depends on the physical characteristics of the environment. These characteristics tend to be variable, so the propagation loss is a random variable. The average value of the received power is called nominal received power, and a significant reduction of received signal power is called a fading. The difference between the nominal level and the reduced received level is called fading depth, and it is expressed in dB. The time passed between the decrease and the recovery of the nominal value is called fade duration. Figure 2.7 shows an example of fading.

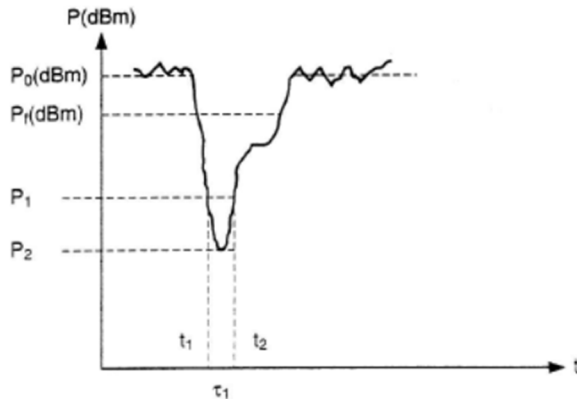


**Figure 2.7.** Fading. Figure obtained from [Rab95].

where  $P_0$ (dBm) represents the nominal value;  $P_1$ (dBm) is the average power level when a fading occurs, which is lower than the nominal value;  $P_2$  is the minimum level of the fading, so the fading depth is  $P_0$ (dBm) –  $P_2$ . Finally,  $\tau_1$  is the fading duration.

There are several types of fading, but the one that affects strongly in the environments presented in this work is the multipath fading. It is generated by the appearance of multiple propagation paths, so interference occurs between the direct or main path and the paths that reach the receiver at different angles. As shown previously, the resulting received signal will depend on the amplitudes and phases of those different signals.

The multipath fading is very selective in frequency, or what is the same, it affects a very narrow frequency range. It is also very deep (>20dB), but has a very short duration. Because of this intensity and the frequency selectiveness, the multipath fading often causes important attenuation and distortion in the received signal, affecting greatly the quality of the communication.

## 2.3 Wireless Communication Systems

Once the main electromagnetic propagation phenomena have been briefly presented, in this subsection an overview of the main wireless communication systems is presented.

One of the possible classifications for wireless communication systems is based on the communication range of the networks. From the higher range to the lower range (see Figure 2.8): WWANs (Wireless Wide Area Networks), WMANs (Wireless Metropolitan Area Networks), WLANs (Wireless Local Area Networks), WPANs (Wireless Personal Area Networks) and WBANs (Wireless Body Area Networks).

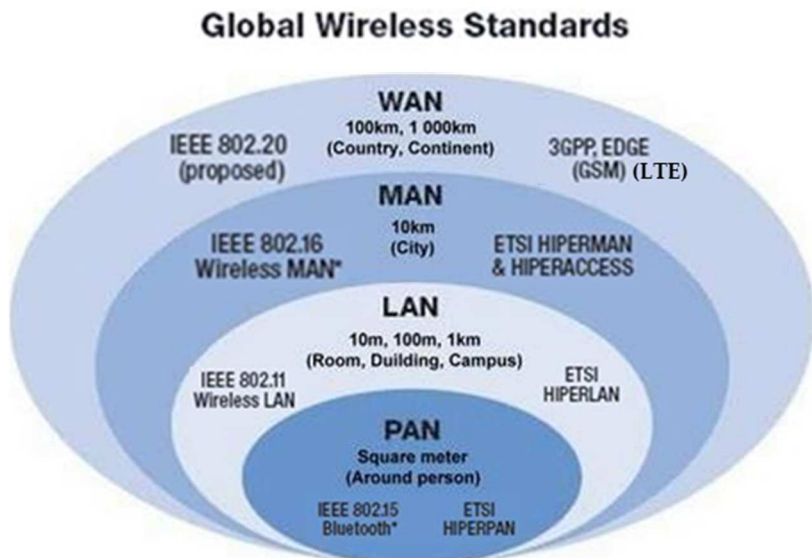


**Figure 2.8.** Wireless communication systems classification by range and their corresponding standards.

The wireless communication systems covered in this thesis work are classified as WLAN and WPAN, as they are the wireless communication systems used for the deployment of WSNs. Figure 2.9 shows the typical WLAN and WPAN standards with their range and data rate. As can be seen, depending on the requirements of specific

applications, different technology will be chosen to use for the deployment of WSNs. Besides, there are other parameters such as energy consumption or number of devices that can be part of the same network that should be taken into account. Due to its characteristics, ZigBee-based devices have been chosen in order to develop this thesis work. Following, the most representative characteristics of the ZigBee standard are presented.

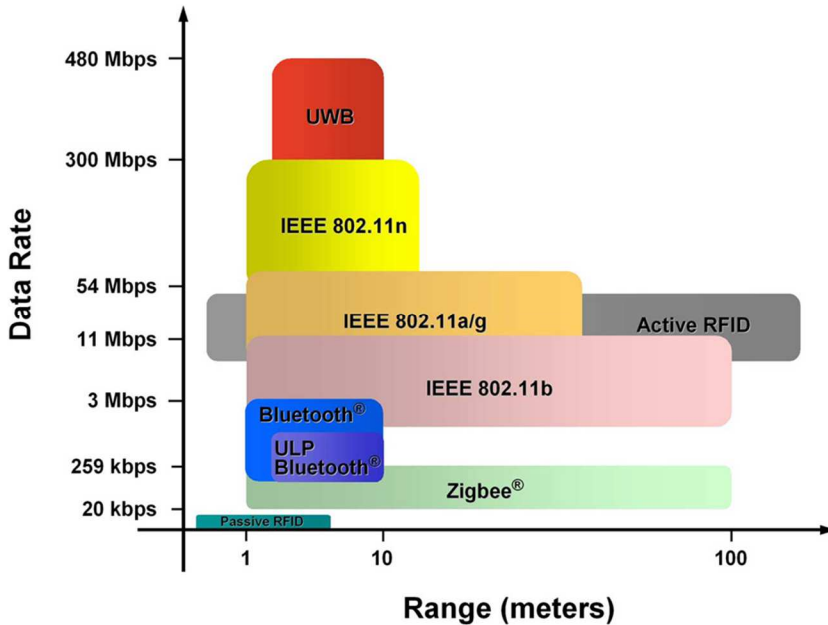


Figure 2.9. Wireless PAN and LAN communication standards. Figure obtained from [<http://simba1980.spaces.eepw.com.cn/>].

### 2.3.1 ZigBee

ZigBee is the name of the most widely used standard for the deployment of WSNs. ZigBee-based devices operate in the 868 MHz, 915 MHz and 2.4 GHz bands and the data rate is fixed at 250 Kbps. ZigBee was designed for low data rate, low cost and low energy consumption. Usually, the devices are powered by batteries and in

many applications the total time that the wireless device is active is very limited. The device spends most of the time in a power saving mode called sleep mode, extending the battery life up to several years.

The ZigBee standard was created and developed by The ZigBee Alliance, an open group born in 2002. This group consists of hundreds of companies, which many of them are market leaders in their respective fields (see Figure 2.10).



Figure 2.10. The ZigBee Alliance members. Figure obtained from [Gis].

The ZigBee standard adopted the physical and MAC (Medium Access Control) layers from the IEEE 802.15.4 standard (see Figure 2.11).

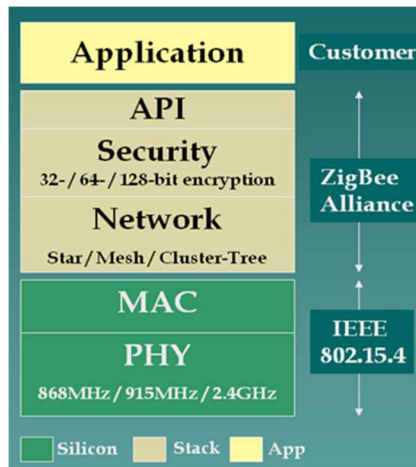


Figure 2.11. ZigBee and IEEE 802.15.4 standard.

The most relevant characteristics of the ZigBee standard are:

- High reliability.
- Low cost.
- Low energy consumption.
- Highly secure.
- Open standard.
- Low transmission data rate.

### High Reliability

Wireless communications are inherently vulnerable. They can be blocked by some metal or water. Besides, they vary widely due to factors such as the antenna design, transmitted power, weather conditions and interferences.

ZigBee provides high reliability in different ways:

- IEEE 802.15.4 with O-QPSK (Offset-Quadrature Phase-Shift Keying) and DSSS (Direct Sequence Spread Spectrum) provides excellent performance in low SNR environments.

- CSMA-CA (Carrier Sense Multiple Access Collision Avoidance) avoids collisions on the channel. ZigBee listens before transmitting and only transmit when the channel is free.

- CRC of 16 bits, used in every transmitted packet, ensures that each bit of the transmitted data is correct.

- The use of ACKs at each transmission hops. Each packet can be retransmitted up to three times (a total of four transmissions).

- Mesh network topology allows choosing the most reliable route. When an established route is cut, ZigBee can find an alternative route, as shown schematically in Figure 2.12 (node 1 transmits to node 3). Additionally, ZigBee provides broadcasting and multicasting transmission.

- End-to-end ACKs verify the reception of the data by the end user.

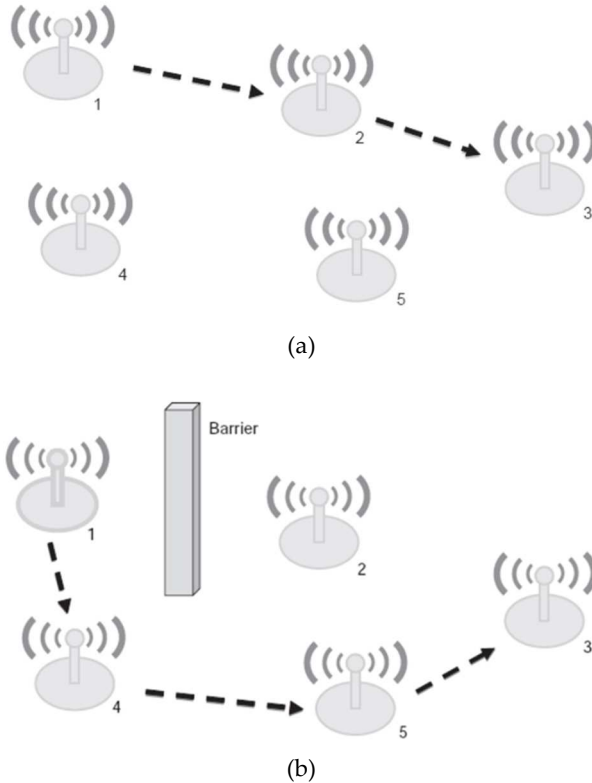


**Figure 2.12.** (a) Established route in a mesh topology. (b) Alternative route in a mesh topology. Figure obtained from [Gis].

### Low Cost

The cost of the deployment of a ZigBee network depends on the size of the network in terms of number of deployed devices. But comparing with other wireless technologies, the cost of the chips and transceivers is lower. It can be less than 1 euro, and ZigBee modules cost between 15 and 25 euro. The cost will be reduced if large number of devices is purchased. It is also possible to purchase only the transceiver or chip. In this case, prices vary between 2 and 6 euros each, and if the number of units is high the price can be reduced to less than 1 euro/unit. Texas

instruments, Ember and Freescale have a variety of chips and transceivers at these prices.

Another very important issue is that the frequency band of 2.4 GHz, which is the most common band used for ZigBee, is open worldwide and is not necessary to pay a license.

### Low Energy Consumption

A ZigBee device can operate for several years with a couple of AA batteries. The main reason for this low consumption is its duty cycle. A node in a network does not need to be permanently connected to remain in the network. For example, a temperature sensor may have to transmit only once per hour unless there is an abrupt change in temperature, so the demand of energy is very low. The following graph shows the approximate battery life of a ZigBee-based security sensor compared to the interval time between communications:

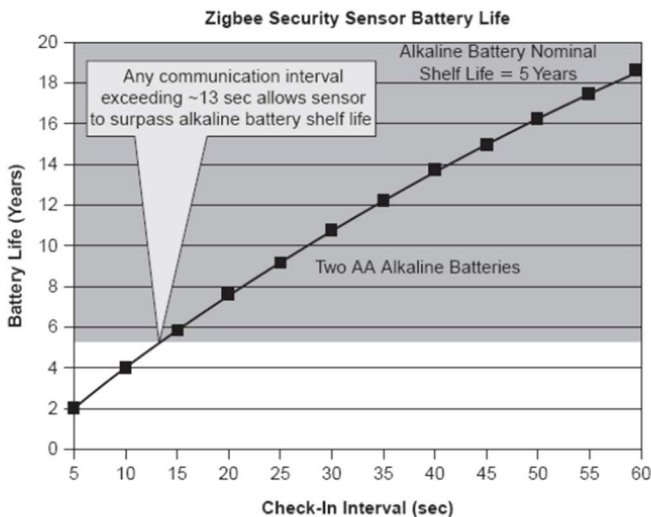


Figure 2.13. AA battery life for ZigBee. Figure obtained from [Gis].



### High Secure

In order to provide the network with the maximum security possible, ZigBee uses AES (Advanced Encryption Standard)-128 NIST (National Institute of Standards and Technology). This standard is a cipher block that encrypts packets. Besides, provides authentication to ensure the received packets are from the own network.

ZigBee is a reliable and internationally recognized standard, is free of patent infringements and can be implemented on 8-bit processors.

### Open Standard

ZigBee is an open global standard. It can be downloaded from the website [www.zigbee.org](http://www.zigbee.org). The mentioned The ZigBee Alliance, in addition to developing the standard, also specifies several tests for companies to develop their ZigBee compliant devices. This ensures compatibility between devices developed by different companies.

The ability of different devices and applications to work perfectly together is essential because it allows a ZigBee network to be formed by products from different companies.

### Low Transmission Data Rate

Nowadays, in most cases the objective is to increase the data transmission data rate. With ZigBee, it does not happen. Although there are specific applications where it is necessary high data rates, when ZigBee is used, a low data rate is required in most of the cases.

As it is said, ZigBee is based on the 802.15.4 standard, in which the maximum speed operating at 2.4 GHz is 250 Kbps.

Once the main characteristics of the ZigBee standard have been presented, other issues such as frequency band allocation and data rates are now presented.

There are three frequency bands available in the IEEE 802.15.4 version of 2006:

- 868 MHz band: 868-868.6 MHz.
- 915 MHz band: 902-928 MHz.
- 2.4 GHz band: 2400-2483.5 MHz.

The 868 MHz band is used in Europe for several applications, including short-range wireless networks. The other two bands are ISM frequency bands, so do not require a license. The 915 MHz band is used mainly in the USA, whilst the 2.4 GHz is used worldwide. Figure 2.14 shows more details on the frequency bands used by the IEEE 802.15.4 standard.

	Frequency (MHz)	Number of Channels	Modulation	Chip Rate (Kchip/s)	Bit Rate (Kb/s)	Symbol Rate (Ksymbol/s)	Spreading Method
	868-868.6	1	BPSK	300	20	20	Binary DSSS
	902-928	10	BPSK	600	40	40	Binary DSSS
<b>Optional</b>	868-868.6	1	ASK	400	250	12.5	20-bit PSSS
	902-928	10	ASK	1600	250	50	5-bit PSSS
<b>Optional</b>	868-868.6	1	O-QPSK	400	100	25	16-array orthogonal
	902-928	10	O-QPSK	1000	250	62.5	16-array orthogonal
	2400-2483.5	16	O-QPSK	2000	250	62.5	16-array orthogonal

**Figure 2.14.** Operating frequencies and data rates for IEEE 802.15.4. Figure obtained from [Far08].

The number of channels for each frequency band is different. The 868 MHz band has only one, the 915 MHz (excluding optional channels) and the 2.4 GHz band has 16 channels. Figure 2.15 shows the distribution of the channels.

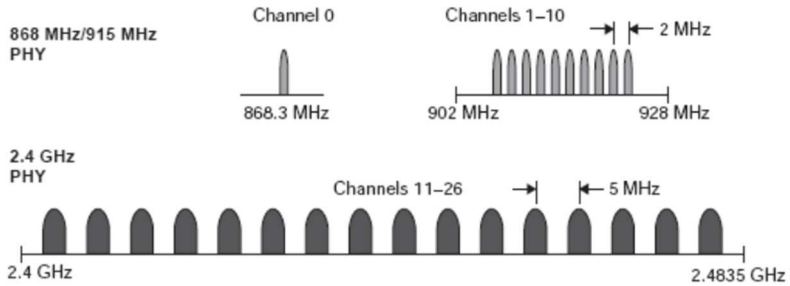


**Figure 2.15.** IEEE 802.15.4 frequency channels. Figure obtained from [IEEE Std 802.15.4<sup>TM</sup>-2006].

The 2.4 GHz band is accepted worldwide and is the one with the highest data transmission rate and the greatest number of channels. It is the most popular choice to develop transceivers. This band also has some disadvantages, such as possible problems of coexistence with IEEE 802.11 and other technologies which operate at the same frequency. Furthermore, there are interferences, such as the interferences produced by the microwave ovens, which can affect the quality of the transmission.

Regarding the topology of ZigBee networks and the role that each of the nodes can take, there are two types of devices in IEEE 802.15.4 wireless networks:

- 1- FFD (Full Function Device): Able to perform all the functions described in the IEEE 802.15.4 standard and able to accept any role in the network.
- 2- RFD (Reduced Function Device): Limited ability to perform functions. For example, while a FFD can communicate with any other device in the network, RFD can only communicate with another RFD. The processing capacity and memory in RFD devices is usually lower than in FFD.

In an IEEE 802.15.4 network, a FFD device can take three different

roles: Coordinator, PAN coordinator and Device. A Coordinator is a device that is capable of routing messages. If the Coordinator is also the main device of the network, it is called PAN coordinator. If a FFD device is not acting as a coordinator, then it is simply called Device.

The ZigBee standard uses a different terminology. A ZigBee coordinator (ZC) is an IEEE 802.15.4 PAN coordinator. A ZigBee router (ZR) is a device that can act as an IEEE 802.15.4 coordinator. Finally, a ZigBee End Device (ZED) is a device that it is neither a coordinator nor a router. ZigBee End Devices have the least processing power and memory. Typically, they are the cheapest devices in the network. In Figure 2.16 the mentioned different device roles can be seen.

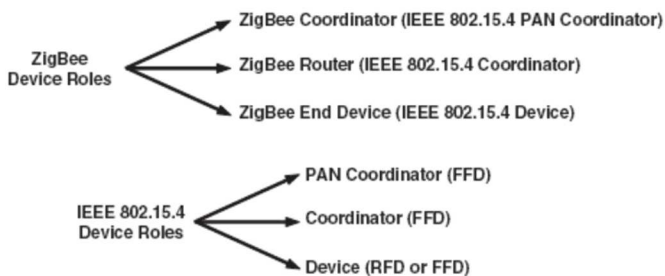


**Figure 2.16.** ZigBee and IEEE 802.15.4 device roles. Figure obtained from [Far08].

The ZigBee coordinator (ZC) is the only device that can form a network, so each network has only one ZC. If the network is open and new devices are expected, the ZC must be present because it is responsible for deciding the joining or the rejection of a new device. On the other hand, if the network is completely configured and the incorporation of new devices is not expected, the ZC behaves like a ZigBee router (ZR). When the used network topology is Tree topology, the ZC is the root node.

The ZigBee router (ZR) is an optional component of the network. It extends the network coverage connecting with a ZC or other ZRs. It participates mapping local addresses and the routing of messages.

When a simpler device is needed, a ZED is used, which can switch to the idle state (sleep mode) to consume less energy. ZigBee standard

imposes no time limit on the energy-saving state, so this time will depend on the needs of each application. It is also an optional network device and extends the network coverage communicating with ZC and ZR, but not with other ZED. A ZED does not participate in routing.

The following figures show a summary of the main features of each ZigBee device type and the different allowed associations between them:




Node Type	Features
	Forms network Routes packets Security Trust Center Allows nodes to join network
	Joins network Routes Packets Allows nodes to join network
	Joins network Battery operated and may sleep Smallest code size Can be RxOnIdle = true (no polling) or RxOnIdle = false (polling)

Figure 2.17. ZigBee node types.

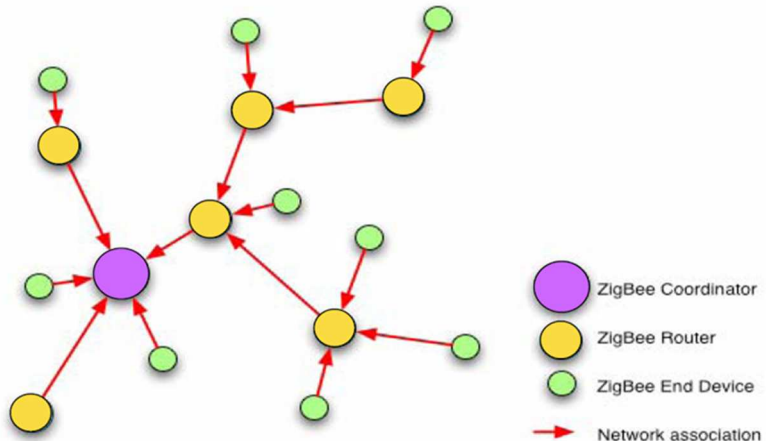
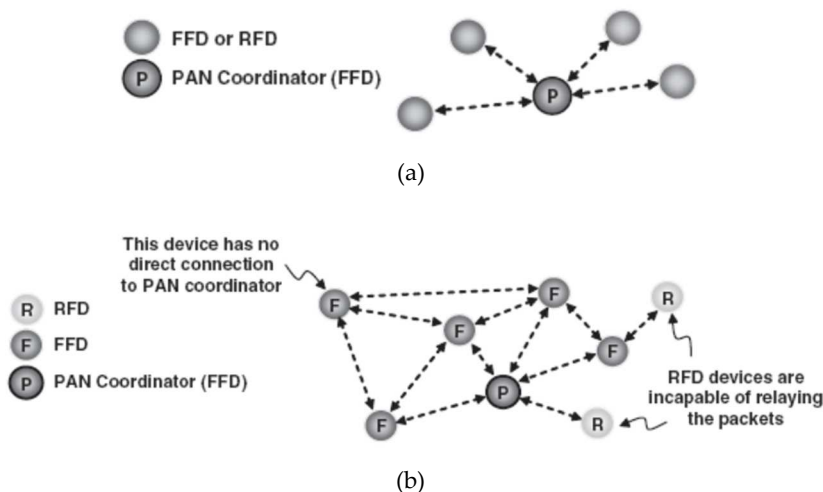


Figure 2.18. Allowed associations in a ZigBee network.

The ZigBee network layer is responsible for forming and managing the network. The network must be formed in one of the two topology types specified in IEEE 802.15.4: star and peer-to-peer.

In the star topology, shown in Figure 2.19a, the network devices can only communicate with the PAN coordinator. In a peer-to-peer topology, shown in Figure 2.19b, each device can communicate directly with any other device on the same network as long as the distance between them permits it. In this case, any FFD device could have the role of PAN coordinator. Usually, the first FFD device beginning a communication in order to create a new network will be the PAN coordinator.



**Figure 2.19.** (a) Star topology. (b) Peer-to-peer topology (mesh). Figure obtained from [Far08].

Peer-to-peer networks can take different forms defining some restrictions in the communications. When there are no restrictions, it is called mesh topology. Another form of peer-to-peer topology is the tree topology. In Figure 2.20 an example of tree topology is shown.

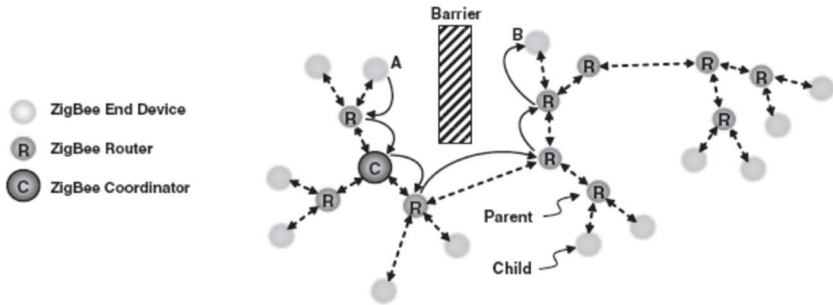


**Figure 2.20.** Tree topology. Figure obtained from [Far08].

Due to the amount of work that PAN coordinator has to do, it is active for long time periods. Because of this, it is normally fed with a larger power source than a simple battery. Other devices are typically powered by batteries.

## 2.4 Wireless Interferences

The quality of the information transmitted via a radio link between transceivers of a wireless communication system can be highly impacted by the presence of disturbances to the desired signal. Unfortunately, the wireless channel suffers interferences inevitably due to its lack of physical borders. Typically, interferences impact destructively the content of the received information. Depending on the random processes that occur in the receiving device, these interferences are classified in two families: Additive and Multiplicative interferences.

Multiplicative interferences occur mainly due to the own characteristics of the specific communication system itself, such as frequency of operation, radio propagation phenomena of the transmitted signal, required delay and the coherence time of the channel.

On the other hand, Additive interferences occur when radiating sources external to the desired wireless communication system affect the desired received signal. Additive signals can be classified as Natural and Man-made. In this thesis work, the presented interference analysis is focused on Man-made interferences, specifically on

interferences from other RF systems (which exist since the generation of the spark for the experimental verification of the existence of electromagnetic waves made by Hertz) and interferences from electric devices and appliances. Figure 2.21 shows the classification of interferences in RF communication links.

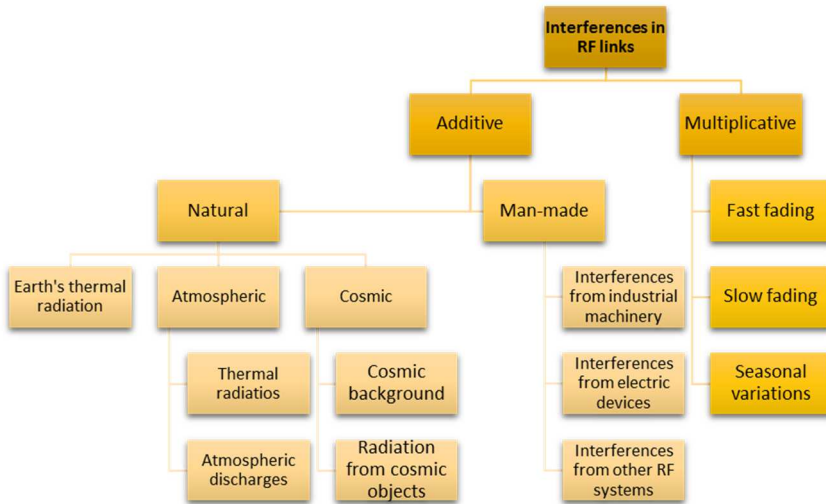


**Figure 2.21.** The classification of interferences associated with RF signals.

## 2.5 Radio Propagation Models

The importance of the study of the radio propagation has increased enormously in recent years because of the increasing amount of wirelessly connected devices that exist and are expected to coexist in a near future. For that purpose, the propagation models have great importance since they provide RF power level estimations within the scenarios where the wireless communication systems are going to be deployed. A propagation model is a set of mathematical expressions, diagrams and algorithms used to represent the radio propagation characteristics of an environment. Prediction models can be classified into theoretical, empirical or statistical and deterministic models.



In this subsection, a brief description of the existing propagation models is made, from empirical and statistical techniques that offer high computational simplicity but little accuracy in the results, to deterministic methods based on the calculation of electromagnetic fields that provide high accuracy, but also a high computational cost.

### **2.5.1 Theoretical models**

The purely theoretical treatment of radio propagation within complex scenarios such as urban, suburban or indoor areas is basically an intractable electromagnetic problem because of the general non availability of a detailed geometric description of the coverage area and the numerous boundary conditions. Theoretical models are derived physically assuming some ideal conditions. For example, the diffracting screens model is derived using physical optics assuming uniform spacing and heights of buildings. Free space model and Diffracting screen model are some examples of theoretical models.

### **2.5.2 Empirical models**

Empirical or statistical models are based on measurements. They are usually a set of equations derived from extensive field measurements. Empirical models are simple, efficient to use and accurate for environments with the same characteristics as those where the measurements were made. Important models in this group are Okumura model, who is one of the most widely used in urban areas, Hata model, which is an empirical formula of the graphical Okumura model, and COST 231.

These models are recommended when no high accuracy is required. One of the main drawbacks of empirical models is that they cannot be used for different environments without modification. For example, the empirical model for macro-cells cannot be used for indoor pico-cells. The validity of the models is highly dependent on the measurement environment because of the regressive process used to obtain them.

### 2.5.3 Deterministic models

In order to increase accuracy and minimize the dependence on the measurement environment, deterministic methods were developed. These site-specific methods are based on numerical methods. They use Maxwell's equations to calculate the full electromagnetic propagation characteristics. Some examples are the Ray-Tracing method, the Finite Difference Time-Domain (FDTD) method and the Method of Moments (MoM).

These methods are definitely better than the methods explained above in terms of accuracy. Even more for the environments studied in this work, which are complex scenarios, most of them indoor. The main disadvantage of the deterministic methods is the large computational overhead that could be prohibitive for some big complex environments.

Especially in complex and indoor scenarios, the behavior of the radio channel is not a trivial issue and heavily depends on the complexity of the environment [Fin09]. The appearance of degradation effects fundamentally due multipath components but also of phenomenon like reflection, refraction, diffraction and scattering among others make the study of the associated radio channel a really complex task [Wan12]. For these cases, Ray Tracing and Ray Launching methods offer a good trade-off between accuracy and calculation time, providing quite accurate RF power estimations for a whole scenario [Isk02,Rez10].

A comparison between the mentioned radio propagation models is depicted in Figure 2.22, where the trade-off between the accuracy of estimated RF values and simulation time can be seen. As previously said, the Ray Tracing techniques are very consistent and acquire a good compromise between the accuracy of the results and the computational time. Because of that, an in-house developed Ray Tracing technique has been used in this thesis for the analysis of radio propagation within complex environments: the 3D Ray Launching method.

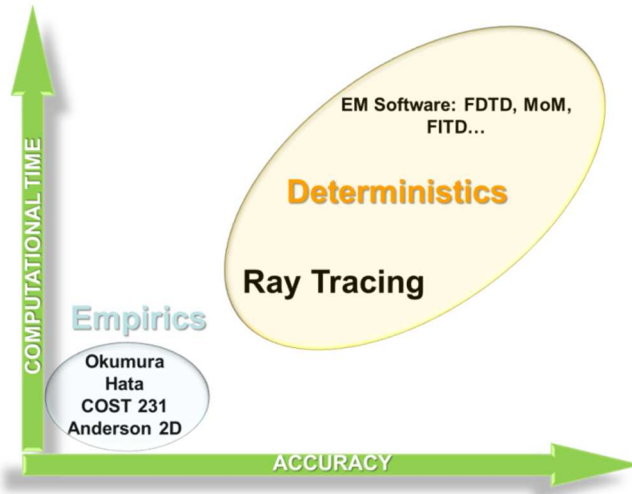


**Figure 2.22.** Accuracy vs. Computational cost of different radio propagation models.

# Chapter 3

## 3D Ray Launching

**T**HIS chapter presents the 3D Ray Launching algorithm, the in-house developed deterministic simulation tool used in this research work for the analysis of radio propagation phenomena within different complex scenarios. In Section 3.1 the description of the 3D Ray Launching simulation technique is presented. Then, in order to validate and show the accuracy of this simulation procedure, in Section 3.2 the radio propagation analysis carried out for different complex scenarios are presented. Finally, in Section 3.3 the contributions to the state of the art specifically related to the results shown in Section 3.2 are cited.

### 3.1 The 3D Ray Launching simulation tool

In complex environments, both indoor and outdoor, where the morphology of the scenario, the topology of the wireless systems and the presence of human beings greatly affect the electromagnetic wave propagation, it is a major issue to conduct a radio propagation analysis

before the deploying of WSNs or any other wireless communication system. Providing accurate radio propagation estimations in order to obtain valuable information regarding the performance of wireless devices deployed within complex environments is the aim of the 3D Ray Launching simulation method used in this work.

This 3D Ray Launching algorithm has been entirely created and developed in the Public University of Navarre. It is based on Matlab programming environment, and as a Ray Launching and Ray Tracing technique, it is a deterministic method based on Geometrical Optics (GO). The rays considered in GO are direct, reflected and refracted (transmitted) rays. Because of this, abrupt transitions areas may occur, corresponding to the boundaries of the regions where these rays exist. To complement the GO theory, the diffracted rays are introduced with the Geometrical Theory of Diffraction (GTD) and its uniform extension, the Uniform GTD (UTD). The purpose of these rays is to remove the field discontinuities and to introduce proper field corrections, especially in the zero-field regions predicted by GO.

The principle of operation of the algorithm lies in the rays that are launched in 3D directions (at an elevation angle  $\theta$  and with an azimuth angle  $\phi$ , as defined in the usual spherical coordinate system) with a predetermined angular separation from a specified source placed within a scenario under analysis. Figure 3.1 shows schematically the Ray Launching concept. The launched rays correspond to single points of the wave front of the radiated electromagnetic wave (see Figure3.2), and they propagate along the 3D space following a combination of optic and electromagnetic theories.

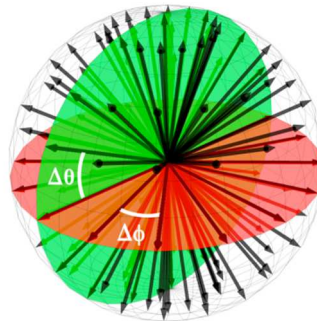


**Figure 3.1.** Schematic representation of Ray Launching concept.

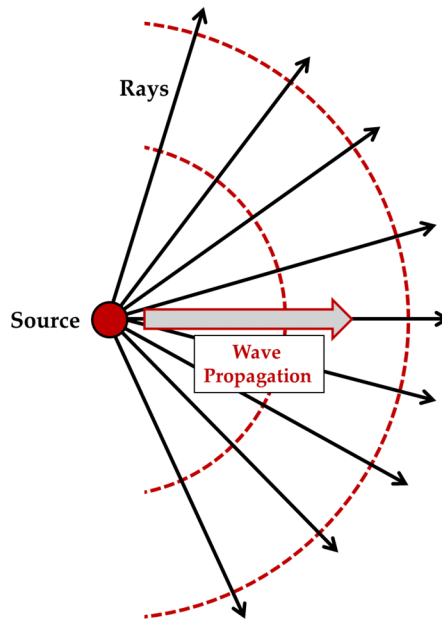


**Figure 3.2.** Wave front propagation associated with launched rays.

Thus, each ray propagates in the space as a single optic ray, being affected by propagation losses. The electric field components values corresponding to the launched rays are calculated by the following formulas, which represent the electric field created by an antenna with radiated power  $P_{rad}$  with directivity  $D_t(\theta_t, \phi_t)$  and polarization ratio ( $X^\perp$ ,  $X^\parallel$ ) at a distance  $r$  in free space [Car93]:

$$E_i^\perp = \sqrt{\frac{P_{rad} D_t(\theta_t, \phi_t) \eta_0}{2\pi}} \frac{e^{-j\beta_0 r}}{r} X^\perp L^\perp \quad (3.1)$$

$$E_i^\parallel = \sqrt{\frac{P_{rad} D_t(\theta_t, \phi_t) \eta_0}{2\pi}} \frac{e^{-j\beta_0 r}}{r} X^\parallel L^\parallel \quad (3.2)$$

where  $\beta_0 = 2\pi f_c \sqrt{\epsilon_0 \mu_0}$ ,  $\epsilon_0 = 8.854 \cdot 10^{-12}$  F/m,  $\mu_0 = 4\pi \cdot 10^{-7}$  H/m and  $\eta_0 = 120\pi$  ohms.  $f_c$  is the frequency of operation and  $L^\perp$  and  $L^\parallel$  are the path loss coefficients for each polarization.

When a ray impacts the planar interface of an object, a reflected and a transmitted (i.e. refracted) ray are created with a new angles provided by the well-known Snell's law [Hri00], shown in Figure 3.3. According to this law, the coefficients for the vertical and horizontal polarization for the reflected and transmitted rays are given by

$$T^{\perp} = \frac{E_t^{\perp}}{E_i^{\perp}} = \frac{2\eta_2 \cos(\Psi_i)}{\eta_2 \cos(\Psi_i) + \eta_1 \cos(\Psi_t)} \quad (3.3)$$

$$R^{\perp} = \frac{E_r^{\perp}}{E_i^{\perp}} = \frac{\eta_2 \cos(\Psi_i) - \eta_1 \cos(\Psi_t)}{\eta_2 \cos(\Psi_i) + \eta_1 \cos(\Psi_t)} \quad (3.4)$$

$$R^{\square} = \frac{E_r^{\square}}{E_i^{\square}} = \frac{\eta_1 \cos(\Psi_i) - \eta_2 \cos(\Psi_t)}{\eta_1 \cos(\Psi_i) + \eta_2 \cos(\Psi_t)} \quad (3.5)$$

$$T^{\square} = \frac{E_t^{\square}}{E_i^{\square}} = \frac{2\eta_2 \cos(\Psi_i)}{\eta_1 \cos(\Psi_i) + \eta_2 \cos(\Psi_t)} \quad (3.6)$$

where the index of refraction of both mediums are  $\eta_1 = 120\pi/\sqrt{\epsilon_{r1}}$  and  $\eta_2 = 120\pi/\sqrt{\epsilon_{r2}}$  and  $\Psi_i, \Psi_r$  and  $\Psi_t$  are the incident, reflected and transmitted angles respectively.

Once the parameters of transmission  $T$  and reflection  $R$  as well as the transmission and reflected (which is the same as the incident) angles are obtained, the new reflected and transmitted rays are launched from the impact point of the original incident ray with the new spherical angles  $(\theta_r, \phi_r)$  and  $(\theta_t, \phi_t)$  respectively.

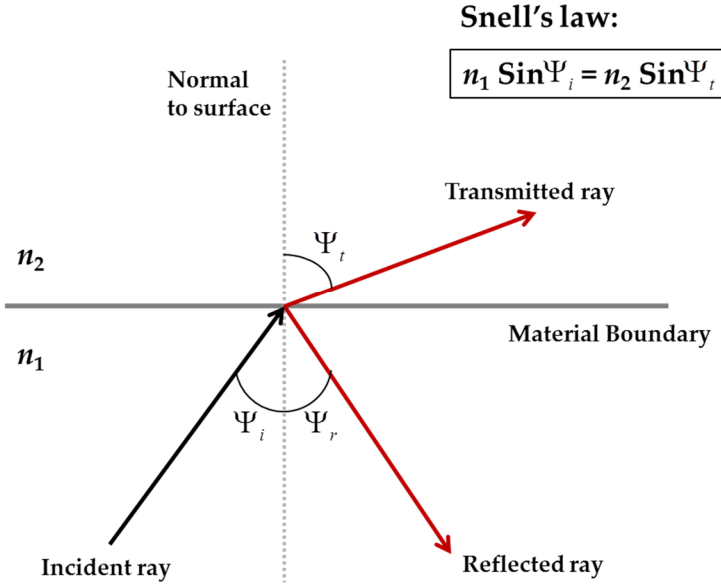


Figure 3.3. Snell's law representation.

Furthermore, this 3D Ray Launching algorithm takes into account the diffraction phenomenon, which happens when a ray impacts an object's edge. For that purpose, the UTD has been implemented in the GO algorithm by computing the diffraction coefficients on the edges of the diffractive elements with the finite conductivity two-dimensional diffraction coefficients given by [Lue88][Lue89][Rec09]:

$$D^{\parallel\perp} = \frac{-e^{-j\pi/4}}{2n\sqrt{2\pi k}} \left\{ \begin{array}{l} \cot\left(\frac{\pi+(\Phi_2-\Phi_1)}{2n}\right) F(kLa^+(\Phi_2-\Phi_1)) \\ + \cot\left(\frac{\pi-(\Phi_2-\Phi_1)}{2n}\right) F(kLa^-(\Phi_2-\Phi_1)) \\ + R_0^{\parallel\perp} \cot\left(\frac{\pi-(\Phi_2+\Phi_1)}{2n}\right) F(kLa^-(\Phi_2+\Phi_1)) \\ + R_n^{\parallel\perp} \cot\left(\frac{\pi+(\Phi_2+\Phi_1)}{2n}\right) F(kLa^+(\Phi_2+\Phi_1)) \end{array} \right\} \quad (3.7)$$

where  $n\pi$  is the edge angle,  $F$ ,  $L$  and  $a^\pm$  are defined in [Rec09],  $R_{0,n}$  are the reflection coefficients for the appropriate polarization for the 0 face or  $n$  face, respectively. The  $\Phi_2$  and  $\Phi_1$  angles in (3.7) refer to the angles in Figure 3.4.



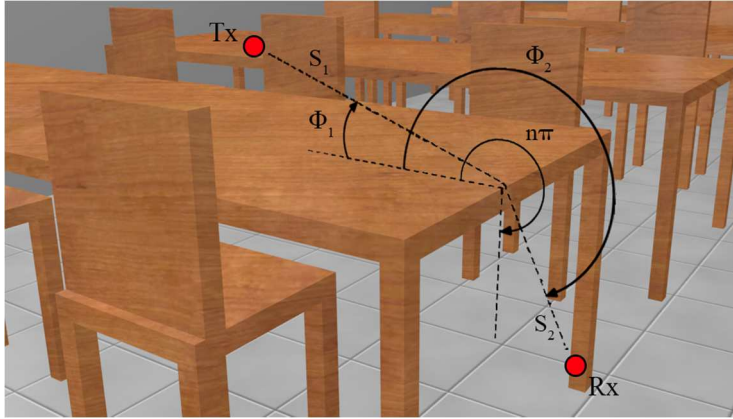


Figure 3.4. Geometry for edge diffraction coefficients.

When diffraction phenomenon occurs, the diffracted field is calculated by [Lue89]:

$$E_{UTD} = e_0 \frac{e^{-jks_1}}{s_1} D^{\perp\parallel} \sqrt{\frac{s_1}{s_2(s_1+s_2)}} e^{-jks_2} \quad (3.8)$$

where  $s_1$ ,  $s_2$  are the distances represented in Figure 3.4 from the source (Tx) to the edge and from the edge to the receiver point (Rx), respectively.  $D^{\perp\parallel}$  are the diffraction coefficients calculated from (3.7).

Figure 3.5 shows schematically the reflection, transmission and diffraction phenomena when a launched ray impacts a cuboid generated in the 3D Ray Launching simulation tool. The red dots represent the transmitter or the source of the launched ray.

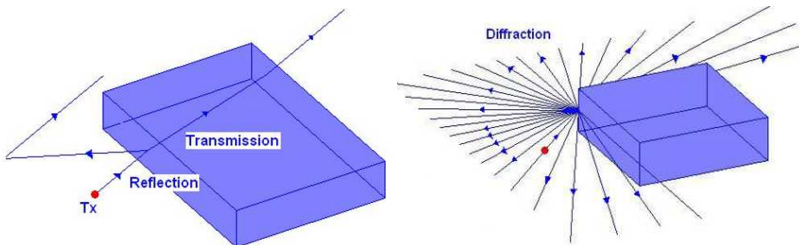
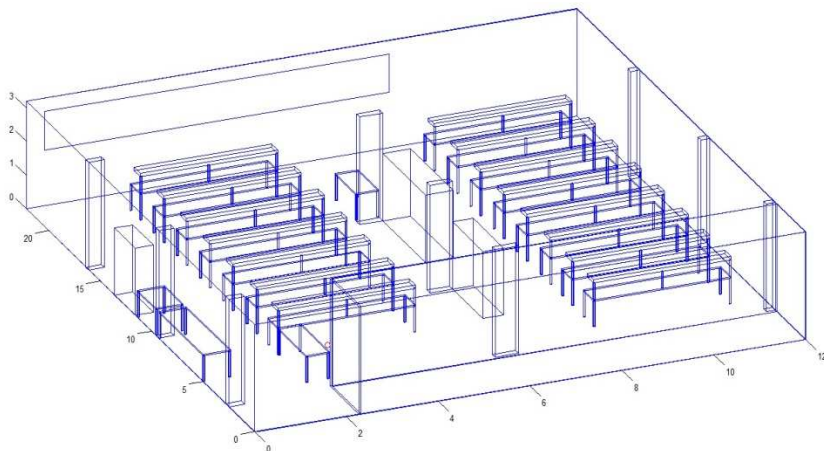


Figure 3.5. Reflection, transmission and diffraction phenomena.

Once the principle of operation of the 3D Ray Launching algorithm has been presented, i.e. how the launched rays represent the propagating electromagnetic wave and their interaction with the objects within the scenario creating the electromagnetic phenomena of reflection, refraction (transmission) and diffraction, other important aspects of the in-house 3D Ray Launching algorithm are presented.

The main of these aspects is the creation of the scenario under analysis. A full 3D scenario is created before the simulation procedure, considering all the objects, walls, columns, windows, doors, transmitters, receivers and all the elements that are present within the environment. The real size of the scenario itself and the elements within is taken into account, with the drawback that only hexahedral shapes can be defined. Figure 3.6 shows a schematic view of a scenario created by the 3D Ray Launching tool. Furthermore, the material properties of all the elements within the considered scenario are also taken into account, by defining the dielectric constant (i.e. the relative permittivity) and the conductivity for the frequency range of operation of the wireless system under analysis, which leads to providing very accurate simulation results. The materials are assumed to be spatially homogeneous and temporally non-dispersive.



**Figure 3.6.** Schematic view of a scenario created with the 3D Ray Launching simulation tool.

It must be pointed out that a grid is defined for the whole volume of the simulation space in order to save the parameters of each ray. Accordingly, the 3D environment is divided into a specific number of cuboids of a size fixed by the user. The size of the cuboids leads to higher or lower resolution, making the obtained results more or less accurate respectively. The cuboid size or resolution also affects the required computational time, being higher when the cuboids are smaller, as the number of cuboids and hence the number of mathematical calculations grow.

The calculated results, such as the received power level or the Power Delay Profiles, are stored in the cuboids that fill the entire volume of the scenario under analysis. For that purpose, when a ray enters a specific cuboid, its parameters are saved in a matrix with the value of the received power and the time of arrival. This happens until the ray has a certain number of permitted reflections (i.e. impacts on objects) or it exceeds the propagation time set, both parameters defined by the user.

Finally, but not less important in order to obtain accurate simulation results, the characteristics of the deployed wireless transceivers are predefined. Following, the main parameters of the transmitter as well as the receiver transceivers are shown:

- Location within the scenario under analysis (Cartesian coordinates, in meters)
- Radiated power level (Watt)
- Frequency of operation (Hz)
- Number of launching rays
- Separation angle between rays ( $\theta$  and  $\phi$ , in degrees)
- Antenna type and Directivity (radiation pattern)
- Antenna Gain

For an in-depth description of the in-house 3D Ray Launching simulation tool and the detailed operating mode of the algorithm, such as the mathematical calculation of the received power, consult the previously published work [Azp14].

As it is stated in the previous section of this work, the Ray Launching methods offer a good trade-off between accuracy and calculation time, providing quite accurate results. In order to confirm this statement for the presented in-house 3D Ray Launching algorithm, radio propagation analysis works have been performed for different complex environments. The obtained results are shown and discussed in the following section.

## **3.2 Modeling of complex environments and validation of the 3D Ray Launching method**

Once the 3D Ray Launching simulation tool has been shown, in this section its use for radio propagation estimations within complex environments is presented. For that purpose, the modeling of various complex environments has been carried out by creating schematic representations of the real scenarios with the aim of the 3D Ray Launching algorithm. Then, simulations have been performed in order to compare the estimated results with measurements, thus validating the simulation procedure. The results show that the in-house developed 3D Ray Launching method provide accurate RF power distribution estimations for morphologically different complex indoor scenarios, mainly indoor but also outdoor.

### **3.2.1 Office environments**

As a first step, office environments have been analyzed, as they are one of the most common indoor scenarios where a WSN can be deployed. Specifically, the influence of the topology as well as the morphology of this kind of indoor scenarios in the deployment of WSNs and wireless systems oriented to be applied to Building Automation Systems has been analyzed, as the use of these automation systems has been growing all over the world in the last years [Frä09][Bac10][Zam10][Rui12].



\*Figure obtained from <http://timesofkabul.com>

As time goes by, more buildings integrate an automation system for intelligently controlling elements such as light, heating, energy management, etc. The application of Building Automation Systems to any kind of building (including residential environments) is also called Smart Building (or Home) Systems. In this way, a Smart Building can be defined as the application of automation and integration systems on building facilities in order to improve the daily life of final users, to reduce energy consumption, to improve security and to reduce overall maintenance cost. This technology has been under development during many years with different standards and technologies such as KNX, BACnet or LON, allowing the development of different applications and systems in the last few years. All Smart Building networks are based on communication between sensors and actuators governed by the intelligence of the system. Over time, these systems have evolved incorporating more and more intelligence and decision making, up to Ambient Intelligence (AmI) concepts. Nowadays, AmI is described as an emerging discipline that brings intelligence to our everyday environments and makes them sensitive to end users. In order to obtain this level of intelligence, the hardware becomes more complex and is necessary to involve a larger number of sensors to obtain a large

amount of information achieving a more accurate response.

The connection between the components of these systems has been made typically via electric conducting cables, but nowadays the use of wireless technologies for communication with each other is taking a predominant role, bringing the Internet of Things to this kind of environments, providing communications and intelligence to the devices that surround us in everyday life defining “new” ambient intelligence environments.

With the rapid development of the wireless network technologies, the Building Automation Systems based on the WSN becomes more and more popular [Ost07][Wen10][Sun11]. The main advantage of using these wireless sensors is that they are easy and fast to deploy, not requiring any kind of wiring infrastructure. On the other hand, as the foreseen scenario for Building Automation Systems is an indoor scenario, it has a high complexity related to the topology as well as the morphology in terms of radio propagation. This leads to increased losses, in terms of material absorption as well as to strong multipath propagation. Besides, future systems will tend to use a large number of sensors, in which energy consumption and capacity are key issues to be considered.

There are many wireless communication technologies available (i.e. Bluetooth, ZigBee, Wi-Fi, NFC, etc.), most of them working in any of the existent ISM (Industrial, Scientific and Medical) free bands. For Building Automation Systems, aspects like low power consumption and low cost are typical parameters desirable in this kind of networks and because the data amount to exchange is usually small, the transmission data rate is not a determining factor. There are several products in the market that fulfill these characteristics and most of them are IEEE 802.15.4 compliant devices, which also is the most used standard for wireless Building Automation Systems [Bol06][Tae07][Dae10]. The main radio characteristics of the IEEE 802.15.4 protocol are shown in Figure 3.7.

<i>Frequency</i>	<i>Band</i>	<i>Coverage</i>	<i>Data Rate</i>	<i>Number of channels</i>	<i>Rx Sensitivity</i>	<i>Modulation</i>
2.4 GHz	IMS	Worldwide	250 Kbps	16	-85 dBm	O-QPSK
868 MHz		Europe	20 Kbps	1	-92 dBm	BPSK
915 MHz	IMS	America	40 Kbps	10	-92 dBm	BPSK

Figure 3.7. IEEE 802.15.4 radio characteristics.

The goal of the following analysis is to assess the radio coverage and link quality of IEEE 802.15.4 compliant devices in typical real indoor scenarios, for optimizing their deployment into WSNs for using them on Building Automation Systems. The proposed analysis is applicable in principle to a wide range of wireless systems, although it has been particularized for 802.15.4 devices. This type of Wireless Sensor Network exhibit properties such as 5 MHz bandwidth channelization (3 MHz real channel bandwidth), channel access based on CSMA/CA and low output power in the order of 0dBm, just to name a few. These properties, together with multiple network configurations and the possibility of including a large number of nodes, pose 802.15.4 networks and ZigBee as candidates in Building Automation Systems for control illumination, household appliance intercommunication, control of climate systems, presence-intrusion detection or entertainment, among others.

The main analyzed parameter has been link quality, which is given by the Packet Error Rate (PER), directly related to the Signal to Noise ratio to be achieved as a function of transceiver sensitivity. In the same way, the Signal to Noise ratio is strongly conditioned by the received power levels, which depend on the morphology of the environment where the wireless transceivers are deployed. For that analysis, simulations and measurements have been made in two laboratories of the Public University of Navarre: R&D building's laboratory N<sup>o</sup> 5 (scenario 1) and the Radio communication laboratory (scenario 2) depicted in Figure 3.8a and Figure 3.8b respectively.



These scenarios are complex environments composed of different types of walls (concrete, plywood, etc...) and a variety of different furniture (metallic cupboards, tables, chairs, computers, etc.), heavily affected by signal degradation due to multipath components. The proposed scenarios emulate the behavior of a typical small office and a more complex and bigger office or workplace.



(a)

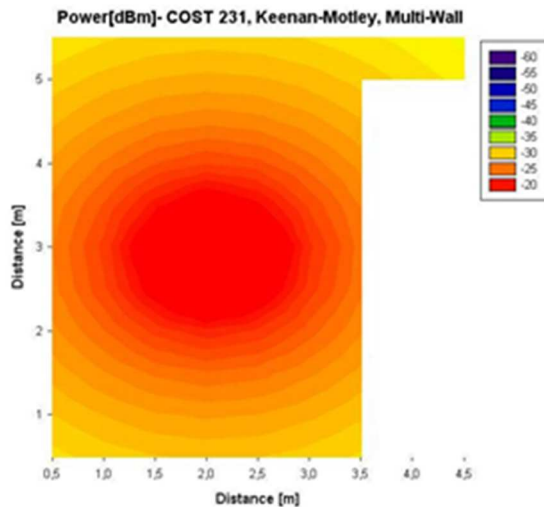


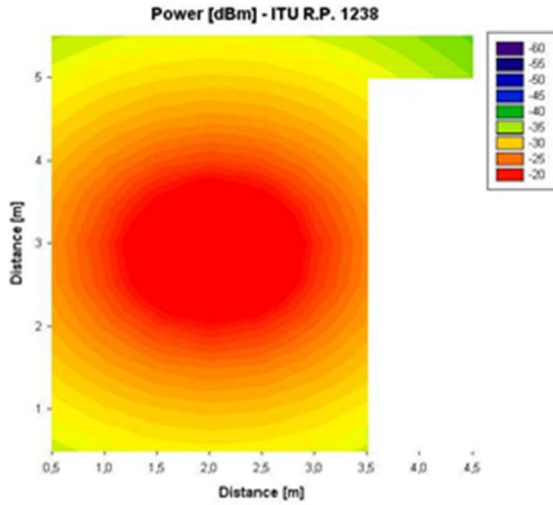
(b)

**Figure 3.8.** (a) R&D building's laboratory N° 5 picture. (b) Radio communication laboratory picture.

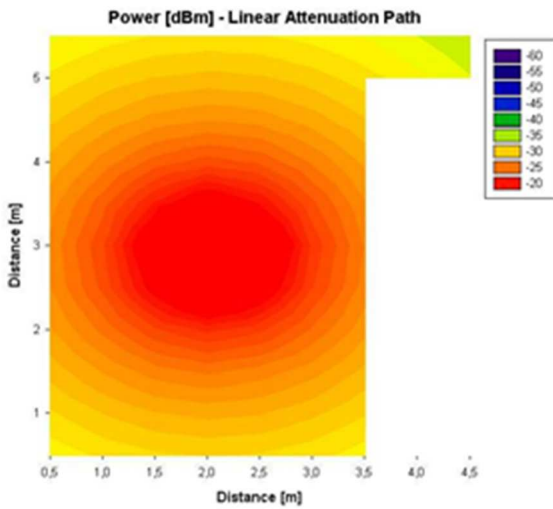


In order to analyze the impact of the topology and morphology of the proposed indoor scenarios in wireless system behavior, a first approximation can be given by means of empirical based models, based on analytical expressions derived from non-linear regression of the scenario under analysis. As it has been commented in previous sections, these models give rapid results, but require calibration based on measurements in order to give an adequate fit of the result, since it is strongly dependent on the environment where the results are being obtained. In this study, the estimation of the RF power distribution within the scenario depicted in Figure 3.8b has been obtained by applying different empirical models, such as Cost 231, Keenan – Motley, Multi-wall models (see Figure 3.9a), ITU R. P. 1238 model (see Figure 3.9b) and Linear Attenuation Path model (see Figure 3.9c). The calculations have been obtained considering a source placed in the center of the scenario operating at a frequency of 2.45 GHz and a transmitted power of 18dBm. As it can be seen from the figures, these models give simplified estimations, in which the complexity of the indoor elements (such as material changes, furniture, windows, etc.) has no significant effect.





(b)



(c)

**Figure 3.9.** RF power distribution for a height of 1.05m within the scenario of Figure 3.8a, calculated by (a) Cost 231, Keenan – Motley and Multi-wall models, (b) ITU R. P. 1238 model, (c) Linear Attenuation Path model.

Once the estimations obtained by different empirical models have been presented, the in-house 3D Ray Launching method has been used in order to analyze the same indoor scenarios with the aim of comparing its results with the results shown in Figure 3.9. A schematic view of the created indoor scenario corresponding to the “R&D building’s laboratory N° 5” of Figure 3.8a, is shown in Figure 3.10a, where the inclusion of indoor elements such as furniture, doors, walls and windows can be seen. It is important to note that the results shown in Figure 3.8 and Figure 3.9 correspond to a single room of the scenario represented in Figure 3.10a. In Figure 3.10b, a representation of the ray launching procedure is shown, with a three dimensional calculation scheme. Rays are launched given the solid angle definition within the simulation parameters. The scenario is subdivided in cuboids, in which the calculation of electrical field values in vector format are performed and processed in order to estimate parameters such as received power levels or Power Delay Profiles, as a function of the spatial observation point.

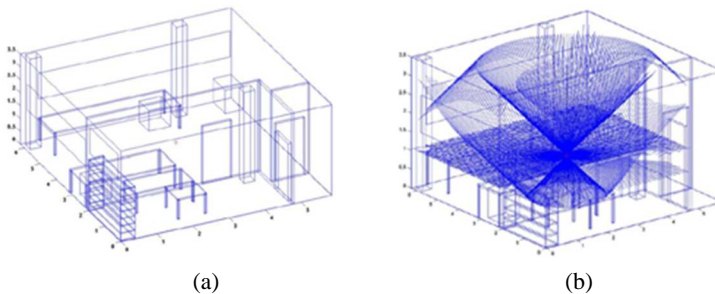


**Figure 3.10.** (a) R&D building’s laboratory N° 5. (b) Ray launching representation for the indoor scenario.

Figure 3.11 shows the RF power distribution results obtained by the 3D Ray Launching method at some specific points (the points where measurements were taken) of a plane at 1.05m height. The simulations have been performed considering the same parameters used for the estimations with the empirical models, i.e. a frequency of operation of 2.45 GHz and a transmitted power level of 18dBm. It is observed how the 3D Ray Launching results represent better the expected RF

distribution within indoor scenarios, showing the power variations due to the multipath propagation generated by the consideration of the elements within the scenario.

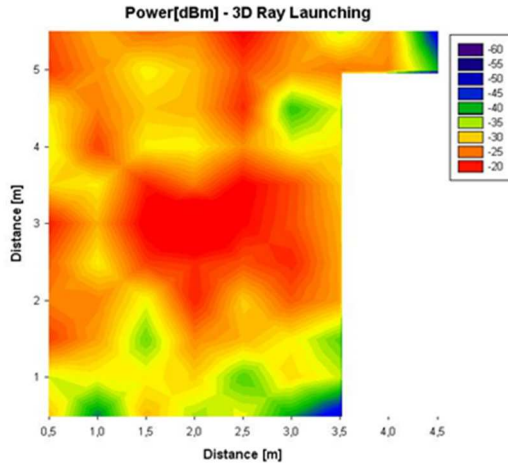


**Figure 3.11.** RF power distribution for a height of 1.05m within the scenario of Figure 3.8a, calculated by the 3D Ray Launching method.

In order to show clearer the difference of using empirical models or the 3D Ray Launching algorithm, in Figure 3.12 the results obtained by empiric models and the 3D Ray Launching algorithm are compared with measurements taken within the scenario under analysis. As it can be seen, there is quite good agreement between measurement results and 3D Ray Launching results, whereas there is worse agreement with empirical based models in general. The results obtained by the empirical models only follow the tendency of the power distribution, while the 3D Ray Launching results also represent the short term variations as they take into account the elements within the specific scenario under analysis. The measurement points represented in the graph correspond to the values of  $X=0.5\text{m}$  along the Y-axis, with higher discrepancies at certain points, due to averaging differences in the cuboid and equivalent antenna volume, as well as the unavoidable errors due to the differences between the real scenario and the created one. The adequate correlation between simulation and measurement

results validates the use of the 3D Ray Launching simulation tool for the complete scenario.

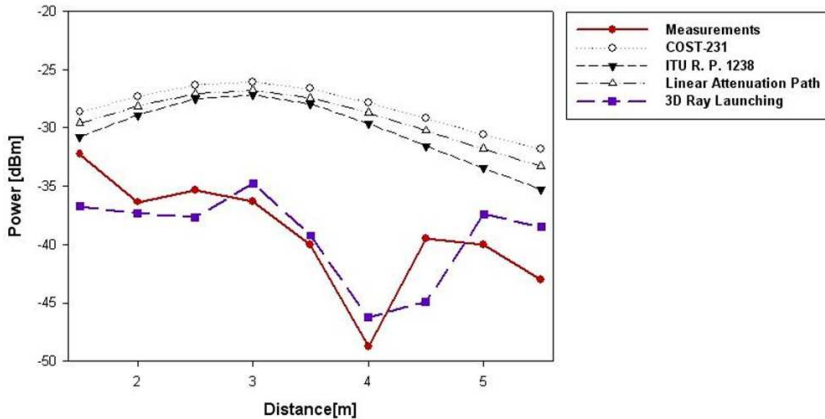


**Figure 3.12.** Received power vs. Linear path results. Comparison between Measurements and different Propagation models.

As stated previously, the determination of the received signal levels is the key parameter in order to analyze the overall link quality of the Wireless Sensor Network nodes. In order to gain insight in the performance of the presented 3D Ray Launching algorithm and the calculation of the RF power level distribution, several additional simulations have been carried out for different locations of the transmitter to verify that the interaction with the elements within the indoor scenario are considered and to stress the fact that both the morphology of the scenario and the location of the transmitter (as well as the potential receiver) play a key role in the overall performance of the wireless system. Figure 3.13 shows the RF power distribution for two different heights when the transmitter is fixed at a different location ( $X=1.8$ ,  $Y=5.34$ ,  $Z=1.05$ ) meters. As can be seen, there is a noticeable variation of power level even in the case of relatively small distances. This is due to the particular electromagnetic phenomena occurring within indoor scenarios like home and office environments, such as fast fading, which is the most relevant, which is due to the multipath propagation components, strongly dependent on the

morphology and topology of the scenario considered. In order to illustrate this dependence with spatial distribution, Figure 3.14 represents how the received power is distributed along the X and Y-axis for different heights. The strong dips in received power level are due to destructive addition of multipath components, described statistically by fast fading.

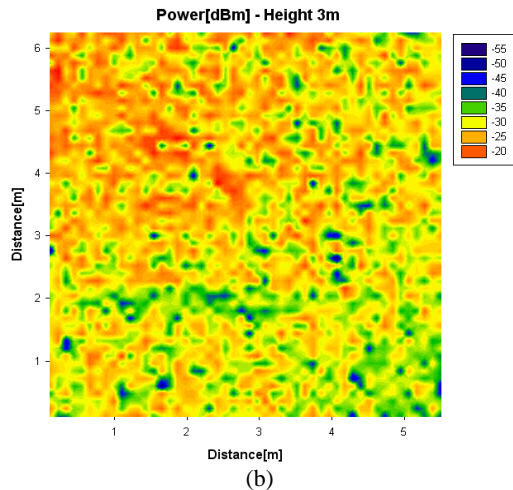
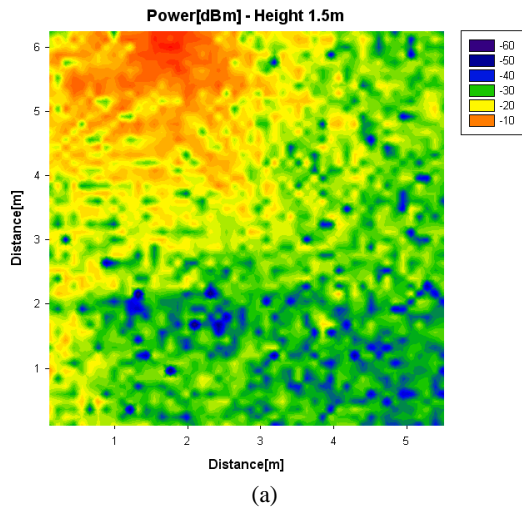


**Figure 3.13.** RF power distribution for different heights within the scenario of Figure 3.10a. (a) 1.5m height. (b) 3m height.

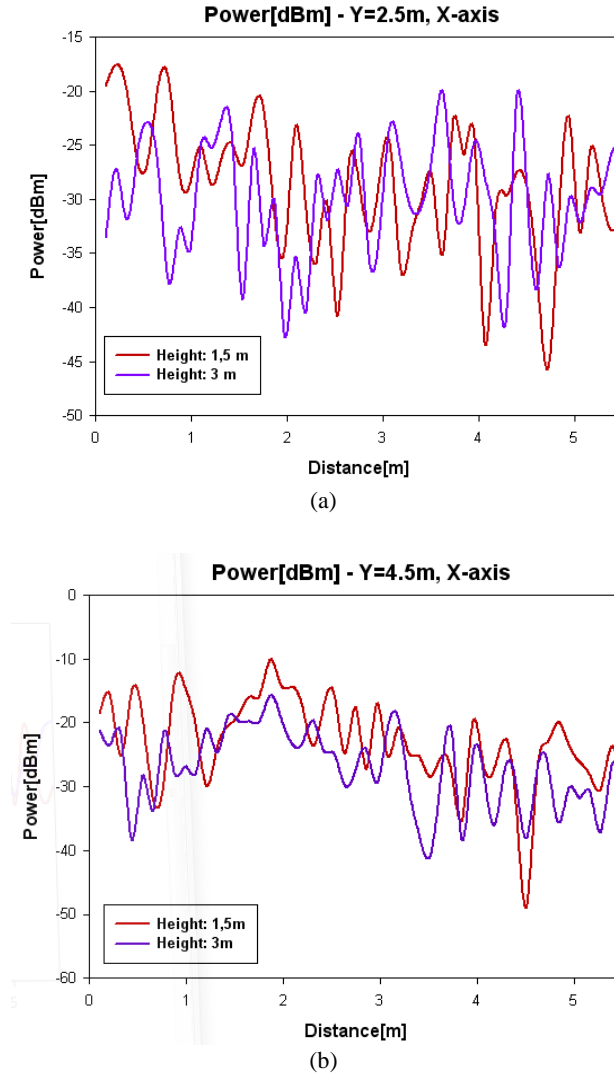


**Figure 3.14.** Distribution of RF power for different points of Y along the X-axis, for different heights. (a) Y=2.5m. (b) Y=4.5m.

To illustrate the relevance of this propagation mechanism, the Power Delay Profile for a given point of the scenario is shown in Figure 3.15. As it can be seen, there is a large number of echoes in the scenario, within a time span of approximately 15ns to 90ns, corresponding to

distances from 0.5 meters to 2.5 meters. The large amount of echoes within such a short distance is coherent with the complexity of the scenario (elements such as furniture) as well as the material properties at the frequency of operation.

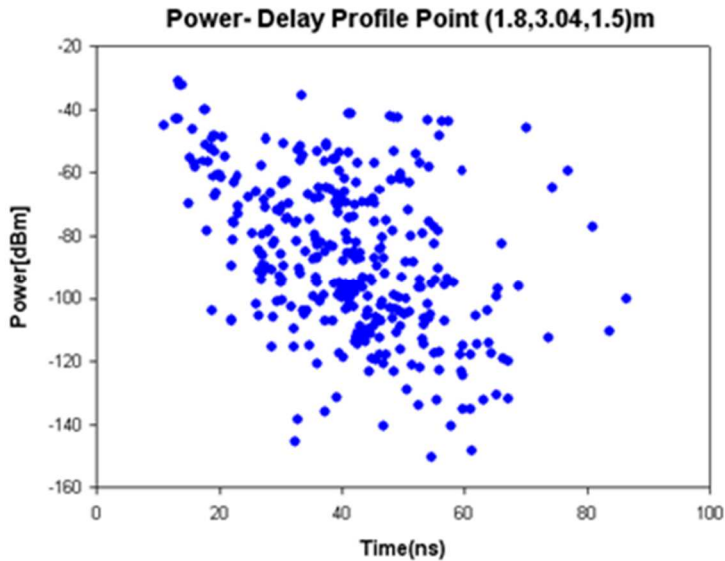


**Figure 3.15.** Power Delay Profile at Point (1.8, 3.04, 1.5) m within the scenario under analysis (Figure 3.10a).

Additionally, several simulations of the other presented indoor scenario, called “Radio communication laboratory” (Figure 3.8b) have been done. Figure 3.16 shows the schematic representation of this scenario created with the 3D Ray Launching simulation tool. In this case, the scenario has a larger size, with a great deal of furniture, typical of laboratory/technical office environment, including two metallic lockers in the center of the scenario. Figure 3.17 shows the spatial distribution of RF power for different heights when the transmitting antenna is placed at the point (X=2, Y=2, Z=0.81) m. Once again, the morphology and the topology of the scenario play a key role in the values of received power levels and the same effects shown in the previous scenario are seen. It is worth noting the expected effect



that the two metallic lockers have in the propagated signal (see Figure 3.17a): the signal does not penetrate the lockers and the RF power behind them decreases significantly, due to the properties of the metallic material of the locker.

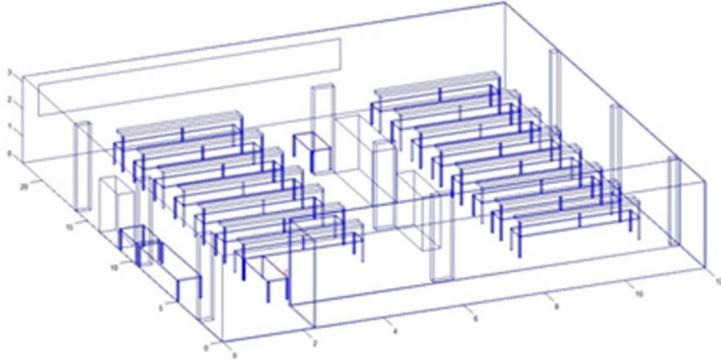
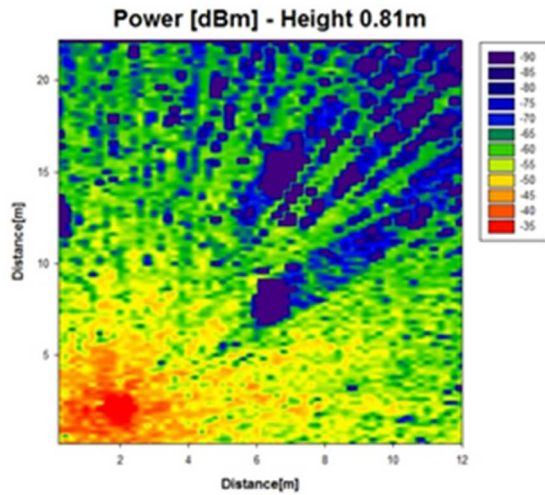
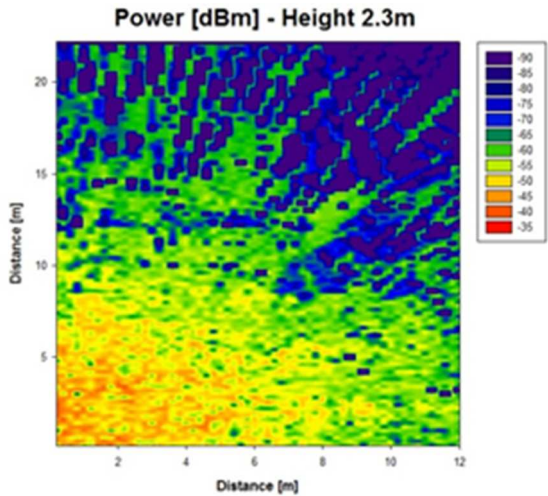


Figure 3.16. Radio communication laboratory.



(a)



(b)

**Figure 3.17.** RF Power distribution estimations for different heights within the scenario of Figure 3.16. (a) Height=0.81m. (b) Height=2.3m.

The simulation results show the relevance of the layout of the working scenario in the deployment of WSNs. Validation is now sought in terms of experimental results, with the aid of realistic wireless transceivers. As it has been previously stated, due to the performance in terms of unit cost, power consumption and spectrum availability, IEEE 802.15.4 based devices have been employed for the experimental setup. Specifically, the wireless communication devices used in this work have been XBee Pro models, from Digi International Inc, shown in Figure 3.18a. The transmission RF power level of these devices can be adjusted with a maximum default value of 18dBm, which has been used in the experimental setup. The module has different antenna options (i.e., external antenna, usually a whip antenna or a compact integrated chip antenna) with election, in terms of size and integration of chip antenna, which leads to a low antenna gain, in the order of -1.5dBi. For simple standalone operation, the transmitter XBee Pro module and the associated components can be plugged into a solderless breadboard powered by two 1.5 VDC AA batteries. For transmitting arbitrary data or processing receiving data,

the connection with a PC is required. For that purpose, the XBee Pro module is plugged into an XBee Explorer USB unit (see Figure 3.18b). In this way, the XBee Pro modules' UART appears as a USB serial port in the connected PC and can be accessed for reading/writing data using RS 232 protocol.

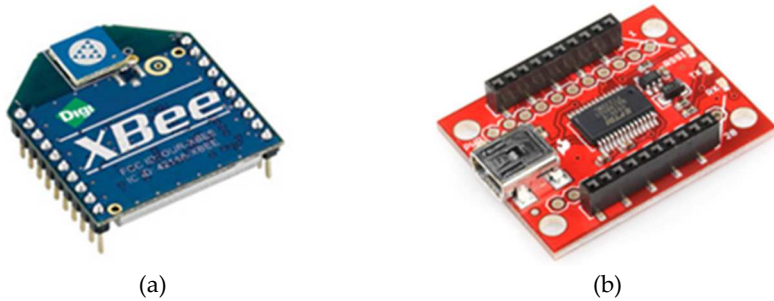


**Figure 3.18.** (a) XBee Pro module. (b) XBee Explorer USB.

The initial experimental setup has been deployed in the scenario of Figure 3.8a. In order to analyze the radio propagation characteristics of the scenario, a transmitting XBee Pro module has been placed in the center of the room and the received RF power has been registered in several different points. The received power values have been measured with the aid of an omnidirectional antenna connected to an Agilent N9912A FieldFox RF Spectrum Analyzer of Agilent, with a central detection frequency fixed at 2.4 GHz. The spectrum analyzer is capable of measuring signals from 5 KHz to 4/6 GHz with a DALN (Displayed Average Noise Level) of -148dBm, a sufficient dynamic range to analyze the XBee Pro transmitted RF signal. In order to improve the spectrum analyzer's measurement time, the transmitter has been configured to operate sending one packet of data per millisecond, which is the maximum achievable data rate.

As shown in the previous Figure 3.12, where the comparison between the these measurements and the estimations of the received RF power is depicted, it can be seen that the received RF power differs greatly from the values predicted by the propagation models and adjusts more precisely to the ones predicted by the 3D ray launching algorithm. As for consideration of computational error, the corresponding simulation error of the 3D Ray Launching algorithm is

defined as the difference between the measured and simulated values of the path loss at any time. For this case, the resulting mean error is 0.50dB, with a standard deviation of 1.58dB, indicating that the simulation method is working properly within this scenario. It is also worth noting that the simulation results indicate that the received signal levels are above the sensitivity threshold of conventional IEEE 802.15.4 transceivers, usually below -80dBm.

Another important aspect of a wireless communication system is the quality of the radio link. It is significant to determine how the received packet's RSSI affects the links PER (Packet Error Rate), as already stated previously. To obtain the data, XBee Pro module's functionality of estimating each received packet's RSSI has been used. The aim is to analyze the relation between the PER of the radio link and different values of RSSI, since this will give a direct correlation between both values and hence allow an estimation of the overall observable radio link quality. For that purpose, in a random point within the room, an XBee Pro module emulating a transmitter has been placed and connected to a computer via a USB cable. In the same computer, a Java application runs. This was programmed in-house for the purpose of broadcasting a quantity of packets determined by the user. On the other hand, another XBee Pro module has been connected, also via a USB cable to a laptop. In that laptop another in-house Java programmed application runs. This application determines the average RSSI of the received packets and the corresponding PER value, storing them in a text file along with the values of the arriving time, RSSI value and the sequence number of every received packet. The receiver position has been changed randomly throughout the scenario for obtaining different values of average RSSI and its corresponding PER values. In order to obtain meaningful data, it is important to send a significant amount of packets. Taking this into consideration, the number of packets used for every PER measurement has been of 1,000,000. In Figure 3.19 the representation of the measured PER versus the average RSSI is shown. It can be seen that the packet errors are very low until a RSSI value of -75dBm is reached. Then, the curve behavior follows an exponential trend, losing many packets when the RSSI value

approximates to -100dBm, which is the sensitivity value of the used XBee Pro devices. This behavior is due to the receiver begins to have problems retrieving the original data correctly when the SNR becomes too low, i.e., when the RSSI becomes too low.

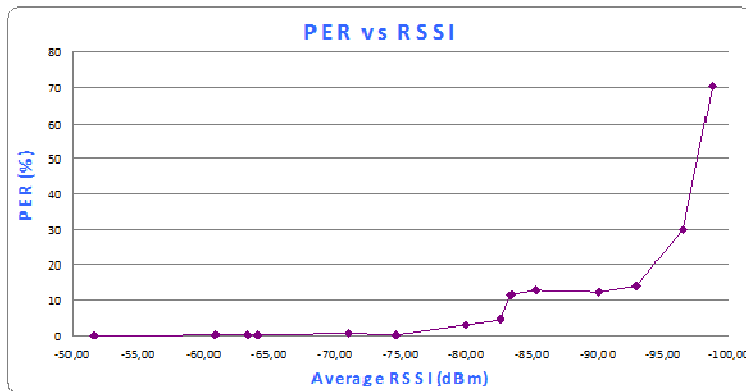


**Figure 3.19.** PER vs. Average RSSI in the scenario of Figure 3.8a.

In order to improve the performance of the wireless communication, the XBee Pro modules have the capability of sending ACK (Acknowledgement) packets for error recovering. When a packet is sent by the transmitter, an ACK packet is sent back from the receiver. If the ACK packet is not received, another packet is sent by the transmitter with the information of the lost packet. The IEEE 802.15.4 protocol provides a maximum of 3 ACK retries after the packet emission is considered a failure. The difference in the link quality between using ACK packets could be very significant, as it is shown in Figure 3.20, where a comparison between measurements without ACKs and using ACKs is depicted. It can be seen how the trend of both curves is similar; however, the degradation in the percentage of received packets starts at RSSI value of -75dBm for the case without ACKs and at -90dBm when the ACK option is activated. This 15dB difference in RSSI would have a strong impact on the overall coverage radius of the wireless system.

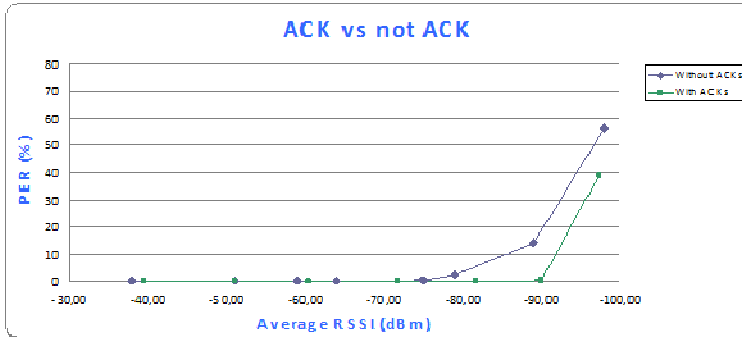


**Figure 3.20.** Representation of wireless link degradation in terms of percentage of PER, with and without use of ACK packets.

Further measurement results have been obtained for the scenario of Figure 3.8b, which is a larger and more complex environment as it has a higher density of furniture elements. Figure 3.21 shows the obtained PER vs. RSSI results. As it is expected, similar behavior is observed as in the previous case of the previous scenario. Even so, in this case, the degradation in the percentage of received packets starts at RSSI value of -84dBm approximately, while in the previous scenario starts at -75dBm. This is due to the fact that the morphology of both scenarios is different and hence, the wireless communication within them is differently affected by the multipath propagation, which leads to more or less conservative network deployment of the wireless sensors.

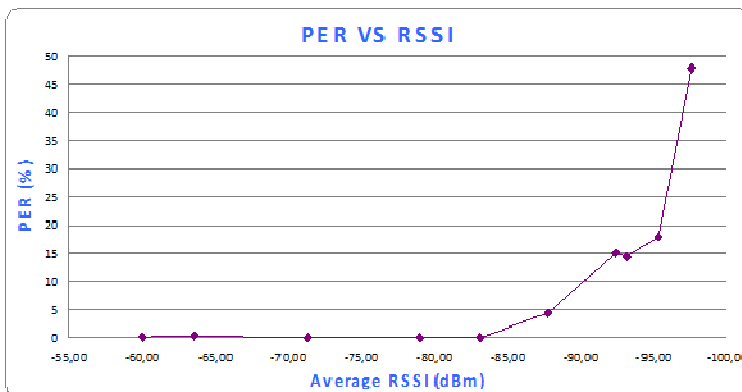


**Figure 3.21.** PER vs. Average RSSI in the scenario of Figure 3.8b.

As it has been seen in both measurements and simulation results, the layout and composition of elements within an indoor scenario, such as office environments, play a key role in the overall effect in terms of losses in the propagation channel used in WSNs and systems. As showed, initial considerations are usually based on simplified empirical models, which lead to large errors in received signal estimations. To overcome this limitation, the in-house developed deterministic code based on 3D Ray Launching has been used to analyze the effect of the indoor topology and morphology in the operation of wireless links within two different realistic scenarios. Experimental validation has been obtained by performing tests with wireless sensors. The results confirm that the analysis of the topology of the WSN has a strong impact in complex indoor scenarios, in which small distances represent relevant changes in the received level as well as the overall quality of the wireless system. The application of the 3D Ray Launching technique in the planning phase of wireless sensor networks and systems can lead to the optimization of the quality of service, capacity and overall energy consumption of the WSN, which is of great importance in the deployment strategy of future high density sensor configurations, present in Building Automation Systems of the future.

### **3.2.2 Home environments**

Another typical indoor environment where WSNs can be deployed is the home environment. As in the previous case of office environments, home environments also are complex scenarios in terms of radio propagation due to the furniture elements and walls within them. While in the previous subsection single office rooms have been studied, in this subsection a radio propagation analysis within a whole home is presented. The aim of this study is to analyze the radio propagation of a ZigBee-based WSN oriented to enable a potential deployment of wireless Ambient Assisted Living (AAL) system within a common home environment.



\*Figure obtained from <http://www.truste.com>

AAL systems are possible due to the wide adoption of diverse technological elements, which have been key drivers in the transformation, provision and delivery of healthcare services. In particular, those related to Information and Communication Technologies. Traditionally, healthcare services entailed large amounts of resources, many of which required patients to be in direct contact with health specialists, for diagnostics as well as for treatment. In the past decade, with the steady adoption of software solutions and seamless connectivity, electronic health (e-Health) as well as mobile health (m-Health) have enabled Ambient Assisted Living (AAL) and Context Aware scenarios, where real time monitoring and interaction of patients and users with health specialists can be performed remotely [Pal13][Leo13], decreasing overall cost and increasing overall quality of life, reducing patients displacement and allowing them to live in their homes [Led13][Mor12]. Parameters such as biomedical signals, drug



distribution, patients' behavior and interaction and alarm signals can be readily collected and analyzed. An evolution in the concept of AAL is the interaction of these localized solutions within a Smart City or Smart Region, giving rise to the Smart Health concept [Sol14].

In order to collect the amount of information required for the deployment of an AAL system within a home environment, the number of wireless transceivers within the scenario is supposed to be quite high. Because of this, a dense ZigBee network deployed within a home environment is analyzed in this section of the work. The scenario considered is a common apartment located in the neighborhood of 'La Milagrosa' in the city of Pamplona, Navarre. The apartment has approximately 65m<sup>2</sup> and it consists of 2 bedrooms, 1 kitchen, 1 bathroom, 1 study room, 1 living room and 1 small box room, as it is shown in Figure 3.22. The dimensions of the scenario are 9.05m × 7.255m × 2.625m, and it is completely furnished. For its construction by means of the 3D Ray Launching tool, the real size and material properties (dielectric constant as well as conductivity) of all the furniture and elements such as chairs, tables, doors, beds, wardrobes, bath, walls, etc. have been taken into account, which will lead to obtain accurate simulations results. The properties of the materials with greater presence in the scenario are listed in Table 3.1.

Material	Permittivity ( $\epsilon_r$ )	Conductivity ( $\sigma$ )[S/m]
Air	1	0
Plywood	2.88	0.21
Concrete	5.66	0.142
Brick wall	4.11	0.0364
Glass	6.06	10 <sup>-12</sup>
Metal	4.5	4×10 <sup>7</sup>
Polycarbonate	3	0.2

**Table 3.1.** Properties of the most common materials used for 3D Ray Launching simulations.

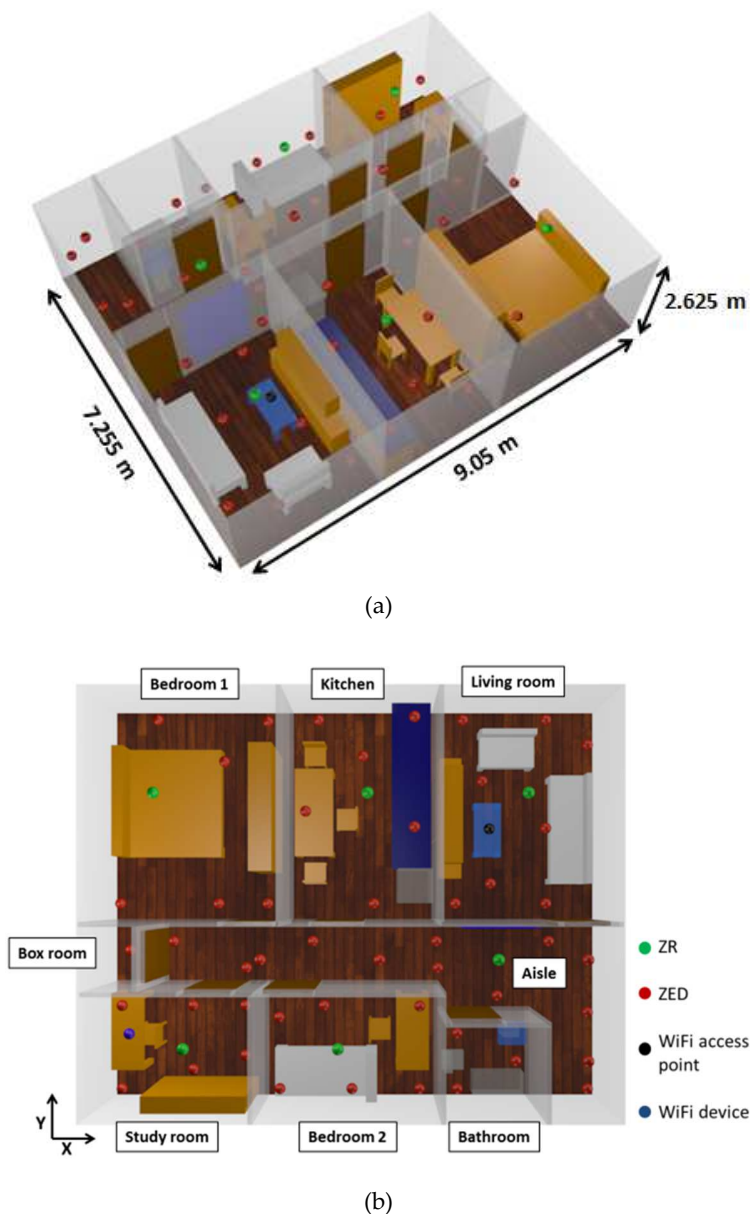


**Figure 3.22.** (a) 3D simulated scenario with wireless devices shown in colored dots, (b) top view of the scenario.

Once the simulation scenario has been defined, a measurement campaign has been carried out in the real scenario in order to validate the results obtained by the 3D Ray Launching algorithm. For that purpose, a ZigBee-compliant XBee Pro module connected to a computer through a USB cable has been used as a transmitter (see Figure 3.23a). The transmission power level of the wireless device can be adjusted from 0dBm to 18dBm. For the validation, the 0dBm level has been set, which will be the level used for the simulations of the ZigBee network reported in the following sections. Received power values in different points within the scenario have been measured by means of a 2.4GHz-centered omnidirectional antenna connected to a portable N9912A FieldFox spectrum analyzer (see Figure 3.23b). In order to minimize the spectrum analyzer's measurement time, the transmitter has been configured to operate sending one data packet per millisecond. The measurement points and the position of the transmitter element can be seen in the schematic view of the scenario shown in Figure 3.24, which are represented by green points and a red rectangle respectively. The transmitter has been placed at height 0.8m and the measurements have been taken at height 0.7m. The obtained measured power levels for each measurement point have been depicted in Figure 3.25, where a comparison between the measurements and 3D Ray Launching simulation results is shown. As can be seen, the 3D Ray Launching simulation tool provides accurate estimations. In this case, taking into account the 14 measurement points, a mean error of 1.38dB with a standard deviation of 2.55dB has been obtained.

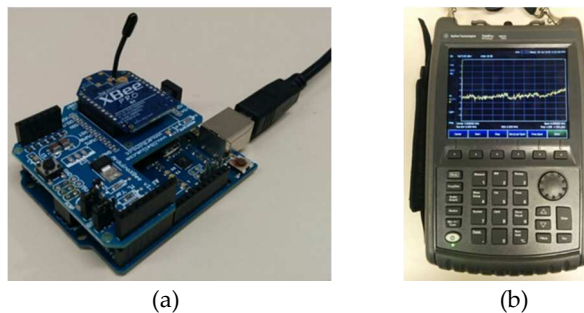


**Figure 3.23.** (a) XBee Pro module. (b) N9912A FieldFox spectrum analyzer.

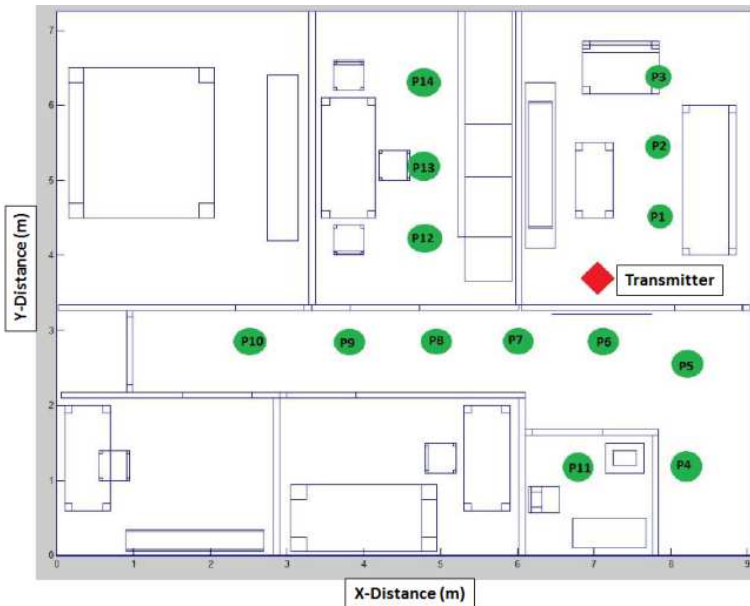


Figure 3.24. Schematic upper view of the scenario. Measurement points are shown in green and the transmitter location in red.

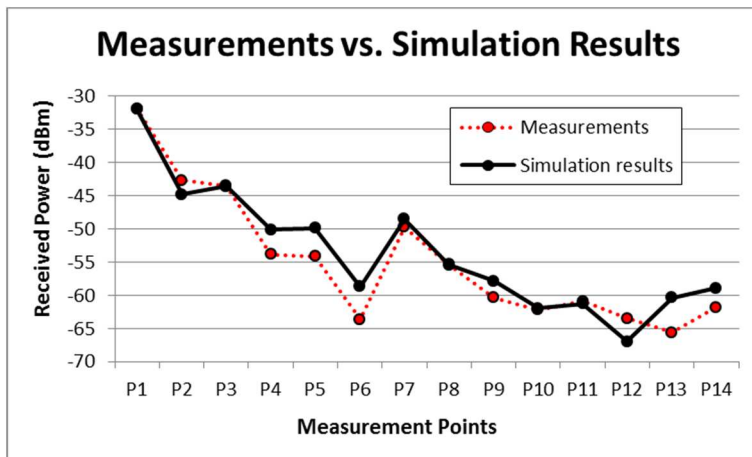


Figure 3.25. Measurements vs. 3D Ray Launching simulation results for different points within the scenario (see Figure 3.24).

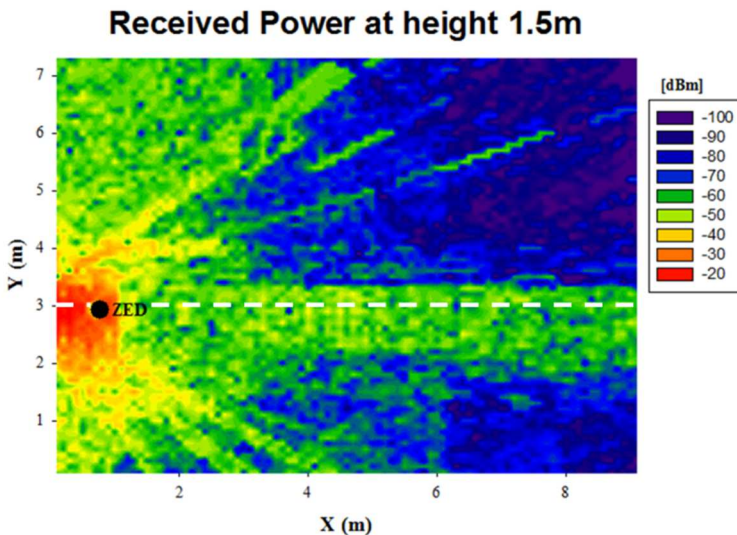
Following the validation of the 3D Ray Launching simulation algorithm, the radio propagation within the presented home environment is analyzed. For that purpose, a ZigBee-based wireless network has been deployed within the scenario (see Figure 3.22b). The network consists of 50 ZED (ZigBee End Device), which emulate different kinds of sensors distributed throughout the apartment and 6 ZR (ZigBee Router), which emulate the devices that will receive the information transmitted by the ZEDs included in their own network. There are also WiFi devices, but they are used for another analysis in later sections of this work.

The performance of a WSN in AAL environments in terms of received power distribution is a major issue, especially in complex indoor environments where radio propagation phenomena like diffraction and fast fading are very strong. Besides, the deployment of ZigBee-based WSNs is versatile and allows several topology configurations such as star, mesh or tree. Furthermore, due to the wireless inherent properties and the size of the motes, their position as well as the network topology itself can be easily changed and reconfigured. Thus, very different networks and sub-networks can be found in a single AAL environment. The aim of the following study is to analyze the propagation phenomena, as well as the effect of the topology and the morphology of the scenario under analysis, by means of the 3D Ray Launching simulation method. For that purpose, the simulations of the ZED devices shown in Figure 3.22 have been made. The used simulation parameters are shown in Table 3.2.

Parameter	Value
Frequency	2.4 GHz
ZigBee Transmitted power	0 dBm
Antenna gain	1.5 dBi
Launching angle resolution	1°
Maximum permitted reflections	7
Cuboids resolution	10cm × 10cm × 10cm

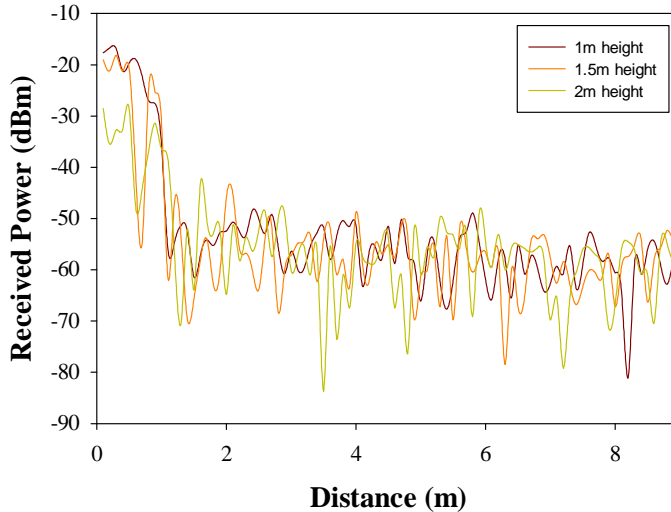
**Table 3.2.** Parameters for the 3D Ray Launching simulations.

The main result provided by the simulations is the RF power level distribution for the whole volume of the scenario. Figure 3.26 shows an example of the received power distribution in a plane at height of 1.5m of the scenario for the transmitting ZED placed within the box room. It can be observed that the morphology of the scenario has a great impact on the results. In this example, it is clearly shown how the radio propagation through the box room’s gate and through the isle is greater than the rest of the farthest rooms of the scenario, as there are less obstacles and walls in the rays’ path. Due to the topological complexity of this kind of scenarios, the multipath propagation is expected to be the main propagation phenomenon, which appears due to the strong presence of diffractions, reflections and refractions of the transmitted radio signals. Multipath propagation typically produces short-term signal strength variations. This behavior can be observed in Figure 3.27, where the estimated received power vs. linear distance is depicted for 3 different heights corresponding to the white dashed line of Figure 3.26.



**Figure 3.26.** RF power distribution plane at height 1.5m when the ZED within the box room is transmitting. The white dashed line corresponds to the data shown in Figure 3.27.

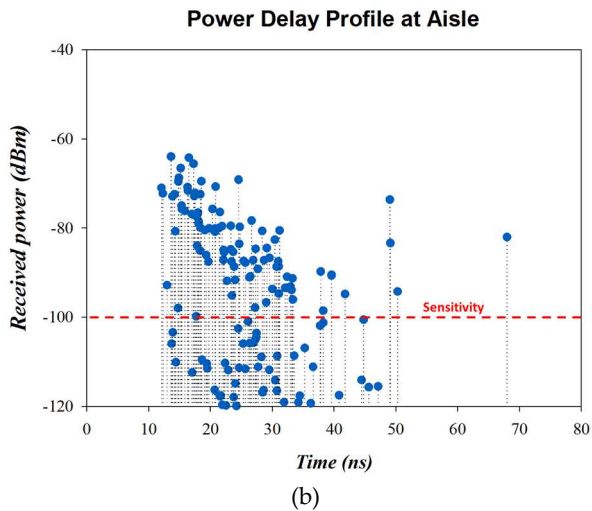
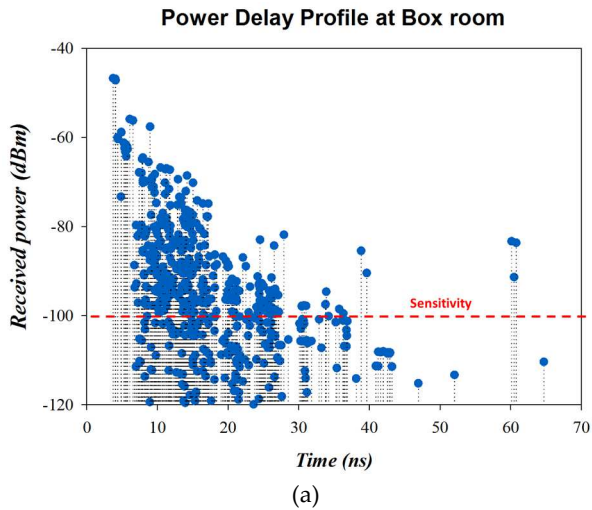
## Received Power vs. Linear distance



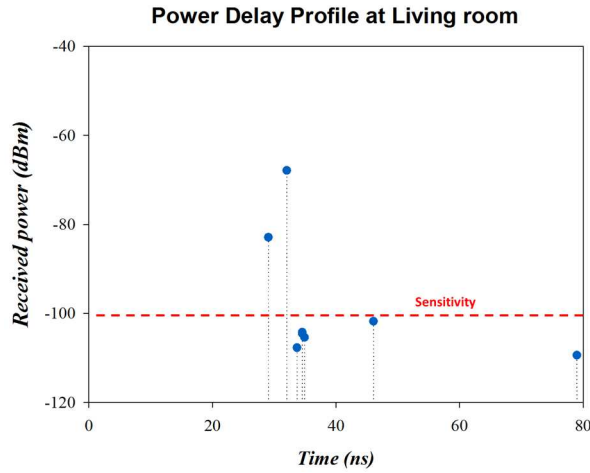
**Figure 3.27.** Estimated received power vs. linear distance for 3 different heights corresponding to the white dashed line depicted in Figure 3.26.

The relevance of multipath propagation within the scenario can be determined by the estimation of the values of all the components reached at a specific point, usually the receiver. In order to assess this, Power Delay Profiles are used. This kind of results can be obtained with the presented 3D Ray Launching tool. As an example, Figure 3.28 shows the Power Delay Profiles for 3 different positions within the scenario, when the ZED of the box room is emitting (the case represented in Figure 3.26). As it can be observed, the complex environment creates lots of multipath components, which are very strong in the box room as the transmitter is in it (Figure 3.28a). As expected, these components are fewer and weaker (i.e. lower power level) as the distance to the transmitter grows, as it can be seen in the Power Delay Profiles of randomly chosen points within the aisle (Figure 3.28b) and the living room (Figure 3.28c). Note that the arrival time (x-axis) of the first component of each graph clearly shows the increasing distance, being higher while the distance grows. The dashed red lines depicted in the Power Delay Profiles correspond to the

sensitivity of the XBee Pro modules, indicating which of the received components can be read by the receiver: those with a power level higher than -100dBm.







(c)

**Figure 3.28.** Estimated Power Delay Profiles when the ZigBee mote within the box room is emitting, for different points within the scenario; (a) Box room, (b) Aisle and (c) Living room.

An alternative approach to show the impact of multipath propagation is the use of Delay Spread graphs, which provide information for a whole plane of the scenario in a single graph, instead of the ‘point-like’ information provided by Power Delay Profiles. The Delay Spread is the time span from the arrival of the first ray to the arrival of the last ray, at any position of the scenario; i.e., the time span between the first and the last element depicted in Power Delay Profile figures. Figure 3.29 shows the Delay Spread for a plane at height 2m when the ZED placed in the box room transmits. As expected, larger timespan values can be found in the vicinity of the emitting ZED since this is the area where the reflected valid rays (i.e. rays with power level higher than the sensitivity value) arrive sooner. In other areas, Delay Spread values vary depending on the topology of the scenario.

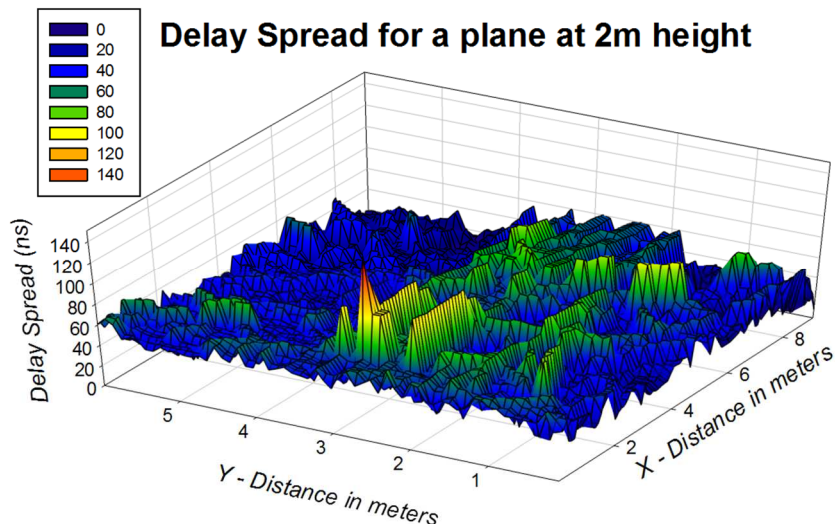


**Figure 3.29.** Delay Spread at 2m height when ZED transmits in the box room ( $X=0.5\text{m}$ ,  $Y=2.8\text{m}$ ,  $Z=1\text{m}$ ).

The presented results show that the in-house 3D Ray Launching simulation tool is valid for simulating home environments, and that this kind of AAL indoor complex scenarios need a thorough and personalized radio planning analysis as the radio propagation has a strong dependence on the network topology and the indoor scenario configuration.

### 3.2.3 Vehicular environments

After the use and validation of the 3D Ray Launching algorithm within office and home environments, in this section more complex and less studied indoor environments are presented. These new type of scenarios are vehicular environments, which in recent years have gained importance due to the development of intelligent transportation systems. Specifically, intra-vehicular propagation has been studied, within vehicles such as cars, aircrafts or trains. Comparing with home and office environments, these kinds of scenarios are usually smaller and they have a strong presence of metallic elements. As in the

previous environments, a radio propagation analysis is carried out, and measurements within real scenarios help to validate the results obtained by our 3D Ray Launching algorithm.



\*Figure obtained from <https://jaxenter.com>

First, the influence of the topology and morphology of a particularly complex scenario for the deployment of ZigBee wireless sensor networks is analyzed. This complex scenario is a common car. The existence of loss mechanisms such as material absorption (seats, dashboard, etc.) and strong multipath components due to the great number of obstacles in a small scenario and the metallic environment (bodywork), as well as the growing demand for wireless systems within a vehicle emphasizes the importance of the configuration of the heterogeneous intra-car wireless systems.

As it is well known, WSNs are growing rapidly into a large number of fields of application. The most popular application fields have been building automation systems, location, industrial and structural monitoring, farming and agriculture, defense, security and healthcare, among others. Recently, vehicular wireless applications have had great relevance due to the increasing number of sensors used in cars for

different functions as engine management, comfort or intelligent brake systems, just to name a few. Traditionally, these sensors have been wired, but replacing these wires with wireless technologies (e.g. ZigBee or RFID) could lead to a significant weight and cost reduction [Mir06][Lee11]. Besides, wireless technologies provide easier and cheaper deployment, system maintenance and upgrade.

Car manufacturers as well as research groups around the world have shown great interest in the development of wireless systems for automotive applications. In fact, there are study groups working on car communications with the aim of defining standards: 802.11p and IEEE 1609 family of standards for Wireless Access in Vehicular Environments (WAVE), among others. These emerging vehicular networks, which can be vehicle-to-infrastructure, vehicle-to-vehicle and intra-vehicle communications, could provide a wide variety of new applications. For vehicle-to-infrastructure communications, the most popular wireless technologies are WiFi (or IEEE 802.11) [Hyn12], cellular technologies as GSM/GPRS [Chu10] and mainly ZigBee (or IEEE 802.15.4) [Wei08][Pop09][Min10][Chu10][Hyn12]. One of the main goals in vehicle-to-infrastructure communications is the security and the avoidance of traffic accidents [Wei08][Hua08][Foi09][Shi10] but the number of applications is wide, and there are very interesting applications as the management of charging systems for electric cars [Lem11] and CO2 monitoring [Shu09], also mainly based on ZigBee wireless communication.

Another interesting field of these kinds of communications is the so called inter-vehicular communications (IVC), which can interact with the previously mentioned vehicle-to-infrastructure networks to improve the performance and capabilities of the system. Nowadays the main wireless technology used for that is ZigBee, usually combined with others, as IEEE 802.11 standards, GSM or GPS [Eam08][Guo11]. This issue has been treated in the literature since several years ago, with the design of antennas and systems for car communications [Aus98][Gsc03], as well as other related aspects such as the improvement of the communication security and protocol [Hai06][Lee09].

Finally, there are intra-vehicle communications, in which the complete communication process takes place among devices placed on or inside a single car or vehicle. In the literature there are wired solutions to provide a communication inside a car, mainly based in power line communications (PLC) [Nou09]. But since the minimization of weight became an important issue in order to gain capabilities and reduce fuel consumption, there has been an increasing interest on using wireless communication systems [Ahm07][Nou08]. Besides, as stated previously, wireless technologies provide easier and cheaper system deployment and maintenance. The wireless channel for intra-vehicle communications has been studied previously for different frequencies [Mog09][Rao12], and hybrid solutions have been also proposed in order to reduce free space propagation losses [Fuj10].

In this work, wireless intra-car communications are analyzed, focusing on WSNs. Several wireless technologies or frequency bands have been used for the implementation of intra-car WSNs, as RFID [Ton07], 60 GHz band [Saw09] or ultra wideband (UWB) [Yon12]. But due to the complex characteristics of the environment and the requirements of the applications (low cost, low energy consumption, low data rate and energy supply by batteries), the most widely used technology is ZigBee, based on IEEE 802.15.4, which fulfills the typical requirements. The range of applications in which ZigBee is used for intra-car communications is wide, e.g. tire safety detecting systems [Wan10], CO<sub>2</sub> monitoring [Guo11], safety [Jiu11], noise reduction [Mie11], vehicle identification and driver authentication [Dis08] and multimedia applications for environmental control [Bur07]. It is important to note that the increasing number of portable electronic devices and wireless systems (e.g. laptops, smartphones) could interfere with those ZigBee WSNs, as they operate in the 2.4 GHz ISM (Industrial, Scientific and Medical) band [Hsi07][deF09].

The emerging interest on intra-car applications leads to an increasing number of deployed wireless sensors inside cars. Therefore, taking into account that a car is a highly complex environment where strong degradation effects due to multipath components and phenomena like reflection, refraction and diffraction are present, the radio channel

requires an in-depth radio propagation analysis. Different simulation methods can be found in the literature to obtain propagation estimations and characterization of the radio channel for intra-car communications. Typically, statistical characterization of the radio channel has been obtained performing measurements within the car [Bel09][Tsu09][Bas13]. There are other channel modeling simulation methods as the system simulator for Tire Pressure Monitoring System (TPMS) [Hua12] and the ones based on the channel model specified in the IEEE 802.15.3a indoor model for UWB [Lei10]. All these methods usually define a simple and not highly accurate radio channel.

Deterministic simulation methods (Finite Difference Time Domain (FDTD) method and the Method of Moments (MoM)) have been also used for intra-car environments, improving strongly the accuracy and precision of the simulation results, thus obtaining reliable estimations of the propagation. But due to the high computational cost, they have been used for modeling specific systems, as the performance of tire pressure monitoring system [Son06]. But for the simulation of a complex intra-vehicular environment, they can be highly time-consuming due to the high computational cost. As we already know, there are also the deterministic ray tracing and ray launching methods offering a reasonable trade-off between precision and required calculation time, which have been also used in car environments with the aim of parameterization of cars as scattering centers for car-to-car or car-to-infrastructure communications [Bud12].

In the following study, an in-depth propagation study for ZigBee motes operating at ISM 2.4 GHz band inside a common commercial car is presented, emulating an operating WSN. The simulation of the radio propagation within the car has been carried out by means of the in-house 3D Ray Launching method, which is a novel method for analyzing the radio channel inside cars, and which has been already used for the modeling of a UHF-RFID system in a van [Azp12]. Power distribution planes and consumption planes inside the car are presented as radio propagation results. Also time domain results are presented, as Power Delay Profiles and delay spread.

Finally, in order to validate all the simulation results presented

throughout the paper, a test-bed with a real car has been set, in which received power measurements have been performed to compare them with the simulation results. System measurements have been also performed in order to analyze the link quality inside a car. The PER (Packet Error Rate) is the parameter that has been measured for that analysis.

In this study, a car model based on the real dimensions (4.57m x 1.6m x 1.46m) of the 406 model of the brand Peugeot has been implemented in the 3D Ray Launching software for the simulations (see Figure 3.30). The simulation tool has the limitation of representing shapes by parallelepipeds, but on the other hand, the constitutive materials of the different parts of the scenario, as dashboard, seats, windows, engine and the car body have been accurately defined, taking into account their real size and dielectric characteristics. Besides the material characterization of the objects within the scenario, the parameters that are set in the simulator (antenna type, transmitted power, radiation pattern, cuboids size, etc.) are determinant in order to calculate accurate results of the radio propagation due to the phenomena associated to it (i.e. diffraction, refraction and reflection).

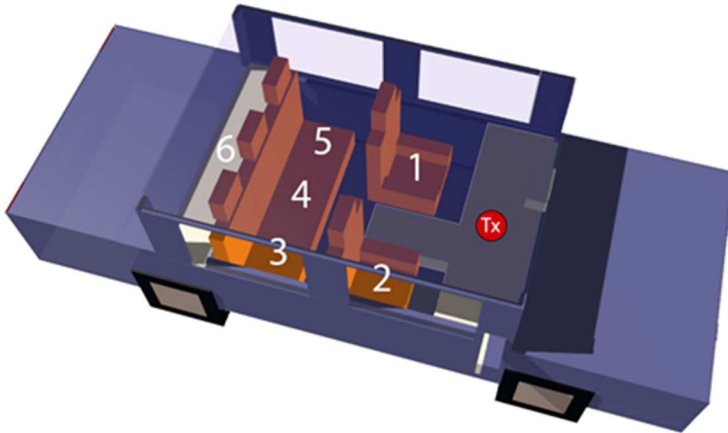


**Figure 3.30.** 3D Ray Launching car model for the Peugeot 406.

For all the simulations, an antenna has been placed inside the car, just over the dashboard (red dot in Figure 3.30), considering that position a place where a real device could be situated. This transmitting antenna has been configured as a dipole, transmitting 18 dBm at 2.41 GHz, as they are the characteristics of the real device used for subsequent measurements. Table 3.3 shows a summary of the parameters set for the simulations.

Parameter	Value
Frequency	2.41 GHz
Transmitted power	18 dBm
Antenna type	Dipole
Launching angle resolution	1°
Maximum permitted reflections	5
Cuboids resolution	5cm × 5cm × 5cm

**Table 3.3.** Parameters for the simulation of the car model.

In order to show the obtained simulation results, two different cutting planes have been set at different heights (1 and 1.2 meters), as can be seen in Figure 3.31. The plane at height 1 meter corresponds to the height where the transmitter is placed at and the 1.2-meter-height plane corresponds approximately to the height of the head of a person sitting in the car.

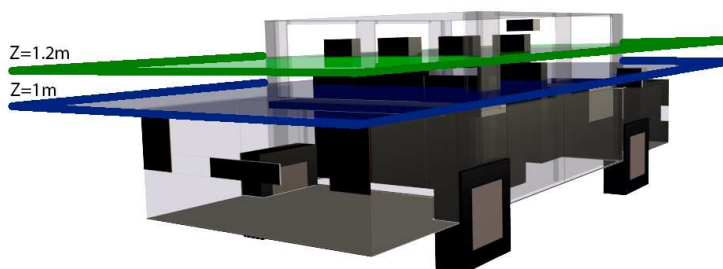


**Figure 3.31.** Representation of the two cutting planes for which the simulation results are shown.



The following simulation results show the RF power distribution planes and the energy consumption planes for the two different heights represented in Figure 3.31. First, the distribution of the estimated RF power distribution is presented in Figure 3.32. The radiating element, which represents a wireless ZigBee mote placed on the dashboard, is depicted by a black circle in the 1meter-height plane (the same place as the transmitter in Figure 3.30).

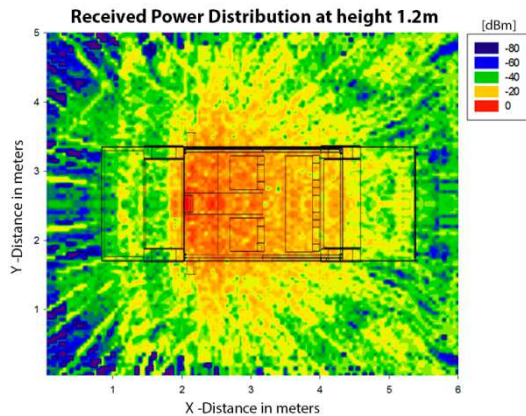
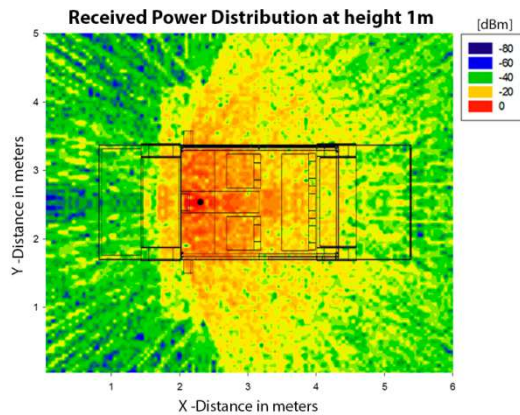


**Figure 3.32.** Estimation of RF power distribution for different cutting planes at different heights: (a) 1 m, and (b) 1.2 m.

As expected, the highest power values can be found for the plane at height of 1 meter (Figure 3.32a), since it is the height where the transmitter is placed. The influence that obstacles (like seats and dashboard) have on the radio propagation inside the car can be also appreciated, as they absorb and reflect part of the emitted power, creating behind them zones which receive lower power levels. The metallic body of the car makes most of the power remain inside the car due to the reflective properties of metals, but a significant amount of energy leaks through the windows. Low received power zones can be also found in the engine area, as well as the car trunk area, also due to the metallic parts of the car. There are also some points within the car where the received power level is low, which can be generated due to the multipath propagation. In order to show better these phenomena, received power versus linear distance graphs are shown in Figure 3.33. Specifically, those corresponding to a line that passes through the center of the car for 3 different heights are represented. The mentioned line can be seen in the inset (top right of the picture). The represented heights correspond to the planes shown in Figure 3.31 (1m and 1.2m) and the 0.7m height corresponds to the height where the measurements have been taken, i.e. on the seats, as later is shown.

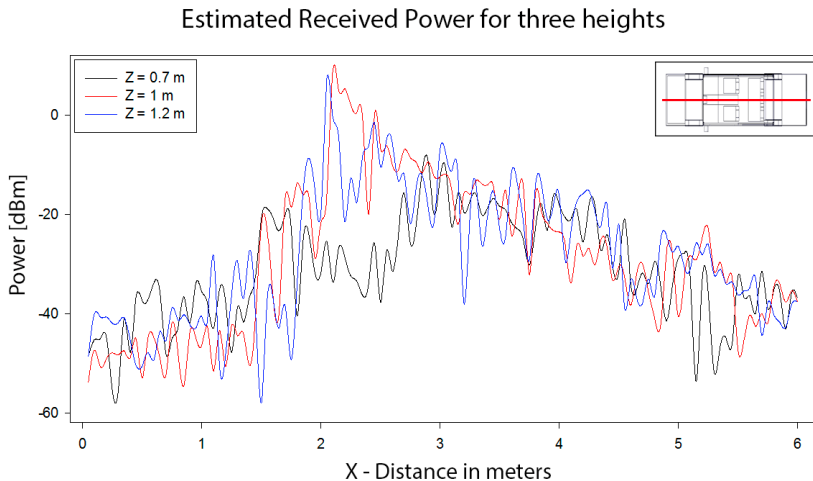
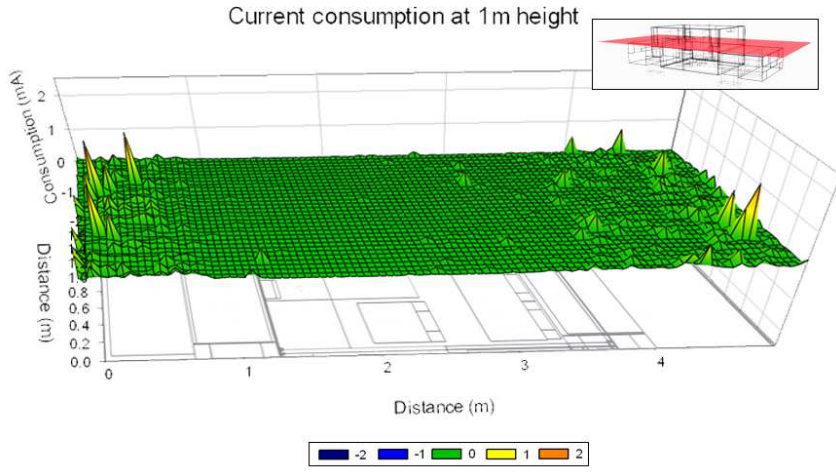


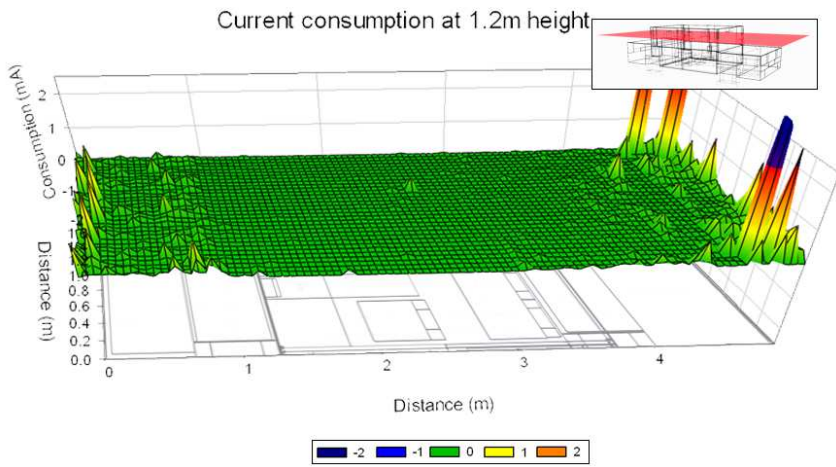
**Figure 3.33.** Received RF power versus linear distance for different heights of the central linear path (see inset).

The results depicted in Figure 3.33 show a noteworthy received signal variation, as it is expected for an indoor environment due to the occurring electromagnetic phenomena such as fast fading, which occurs due to multipath components. In this case, those multipath components appear especially due to the high reflectivity (great amount of metallic content) and diffraction (many obstacles). The distance dependence is also visible, as the received power level decreases as the distance from the antenna increases. Furthermore, comparing the 3 linear graphs at different heights, lower power level is visible at height 0.7 meters, particularly in the central area of the car and behind the position of the transmitter. It is mainly due to the absorption caused by the dashboard.

As can be seen in the estimations of received power level (Figure 3.32 and Figure 3.33), both topology and morphology affect the expected value, which depends on the location within the scenario. This variability of the received power value impacts directly on the deployment of wireless nodes within the car, as the coverage radius could be affected. Thus, the link balance also varies, modifying the required current consumption for the transceiver to operate. In Figure 3.34 an estimation of the extra current consumption that the transmitting transceiver will suffer as a function of receiver mote location is shown. The same link balance has been maintained between the transmitter and each point within the scenario in order to calculate the required extra transmitted power. This value will depend mainly on the received power in each point. The calculated increase on the transmitted power leads to the increase of the transmitter current consumption, which is what is shown in Figure 3.34. The two current consumption maps depicted correspond to the received power planes shown in Figure 3.32, but only the part that covers the car is shown (the schematic below the graph shows the upper cut of the car). In general, the current consumption within the car does not increase significantly and is not strongly dependent on the location, as usually happens in other bigger scenarios [Gil15]. That is because enough signal level reaches almost all points within the car due to the short distances and the great number of reflections.



(a)



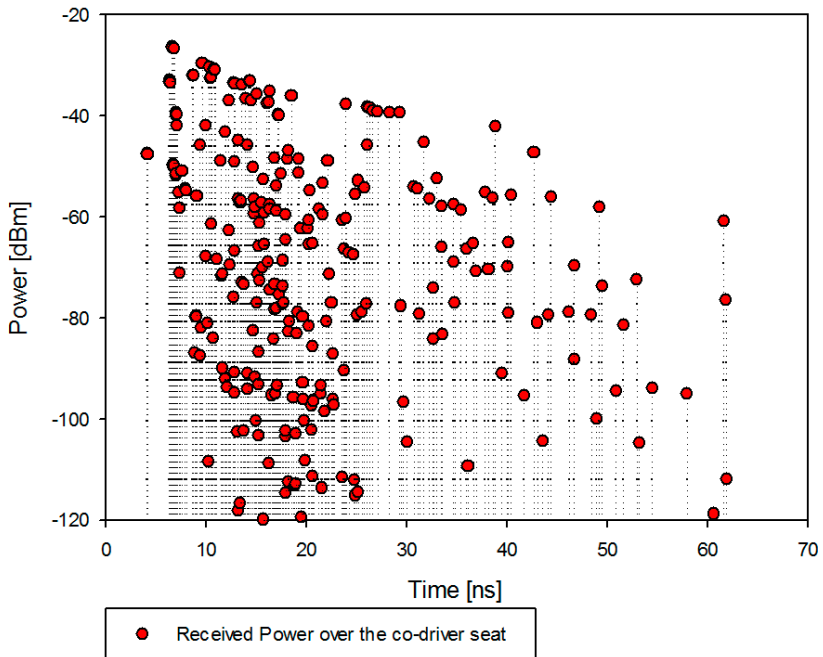
(b)

**Figure 3.34.** Estimated extra current consumption vs. position for different cutting planes at different heights: (a) 1 m, and (b) 1.2 m.

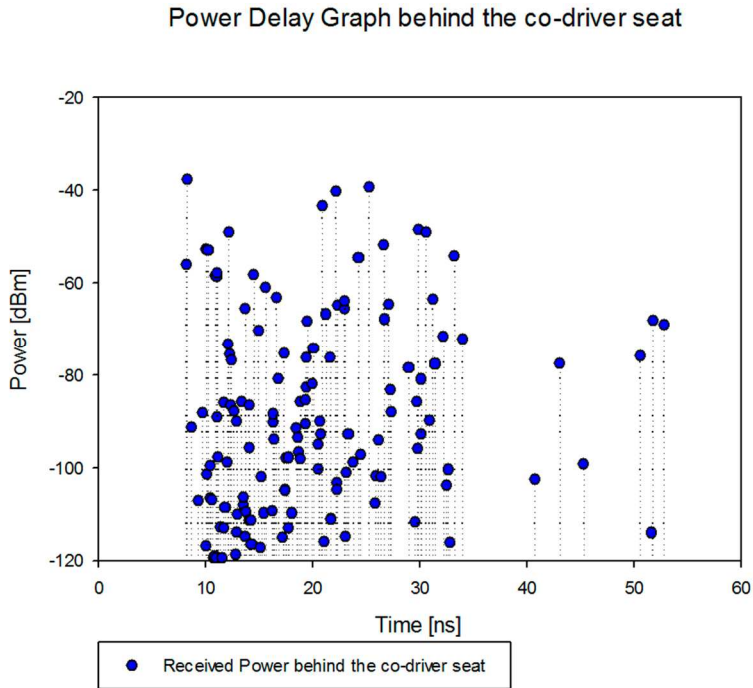
Due to the expected big impact of the multipath propagation inside the car, a more detailed analysis of such phenomenon is presented, since it is a key issue in the study of radio propagation in this kind of scenarios. As previously said, the scenario is a highly reflective environment where a high amount of reflections are produced due to

the metallic parts of the car body. This reflection quantity increases the probability that rays have of crossing the same observation point. In order to analyze this phenomenon, Power Delay estimations obtained by the 3D Ray Launching algorithm are presented in this section. A Power Delay profile shows the power level and arrival time of each ray that crosses a single point (cuboid) in the scenario. In Figure 3.35 two Power Delay profiles for two different points can be seen. These two points have been chosen to show the differences that can be found in the same scenario due to the effect that obstacles (e.g. seats) have in the radio propagation. The red dotted profile (Figure 3.35a) represents a point situated on the co-driver seat, which receives a lot of rays with a high power level. On the other hand, blue dotted graph (Figure 3.35b) represents the Power Delay for a point situated behind the co-driver seat, which receives less multipath components and with lower power level.

Power Delay Graph over the co-driver seat



(a)



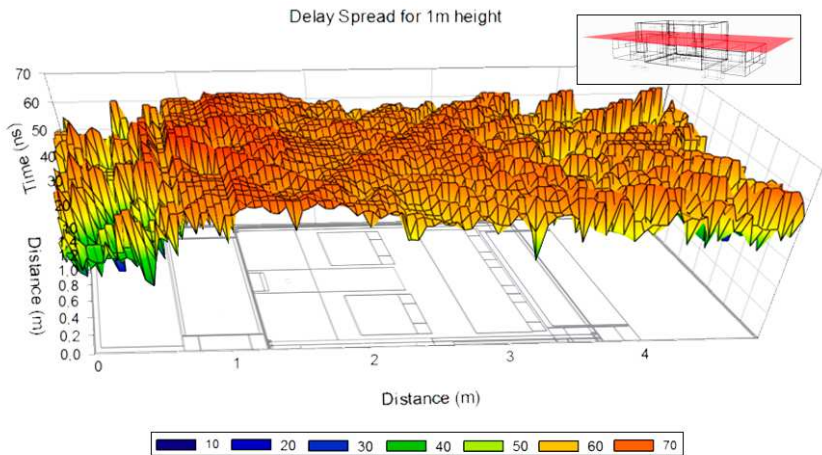
(b)

**Figure 3.35.** Power Delay comparison between two different points within the car, (a) on the co-driver seat and (b) behind the co-driver seat.

As can be seen in Figure 3.35, the point situated on the seat receives significantly higher amount of rays and with higher power level than the point situated behind the seat. This result is expected because the point behind the seat is crossed by fewer rays as the driver and co-driver seats themselves behave as absorptive objects. Therefore, a considerable amount of emitted energy is lost, decreasing the number of rays which can reach the point behind the seats. Despite this, the number of rays reaching the point behind the seat is also high due to the general reflective characteristic of this kind of scenarios.

In order to have a better understanding of the global performance of the multipath propagation inside the car, in Figure 3.36 Delay Spread graphs are depicted for the same 2 different height planes used so far (1m and 1.2m). The Delay Spread is the elapsed time between the

arrival of the first and the last ray, for a single defined cuboid in the scenario. Thus, the strong dependence between the observation point and received multipath components given by the complex morphology of the car environment can be clearly seen. Specifically, in these graphs, the effect that the metallic car body has can be observed, since the Delay Spread values within the car body are much higher than the values just outside, due to the reflections caused by the metallic elements, which make the signal remain inside. The noticeable difference between two heights is also expected, since at 1 meter, apart that it is the height in which the transmitter antenna has been placed and hence the number of reflections will be higher due to the higher power level of the rays, there are more obstacles and metallic elements producing reflections and diffraction than at 1.2 meter height. So some rays will be received later than at height 1.2m, where a significant amount of power (i.e. rays) will be lost through the windows.



(a)



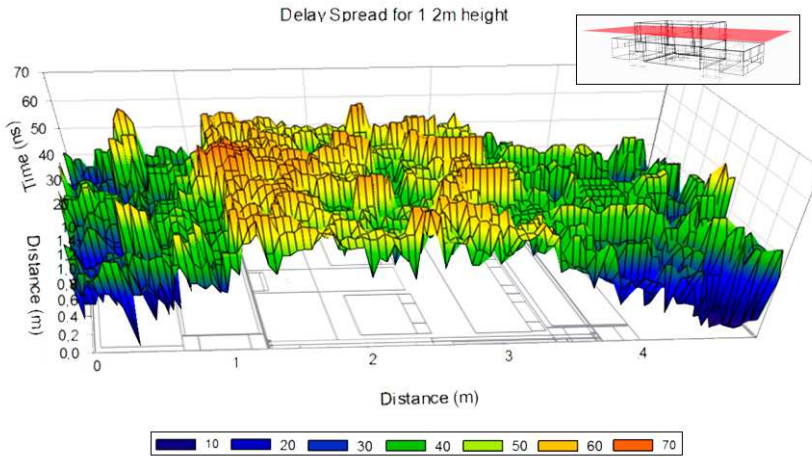


**Figure 3.36.** Estimated Delay Spread for different cutting planes at different heights: (a) 1 m, and (b) 1.2 m.

As in previous sections of this work, an experimental setup has been set with the aim of validating the simulation results obtained in the car. The scenario where the measurements have been performed is presented in Figure 3.37. It is located in one of the car parks at the Public University of Navarre. The car is a Peugeot 406, i.e. the model in which the 3D Ray Launching car model is based. All the measurements presented in this section have been taken without persons inside the car, with the engine off and taking maximum care to have car-free surroundings in order to avoid possible interferences due to reflections from objects around the car. As said, ZigBee technology has been chosen for emulating a WSN. Specifically, the wireless devices used for the measurements have been the XBee Pro motes from Digi International Inc, shown in Figure 3.38. These wireless communication devices operate in the unlicensed ISM 2.4 GHz band and the whip antenna mounted on it has an omnidirectional diagram with an average gain of 1.5 dBi, which has been taken into account to calibrate the measured values. For transmitting and processing received data, the motes have been connected to a PC via USB cable after being plugged into an XBee explorer unit.





**Figure 3.37.** The scenario where the measurements have been taken. Notice that there is not any other vehicle or obstacle near the car.



**Figure 3.38.** The ZigBee mote used for ZigBee wireless communications inside the car.

Two different measurement campaigns have been carried out. In first place, the radio propagation inside the car has been characterized setting a transmitting ZigBee mote on the dashboard, at the point indicated in Figure 3.30. Then, the points numbered from 1 to 6 in the same figure indicate the measurement points (seats and the tray on the back side of the car), where the received power level has been measured by means of a N9912 Field Fox spectrum analyzer of Agilent. The omnidirectional antenna coupled to the analyzer operates at ISM 2.4 GHz band and has a gain of 5 dBi. The parameters of the transmitting ZigBee mote can be seen in Table 3.4.

Parameter	Value
Frequency	2.41 GHz (ZigBee channel 12)
Transmitted power	18 dBm (max. default value)
Antenna type	Monopole
Measurement time	5 minutes

**Table 3.4.** Configuration of the parameters of the XBee Pro wireless devices to measure the received power level inside the car.

The obtained received power measurements in the mentioned measurement points can be seen in Figure 3.39. The 3D Ray Launching simulation results are also shown, for an easier comparison with the measurements. It can be clearly seen that a very good agreement between the simulation results and the measurements has been obtained. The resulting error mean for those measurement points is 0.08 dBm, a very low error that indicates that the proposed in-house 3D Ray Launching simulation method works properly, validating the simulation results obtained and shown in this work for this kind of scenario.

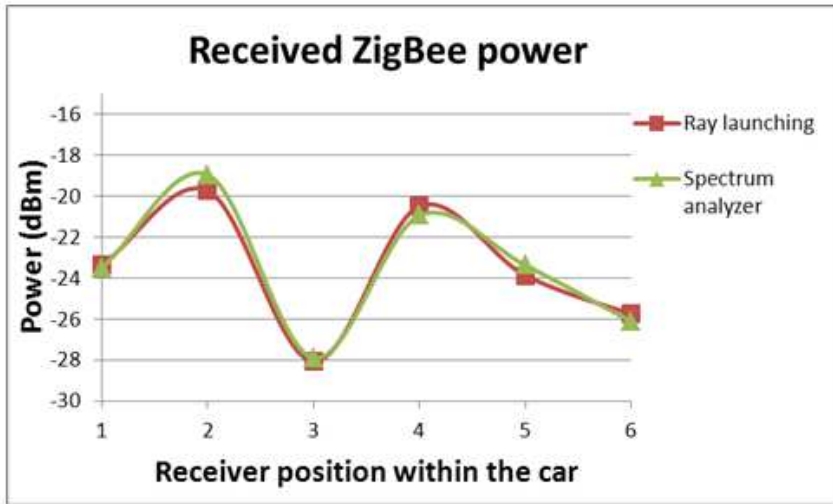


**Figure 3.39.** Received power measurements and simulation results within the car for the positions shown in Figure 3.30.

Once the received power level for different positions within the car has been measured and the simulation method has been validated, the second measurement campaign has been performed. The aim of these new measurements is to deepen the analysis of the radio propagation in a highly complex indoor environment such as the car. For that purpose, the quality of the ZigBee channel has been measured. Specifically, the value of PER (Packet Error Rate) has been used as quality parameter, which indicates the percentage of transmitted packets that has been lost and do not reach properly the receiver. The position of the transmitter and the measurement points have been the same as in the first measurement campaign. But in this case, instead of the spectrum analyzer, another XBee Pro mote has been placed on the measurement points in order to create ZigBee radio links. Table 3.5 shows the configuration of the wireless mote's parameters used for measuring the PER. Notice that ACK options have been disabled to avoid packet retransmissions and the transmitted power level has been reduced to the minimum default value in order to analyze the worst case, in which the lost packet quantity will be the highest. It is worth

noting that 10 dBm is the lowest transmitted power level for these particular devices, but it is the highest transmitted power allowed by European legislation for this kind of wireless communications at 2.4 GHz ISM band. The PER value has been calculated transmitting 100,000 packets. Two in-house developed applications based on Java, one for the transmitter and the other for the receiver, have been used in order to configure easily the parameters shown in Table 3.5, as well as to calculate the PER by reading the sequence number of the received packets.

Parameter	Value
Frequency	2.41 GHz (ZigBee channel 12)
Transmitted power	10 dBm (min. default value)
Transmitted packets	100,000

**Table 3.5.** Configuration of the parameters of the XBee Pro wireless devices to measure the ZigBee radio link quality inside the car.

The measured values of PER are shown in Figure 3.40. As can be seen, the values are very low, so the number of lost packets is very low too. This is as expected, since although the environment is very complex with a high number of multipath components, the size of the scenario is very small and the received power level within the car is enough to have a good channel quality. It is worth noting that the PER depends strongly on the received power level (but not exclusively), as can be seen in the measurement point 3, where in Figure 3.39 receives the lowest power level and in Figure 3.40 has the highest PER value. So, taking into account that the measured PER results have been obtained with the ACK option disabled, it can be concluded that no channel quality problems in terms of packet losses would be within this kind of scenarios. Furthermore, PER could be improved activating ACK options.

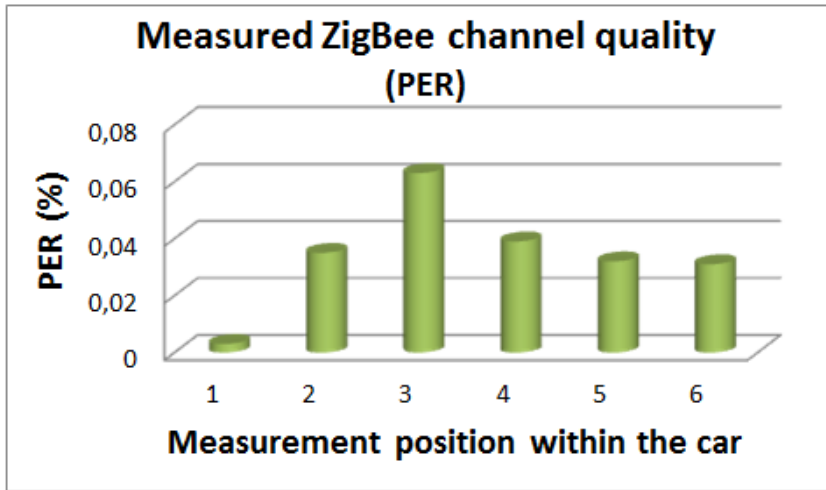


**Figure 3.40.** ZigBee wireless channel quality measurements within the car for the configuration shown in Figure 3.30.

Summarizing, the characterization of ZigBee wireless propagation inside a car has been analyzed by means of the in-house developed 3D Ray Launching simulations and measurements. Inherently, cars are complex indoor scenarios due to the small size, the large amount of metallic elements that can be found (mainly the bodywork) and the high density of obstacles. The high percentage of occupied space due to the great number of obstacles generates phenomena as absorption as well as diffraction. The metallic elements within the car, especially the bodywork, makes the environment highly reflective, generating great number of multipath components, as can be seen in Power Delay Profiles and Delay Spread results.

Although the received power level is high enough to assure good channel quality in most points within the car, as shown in current consumption estimations as well as in PER measurements (note that ACK option was disabled), the great number of multipath components generates points within the car where the received power is lower. Therefore, there are points where the PER could be significantly higher, especially taking into account that the highest power level permitted by

the ZigBee nodes has been used in this study.

The low error between the simulation results and measurements (0.08 dBm) validates the deterministic 3D Ray Launching technique used in this work, making it adequate for radio planning analysis with the aim of deploying ZigBee-based WSNs within common cars. Results also show that ZigBee is a viable technology for successfully deploying intra-car wireless sensor networks.

Once the intra-car environment has been analyzed, now a bigger and more complex intra-vehicle scenario is presented: a train's passenger wagon, which is an interesting scenario since high-speed trains are developing rapidly with the growing demand for fast and safe transportation, leading to an increase in the number of users of this type of transportation. In addition, mobile services have experienced a tremendous growth, from traditional voice services, to mobile office and interactive services, such as online gaming or social networking. In the near future, railway systems will be integrated within the framework of Smart Cities, to achieve a safe, accurate and efficient transportation system.

Traditionally, railway communications have relied on mobile networks, such as PLMN based on GSM/UMTS networks [Web94][Abr00], or more specifically for the railway sector, GSM-R system to provide narrow band service, usually relying on base stations deployed in the vicinity of the railroad tracks. However, in the new high-speed trains, due to their design, larger penetration losses occur. Hence, an additional node should be introduced and the assessment of the signal propagation between the base station to the node (outdoor part) and node to terminal (indoor part) are needed. On-board networks implemented in trains integrating both the control and the entertainment information using the Ethernet protocol have been analyzed and results have shown that such a shared infrastructure is a practical solution while guaranteeing correct performance [Azi08][Has08][Cla11]. Moreover, with the increased demand for railway services, wireless sensor networks are widely used in this sector, for multiple functions, such as the control of railway tracks and

irregularities, the detection of abandoned objects in railway stations or secure railway operations [Sha07][Gao11][Fla10][Gru09].

With the aim of enhancing the performance of these applications, the assessment of radio wave propagation within the indoor environment of a train wagon is compulsory. Different simulation methods can be found in the literature to obtain propagation estimations and characterization of the radio channel for intra-vehicle communications. Typically, statistical characterization of the radio channel has been obtained performing measurements within vehicles, such as the previously mentioned works for intra-car environments [Bel09][Tsu09]. Besides, the statistical characterization has been also made for a commercial aircraft cabin [Dia04][Mat08][Mor08][Skr11] and trains [Don10]. Again, we know that these methods usually define a simple and not highly accurate radio channel, with low computational cost but limited accuracy. And in order to improve strongly the accuracy of the estimated values, a deterministic method such as the presented 3D Ray Launching algorithm is required, which in addition to the accurate results, the computational cost will be much lower than that offered by the common deterministic methods.

Following, an in-depth propagation study within a railway wagon train is presented, emulating an operating Wireless Sensor Network (WSN). This is an important task due to the occurrence of significant multipath propagation in this type of environments because of the major metallic mass of the vehicles. In [Sal14], a proposal of communication architecture to provide ubiquitous connectivity needed to enhance the smart train concept is presented. It combines an intra-wagon communication system based on nomadic devices connected through a Bluetooth Piconet Network with a highly innovative train-to-ground communication system. The difference with the work presented here is that the following study is focused in the intra-wagon communication, showing an in-depth analysis of the electromagnetic waves behavior which is necessary before the deployment of a WSN within the train. Specifically, this work pursues characterizing the effect of radio propagation phenomena in on-board transceivers in order to assess the impact of the morphology of the train as well as the topology

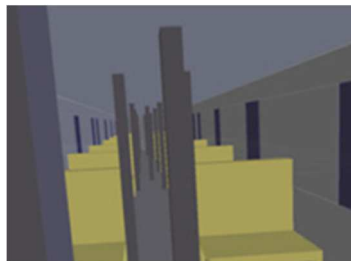
of the wireless system, in order to optimize system performance. The appropriate election of the emplacement of the devices, the RF frequency to use and the optimal selection of the topology of the WSN may provide better results on communication efficiency, reduce interference and therefore minimize the energy consumption of the nodes.

The simulation scenario that has been implemented corresponds to the interior of a real passenger wagon, built for railway operator Euskotren by the company CAF. A view of the wagon under consideration can be seen in Figure 3.41a and the wagon model developed for the simulation with the 3D Ray Launching code is depicted in Figure 3.41b. Figure 3.41c shows the schematic view of the whole indoor wagon train implemented for simulation (ceiling and a side wall have not been shown for a better illustration of the inside).

For the radio propagation study within the scenario, a transmitting antenna has been placed at coordinates  $(X=3\text{m}, Y=1.24\text{m}, Z=1.1\text{m})$ , which correspond to the point with the text 'TX' in Figure 3.41c. The frequencies under analysis have been 2.43GHz and 868MHz, since they fall into the most common frequency bands used for the deployment of WSN within indoor environments. The created wagon model was furnished with metallic floors and walls, and rows of seats with a polycarbonate base. The material parameters (as given by the train manufacturer) used in the model are defined in Table 3.6, where both operating frequencies have been taken into account. The simulation parameters are shown in Table 3.7. The cuboids resolution and the number of reflections have been set to 10cm and 5 respectively, in order to balance accuracy and simulation time.

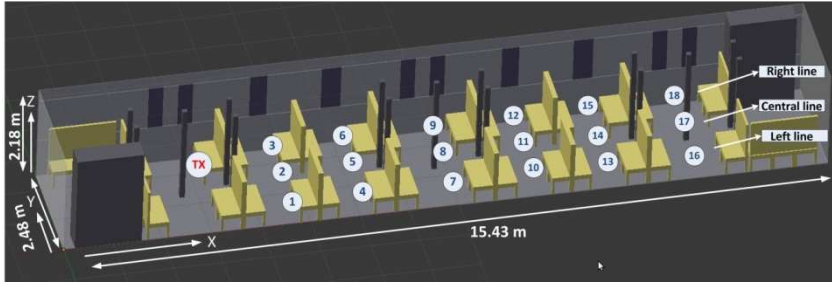


(a)



(b)





(c)

**Figure 3.41.** (a) Real passenger wagon, (b) 3D Ray Launching simulation scenario, (c) Schematic view of the whole indoor wagon train.

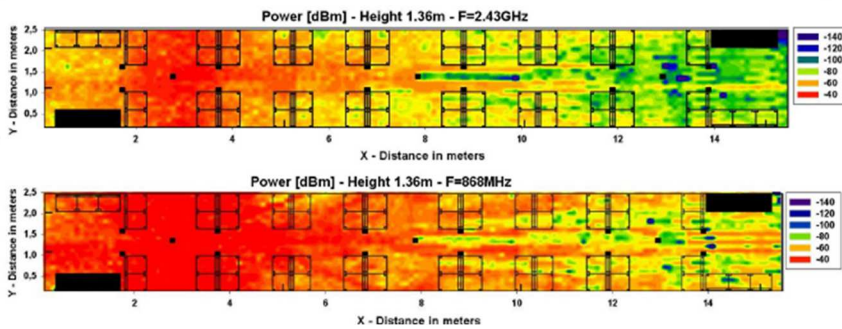
Material	Permittivity ( $\epsilon_r$ )		Conductivity ( $\sigma$ ) [S/m]	
	868 MHz	2.4 GHz	868 MHz	2.4 GHz
Air	1	1	0	0
Polycarbonate	3.2	3	0.2	0.2
Glass	5.5	6.06	$10^{-12}$	$10^{-12}$
Aluminum	4	4.5	$4 \times 10^{-7}$	$4 \times 10^{-7}$

**Table 3.6.** Electromagnetic properties of the main materials used in the wagon model.

Parameter	Value
Frequency	2.43 GHz 868 MHz
Vertical and Horizontal angular resolution	$1^\circ$
Transmitted Power	-10 dBm
Cuboids size	10cm $\times$ 10cm $\times$ 10cm
Permitted reflections	5

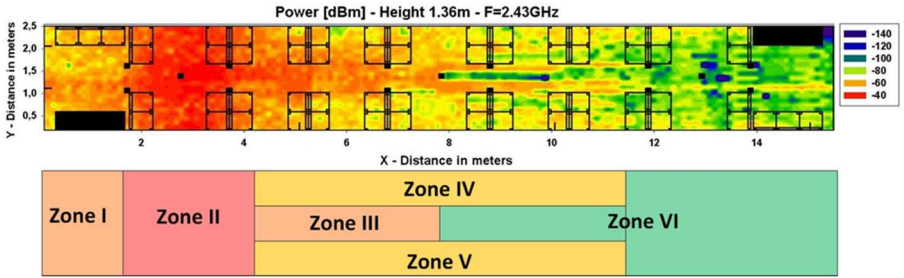
**Table 3.7.** Parameters for the 3D Ray Launching simulations.

Figure 3.42 shows the received power simulation results obtained by means of the 3D Ray Launching algorithm for the received power for both frequencies. The figure represents a 2-D longitudinal cut plane at 1.36 meters height, although simulation results have been obtained for the whole volume of the scenario. In both figures how the spatial distribution of power is strongly dependent on the observation point can be seen, which stresses the strong influence of the morphology of the scenario under analysis. Elements such as passenger seats produce power absorption as well as scattering, leading to increased losses. It can be also seen that the use of a lower frequency band (868MHz) leads to less propagation losses, as expected.



**Figure 3.42.** Received power distribution within the wagon train at 1.36 meters height for frequencies 2.43GHz and 868MHz.

In order to gain insight into the influence that the morphology of the scenario has in radio wave propagation, Figure 3.43 shows different zones, delimited by the estimated mean received power, for 2.43GHz frequency. It can be seen that the values of the mean received power depend strongly on the morphology of the wagon train and the position of the transmitter itself. In Table 3.8 the mean power with the standard deviation of each zone are shown. In addition, the obstacle density of the zones is also given. It is observed that the obstacle density has a great influence on the received power, but the size of the area for a specific zone has to be taken into account, as can be seen if zone I and zone VI are compared.



**Figure 3.43.** Estimated received power divided by zones for 1.36 meters height at 2.43GHz frequency.

Zone	Area (m <sup>2</sup> )	Mean Power (dBm)	Standard deviation (dB)	Obstacles Density (%)
I	4.712	-61.51	7.89	14.4
II	5.456	-46.33	2.54	0.54
III	2.280	-57.88	3.08	1.75
IV	6.480	-69.62	1.98	4.32
V	6.480	-68.94	1.97	4.32
VI	12.31	-82.51	6.26	10.19

**Table 3.8.** Simulation results divided by zones.

From these results, it is deduced that received power in different points of this kind of scenarios depends greatly on the position of the transmitter, the obstacle density of the different zones and the different material properties of the obstacles. All these issues are taken into account by the 3D Ray Launching simulation tool, which provides accurate results for such environments where the multipath propagation has a great impact on the RF power distribution. In order to illustrate the impact of the multipath propagation within the scenario under analysis, the Power Delay Profile at a central location ( $X=6.3\text{m}$ ,  $Y=1.38\text{m}$ ,  $Z=1.1\text{m}$ ) has been obtained and shown in Figure 3.44. As can be seen, there are a large number of echoes in the scenario

in a time span of 12 to 33 ns. But it is worth noting that many of them reach the receiver point with a power level lower than -100 dBm, which is a typical sensitivity value of motes operating at 2.4GHz band. Time dispersion varies widely in a mobile radio channel depending on the geometrical position relationships among the transmitter, the receiver and the surrounding physical environment. Due to this fact, another parameter that can grossly quantify the multipath channel is the delay spread, which shows the effects of dispersion and is depicted in Figure 3.45 for the passenger wagon environment. The delay spread has been defined as the time delay between the first and the last ray which arrives to each spatial point. It has been calculated using as threshold the noise floor, with a value of -120dBm. In addition, in Figure 3.45 two Power Delay Profiles are shown as an example, where the difference effect of the multipath propagation on different zones of the wagon can be clearly seen. In this specific case, multipath propagation has a greater impact in the surroundings of the transmitter antenna due to the morphology of the scenario and the distribution of the obstacles.

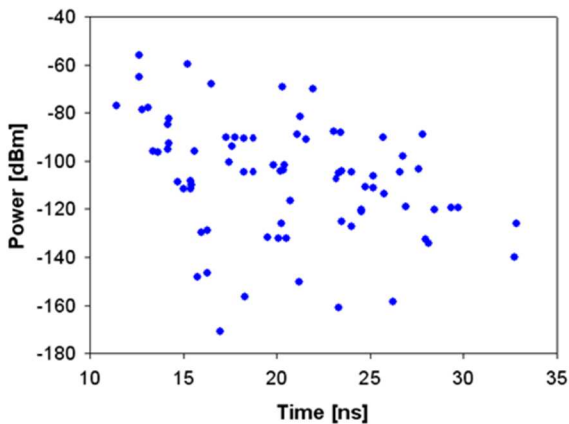


**Figure 3.44.** Power Delay Profile at a given cuboid, located at the center of the wagon (X=6.3m, Y=1.38m, Z=1.1m) for 2.43GHz frequency.

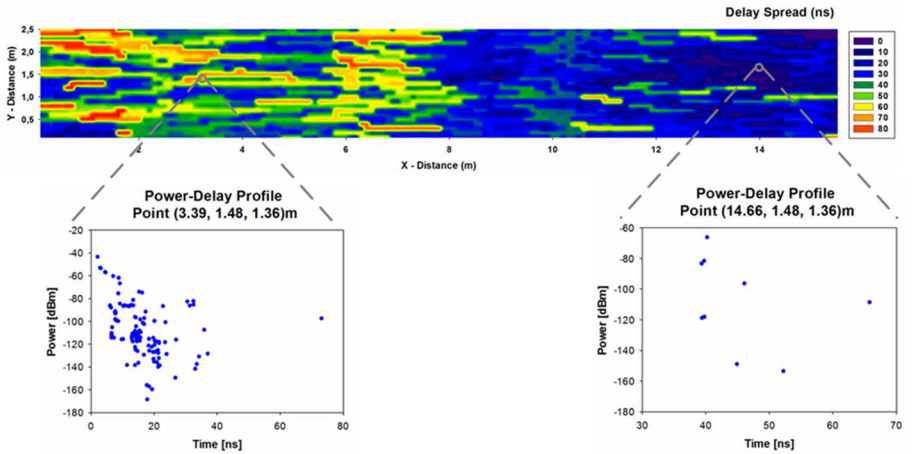
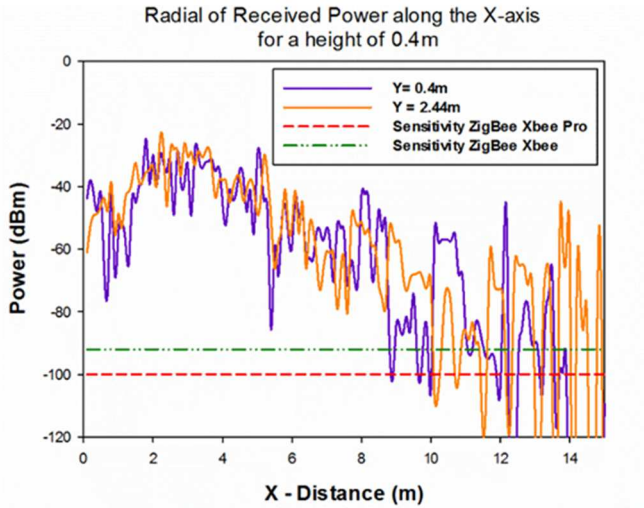


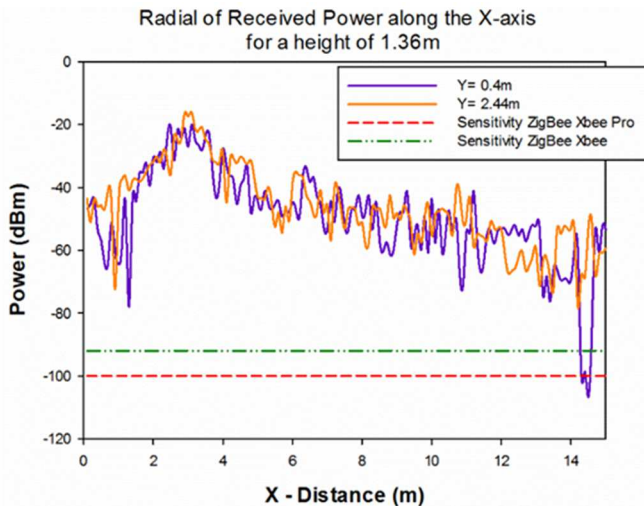
**Figure 3.45.** Delay Spread estimation within the train wagon at 1.36 meters height for 2.43GHz frequency. The Power Delay Profiles at two particular spatial samples are also shown.

In order to assess the deployment of WSNs in this complex indoor environment, the potential deployment of two different wireless communication modules have been studied. Specifically, ZigBee-based technology has been evaluated again by means of XBee Pro and XBee motes from Digi International. The differences between them are mainly the sensitivity and the larger transmitted power of the XBee Pro. For this study, the considered transmitted power level has been set to the minimum default value of the XBee Pro (i.e. 10dBm), which also is the maximum default value of the XBee motes. Besides, this is the maximum power level allowed for this kind of narrow band communications in Europe at ISM 2.4GHz band. Figure 3.46 shows the linear distributions of received power (called ‘Radials’) along the X-axis for two different values of Y-axis. Figure 3.46a shows the results for a height of 0.4m and Figure 3.46b for a height of 1.36m. Additionally, the sensitivity of the XBee Pro (-100dBm) and XBee (-92dBm) modules is represented by a dashed red line and a green dashed line respectively. It can be seen that there are some points where the received power falls below the sensitivity level, which means that there are locations within the wagon where the communications between these motes will not be

possible. These results show that a radio planning is mandatory if ZigBee-based communication systems are to be deployed within common passenger train wagons.



(a)



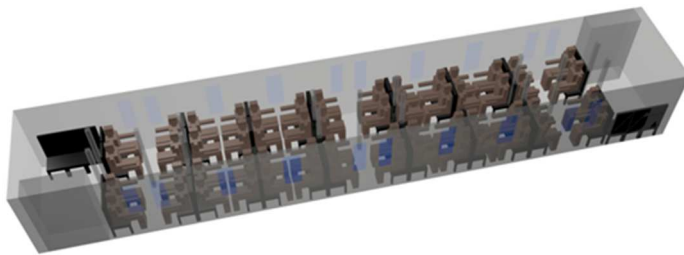
(b)

**Figure 3.46.** Comparison of received power vs. linear distance for XBee Pro and XBee modules along the X-axis: (a) 0.4m height (b) 1.36m height.

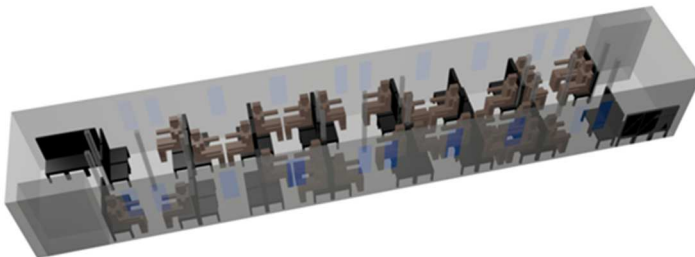
Thus far in this analysis of radio propagation within a passenger wagon, the simulations have been made without the presence of persons. But in a real scenario, the most common scenario is when people are within the wagon. Therefore, in order to characterize the radio channel more realistically, it is important to consider the impact of human beings within the train. In this regard, simulations of a walking human have been done using a phantom created with an animation software package for 2.45GHz communications [Nec10]. However, accurate results regarding the effect of a human body will require full wave simulations (e.g. by means of software such as CST Microwave Studio), but taking into account that in this case the persons are within a complex environment, an enormous computational cost would be necessary for simulating the whole scenarios. Trying to solve this issue, in [Hal12] a method that allows modeling separately propagation around the body and in the environment is proposed. The approach considers that there are three components of the average received power: power of the strongest or direct ray, average power delivered by the multipath components propagating around the body itself and the average power scattered from the objects in the environments surrounding the body. This assumes that scattering from the body and scattering from objects in the environment are independent from each other. Thus, the parameters regarding scattering of the body can be measured on a person in an anechoic environment or simulated on a human body model in isolation and the parameters with regard to the multipath propagation in the environment can be obtained by 3D Ray Launching simulation excluding the body itself. This approach greatly simplifies the calculations. Following this, in [Agu12] a human body model was created specifically for the 3D Ray Launching code used in this work, which includes the dispersive nature of materials' parameters of internal organs, skin, muscle and bones, and emulates satisfactorily the influence of human beings in RF power distribution in complete volumes of different scenarios.

Therefore, this human model has been included in the wagon scenario in order to assess the impact of the presence of human being in

this kind of scenarios. As the number of persons within the wagon is expected to have a different impact on the radio propagation, three different cases of human being occupation have been considered: 90.3%, 45.16% and 22.5%, which correspond to 56, 28 and 14 persons respectively. These three cases are represented in Figure 3.47. The comparison of path loss between these three cases and the empty wagon has been done and Table 3.9 shows the mean additional path loss for the three cases. As expected, the losses are higher when the wagon is full of people. Although the presence of people leads to additional mean path losses, the morphology of the scenario changes and hence, the multipath propagation is also affected, giving different received power patterns such as the linear path representation shown in Figure 3.48, where the comparison between the four cases for  $Y=0.6\text{m}$  (along X-axis) at a height of 1.36 meters is depicted. The graph shows how the trend of the estimated received power is the same, but there are specific points with significant differences among the cases under analysis. This proves that the presence of human being within this kind of scenarios can be a key issue to take into account for an adequate WSN deployment.

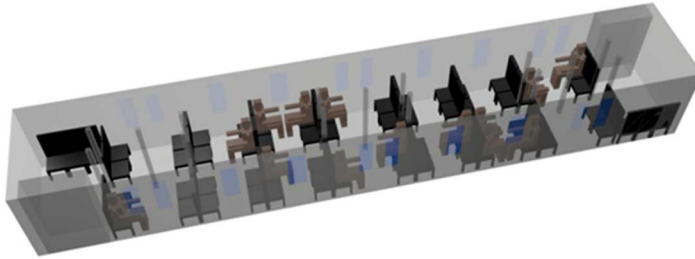


(a)



(b)





(c)

**Figure 3.47.** Different cases of human being occupation within the wagon: (a) 90.3% (b) 45.16% (c) 22.5%.

Occupation (%)	Additional Mean Path Loss (dB)	Standard Deviation (dB)
90.3	12.98	5.79
45.16	10.62	5.06
22.5	9.21	3.62

**Table 3.9.** Additional Mean Path Loss for different human being occupation within the wagon.

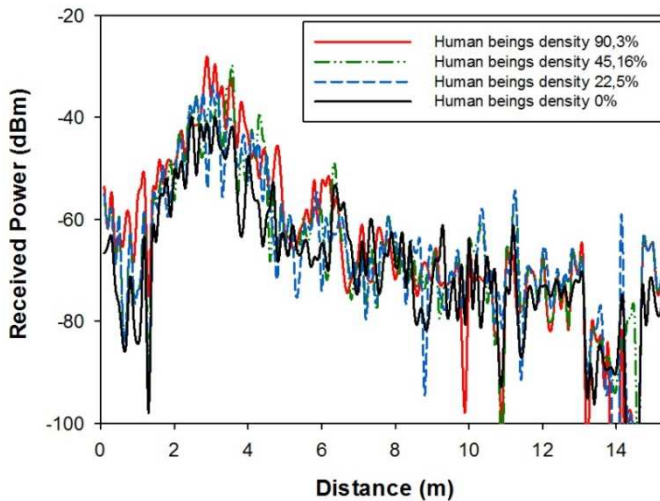


**Figure 3.48.** Estimated received power vs. linear distance along the X-axis, for  $Y=0.6\text{m}$  and  $Z=1.36\text{m}$ , for different human being presence within the wagon.

As it has been done so far in order to validate the 3D Ray Launching predictions, measurements in a real passenger wagon have been performed. For this purpose a passenger wagon of EuskoTren railroad operator from the train manufacturer CAF has been employed for the experimental set up (see Figure 3.41a). RF propagation measurements have been done within the wagon with the aid of a signal generator (Agilent N1996A), a spectrum analyzer (Agilent N9912 FieldFox), and a set of antennas for the 2.43GHz and 868MHz frequency bands (ECOM5-2400 from RS for 2.43GHz and FLEXI-SMA90-868 from RF Solutions at 868MHz, both with an omnidirectional radiation pattern, linear polarization and 5dBi gain). The transmitter antenna has been placed at the coordinates (X=3m, Y=1.24m, Z=1.1m) represented in Figure 3.41c and the transmitted power level has been set to -10dBm. Besides the transmitter location, Figure 3.41c also shows the measurement points (1.36m height) along the passenger wagon, organized in three rows. The comparison between simulation results and measurements for both frequencies of operation is shown in Figure 3.49. The obtained mean error for 2.43GHz frequency is 0.59dB with a standard deviation of 2.08dB, whereas for 868MHz the mean error is 0.99dB with a standard deviation of 1.73dB. The obtained results exhibit good agreement and validate the 3D Ray Launching simulation results for this kind of scenarios.

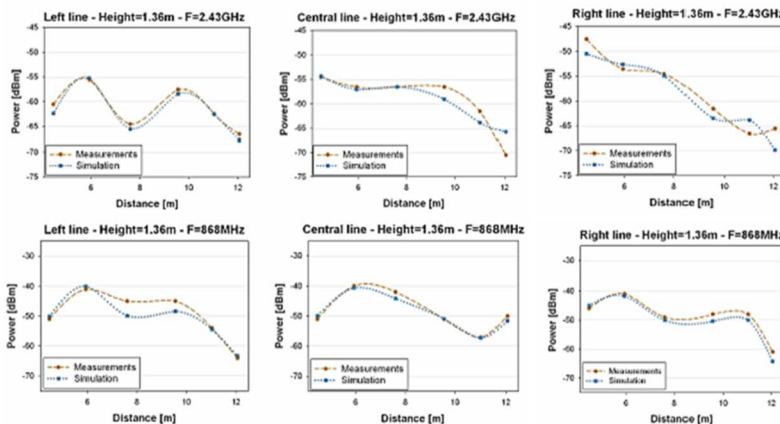


Figure 3.49. Comparison between simulations and measurements for 2.43 GHz (top) and 868 MHz (bottom) frequencies.

### 3.2.4 Sport environments

Another interesting field of application for WSNs is sport. Nowadays there are a lot of sports practiced around the world, and many of them practiced by professional athletes, sportsmen and sportswomen. Although sports have a great impact and presence in our daily life, in general there is a lack of technological application in most of them, especially regarding WSNs and the possibilities that these wireless technologies provide. With the aim of bringing WSNs closer to sport activities, the in-house 3D Ray Launching tool has been used in different sport environments in order to analyze the radio propagation and the viability of deploying WSNs within them.



\*Figure obtained from <http://tech.co>

The first sport environments under analysis have been Judo venues, which can be extended to many other sports, as they are practiced in very similar scenarios, usually small gyms. Judo venues have been chosen due to the morphological characteristics of the venues, which are similar to the typical indoor scenarios analyzed by the 3D Ray Launching tool (office and home), mainly in terms of size. Besides, Judo is one of the most popular martial arts. Originally developed in Japan in the late 19th century by Jigoro Kano, the practice of Judo has become popular all around the world. Judo became an Olympic sport in the 1964 Tokyo games, with active worldwide competitions being held under the auspices of the International Judo Federation (IJF), which is

subdivided in 5 different Judo Federations around the world. The practice of Judo has been widely adopted, not only at competition level but also as part of the physical education programs at different school levels. Judo is considered mainly a body contact sport, in which two different modalities are developed. On one hand, the technical part also known as kata, in which different techniques and movements are evaluated, and on the other hand, the combat modality, called randori. In both cases, a key aspect is the postures (with a wide range of different postures and with competition scenarios at a standing level as well as floor level) and the way contact between opponents is produced. In this sense, the IJF gives assistance and guidelines for the organizers of international competitions.

Following IJF rules, the environments where Judo competitions are held are complex indoor scenarios in terms of radio propagation, as some competition venues have large spectator capacity, multiple competition areas, furniture, and other facilities. Specifically, for holding International competitions, the competition venue has to have room at least for 10,000 spectators, 4 or 5 competition areas, warming up area with minimum 600 m<sup>2</sup>, and the following services and materials must be provided for each competition area: two electronic scoreboards plus one manual, a table for at least 10 people and a smaller table for the check-in and control of Judokas. In addition, a central table for a Jury is needed, with a wireless microphone system connected to the public address system for use only by referees, as well as an audio-visual information system to spectators, where the information about the Judokas and the results of the combats is shown. Apart from the complexity of the morphology of the environment itself, the deployed wireless systems as wireless microphones, WiFi networks, referees' headphones, wireless systems deployed to be used by the media and the huge quantity of portable personal devices that can be found within a crowded venue can make it a very complex task in terms of interference and coexistence. On the other hand, training venues are usually less complex than competition venues in terms of interferences, as they are smaller, the presence of people is much lower and there are less operating wireless communication systems. But they

still have the inherent complexity of indoor scenarios in terms of radio propagation.

In the literature, some WSN-related works for large sport venues can be found, as the development of wireless video services [Xua06] or the design of wireless environmental monitoring system based on ZigBee for stadiums [Che11]. But there is a neediness of in-depth radio planning studies for both large (competition venue) and smaller (training venue) sport environments. Furthermore, taking into account that wearable sensors for monitoring sport performance, training improvement and coaching support have been already developed [Chi05][Hei06][Che08][Zhi13][Pin13]. In the same way, specific wireless-based applications for different sports have been also presented in the literature, as movement activity monitoring for sprinters [Kuz12], investigating arm symmetry for swimmers [Sta12], real-time swimmers monitoring to extract stroke information [Cha13], effort control systems [Val13], tracking hip angles for cyclists [Coc14], detecting of illegal race walking [Lee13] and various general monitoring systems [Val10][Row12][Rod13]. But there are very few that deal with wireless-based applications on martial arts or contact sports [Wad13][Amb13]. Specifically for Judo environments, there is no reported work about radio planning analysis or development of applications.

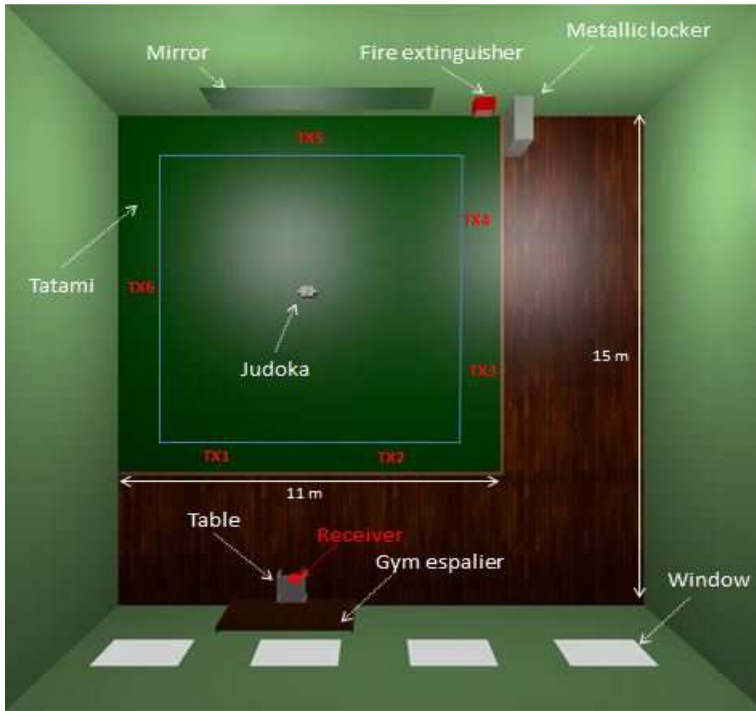
In this work, the characterization of the radio propagation in a real Judo environment for the purpose of developing potential wireless-based applications is presented. ZigBee-based XBee Pro modules operating at ISM 2.4 GHz have been used to emulate a WSN operating within Judo environment, since ZigBee technology has been previously used for other sport monitoring systems [Zul12][Min12]. For the purpose of analyzing this kind of environments, the analyzed real Judo scenario has been simulated by means of the 3D Ray Launching tool, and radio propagation and wireless channel quality measurements have been taken. The following analysis can aid in the optimal wireless network deployment, making the use of WSNs attractive for multiple applications in Judo environments, as monitoring vital signs [Miy13], coaching support, anti-doping control, combat monitoring, Judoka

identification or helping referees (e.g. providing information of a forbidden gripping or when diving head first onto the mat, which is severely sanctioned).

As the goal of this work is to study the feasibility of deploying ZigBee-based WSNs within Judo environments with the aim of implementing useful and novel applications, obtaining realistic radio propagation data within this type of environments is mandatory. For that purpose, a Judo training venue with a competition-size contest area has been chosen to carry out the measurement campaign. Thus, besides a real Judo training venue is analyzed, an approximation to an international competition-size scenario can be studied as the tatami complies with the dimensions specified by the IJF for contest areas for international competitions (10m × 10m). This scenario is located in the facilities of Judo Klub Erice, a local Judo club from Navarre. The dimensions of the whole scenario are 15m (long) × 15m (wide) × 8m (height) and it has a typical morphology of a training venue, as it contains concrete walls, windows, a mirror, parquet flooring and some furniture elements as wooden gym espalier and table, metallic locker and a fire extinguisher inside a metallic box with methacrylate cover. Although most of the scenario is air, the existing furniture and the presence of people make it a complex indoor scenario in terms of radio propagation. Figure 3.50 shows a picture of the real scenario where the measurements have been taken and the schematic scenario created for the later 3D Ray Launching simulations, which represents the real Judo training venue.



(a)



(b)

**Figure 3.50.** Scenario under analysis, (a) real picture, and (b) upper view of the created scenario for 3D Ray Launching simulations.

In order to characterize the radio propagation within the scenario, different measurements have been taken, firstly without and then with the presence of a Judoka on the tatami. The measurements without people on the tatami will give valuable information about the behavior of the radiated electromagnetic waves at the operating frequency band (ISM 2.4 GHz) within Judo environments and they will be used to validate the simulation results. The subsequent measurements with a Judoka on the tatami will give more realistic data since most of the potential applications involving the practice of Judo will presumably include persons.

For the setup of the measurements, a single transmitter and a receiver have been deployed. Due to the performance in terms of power consumption and spectrum availability, IEEE 802.15.4 based XBee Pro ZigBee modules with chip antenna (gain of -1.2 dBi) have been used to act as transmitter. For the measurements without the presence of a Judoka on the tatami, and unlike the receiver, which remains in the same place, the position of the transmitter has been changed in order to cover the perimeter of the tatami. These transmitter positions are represented in Figure 3.50b by red text (TX) and a number. In addition, these chosen transmitter locations can emulate a potential application: by placing pressure sensors throughout the perimeter of the competition area [Maz12][Abd12], a wireless message could be sent to the referee's table to know if a Judoka is inside or outside the competition area, which is decisive data in many occasions in order to validate a Judoka's movement and award it with points or the win of the combat. Figure 3.51 shows an XBee Pro module deployed on the tatami. The transmission power level has been set to the maximum predefined value (18 dBm), transmitting continuously, without time interval between packets. All the measurements have been carried out statically, with the wireless nodes connected to a laptop for charging as well as for data processing duties (e.g. PER data acquisition). The frequency of operation has been set to 2.41 GHz, which corresponds to ZigBee channel number 12 (the lowest channel allowed by this modules). The election of the frequency channel is given by the fact that possible WiFi interferences are wanted to be



avoided. As a receiver, an omnidirectional antenna with 5 dBi gain, connected to a portable spectrum analyzer (Agilent N9912 Field Fox) has been used. Looking at Figure 3.50b again, the red point in the bottom side of the schematic representation of the scenario represents the receiver device, which has been placed on a 0.75m height table, emulating the referees' table with a wireless node receiving the information from the environment or from the Judoka on the tatami (e.g. vital signs during training sessions).

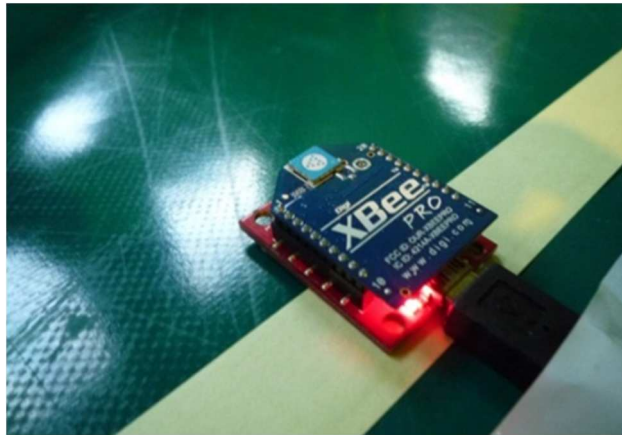


**Figure 3.51.** XBee Pro module deployed on the tatami.

The measured power levels at the receiver position for each of the mentioned 6 different positions of the transmitter along the perimeter of the tatami are shown in Figure 3.52. Thus, the radio propagation from different distances can be analyzed. As can be seen in the obtained values, the distance between the transmitter and the receiver has an important impact on the received power, as expected. But it can be also seen how in some cases more power from further points (e.g. point TX4 versus point TX3) is received. This is mainly due to the multipath propagation, even more important taking into account the height difference between transmitter and receiver, which can lead to a NLOS link.

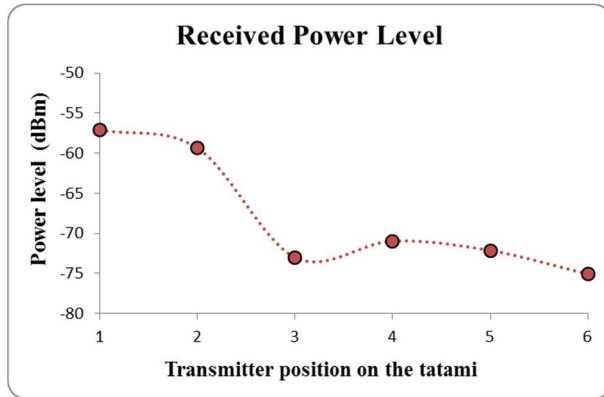


**Figure 3.51.** Received power level for the 6 different transmitter positions.

As it is previously stated, the Judokas will be involved in the most interesting potential Judo applications. Therefore, a second measurement campaign has been carried out with the presence of a Judoka. The Judoka has been placed in the middle of the tatami, facing the receiver point. Like in the previous measurements, the receiver is placed at the same position and it has not been moved. On the other hand, the XBee Pro transmitter has been placed at different parts of the Judoka’s body (chest, back, knee and arm), fixed as seen in Figure 3.52. The notes have been configured as in the previous measurements. It is worth noting that all the measurements have been taken using two different Judogis (jacket, trousers and belt) approved by IJF, in order to make them as close as possible to a realistic high level Judo environment. Figure 3.53 shows the obtained power level values at the receiver location. As can be seen, the position of the transmitter mote on the body has a big impact in the received power level, which could be given by the fact that the receiver is placed on a table at a different height comparing to the transmitter. Note how a significant attenuation appears when the human body is between the transmitter and the receiver (transmitter on the back).

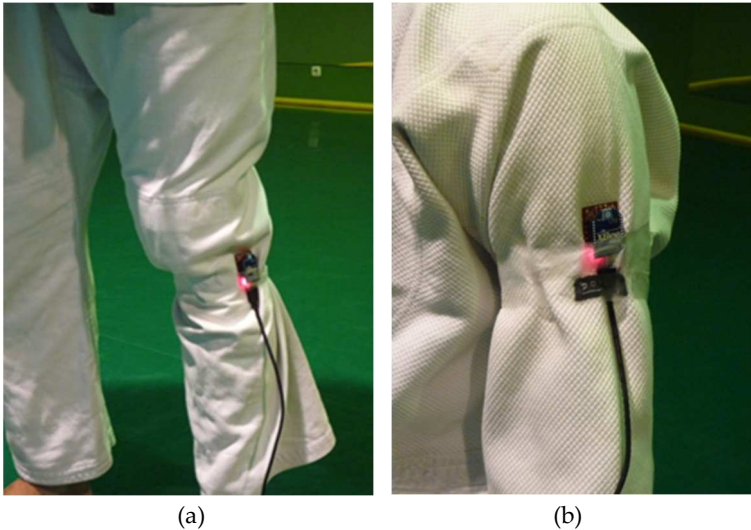


**Figure 3.52.** XBee Pro module on the Judoka's approved Judogi (a) on the knee, (b) on the arm.

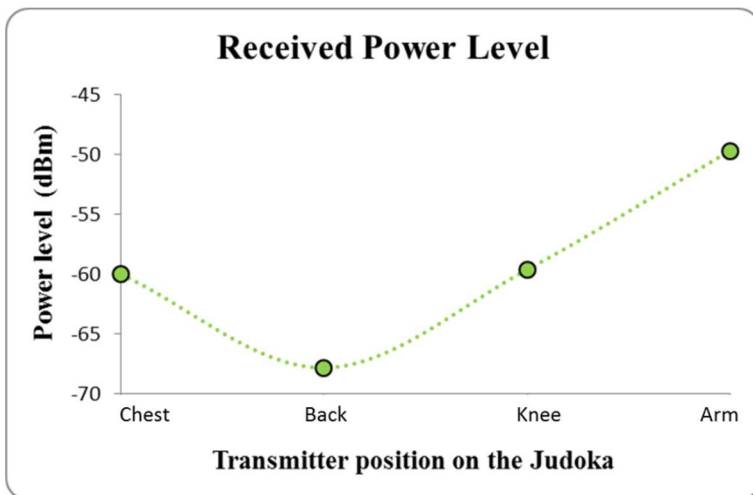
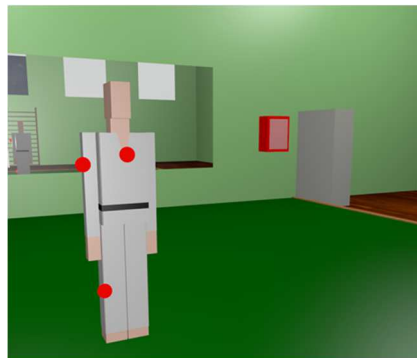


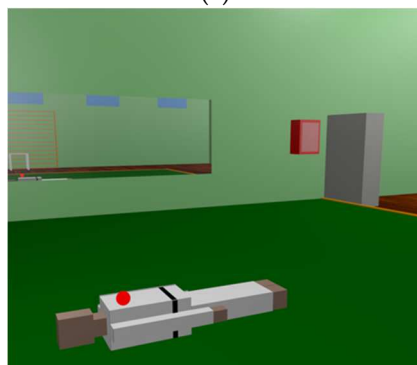
**Figure 3.53.** Received power level for different transmitter positions on the Judoka.

Additionally, wireless channel quality measurements have been taken in order to study if the deployed ZigBee-based communication system between a Judoka/tatami and the referees' table is indeed

feasible. For that purpose, a wireless link has been created between the Judoka/tatami and the table with the aid of two XBee Pro modules. On one hand, the transmitter has been placed on different parts of the Judoka's body, standing as well as lying in the center of the tatami (since during Judo combats there are both standing and ground actions). In Figure 3.54 the transmitter position configurations on the Judoka can be seen, where the red dots represent the XBee Pro modules. On the other hand, the same transmitter positions indicated in Figure 3.50b have been used for the tatami-to-table measurements. The receiver position is also the same as in the previous measurements (Figure 3.50b). All the measurements have been carried out with only one transmitter operating at the same time.



(a)



(b)

**Figure 3.54.** Transmitter positions (red dots) for PER measurements on standing Judoka (a) and on lying Judoka (b).

The parameter chosen for the analysis of the wireless channel quality has been the PER (Packet Error Rate), which gives the percentage of the lost packets during the transmission of a fixed packet value. In this case, 100,000 packets have been transmitted in each PER measurement. The parameters of the XBee motes have been defined like in the previous radio propagation analysis. The transmission has been done without ACK (Acknowledgment) packets. In Figure 3.55 the obtained PER values for the tatami-to-table communication links are shown. Although the PER value varies depending on the position of the transmitter, this variation is very small. Besides, all PER values are very low, i.e. few packets are lost. The standard deviation for each measurement point is also shown, which is also very low, namely 0.02% in terms of PER. This means that the PER variation is strongly dependent with the position of the transmitter but constant in a static scenario. Similar results can be deduced for the case with the transmitters placed on the Judoka's body. In Figure 3.56 and Figure 3.57 measured PER values for standing and lying Judoka can be seen respectively. In this case, besides the fact that the PER will change depending on the position, other issues affect the transmission, like the difference transmitter position heights or the polarization of the transmitter antennas, which is the opposite for the standing Judoka measurements. For a more in-depth analysis for the motes placed on the Judoka, the effect of the Judogi in the transmission has been analyzed. Specifically, for the standing Judoka, measurements on and under the Judogi for each position have been carried out in order to quantify the PER difference. The results show that it has not great impact and the number of lost packets is still very low (see Figure 3.56). Finally, it is worth noting how the PER value changes when the Judoka is lying faced up on the tatami: comparing with the case of the mote on the chest, significantly more packets are lost when the transmitter is on the Judoka's back and the body lies over the device (see Figure 3.57). Even so, the PER values remain low. The obtaining of these low PER values is mainly due to the sensitivity level of the XBee Pro modules, which is significantly lower (-100 dBm) than the received power levels at the receiver position (see Figure 3.51 and Figure 3.53).

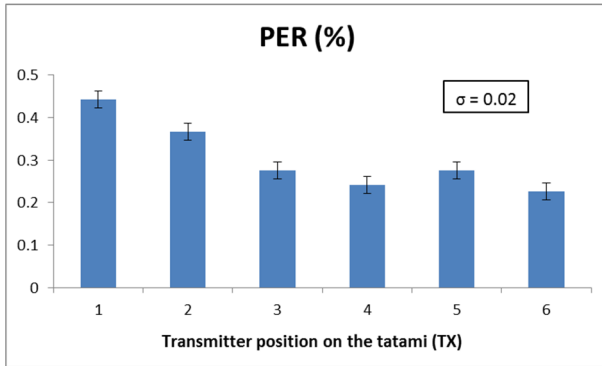


Figure 3.55. PER values obtained for the transmitter placed on the tatami.

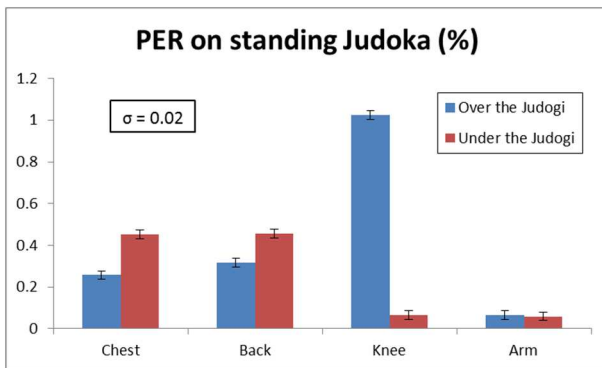


Figure 3.56. PER values obtained for the transmitter placed on a standing Judoka.

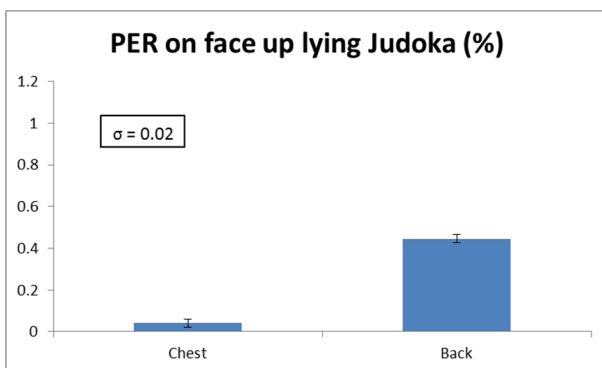


Figure 3.57. PER values obtained for the transmitter placed on a lying Judoka.

From the presented channel quality measurements, and taking into account that no ACK mechanism has been used, which will significantly improve the overall performance of the wireless transmission reducing the PER values, it can be concluded that a ZigBee-based wireless communication system can be deployed in this kind of indoor environments, since its performance is expected to be good enough for potential applications.

The next step in the analysis is to apply the 3D Ray Launching simulation method in order to study if accurate estimations within Judo environments can be obtained. Following, the simulation results obtained by means of the 3D Ray Launching tool are shown, and their suitability for this study is discussed. Creating a detailed scenario and as close as possible to the real one is very important in order to obtain accurate simulation results. Therefore, besides the real sizes of the elements and distances between them have been taken into account, the constitutive materials of all of the objects within the scenario have been carefully defined. A summary of the properties of the main materials used to define the constitutive elements of the created scenario are shown in Table 3.10.

<b>Material</b>	<b>Dielectric constant</b>	<b>Conductivity (S/m)</b>
Wood	2.88	0.21
Plasterboard	2.02	0.06
Concrete	25	0.02
Tatami	4	0.12
Metallic	4.5	$37.8 \times 10^6$
Glass	6.06	0.11

**Table 3.10.** Main material properties for the created scenario.

The parameters defined for the simulations are shown in Table 3.11, which are equivalent to those of the used ZigBee-based motes.

<b>Parameter</b>	<b>Value</b>
Transmitted Power Level	18 dBm
Frequency	2.41 GHz
Launched Rays resolution	1°
Cuboids size	10cm×10cm×10cm
Max. Reflections permitted	5
Transmitter/Receiver antenna gain	-1.2 dBi / 5 dBi

**Table 3.11.** 3D Ray Launching simulation parameters.

Firstly, RF power distribution results have been obtained for the whole volume of the scenario. Figure 3.58 shows the obtained received power planes at height 0.75m (i.e. the height of the receiver on the table), when the transmitter is placed on the tatami at the six different positions shown in Figure 3.50b, without the presence of the Judoka. In the same way, Figure 3.59 shows the estimations for the same plane, but for the transmitter placed on the chest and the back of a standing Judoka (facing the receiver) in the center of the tatami. Note that the previously mentioned detailed human body model created in-house has been used for these simulations. As can be noticed, received power level is dependent on the position of both the transmitter and receiver devices. The influence of the human body is also clearly seen: behind the body the shadow effect is noticeable, receiving lower power values than those in front of the human body where the transmitter is placed. Besides, short term variations of the received power level can be seen throughout the scenario, which is the typical effect due mainly to the multipath propagation, which is in most cases the strongest phenomenon in indoor environments.



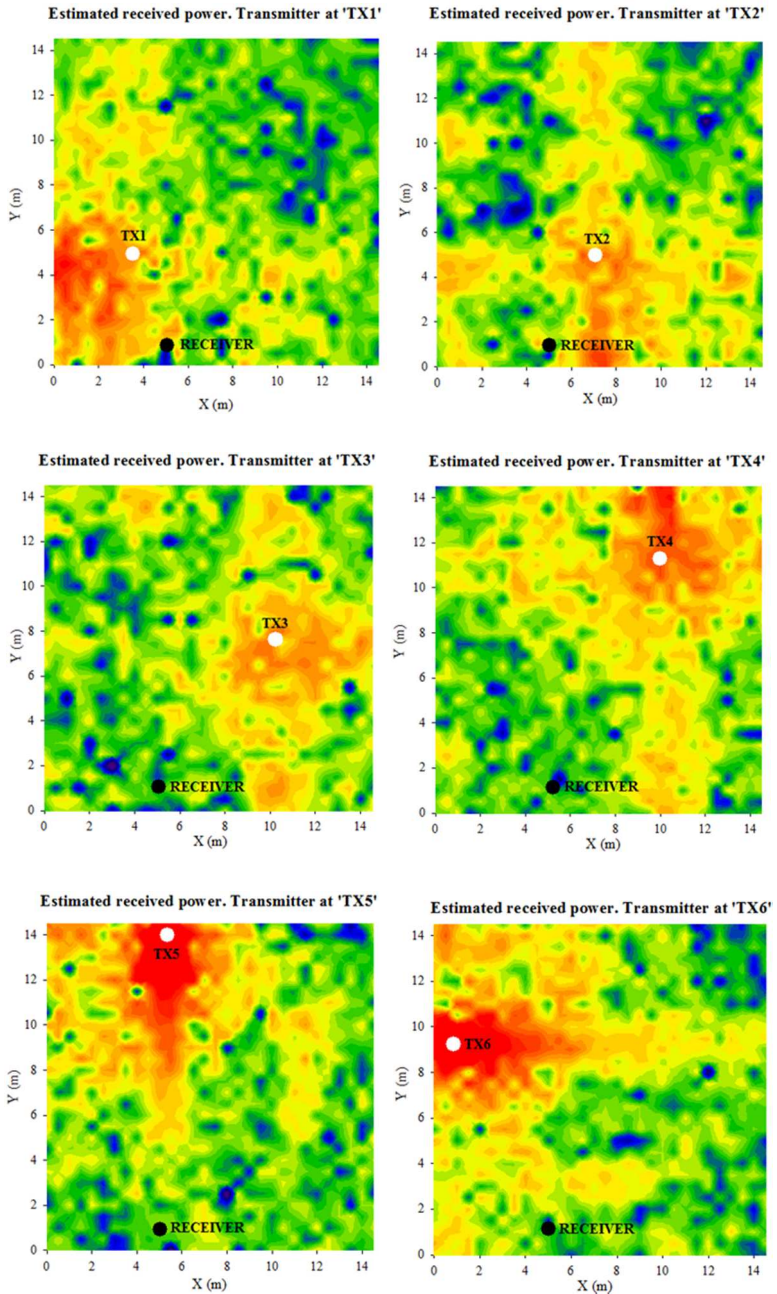
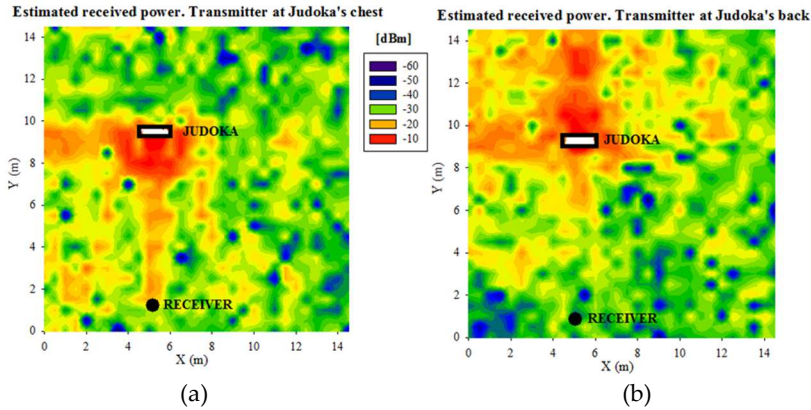
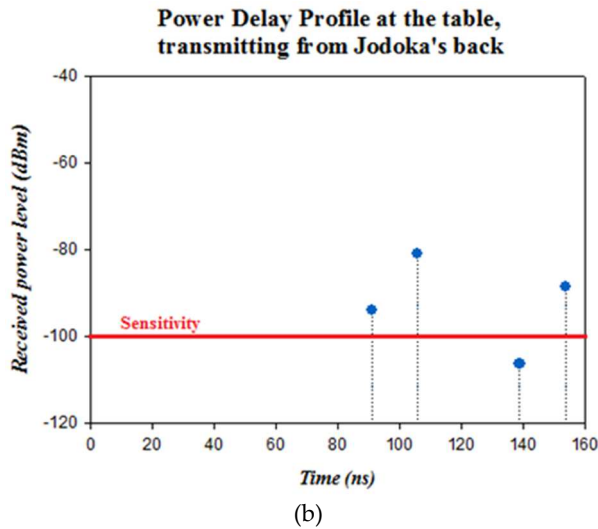
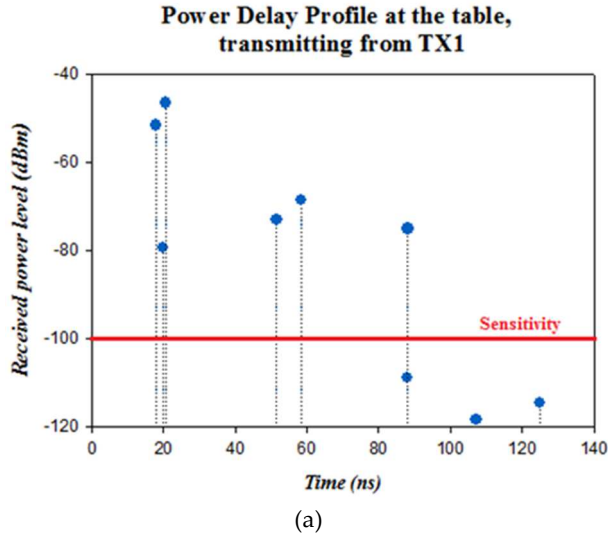


Figure 3.58. Estimated RF power distribution planes at height 0.75m.



**Figure 3.59.** Estimated received power planes at 0.75m for the transmitter placed (a) on the chest, and (b) on the back of a standing Judoka.

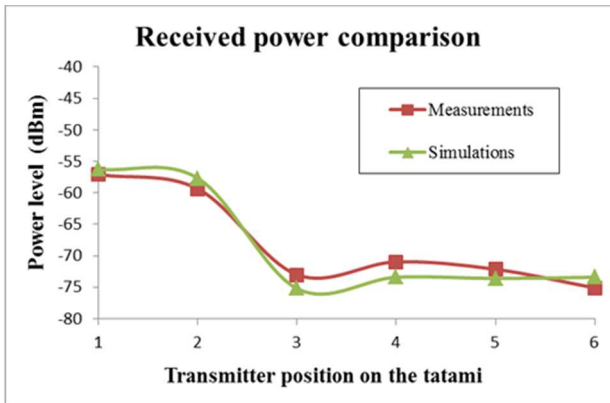
In order to see the impact of the commented multipath propagation in this scenario, in Figure 3.60 two power delay profiles obtained from the simulation results at the center of the table are presented. The transmitter positions have been chosen in order to see the different results that can be obtained depending on the position of the transmitter. These positions correspond to TX1 and the back of the Judoka. The sensitivity of the XBee Pro modules (-100 dBm) has been indicated in the graph by a red line in order to see the components which will be taken into account and which ones will not be ‘seen’ by the device. As expected, more components with higher power level reach the table from position TX1 than position on the back of the Judoka, as the distance is shorter and no human body is affecting the propagation. Regarding the complexity of the scenario, it can be clearly seen that different multipath components reach the receiver point, as it is expected since the scenario is indoor. Anyway, due to the size of the scenario and the low density of elements within it, the impact of the multipath propagation is much less important than in the previously analyzed scenarios such as office, home and vehicular environments, where the PDPs show a larger number of multipath components (see Figures 15, 28, 35 and 44).



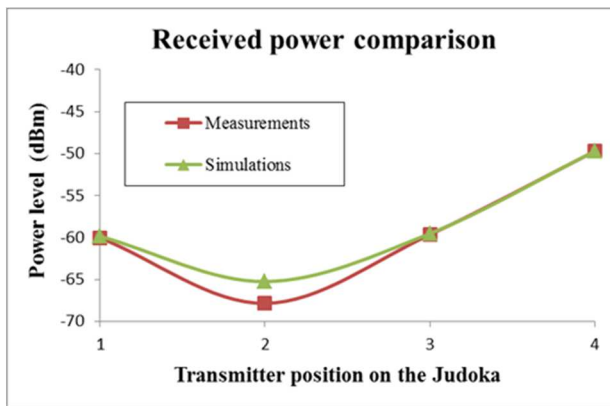
**Figure 3.60.** Power delay profiles at the receiver location for the transmitter placed on the tatami at position TX1 and on the back of the Judoka.

In order to validate the obtained simulation results, in Figure 3.61 a comparison between the simulation results and measurements is shown. Note that in Figure 3.61b, the transmitter positions 1, 2, 3 and 4

correspond to Chest, Back, Knee and Arm respectively. As in the previously studied environments, the received power estimations obtained by means of the 3D Ray Launching method are also accurate for this kind of environments. Specifically, the obtained mean error is 0.104 dB, with a standard deviation of 1.61 dB. Therefore, very accurate estimations can be obtained by means of the presented simulation method, validating it for further simulations in this kind of Judo environments.



(a)



(b)

**Figure 3.61.** Comparison between simulation results and measurements for different transmitter positions, (a) on the tatami, (b) on the Judoka.

Finally, once the simulation results with the presence of a single Judoka have been validated comparing them with measurements, further simulations have been carried out in order to analyze the effect of the presence of two Judokas within the scenario, as Judo combats are played by two Judokas. In Figure 3.62 the scenario with two Judokas in pre-combat position in the center of the Tatami can be seen. Each Judoka has a transmitter placed on their right arm (represented by red dots). The configuration of the wireless nodes (transmitters) and the parameters of the 3D Ray Launching algorithm are the same used for previous simulations (see Table 3.10 and Table 3.11). The estimated received power for the plane at height of the receiver device (0.75 m) when both transmitters are transmitting simultaneously is depicted in Figure 3.63. It can be noticed how received power depends strongly on the position of the transmitters, and it can be guessed that the contribution at the received point will be different. In order to see in detail these different contributions, Figure 3.64 shows the Power Delay Profile at receiver point. As expected, it can be clearly seen that the rays of Judoka 1 reached the receiver with higher power level and sooner than the rays emitted by Judoka 2's transmitter, due mainly to the relative position of each transmitter to the receiver.

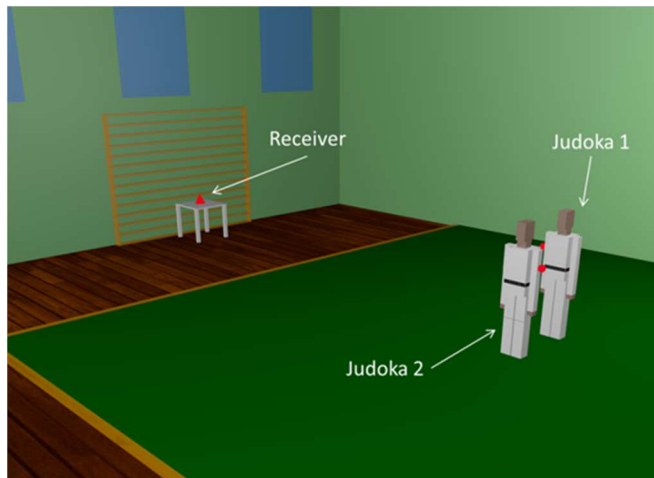


**Figure 3.62.** Scenario under analysis for two Judokas in the center of the Tatami.

Estimated received power. Transmitters at Judokas' right arms

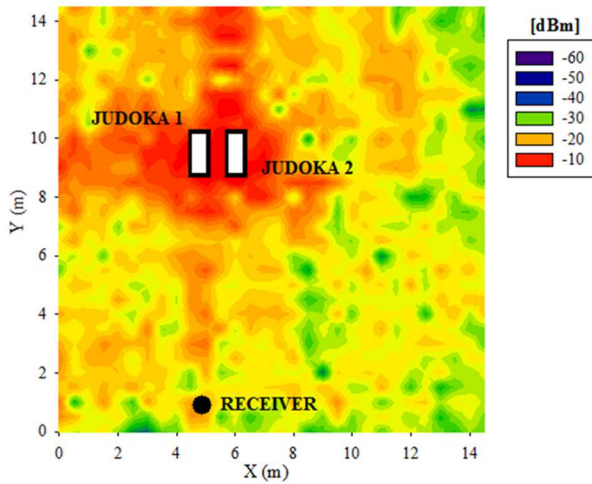


Figure 3.63. RF power plane at 0.75m when the transmitters placed on the right arm of each standing Judoka are transmitting simultaneously.

Power Delay Profiles for both Judokas, at receiver point

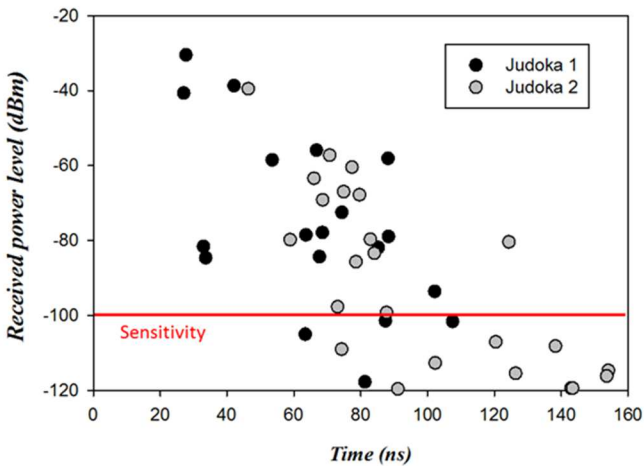


Figure 3.64. Power Delay Profiles at the receiver location for a transmitter placed on the right arm of each Judoka.

Concluding, in this study the influence of Judo environments in the operation of a WSN at ISM 2.4 GHz band has been analyzed by means of an in-house deterministic 3D ray launching algorithm in order to aid in the development of potential monitoring applications. A campaign of measurements in a real Judo training venue has been carried out in order to validate the simulation results. The results show that the topology and morphology of this kind of scenarios have a great impact on the radio propagation and the overall performance of the WSN, due mainly to the effect of multipath propagation, which is the most significant propagation phenomenon in indoor complex scenarios. This leads to the necessity of an in-depth radio planning tool, since the coexistence of the wireless devices of potential applications added to the portable personal devices, the presence of persons itself and other wireless systems such as WiFi networks will make it a very complex task. The high accuracy of the presented in-house 3D ray launching simulation method, including an in-house developed human body model, has been demonstrated, obtaining a mean error of 0.104 dB with a standard deviation of 1.61 dB.

One of the most interesting aspects regarding the radio propagation analysis within sport environments is the study of aquatic sports, due to the difficulties and complexity that the presence of water bring to electromagnetic propagation. As a first approximation to aquatic sports, in this section the radio channel characterization of a wireless communication system between a surfboard and a person (wearable) is evaluated, with the aid of the in-house developed 3D Ray Launching method.

In aquatic environments, researchers have deployed wireless sensor networks above the sea [Jia09][Jam10][Gon12], obtaining environmental monitoring data, and under the sea level developing long distance underwater communications system by using low frequencies [Sen11][Sen12]. More specifically, in the case of surfing, an accelerometer could capture the human body movements and save this information in the surfboard or send it using a wireless link providing real time information to the spectators and sport judges, in the case of



competitions. However, the existence of water surrounding the surfboard must be taken into account in the system analysis, with phenomena such as diffraction, diffuse scattering associated to the rough sea surface and attenuation caused by water absorption taking place. Consequently, many multipath and scattered components can reach the receiver, degrading system operation [Has01][Wes02][Zhu10]. Despite not being a commonly studied topic, in [Bon10] a surfboard full integrated sensor network is presented, enabling sending information of mechanical stress of the board during the activity.

One of the main challenges in aquatic scenarios is the estimation of radio propagation losses in such complex environments. As empirical based estimations will require large measurement sets in order to obtain site specific regressive models and full wave simulation tools require large computational complexity, once more, the 3D Ray Launching algorithm has been used, which provides an adequate tradeoff between precision and computational complexity, particularly for large scenarios. Specifically, the behavior of the radio channel in a surfboard-to-person communication link as well as in a surfboard-to-infrastructure scenario has been analyzed. The simulation parameters employed are shown in Table 3.12.

Parameter	Value
Transmitted Power Level	10 dBm
Frequency	2.4 GHz / 868 MHz
Launched Rays resolution	1°
Cuboids size	5cm×5cm×5cm
Max. Reflections permitted	6
Transmitter/Receiver antenna gain	0.82 dBi / 2 dBi

**Table 3.12.** 3D Ray Launching simulation parameters.

Initially, a test scenario is simulated in order to validate the surfboard model and the human body model (resembling the potential surfer) within the 3D Ray Launching code, verified with measurement



results in the laboratory, which are shown below. To minimize the influence of walls in the received power estimations and therefore, to obtain more reliable results, a wide scenario (8m x 8m x 4m) has been defined, where one person is placed over a surfboard (Figure 3.65). The surfboard has been modeled as a rectangular polystyrene board, having a size of 1.75m x 0.46m x 0.05m, and which includes a wireless transmitter at 0.11m from the left edge, with a radiation pattern corresponding to a short vertical monopole, being the maximum directivity in the horizontal plane.

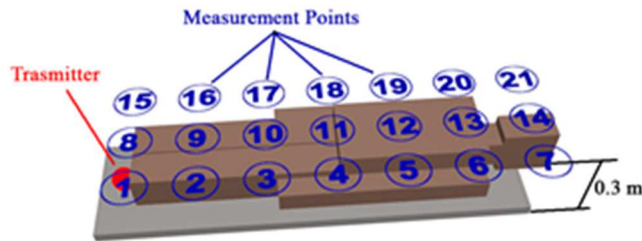


**Figure 3.65.** Model used in the Ray Launching code and measurement points.

Once the scenario has been implemented, simulation results have been obtained for two different heights: 0.3m and 0.9m from the surfboard, considering two typical surfer positions, the person laying (see Figure 3.66) and standing (see Figure 3.67). The estimation of received power level distribution results are represented for 2.4GHz and 868MHz frequencies, which represent the spectral allocation for a wide range of WSN deployments in different regions of the world. The results show that received power values depend on the distance to emitter, decreasing if the distance is greater, and improving when the frequency is reduced from 2.4GHz to 868MHz. Furthermore, outcomes are much better when the person is standing than lying, because the inclusion of a human body in the channel introduces an element with a high absorption coefficient that attenuate signals quickly.

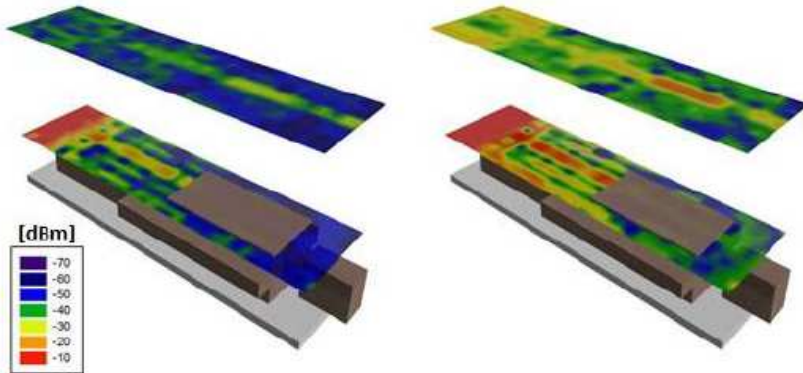


**Figure 3.66.** Simulation results of Received Signal Level at 2.4GHz (left) and 868MHz (right) when the person is lying.

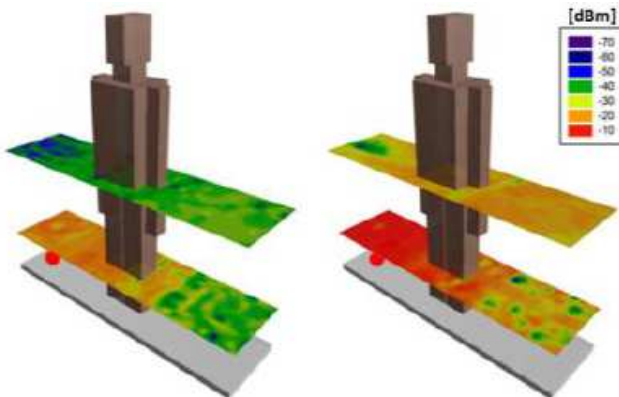


**Figure 3.67.** Simulation results of Received Signal Level at 2.4GHz (left) and 868MHz (right) when the person is standing. The red point is the transmitter.

Further simulation results have been obtained in order to analyze different scenarios. Figure 3.68 shows the differences between the cases of the surfboard placed on water and on a cement floor, when the person is standing on it, for an operating frequency of 2.4GHz. This latter configuration has been employed in order to validate the simulation methodology, which is easily measurable in a laboratory environment.

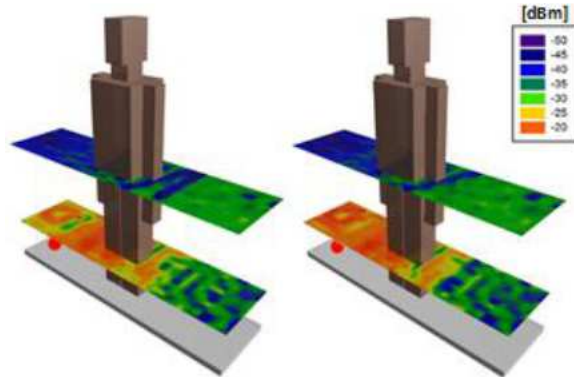


**Figure 3.68.** Estimated RF power levels, considering that the surfboard is on water (left) and on concrete (right).

The material under the surfboard has indeed an impact on the radio propagation estimations. In order to gain insight in this issue, in Figure 3.69 the RF power distribution difference between considering freshwater and seawater (medium salinity) at 20°C of temperature is shown. The receiver node positions correspond to those depicted in Figure 3.65. As can be seen, there are no significant differences for the presented results, which are for a height of 0.3m and 2.4GHz.

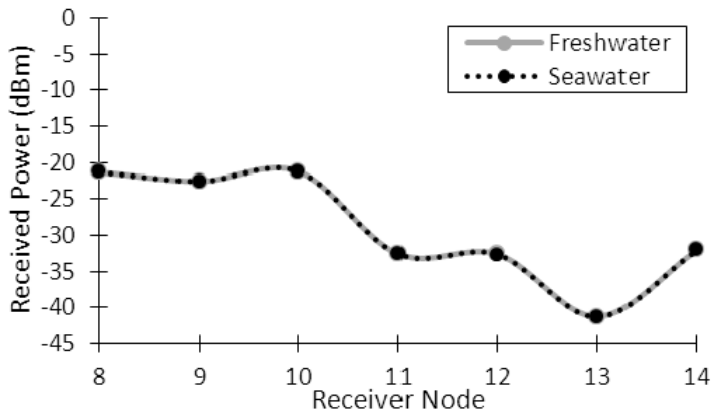


**Figure 3.69.** 3D Ray Launching simulation results depending on water properties.

Furthermore, in order to emulate a true open aquatic environment,

sea surface roughness has been implemented in a larger scenario (with dimensions of 50m x 20m x 10m), considering a potential wireless communication link between the surfer and a receiver on a buoy located at a distance of 42m (see Figure 3.71). Due to the limitations of the simulation code, this buoy has been modeled as a rectangular prism with a size of 1.5m x 1.5m x 2m, although other potential geometries can be implemented.

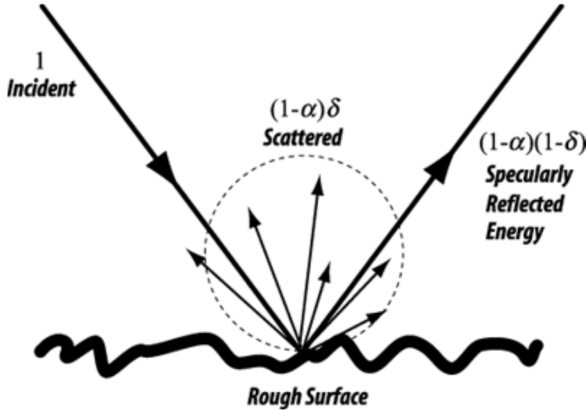


Figure 3.70. Scattering phenomenon on rough surfaces.

It is generally considered that the sea surface is smooth and only produces specular reflection, if Rayleigh criterion (3.9) is satisfied.

$$\sigma_h < \frac{\lambda}{8 \sin \theta_i} \quad (3.9)$$

where  $\sigma_h$  is the standard deviation of sea wave height,  $\lambda$  is the wavelength of the incident ray and  $\theta_i$  is the incident angle.

Otherwise the surface will be rough, causing diffuse scattering and resulting in a power reduction of the specular reflected ray (see Figure 3.70). In order to estimate the scattered power, the Kirchhoff theory proposes an effective reflection coefficient ( $R_{rough}$ ) which is function of  $\sigma_h$  and  $\theta_i$ , besides the specular reflection coefficient ( $R$ ) [Sch86][Yan13]:

$$R_{rough} = R \cdot \exp \left[ -2 \left( \frac{2\pi}{\lambda} \sigma_h \sin \left( \frac{\pi}{2} - \theta_i \right) \right) \right] \quad (3.10)$$

On the other hand, ocean wave behavior depends mainly on the wind speed ( $U$ ). Several works have addressed this relationship by means of the significant wave height ( $H_{1/3}$ ) [Din14], which can be also defined as a function of  $\sigma_h$ :

$$H_{1/3} = 0.0214 U^2 \quad (3.11)$$

$$H_{1/3} = 4\sigma_h \quad (3.12)$$

Applying these formulas, the scattering produced by the sea surface has been implemented in the simulation tool and simulation results have been obtained for a transceiver operating at 2.4GHz, transmit power of 10dBm and a spatial simulation mesh resolution of  $1\text{m}^3$ . Figure 3.71 shows the results for a plane at 1.5m height over the sea surface when the transceiver is embedded in the surfboard.

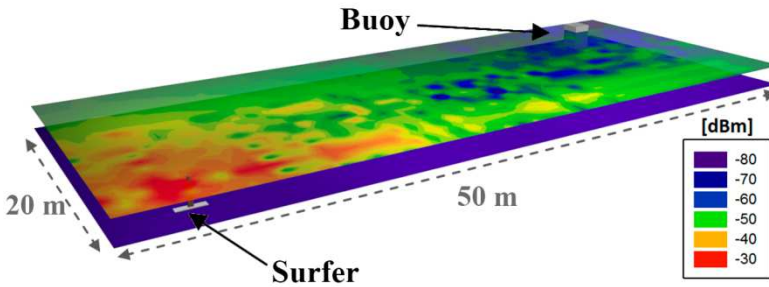


**Figure 3.71.** Simulation results at 2.4GHz considering the rough sea surface. The surfer is placed on the lower left side and the buoy is in the top right corner.

In order to see the effect of the implemented scattering model, Figure 3.72 shows the comparison between a smooth and a rough surface with different degrees of surface roughness. The depicted graph corresponds to the linear path between the surfboard and the buoy. The obtained results show that the received power levels are similar for the compared cases, but at some points the difference can be as high as 8dB between smooth surface ( $\sigma_h = 0$  m) and  $\sigma_h = 0.3$  m. It is worth noting that higher values for the standard deviation of sea wave heights can be

present when surf is practicing, which will affect more significantly the RF distribution.

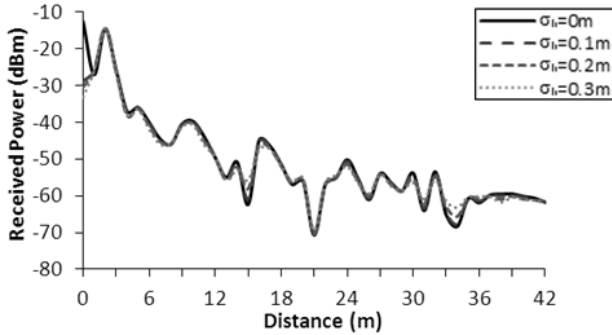


Figure 3.72. Received RF power levels for different standard deviation of wave height.

In order to see clearer the influence of sea height variation in the RF power distribution throughout the presented scenario, the results for two different wave height variation values are depicted in Figure 3.73. As in Figure 3.72, the RF power distribution differences are difficult to see with a naked eye in such a big scenario, but at the zone around the buoy position lower RF values can be seen for the  $\sigma_h = 0.5 m$  case. Therefore, higher values of wave heights and bigger scenarios can lead to quite big differences regarding the RF distribution, affecting the deployment of a potential WSN within this kind of scenarios.

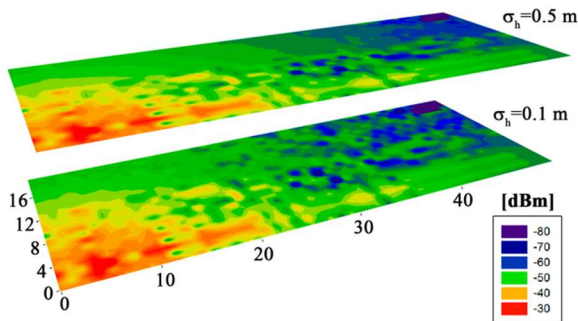
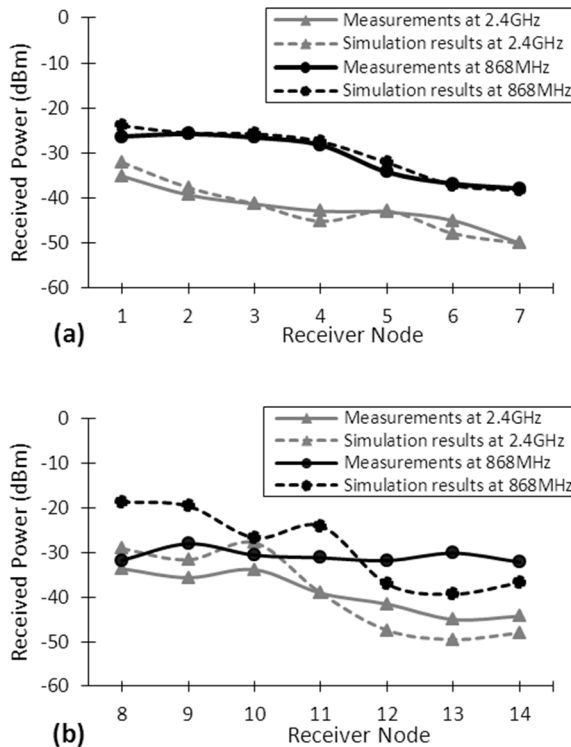
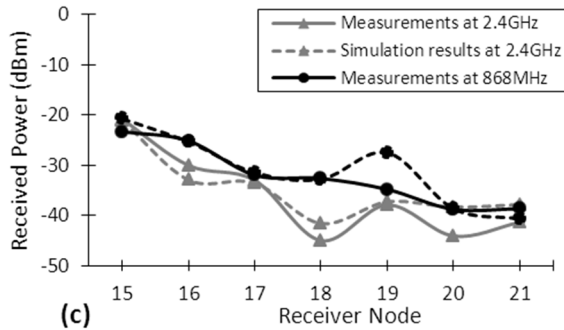


Figure 3.73. Simulation results at 2.4GHz considering the rough sea surface for two different wave height variation values.

In order to validate the presented simulation results, Received Signal Strength Indicator (RSSI) measurement results have been obtained. The experimental setup is composed by a Marconi 2041 signal generator, an Agilent FieldFox N9912A spectrum analyzer connected to corresponding short vertical monopoles. Both 2.4GHz and 868MHz bands have been measured, at maximum transmit power of 10dBm. The transmitter has been fixed on the surfboard and the measurement points have been scanned in three equally spaced rows along the surfboard, at the heights of 0.3m and 0.9m, which is schematically shown in Figure 3.65. The obtained measurement values versus simulation results for a height of 0.3m are shown in Figure 3.74. Good agreement between simulations and measurements can be seen. A mean error of 2.65dB with a standard deviation of 2.85dB has been obtained taking into account the 21 measurement points.





**Figure 3.74.** Received signal strength for the first (a), second (b) and third row (c).

In order to provide more insight in the operation of a potential WBAN/WPAN network, the communication quality has been analyzed by obtaining Packet Error Rate (PER) values of wireless links. For this purpose two XBee Pro modules have been employed, one of them located on the surfboard and the other on several locations of the human body. Every XBee mote is connected to a laptop running specific Java programs implemented in house to send or receive data and generate PER statistics. The link parameters are set up to transmit batches of 10,000 packets with a power of 18dBm, operating at 2.4GHz and employing short vertical monopoles with a gain of approximately 2dBi. The results obtained in all cases are below 0.1% of error, given the fact that XBee modules exhibit receiver sensitivity thresholds of -80 dBm in the most restrictive case (the employed XBee Pro modules have a sensitivity of -100dBm). The employed method can be further extended to obtain quality assessment of wireless links in the case of surfboard or surfer communications towards infrastructure elements, such as buoys or base stations located at the shore.

Summarizing, the characterization of wireless links in the practice of surf for some situations has been presented. Estimations of received power levels have been obtained with the aid of the in-house implemented 3D Ray Launching code, in which a specific simplified surfboard has been generated. Moreover, consideration of dispersive



properties of water (conductivity and dielectric constant) as well as water roughness has been taken into account. In the latter case, water surface roughness is coupled to the 3D RLM code, calculating the equivalent reflection coefficient as a function of average height variations for each ray launched incident on the water surface. Simulation and measurement results have been obtained in a test configuration for several surfboard/surfer position and potential receiver locations, showing good agreement. Once the implemented surfboard and surfer models have been tested, a larger scenario resembling an outdoor aquatic surf location with potential connectivity with an infrastructure element (i.e., marine buoy) has been implemented and simulated for different values of water surface roughness. Bi-dimensional received power plots have been obtained, indicating potential coverage levels, which can be employed in radio planning tasks. The proposed methodology, combining surfboard, surfer and water roughness provides an adequate tool for the estimation of quality assurance parameters in terms of the optimal radio planning configuration in terms of transceiver location in the particular case of outdoor aquatic environments.

### 3.2.5 Commercial area environments

Another environment that has been considered interesting to analyze due to the possibilities that provides for the developing of applications is the commercial areas environment. Nowadays, the use of information and communication technologies has revolutionized the way in which commercial transactions take place, from e-commerce, m-commerce to location based marketing [McG99]. In the case of on-site commerce in retail shops, the introduction of information technologies has aided in logistical processes, stock tracking, automated cashier systems and consumer analysis, among others [Rou06]. It is worth noting that analysis of user interaction in commercial areas takes into account multiple variables, such as user movement patterns or potential user mood [Chu12].



\*Figure obtained from <http://blog.azoft.com>

The inclusion of wireless technologies has provided new means of enhancing procedures related with commercial areas, such as the introduction of RFID in product tracking, development of mobile apps linked with retailer websites and the inclusion of Near Field Communication (NFC) in mobile terminals in order to enhance payment process [Rou06][YuY11]. New functionalities can be envisaged with the advent of wearable technology as well as the steady adoption of Wireless Personal Area Network and Wireless Body Area Network, coupled to Wireless Sensor Networks (WSNs), such as mobility support [Gua16]. Moreover, the evolution of mobile networks, the extension of Internet of Things and the adoption of 5G networks, with Device to Device (D2D) capable connectivity will increase user/environment interaction levels [Aky02][Yic08][Bel13][Ban14]. In this way, traditional information exchange in retail and commercial areas, usually employed for periodic stock management and sales procedures at cashiers, can now be de-centralized and employed for a wider range of applications. Consequently, full advantage of cooperative networking techniques can be used (e.g., CoopMAC protocol, QoS provision via 802.11aa standard, etc.), as well as the possibility of enabling full interaction between the commercial infrastructure (e.g., shelves in which merchandise is contained, exhibition stands, information points). This leads to Context Aware environments, which can be seen as a subset in a larger framework of

Smart City/Smart Regions scenarios, in which larger levels of user/systems interaction are achieved, involving multiple systems and functionalities, such as energy generation and distribution, waste management, Intelligent Transportation Systems or Smart Health, among others [Sol14]. In the specific case of large commercial areas, work has been performed in order to provide context-aware scenarios which lead to ubiquitous shopping malls [Yok06][Eva06][Wic09][Zhi09][WuN12][Zhe12][Goo13][Cha14][She14][Rup15]. In many of the cited works, a higher functionality is provided to shopping carts, as it is an active element within the shopping process.

The wave propagation or the performance of a wireless network within shopping malls has been already analyzed for 320 MHz, 17 GHz and 28 GHz [Unb01][Xia13][Soo14]. In this work, wireless sensor nodes, based on Wireless Body Area Network/Personal Area Network were embedded within a shopping cart and the infrastructure of a large commercial center in order to achieve a context aware shopping environment at 2.4 GHz. Wireless propagation analysis was performed with the aid of the in house deterministic 3D Ray Launching code, in order to account for complex channel characterization, given by the presence of a dense array of multiple obstacles and scatterers (such as merchandise in different container types, materials and volumes), as well as the presence of users within the scenario. This provides information in terms of performance of optimal node configuration in the specific shopping cart/commercial area scenario under analysis. The node configuration allows the analysis of optimal aggregation schemes, as a function of network topology, which has been analyzed for the several cases of interaction between shopping carts and commercial area infrastructure (nodes within shelves or located in diverse access points).

The scenario where the system analysis was carried out is within the E.Leclerc supermarket, located in Pamplona, Navarre, being the largest commercial area in the region. Due to the large size inherent to these kind of commercial areas usually have, the scenario under analysis was limited to a single aisle with its corresponding shelves of the

supermarket, as a first approximation to the problem. The characteristics of the chosen aisle are similar to those that can be easily found in large commercial areas, thus being able to extend the obtained results to any commercial area of this kind. Figure 3.75 shows the real scenario. The antenna used as transmitter can be seen deployed in the shopping trolley. The dimensions of the limited scenario are 25.94 m (length)  $\times$  11.7 m (width)  $\times$  3m (height) (see Figure 3.76). The aisle width is 2.9m and the shelves dimensions are 19.5 m (length)  $\times$  1.5 m (width)  $\times$  2.25 m (height). For the radio propagation study, the trolley was placed at one end of the aisle, between the shelves, as seen in Figure 3.75.



**Figure 3.75.** Real scenario. Note that the shelves on the left are filled mainly with products in glass jars, and the shelves on the right with products in metallic cans. Numbered red dots represent the measurement points.

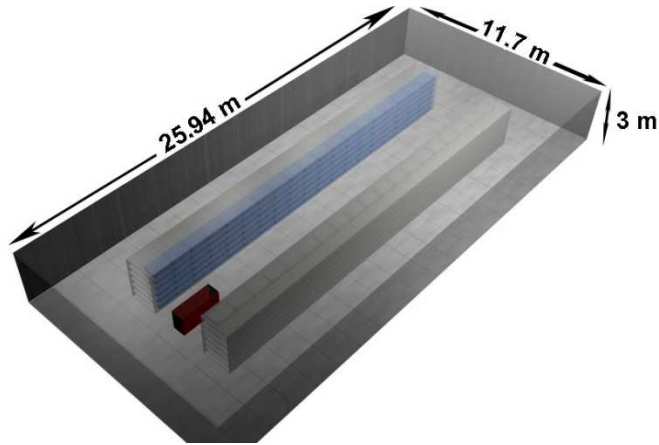


**Figure 3.76.** Schematic view of the scenario generated for the 3D ray launching simulations.

The first step was to analyze the impact of the scenario in the physical layer performance of the wireless sensor network nodes. In the literature, radio-propagation within a shopping mall at 1.9 GHz was performed, comparing measurements, estimations by a statistical method and results obtained by a ray tracing algorithm. The work concludes that the ray tracing method is the most adequate in order to analyze the propagation in this kind of environments [Sam97]. In order to characterize the radio channel in the presented scenario, the in-house developed deterministic 3D Ray Launching code has been used. As it is previously shown in this work, this simulation tool has been previously used and validated for the same purpose in different indoor complex environments. The schematic representation of the scenario created for the 3D Ray Launching simulations can be seen in Fig. 3.76. The shopping trolley is represented by a brown parallelepiped and the antenna has been placed at the same position as the transmitter antenna used for measurements (0.4 m height, in the trolley). Table 3.13 shows the configuration of the most relevant parameters used for the simulations of this scenario.

Parameter	Value
Transmitted Power Level	-10 dBm
Frequency	2.4 GHz
Launched Rays resolution	1°
Cuboids size	10cm×10cm×10cm
Max. Reflections permitted	5

**Table 3.13.** Parameter configuration for 3D Ray Launching simulations.

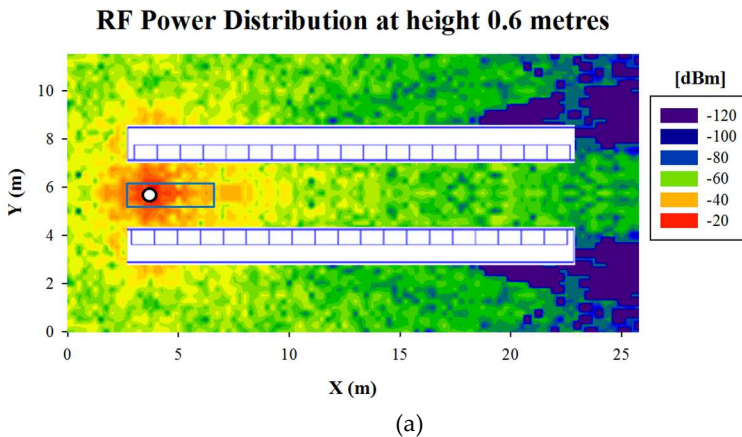
As we know, this 3D Ray Launching simulation tool allows defining the dielectric constant and the conductivity of the materials included in the scenario. As can be seen in Figure 3.75, the left shelves are mainly full of glass jars, and the right shelves have a lot of metallic cans. Therefore, in order to obtain more accurate simulation results, apart from the materials for the floor and walls (concrete), the shelves (aluminum) and the trolley (aluminum), the objects on the shelves have been also defined in accordance with the products found in the real scenario. Table 3.14 shows the main material properties used in the scenario.

Material	Conductivity (S/m)	$\epsilon_r$
Aluminum	$37.8 \times 10^6$	4.5
Glass	0.11	6.06
Concrete	0.02	25

**Table 3.14.** Material properties for 3D Ray Launching simulations.

In order to validate the simulation results obtained by the presented 3D Ray Launching algorithm, 32 different points have been chosen within the scenario under analysis to measure the received power level and compare the obtained values with simulation estimations. The distribution of the 32 measurement points can be seen in Figure 3.75, represented by numbered red dots. As can be seen, they are distributed in two different heights (0.6m and 1.8m) and in both sides of the aisle in order to analyze the effect of different materials on the shelves, as one

side contains mainly glass jars and the other side metallic cans. The measurements have been carried out with the aid of an Agilent CSA N1996A to generate the RF signal and an Agilent FieldFox N9912A portable spectrum analyzer to measure the RF power, both connected to 5dBi monopole antennas. The transmitter antenna has been placed in the trolley, at a height of 0.4m, configured to transmit -10dBm at 2.4GHz. These measurements have been made without the presence of human beings within the scenario. Figure 3.77 shows RF power distribution simulation results for the planes at the heights of the measurement points (0.6m and 1.8m). The transmitter antenna is represented by a white dot inside the trolley. Besides the expected power drop with the increase of the distance (from the transmitter), rapid power variations due to the multipath propagation can be observed. It is also observed how obstacles (shelves) affect the radio-propagation, receiving lower power level behind them.





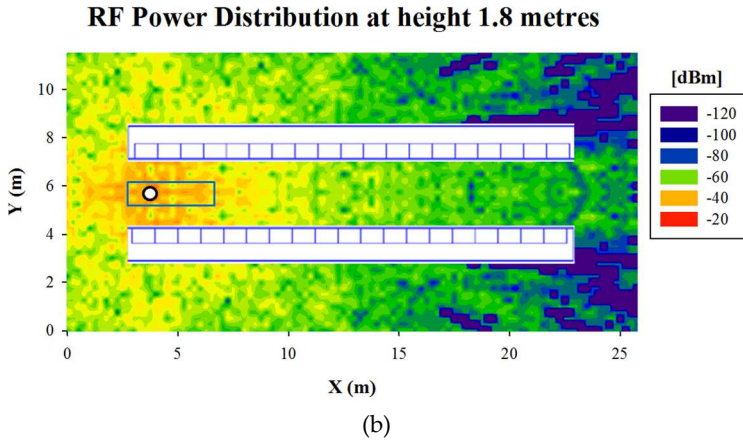
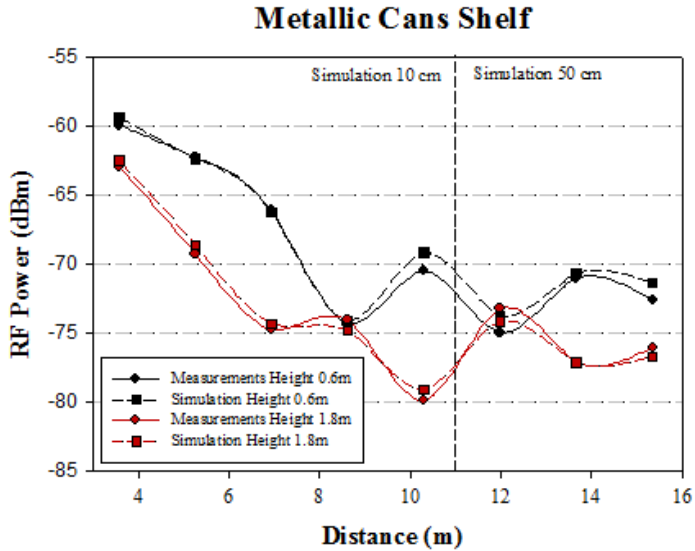


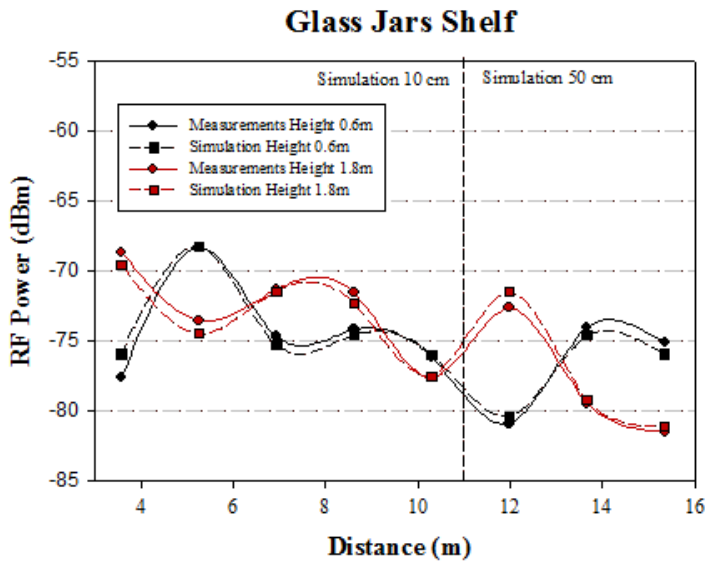
**Figure 3.77.** RF power distribution planes obtained by the 3D Ray Launching method for two different heights: (a) 0.6m and (b) 1.8m.

When the ray launching approximation is used in large scenarios, such as the one presented in this work, divergence takes place. It is directly related with the size of the scenario, the angular resolution of the launched rays and the resolution (cuboids size) set by the user. For small cuboid sizes, large errors occur for big distances, as cuboids without received rays appear. In this scenario under analysis, the divergence phenomenon can be seen for distances larger than 11m approximately. In order to avoid these errors and obtain accurate results, new simulations with lower spatial resolution (higher cuboid size) are required for the mentioned bigger distances. In this case, the new cuboid size was incremented from  $10\text{cm} \times 10\text{cm} \times 10\text{cm}$  to  $50\text{cm} \times 50\text{cm} \times 50\text{cm}$ . The final valid simulation results for both metallic cans and glass jars shelves can be seen in Figure 3.78, where the comparison with measurements is also shown. A vertical dashed line divides the simulation results obtained with cuboids of 10cm and 50cm. In this graphs, the effect of the multipath propagation is more clearly seen, as there are points further which receive lower power levels than closer ones. The results depicted in Figure 3.78 show the validity of the 3D Ray Launching results, with good agreement between measured values and simulation results. The mean error taken into account the 32 measurement points is 0.13 dB, with a standard deviation of 0.72 dB.





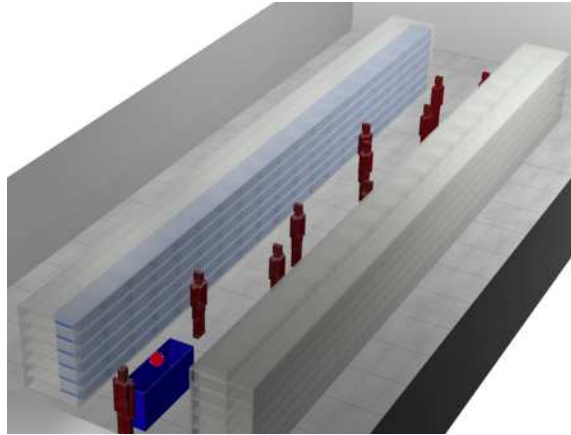
(a)



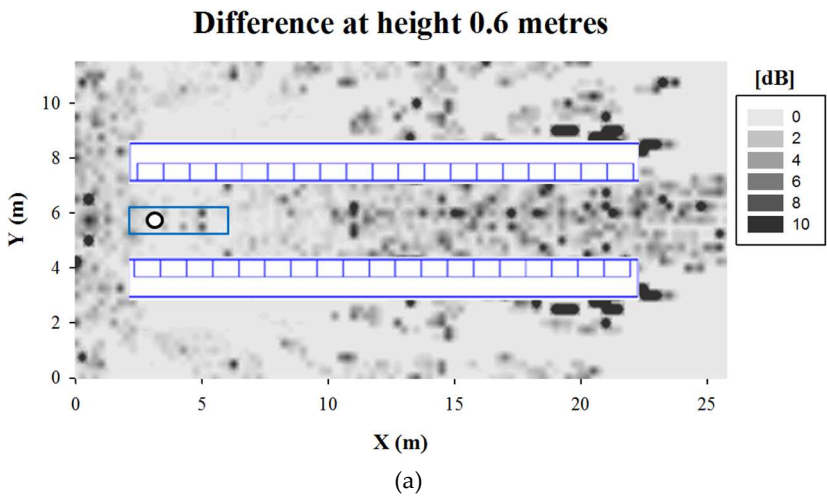
(b)

Figure 3.78. Measurements and 3D Ray Launching simulations results comparison for: (a) Metallic cans shelf and (b) Glass jars shelf.

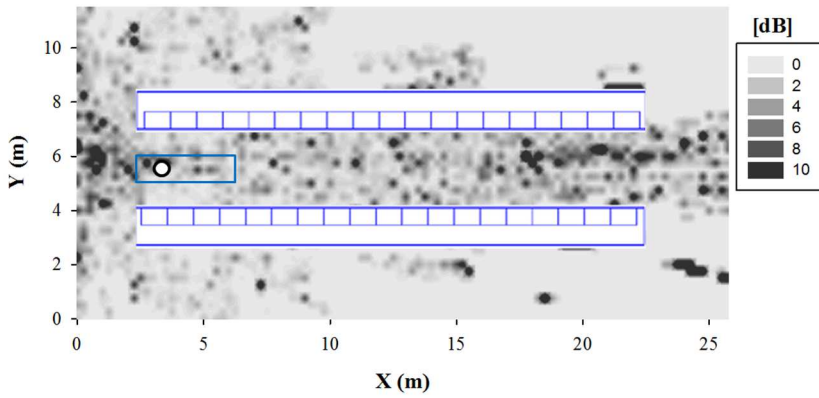
Once the validation of the in-house Ray Launching simulation tool for this kind of scenarios has been done, a new simulation analysis is presented with the aim of studying the presence of human beings, as it is the common situation in this kind of scenarios. Although the number of persons in an aisle of these characteristics varies, for this analysis 10 human beings, all of them adults, were placed randomly throughout the scenario. The used human body model was developed in-house and was previously used and validated [Agu12]. Figure 3.79 shows the schematic representation of the simulated scenario with the person distribution along the aisle. The simulation parameters have been the same that those used in the previous simulations, shown in Table 3.13. In order to show clearly the effect of the presence of persons, in Figure 3.80 the difference between the results with persons and without them is shown, for the planes at heights 0.6m and 1.8m. As expected, the results show that the presence of human beings affect the radio-propagation of the transmitted wireless signal. In some cases, in specific points, the received power level when 10 users are included in the simulation is very close to the value of the case without persons. In other points, the power level difference can be up to 10dB approximately, but in most of the cases it is of a few dB. In order to gain more insight, in Figure 3.81 the comparison between the simulation results without persons and with persons for the 32 measurement points is presented. Specifically for these 32 points, the mean difference is 0.38dB, with a standard deviation of 2.50dB. Although the received power level difference is small in most cases, it can have a huge impact in the performance of wireless notes in terms of energy efficiency, even more if we consider a bigger density of human beings. Thus, apart from the transmitted power level, which can be controlled by the network designer, there are critical issues such as the presence of people and the morphology of the scenario that could affect critically the received power at the receiver position, whatever it is. Therefore, an in-depth radio-planning analysis is required for this kind of scenarios in order to find an optimal wireless network deployment in terms of cost (reducing the number the wireless notes) and energy efficiency (reducing transmitting energy and data rates).



**Figure 3.79.** Schematic view of the simulated scenario with the presence of 10 human beings.



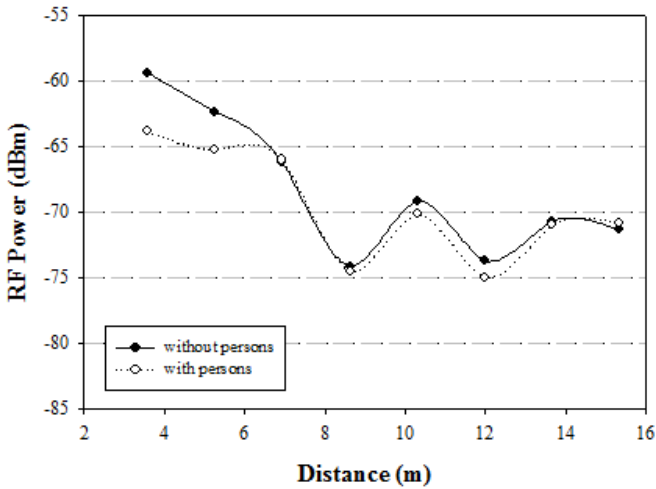
### Difference at height 1.8 metres



(b)

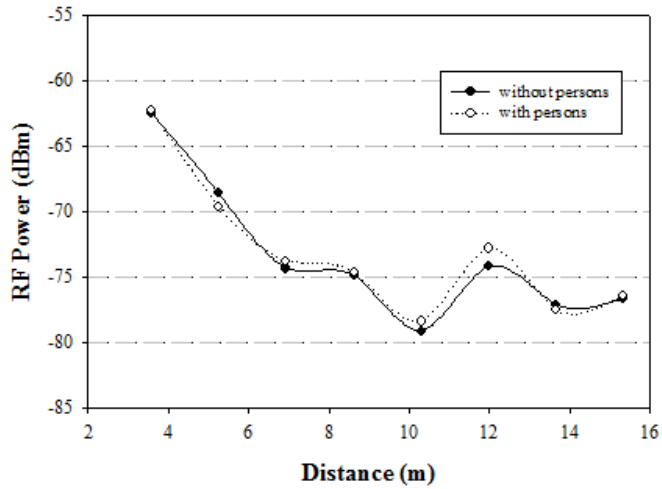
**Figure 3.80.** Received power difference between 3D Ray Launching simulation results with the presence of 10 persons and without persons for the planes at height (a) 0.6m, and (b) 1.8m.

### Simulation results for Metallic Cans at height 0.6m



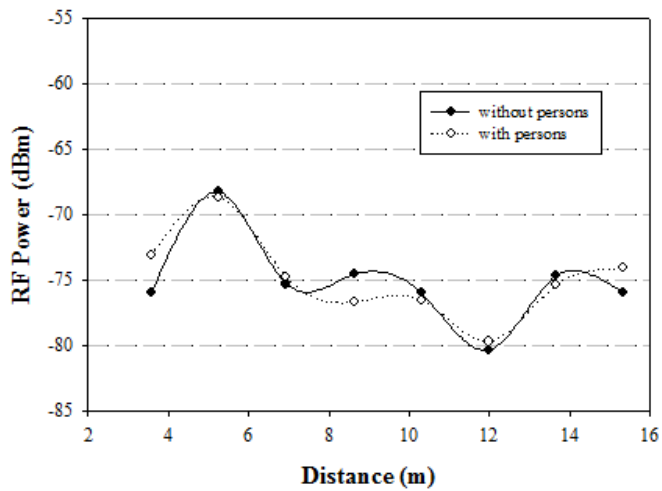
(a)

## Simulation results for Metallic Cans at height 1.8m

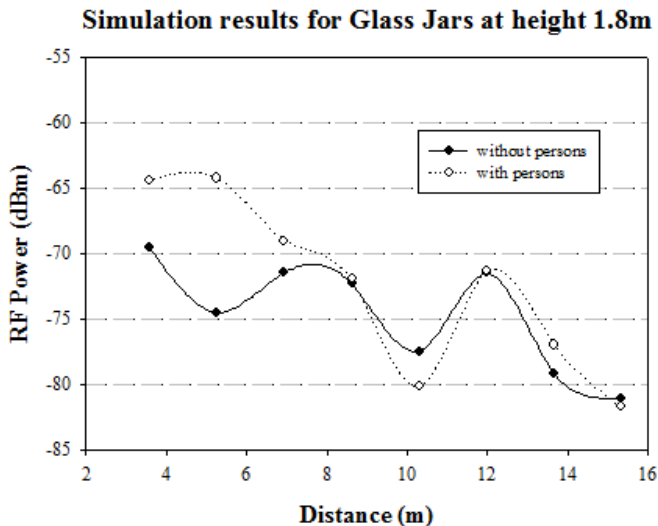


(b)

## Simulation results for Glass Jars at height 0.6m



(c)



(d)

**Figure 3.81.** Comparison between 3D Ray Launching simulation results with the presence of 10 persons and without persons for points at (a) Metallic cans shelf at height 0.6m, (b) Metallic cans shelf at height 1.8m, (c) Glass jars shelf at height 0.6m and (d) Glass jars shelf at height 1.8m.

The simulation results presented in the previous section show the relevance of the layout of the scenario under analysis in the RF power distribution and therefore the potential deployment of WSNs. As one of the main issues when deploying WSNs is the optimization of power consumption and therefore the lifetime of wireless nodes [Tan15][Tya15], a wireless node deployment analysis based on experimental results within the scenario under analysis is presented. Due to the performance in terms of unit cost, power consumption and spectrum availability, IEEE 802.15.4 based devices have been employed for the measurements. Specifically, a wireless system based on Waspnode nodes embedded on trolleys forming a WSN has been deployed. Acting as gateway of the WSN, a Meshlium device (Linux-based router) has been used (also placed on the trolley). Each Waspnode node manages, at least, one RFID transceiver, which obtains the code of each of the products introduced on the trolley and transmits them to the Meshlium gateway. The used Meshlium device supports

four different radio interfaces: WiFi 2.4GHz, WiFi 5GHz, Bluetooth and XBee (i.e. ZigBee-compliant). Figure 3.82 shows the real devices used on the development of the system.

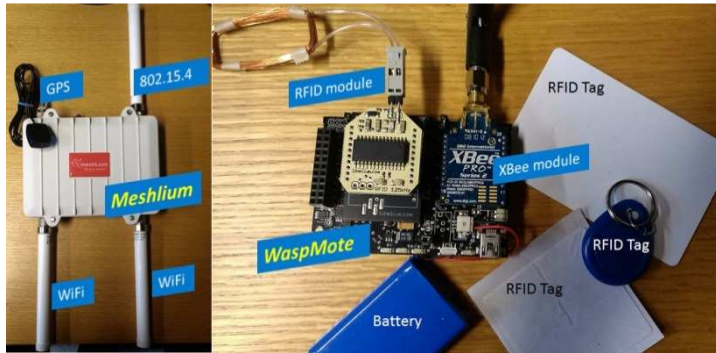


**Figure 3.82.** Hardware used.

The considered WSN includes the placement of sensors equipped with RFID readers on the shelves in addition to those inside the trolleys. Sensors located on the shelves aggregate the information of the detected tags along the mall's aisles. The last node of each aisle will transmit the aggregated information to the central node for its integration into the logistic system of the company (ERP). The goal of this network is to conduct the inventory, which can be performed as a periodic pre-scheduled task, or on demand. Since the detection of many elements (cans, bottles, boxes...) could produce an overload in the network, this activity should be performed during mall's downtime periods (opening and/or closing of the mall, or during the stock replacement process).

On the other side, sensors located inside the trolley (their number and location depends on the size and material of the trolley) are devoted to determine what items have been placed inside the trolley. The key issue will be to discriminate between those products located inside or outside the trolley. The proper location of RFID transceivers and the proper selection of the number of sensors and their coverage areas will allow minimizing the rate of false positives (i.e. item inside the trolley). Figure 3.83 shows the proposed communication schema,

where the nodes placed inside the trolley and the sink nodes of each aisle communicate directly with the central node of the system via WiFi connection, while the rest of nodes communicate among them using IEEE 802.15.4. The nodes located inside the trolley can also communicate with the nodes located on the shelves in order to provide user localization. According to the nodes reachable by the trolley, the system could infer the localization of the trolley.

Two different network topologies of nodes within the scenario under analysis have been studied: linear and zigzag (see Figure 3.84). Each network consists on seven nodes, and a gateway (GW) in charge of data collection on a laptop. Both networks imply the transmission of messages from node  $i$  to node  $i+1$  following a linear or zigzag chain. Communication starts at node 1 and ends at the GW. More than 23,000 iterations (i.e. information sent from node 1 to GW) have been performed, where 98.627% and 99.670% of the iterations are successfully achieved for the linear and zigzag configurations, respectively. Figure 3.85 shows the variation of the RSSI values measured on each node. Nodes #2 and #3 present high variations between the maximum and minimum values for both topologies, while the linear schema also presents a high variation on node #7. It can be also seen that lower RSSI values have been measured for the linear configuration, which get worse as we approach the end of the chain. In fact, Nodes 7 and GW are to blame for 60% of losses for the linear topology. On the other hand, zigzag configuration provides its worst performance at node 3, which is where one third of the total losses happen.



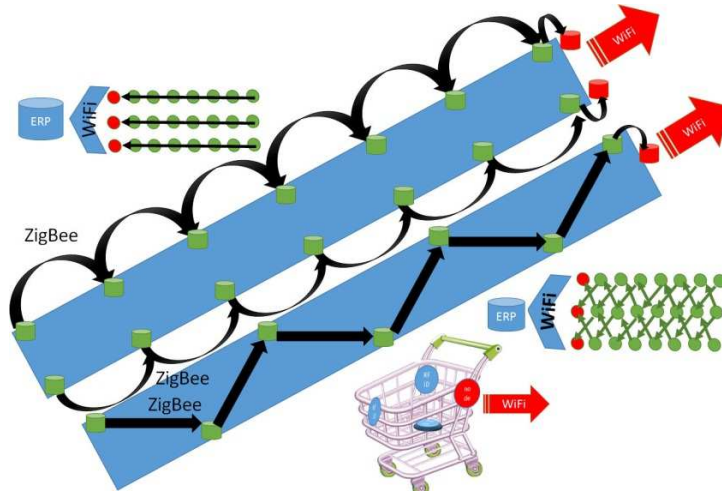


**Figure 3.83.** Communication schema. The trolley includes a Waspote node (in red) with three different RFID transceivers (in blue) and a WiFi transceiver.

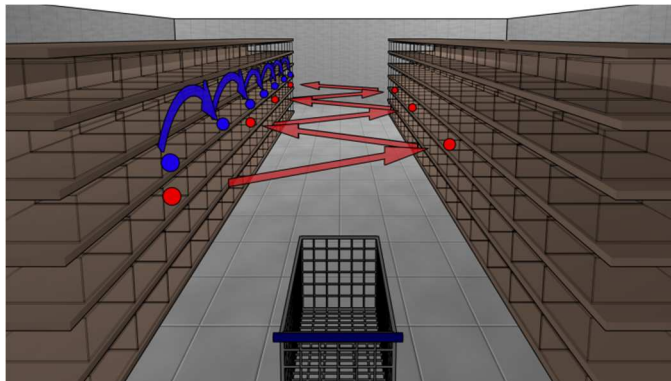


**Figure 3.84.** Node distribution for the linear configuration (blue) and zigzag configuration (red).

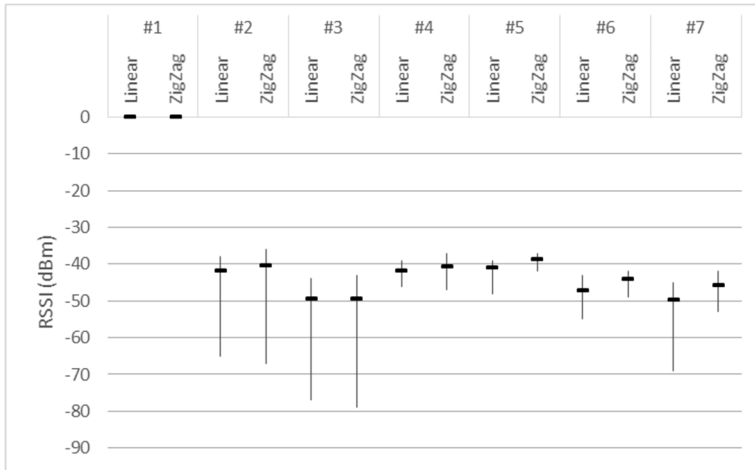


**Figure 3.85.** RSSI variation. Maximum, average and minimum RSSI values measured on each node for both linear and zigzag configurations.

In order to get insight on the performance of the network, Figure 3.86 illustrates the average power consumption by iteration of each node. Message loss along the chain means that the number of iterations successfully accomplished is lower than this of the iterations initiated. The linear configuration involves higher power consumption, ranging from the 76% of node #4 to the 154% of node #6, than that required by the zigzag. The average power saving obtained when using the zigzag configuration is up to 122%. Taking into account the relevance of minimizing energy consumption for the aim of extending the lifetime of the WSN, the zigzag configuration is clearly advantageous within the scenario under analysis.

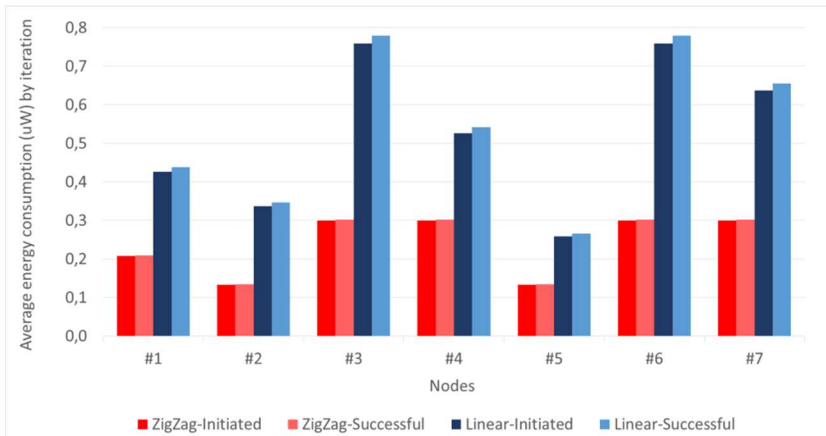


**Figure 3.86.** Average power consumption by iteration, node and topology.

Summarizing the presented results, a Context Aware environment for large commercial areas has been implemented and tested by means of combining WSN nodes to shopping carts and infrastructure nodes. In order to validate system functionality, intensive wireless channel analysis has been performed with the aid of the 3D Ray Launching simulation tool and measurements within a real commercial area environment, where the inherent complexity given by the presence of multiple obstacles and by the inclusion of users within the scenario has been taken into account. The proposed system can be adapted and scaled in order to operate in a wide range of commercial environments. The proposed solution is capable of enhancing user shopping experience with new functionalities, such as indoor guidance, real time cart inventory or location based product alert, as well as providing valuable consumer analysis information to commercial operators in terms of marketing trends as well as optimized logistical and stock procedures.

### 3.2.6 Smart City environments

After using and validating the in-house 3D Ray Launching algorithm in many different environments, in this last subsection an approximation to Smart City environments is presented, as the increasing number of wireless devices and the development of IoT, Intelligent Transportation Systems and s-Health provision, among others, make the radio propagation analysis in this kind of environments necessary and attractive.

But the radio propagation analysis of Smart City environments by means of the 3D Ray Launching method is a challenge due to the big size of the scenarios and the huge amount of elements that can be present, which can lead to high computational costs and problems like ray divergence.

As a first step, a set of buildings has been defined by the 3D Ray Launching, including the existence of indoor dwellings, in order to analyze the performance of wireless systems within a dense urban scenario. This scenario comprises a set of six buildings, each of them with a height of 5 floors. Each building has several flats, with their corresponding indoor distribution of walls, doors and windows. Complete material parameter characteristics have been included for each structural element in order to take into account the possible impact of material choices in the different dwellings. A graphical representation of this scenario is shown in Figure 3.87, in which a constant distribution of buildings can be seen. Note, however, that other configurations could also be implemented if necessary.

The simulation parameters used for the setup are given in Table 3.15. The frequency of operation has been set at 2.4GHz in order to consider multiple wireless systems, such as IEEE 802.15.4 body area networks / personal area networks or IEEE 802.11 Wi-Fi networks, although this frequency can be modified to consider any required frequency band of interest.

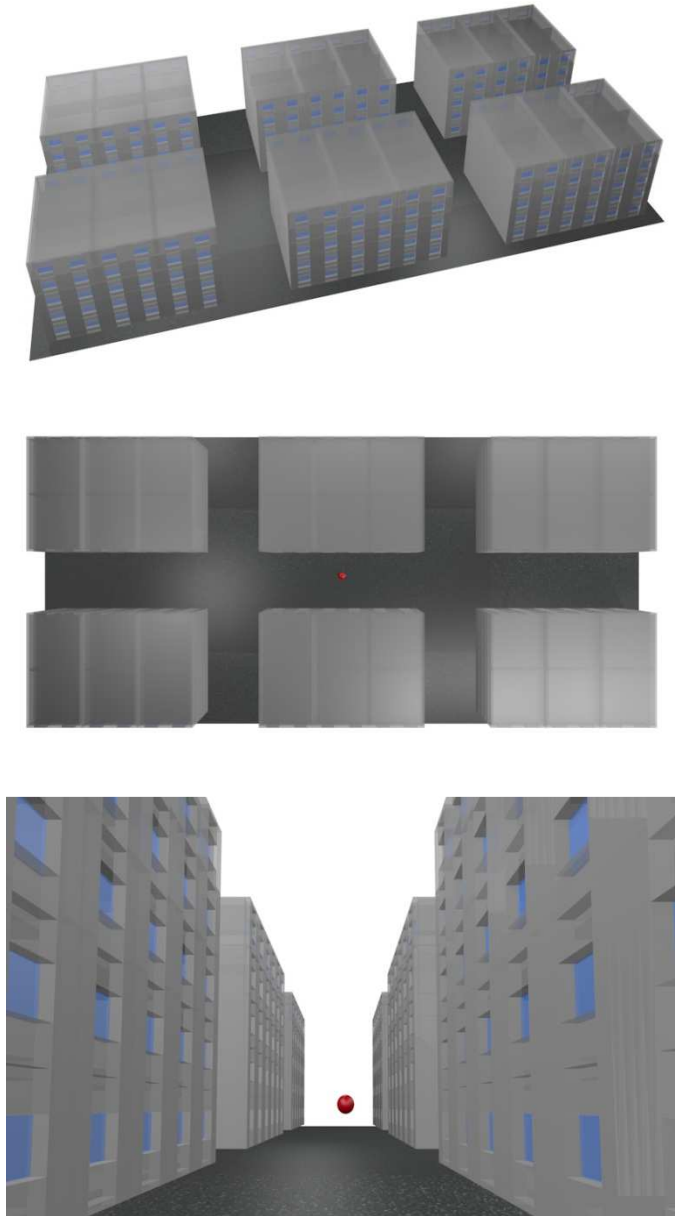


**Figure 3.87.** Simulation scenario representing a section of a dense urban environment, from different visual angles.

Parameter	Value
Transmitted Power Level	30 dBm
Frequency	2.4 GHz
Launched Rays resolution	1°
Max. Reflections permitted	6

**Table 3.15.** Parameter configuration for 3D Ray Launching simulations.

Once the scenario has been implemented, potential transceivers can be located within it in order to emulate wireless communication links and assess the radio propagation. An initial approximation has been taken, placing a transmitter in the center of the scenario (represented by a red point in Figure 3.87). The simulation results have been obtained for the complete volume of the scenario. As an example, bi-dimensional RF power planes are depicted in Figure 3.88 (horizontal cut planes) and Figure 3.89 (vertical cut planes). The inset in Figure 3.89 shows the cutting plane position (represented by red lines). As can be observed, RF power distribution depends on the position within the scenario, where the multipath components due to the interaction with the surrounding elements have a strong influence on the received power level. From these results, RF signal loss values can be obtained, including indoor coverage from a hot-spot located in the street.

Due to the urbanization process that is taking place worldwide, smart cities are gaining importance and the information and communication infrastructures in which they rely have become essential. Those infrastructures have an enormous potential and could be used to improve the mentioned systems provided to citizens such as healthcare, waste management, energy efficiency and intelligent transportation. However, the deployment of these complex communication infrastructures requires deep analysis of their interactions and interferences with the already deployed systems.

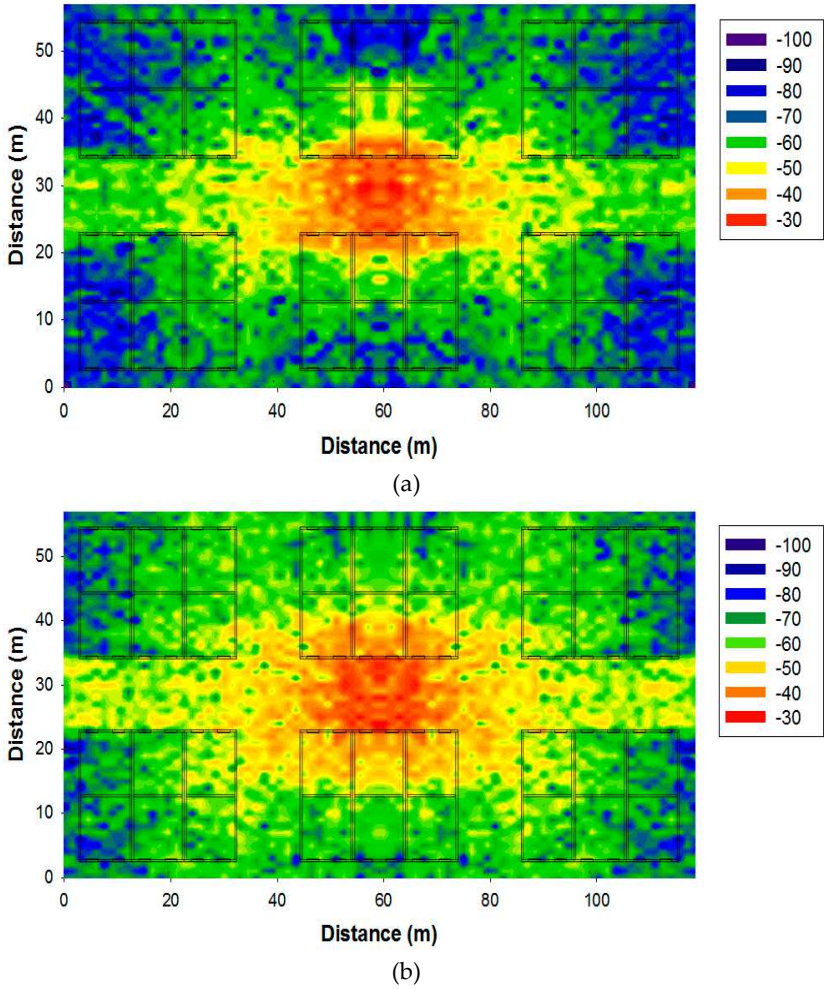


**Figure 3.88.** Received Power Levels (dBm) for the Urban Scenario at different horizontal cut planes: (a) height = 1m, (b) height = 3m.



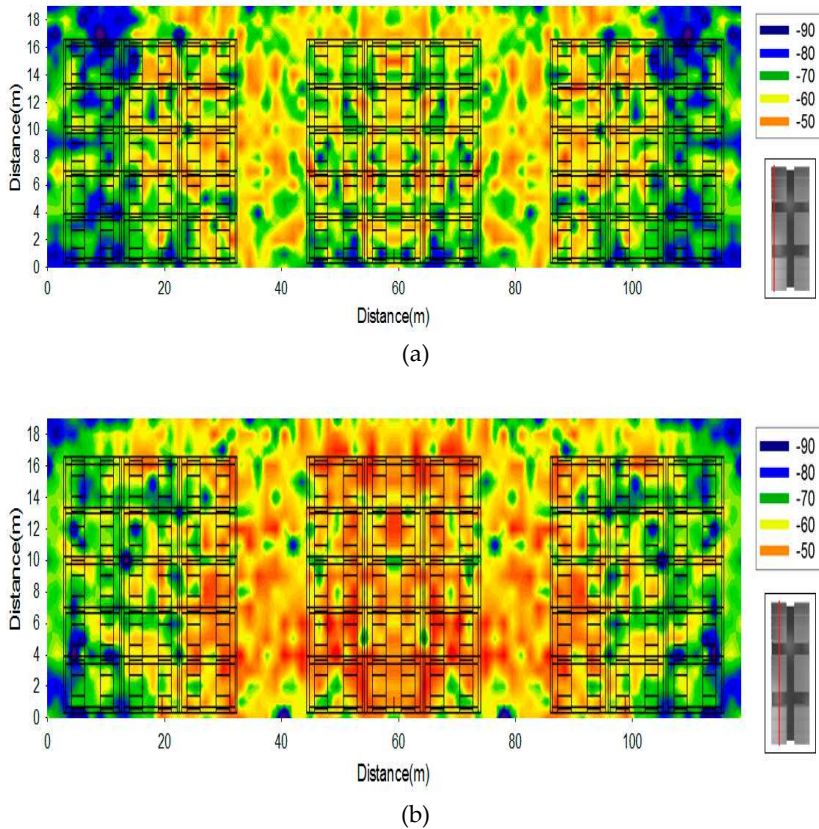


**Figure 3.89.** Received Power Levels (dBm) for the Urban Scenario at different vertical cut planes: (a)  $y = 8\text{m}$ , (b)  $y = 14\text{m}$ .

In order to gain insight in these communication systems within Smart City environments, more realistic scenarios have been analyzed. Due to the relevance that traffic control has acquired in recent years and the growing use of wireless networks in vehicular environments, the following studied scenarios are within the frame of Intelligent Transportation Systems (ITS).

In the past two decades, the number of vehicles circulating in cities has increased considerably. This fact, together with the tendency of citizens to cluster has caused congestion of roads and junctions,



especially in cities with large populations. The existing infrastructures have become inefficient to optimize traffic. The traditional traffic control system based on traffic lights depending on preset date and time patterns is not efficient in reducing waiting times and energy consumption. In fact, simulations show that adaptive traffic control based on information from Wireless Sensor Networks (WSNs) can be improved by 65% in normal traffic conditions compared to traffic management by preset patterns [Abd11]. Since the nineties, there has been extensive research looking for different solutions for ITS, with the aim of improving and performing traffic management. ITS consist of vehicle-to-vehicle (V2V) and vehicle-to-infrastructure (V2I) wireless communications links, contributing to safety improvements and environmentally friendly driving. The ITS road infrastructure has the potential to enhance road safety by helping drivers avoid collisions during basic maneuvers, changing lanes, merging on highways, and driving safely in blind turns. The first implemented ITS were based on counting vehicles through magnetic sensors or artificial vision systems. However, these systems were not completely efficient because line of sight conditions must be fulfilled. Magnetometers sensors based on the detection of magnetic fields on the road lanes have been used to detect the presence of vehicles. These sensors can detect the number of vehicles and their speed, and send their data to the nearest Intersection Control Agent (ICA), which determines the flow model of the intersection depending on sensors' data, using ZigBee technology [Tub07][Fuq09]. For the network architecture, there have been several proposals, ranging from a two sensors architecture [Tub08][Zho10] to several sensors with an ad-hoc network [Kom14][Baa14].

In the past few years, due to the advancement of wireless communications systems, there are new possibilities to manage traffic based on vehicle communications, which make it easier and more accurate than traditional approaches of detecting and counting vehicles. By adding short-range wireless communication capabilities to vehicles, the vehicles can form mobile ad-hoc networks. These are referred to in the literature as Vehicular Ad-Hoc Networks (VANETs). Traffic safety is the main focus of current research on VANETs and the

main motivation of deploying this technology making it ubiquitous. However, there are a number of other applications that could improve the way we drive today. In the future, the main goal for vehicles is to gather sensor data and share information on traffic dynamics with each other and with the road infrastructure.

Traffic lights are regarded as one of the most effective ways to alleviate traffic congestion. However, traditional traffic lights cannot meet the challenges in traffic regulation posed by the fast growing number of vehicles and increasing complexity of road conditions. Because of that, there are many works in the literature that deal with this problem. The work presented in [Gra07] designs an adaptive traffic light system based on short-range wireless communication between vehicles, showing clear benefits compared to adaptive systems based on sensors or cameras. In reference [Alk08], an intelligent dynamic traffic light sequence using radio frequency identification (RFID), which avoids problems that usually arise with standard traffic control systems, especially those related to image processing and beam interruption techniques is described. In [Ais14], a new real-time traffic monitoring is proposed, based on a cluster V2X traffic data collection mechanism, which is able to gather more than 99% of the available data and reduce the overhead to one quarter when compared to other approaches. An intelligent traffic control system to pass emergency vehicles smoothly based on RFID and ZigBee technologies is presented in [Sun14]. In [Ere13], a ZigBee-based wireless system is also presented to assist traffic flow on arterial urban roads. The work proposed in [Shi15] describes a dynamic traffic regulation method based on virtual traffic light for VANETs. The results demonstrate the viability of their solution in reducing waiting time and improving the traffic efficiency.

The operation of WSN is clearly dependent upon having adequate signal levels at the distributed nodes. When designing any wireless network, a significant issue to be considered is the maximum distance between two nodes that still ensures a reliable wireless connection. This depends on a broad range of parameters such as the transmitter power, the receiver sensitivity, the signal propagation environment, the signal frequency and the antennas parameters. In addition, the main challenge

for vehicular communications is the rapidly changing radio propagation conditions. Both the transmitter and the receiver can be mobile, and the scattering environment can rapidly change. Due to this fact, the proper design of a WSN for use in these kinds of environments could be a very challenging process [Ber15]. There are several papers in the literature that present WSN placement optimization mechanisms: In [Sin13] a mechanism for deploying a minimum number of sensors to cover all targets that are randomly placed in a grid environment is presented. Reference [Hua15] proposed a node deployment strategy for blindness avoiding in WSNs on the basis of ant colony optimization. The paper [Lin15] investigates the problem of minimizing the total cost of deploying roadside units and sensor nodes along the two sides and the median island of a two-lane road to cover the whole road, and to form a connected VANET-sensor network. Reference [Xio15] provides analytical modeling for IEEE 802.15.4-compliant WSN in vehicular communications, as well as guide design decisions and tradeoffs for WSN-based VANET applications. In [Ye15], a numerical functional extreme model is proposed for searching the minimum exposure path in WSNs with a hybrid genetic algorithm. Reference [Wan16] also proposes an addressing-based routing optimization scheme for IPv6 over low-power wireless personal area network in vehicular scenarios.

Regarding the wireless communication channel modeling, the geometry-based stochastic models are the most widely used models for propagation prediction in mobile communication channels like V2X communications [Zem12][Bor13][Pat14][Wal14]. However, these approaches do not consider all the elements of the environment, and therefore, they could fail in specific situations when the surroundings have a great impact on the electromagnetic propagation, such as a complex intersection in a large city, which could have vegetation, different type of scatterers including different types of traffic lights, buildings, walking citizens, urban furniture, etc. In order to avoid some of these limitations, the in-house 3D Ray Launching algorithm has been used to assess the radio propagation within this kind of environments, pursuing the characterization of the physical channel for radio planning purposes in urban areas.

As first approximation to vehicular communications in urban areas, the sub-urban scenario depicted in Figure 3.90 has been simulated, where streetlights and trees are placed on the sidewalks. A transmitter antenna (represented by a red point) has been placed on a streetlight, transmitting 0dBm. A car model has been also included for the simulations, located on the road. The obtained RF power distribution is presented in Figure 3.91. Although the scenario has a great percentage of its volume empty, i.e. without obstacles, in Figure 3.91 the typical received power variations due to multipath propagation can be seen. Figure 3.92 shows the estimated PDP at the center of the scenario, where indeed the multipath propagation also has an impact on the radio propagation in this kind of environments.

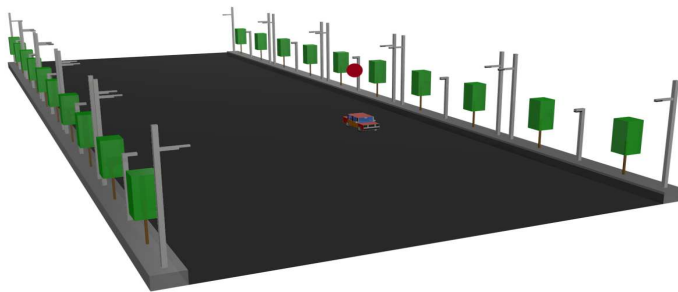


Figure 3.90. Schematic representation of the sub-urban scenario.

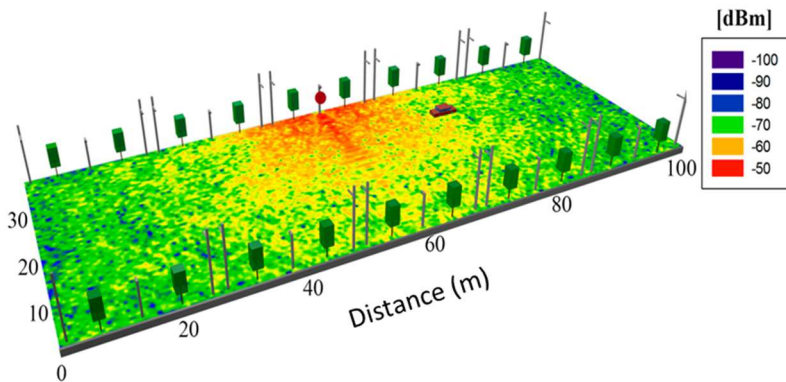
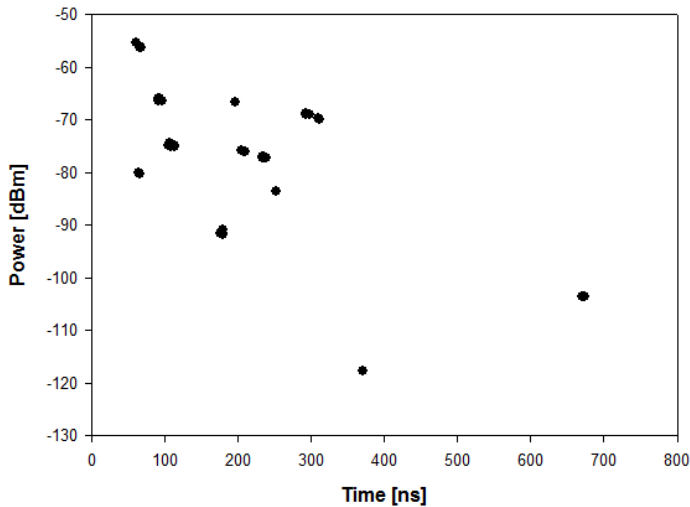
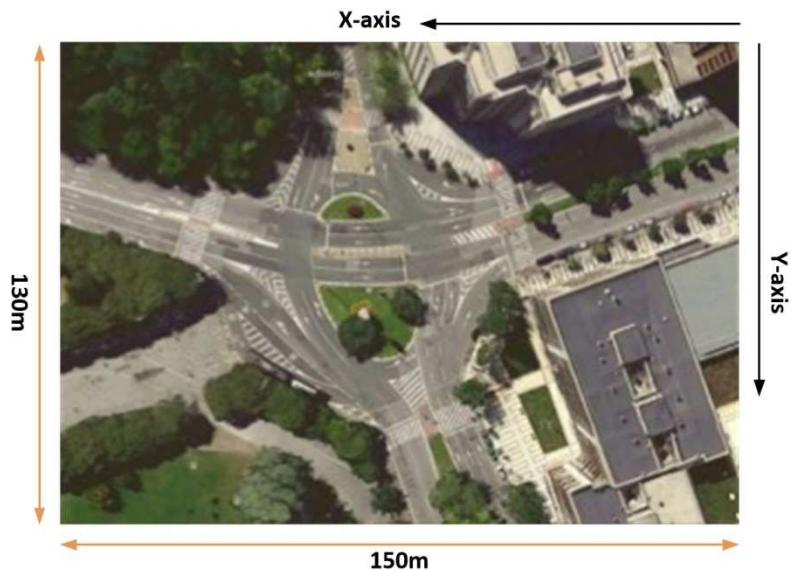


Figure 3.91. 2D map of the received power level for the sub-urban scenario at 1m height.

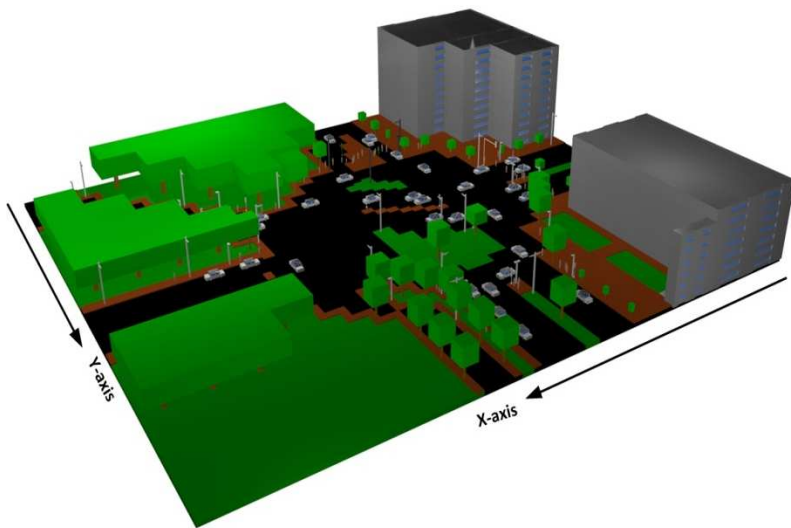


**Figure 3.92.** Estimation of the Power Delay Profile at the center location of the sub-urban scenario.

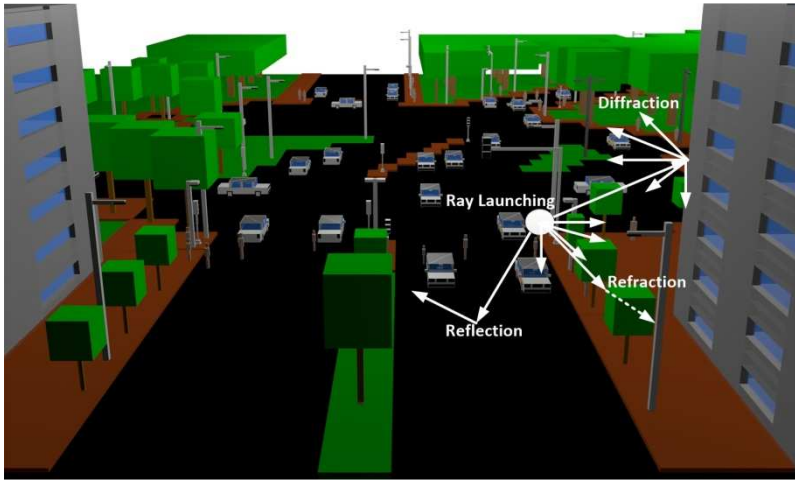
Now, a real and more complex urban scenario is presented in order to assess the usefulness of the 3D Ray Launching method for the radio propagation analysis within urban environments. The considered scenario is an urban area placed near the old town of Pamplona (in Navarre). The dimensions of the scenario are (150m × 130m × 30m) and it contains several buildings, trees of different heights, grass, road junctions, traffic lights, cars, streetlights and people on street. Figure 3.93 shows the real scenario and different views of the created scenario for the simulations. All the material properties for all the elements within the scenarios have been considered, given the dielectric constant and the loss tangent at the frequency range of operation. Taking into account that radio wave propagation in this scenario could change depending on the weather, it is relevant to consider different conditions for the material properties of the vegetation. For that purpose, the values for the material properties of the wood and the foliage have been obtained in [Azp14b]. The previously presented and used human body model and car model have been included in the scenario. The material parameters used in the simulation are defined in Table 3.16.



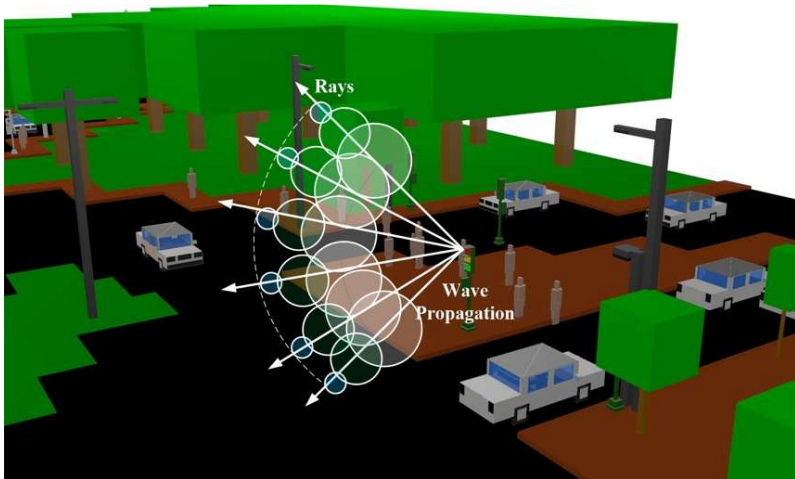
(a)



(b)



(c)



(d)

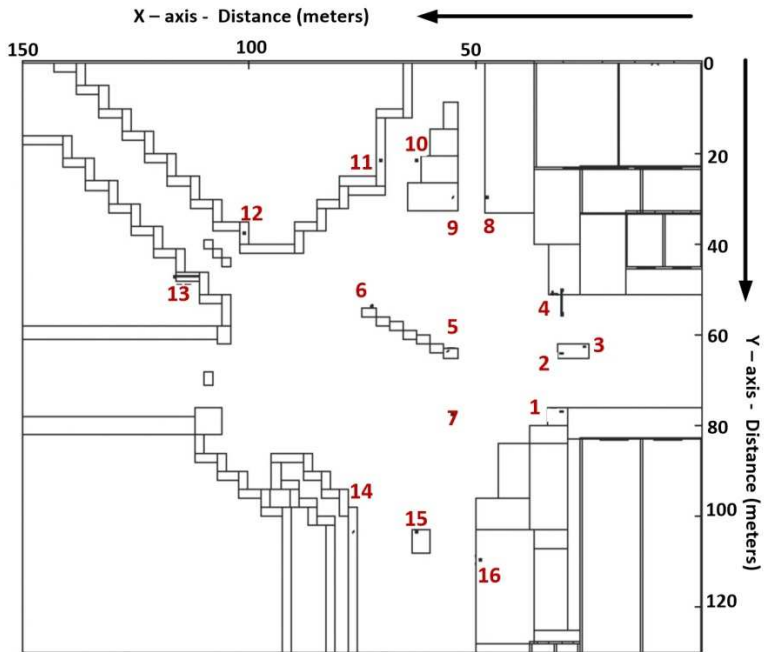
**Figure 3.93.** Real urban scenario under analysis (a), and different views of the created scenario for simulations in the 3D Ray Launching Algorithm.

Material	$\epsilon_r$	Conductivity (S/m)
Air	1	0
Aluminum	4.5	$4 \times 10^7$
Concrete	25	0.02
Polypropylene	3	0.11
Brick	4.44	0.11
Glass	6.06	$10^{-12}$
Plasterboard	2.02	0
Grass	30	0.01
Trunk Tree	[Azp14b]	[Azp14b]
Tree foliage	[Azp14b]	[Azp14b]

**Table 3.16.** Material properties for 3D Ray Launching simulations of the urban scenario.

Once the simulation scenario has been defined, simulation results have been obtained. For the simulations, 16 antennas have been placed throughout the considered scenario, one for each traffic light present within the scenario, since such wireless system could obtain information in relation with pedestrian behavior (e.g., density of users in pedestrian crossings, pedestrian speed or incidentals in pedestrian movement), vehicle behavior or ambient information, among others. The specific position of the antennas within the scenario is shown in the schematic view of Figure 3.94. Each antenna has been placed 10 cm above each traffic light. The radiating element has been configured with the parameters of a wireless ZigBee mote, transmitting 18 dBm at 2.41 GHz. The used simulation parameters are shown in Table 3.17. Figure 3.95 and Figure 3.96 show the RF power distribution within the considered scenario for different heights and planes, and for transmitters placed on different traffic lights. As it can be seen, the influence of the obstacles (like the trees, streetlights, buildings, etc.) as well as the topology of the potential wireless transceivers has a noticeable impact on the radio wave propagation.

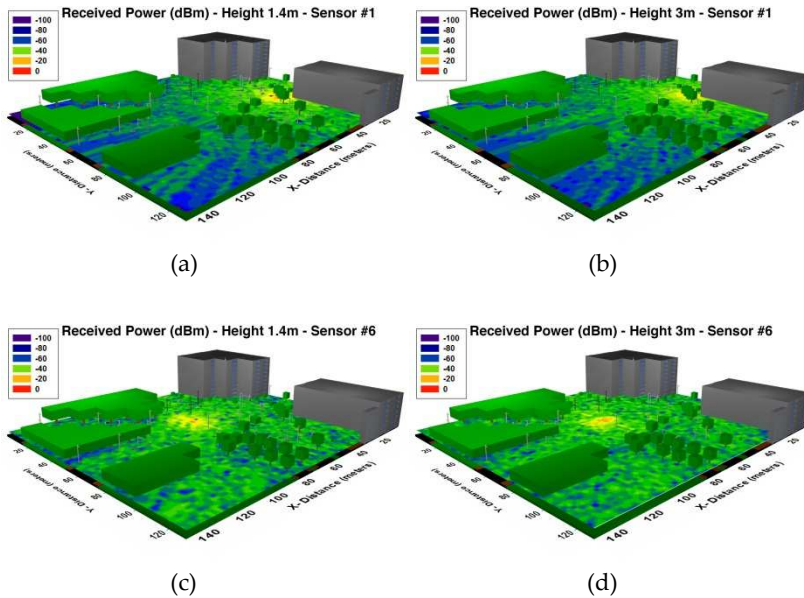




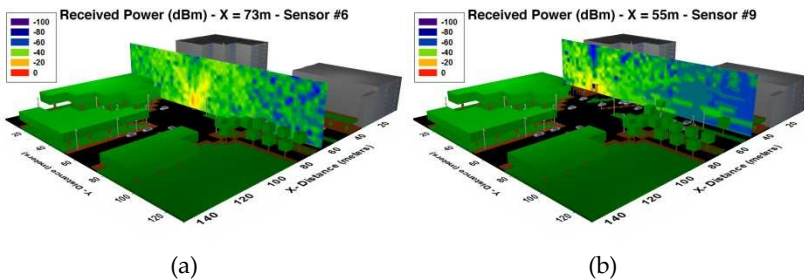
**Figure 3.94.** Schematic view of the position of the 16 antennas within the considered scenario.

Parameter	Value
Transmitted Power Level	18 dBm
Frequency	2.41 GHz
Launched Rays resolution	2°
Max. Reflections permitted	6
Cuboids size	2m × 2m × 2m

**Table 3.17.** 3D Ray Launching simulation parameters.

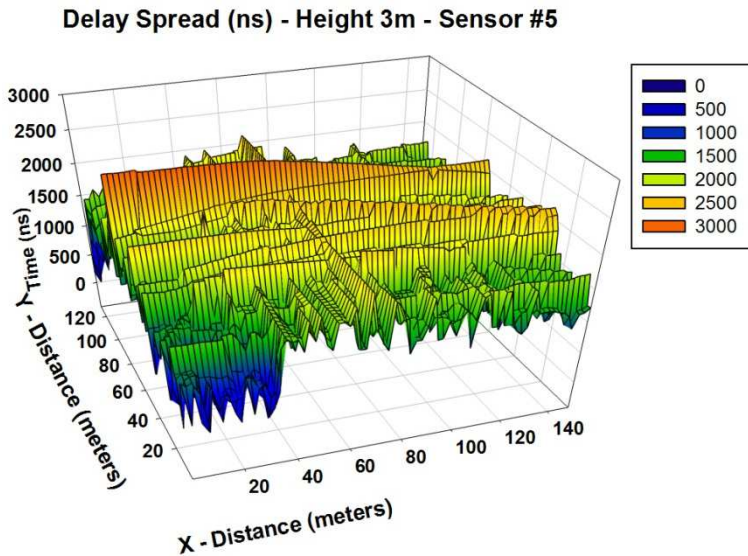


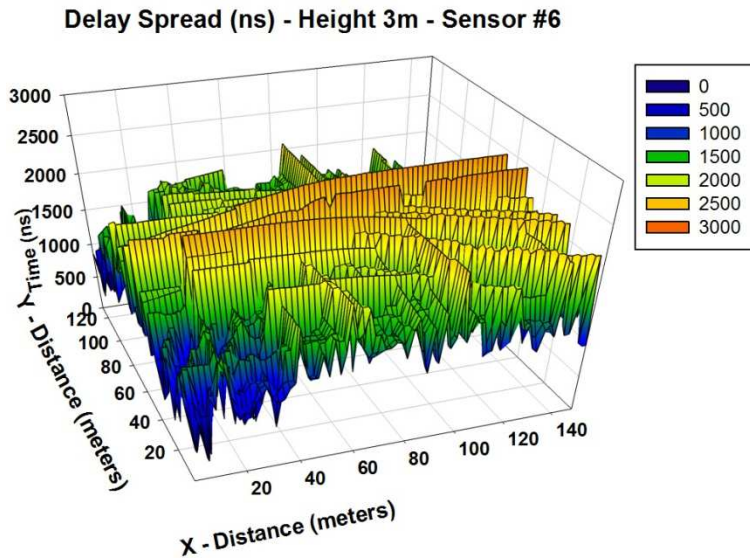
**Figure 3.95.** Bi-dimensional RF power distribution estimations (dBm) within the considered scenario for different heights: (a) 1.4 m height for antenna #1; (b) 3 m height for antenna #1; (c) 1.4 m height for antenna #6; (d) 3 m height for antenna #6.



**Figure 3.96.** Bi-dimensional RF power distribution estimations (dBm) within the considered scenario for different X-axis distances: (a) X = 73 m for antenna #6; (b) X = 55 m for antenna #9.

As it has been previously shown in the sub-urban scenario of Figure 3.90, the multipath propagation plays a significant role within this kind of environments. To illustrate this fact, the Delay Spread for the whole scenario of Figure 3.93 is shown in Figure 3.97. The Delay Spread has been defined as the time delay between the first and the last ray which arrives to each spatial point. It has been calculated using as threshold the sensitivity value of the XBee Pro transceivers, which is  $-100$  dBm. As expected, it can be observed how the Delay Spread is higher in the areas closest to the transmitter antenna and it is lower in other areas due to the larger distances. Additionally, each spatial sample of the Delay Spread is associated with a Power Delay Profile. As an example, in Figure 3.98 the Power Delay Profile at the central position of the scenario is depicted. These results show that the scenario is complex in terms of multipath propagation, even being an outdoor environment, which make the 3D Ray Launching algorithm a really useful tool for radio planning strategies when deploying wireless systems within urban environments.





(b)

**Figure 3.97.** Estimated Delay Spread (ns) at a plane of 3m height for different positions of the transmitter antenna (a) antenna #5; (b) antenna #6.

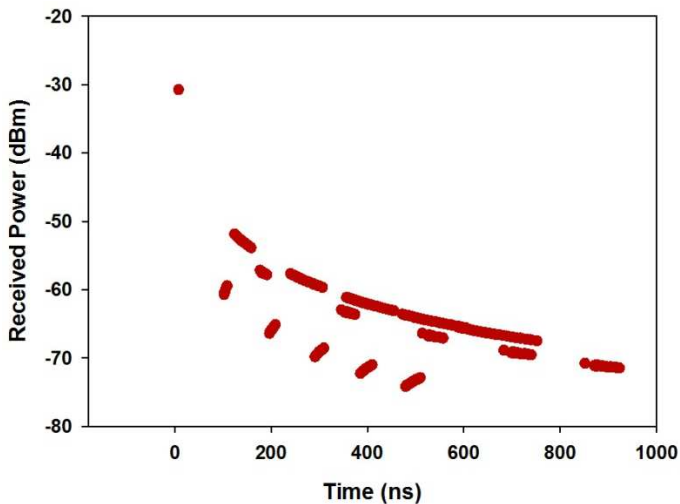


**Figure 3.98.** Power Delay Profile at a central location within the urban scenario.

In order to validate the results obtained by the 3D Ray Launching tool, measurements in the real urban scenario under analysis have been carried out. A transmitter antenna, connected to a signal generator at both 2.41 GHz and 5.9 GHz has been located at coordinates ( $X = 31\text{m}$ ,  $Y = 76.8\text{m}$ ,  $Z = 2.05\text{m}$ ), just above the traffic light #1 (see Figure 3.94). The employed signal generator has been a portable N1996A (Agilent Technologies, Santa Clara, CA, USA) unit and the spectrum analyzer has been an Agilent N9912 Field Fox. The omnidirectional antennas used have been the model ACA-4HSRPP-2458 from Zentri (Los Gatos, CA, USA), which have a gain of 0.3 dBi at 2.41 GHz and a gain of 3.74 dBi at 5.9 GHz. The measurement points are depicted in Figure 3.99 as red numbers, which are 5m away from each other, and all of them at a height of 1.4m.

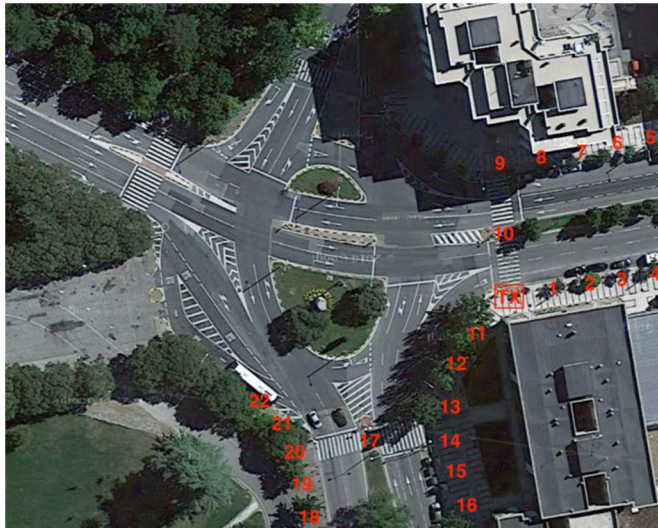


**Figure 3.99.** View of the urban scenario with the transmitter location ('TX') and the measurement points (red numbers).

Before the measurements, in order to see the possible influence of pre-existent interferences in the scenario, a spectrogram has been measured with the aid of the Agilent N9912 Field Fox portable spectrum analyzer. Figure 3.100 shows the measured spectrogram at the transmitter position, for both frequencies in Max Hold mode. It can

be seen that there are not significant pre-existent interferences at the frequency bands of interest (note that the higher value of the scale is -80 dBm). It is worth noting that the noise floor is slightly higher at 5.9 GHz frequency band due to the fact that the gain of the antenna at 5.9 GHz is 3.44 dB higher than at 2.41 GHz.

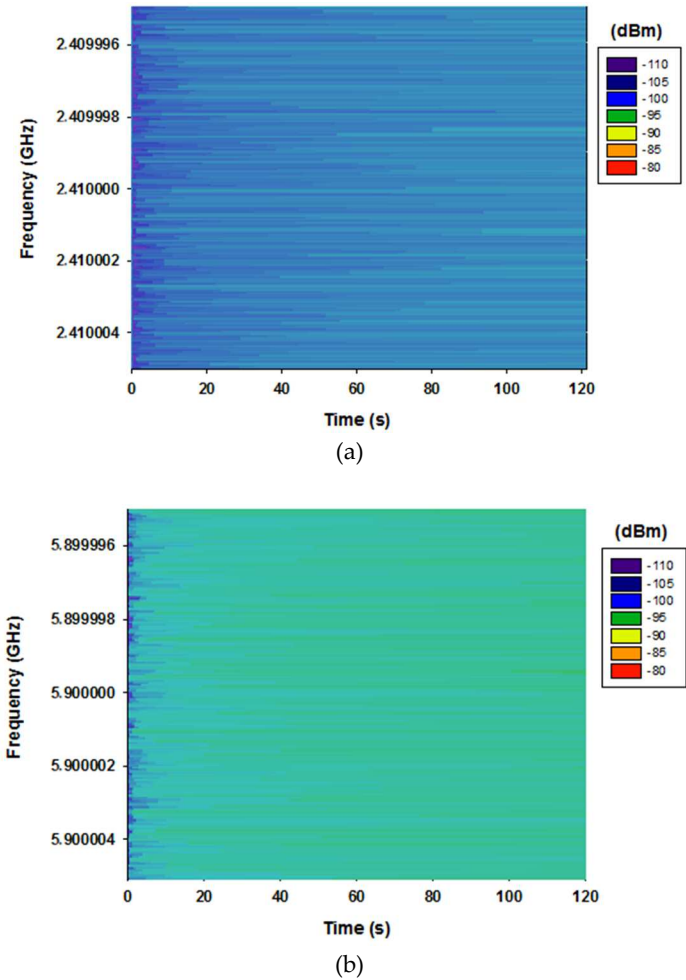
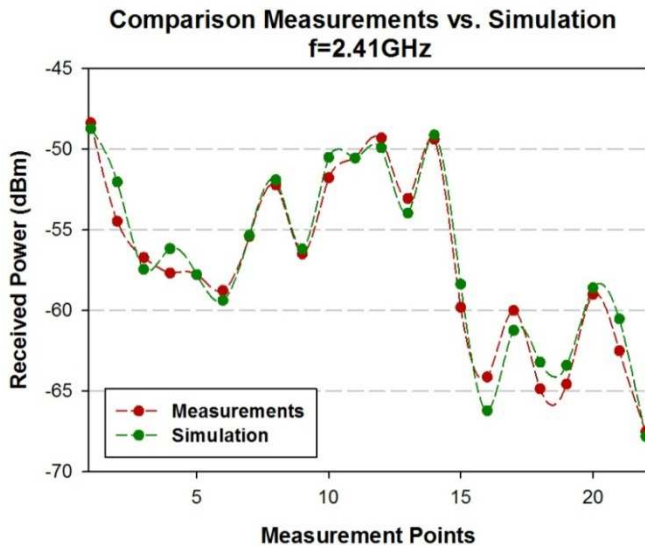


Figure 3.100. Measured spectrogram at (a) 2.41 GHz, and (b) 5.9 GHz band.

Finally, as it has been made for the rest of environments, Figure 3.101 shows the comparison between simulation and measurement results for both operation frequencies. The previously used spectrum analyzer has been used for measure the received power. The measurement time at each point has been 60s and a bandwidth of 100 MHz has been set in the spectrum analyzer for both 2.41 GHz and 5.9 GHz frequencies. The value of received power at each point is the highest peak of power shown by the spectrum analyzer (with MaxHold function activated). The received power values estimated by simulation have been obtained for the same points as the real measurements, considering the corresponding cuboid in the three-dimensional mesh of cuboids in which the scenario have been divided. As it can be observed in Figure 3.101, there is good agreement between simulation and measurement results. Specifically, a mean error of 0.27 dBm with a standard deviation of 1.13 dB has been obtained for 2.41 GHz frequency, and a mean error of 0.66 dBm with a standard deviation of 1.46 dB for 5.9 GHz frequency. The resulting error means are very low, indicating that the proposed 3D RL simulation method works properly, validating in the same way the previously shown simulation results within this scenario.



(a)



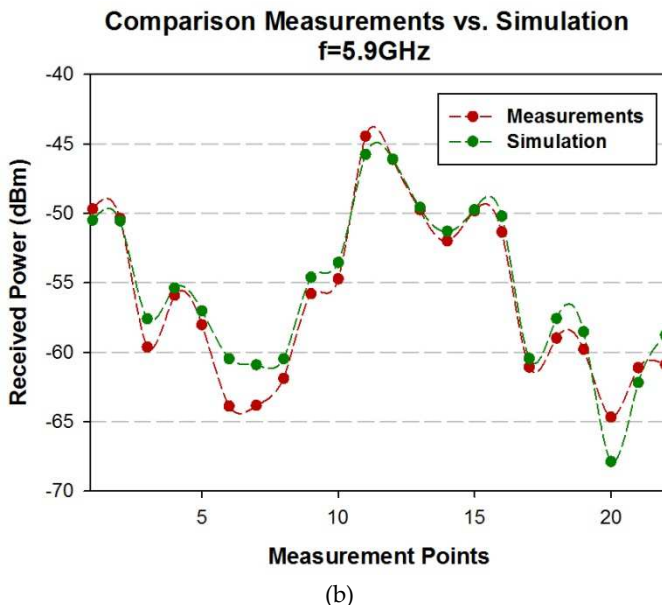


**Figure 3.101.** Comparison simulation vs. measurements for (a) 2.41 GHz and (b) 5.9 GHz in the urban scenario.

### 3.3 Main Contributions

In this last section of Chapter 3, I list only my main contributions (i.e. the articles and conference papers in which I am the first author) regarding the topic covered in this chapter, but as it can be seen in the List of Publications section, I contributed to more works regarding the topic of this section.

Besides, as the published works have been carried out together with other co-authors, I would like to point explicitly what has been my work regarding those published works: My main contributions to the list of publications shown below have been the study of the state of the art, the performance of measurements within the scenarios under analysis, the creation of the scenario for the 3D Ray Launching simulations and the corresponding simulations, the post-processing of the obtained data and the writing of the most of the text of the



manuscripts.

Note that all the research articles have been published in JCR (Journal Citation Reports) indexed journals.

- *Research Articles:*

1. "ZigBee Radio Channel Analysis in a Complex Vehicular Environment," *IEEE Antennas and Propagation Magazine*, vol. 56, no. 4, August 2014.
2. "Radio Characterization for ISM 2.4 GHz Wireless Sensor Networks for Judo Monitoring Applications," *Sensors*, vol. 14, pp. 24004-24028, December 2014.
3. "Implementation of Wireless Sensor Network Architecture for Interactive Shopping Carts to Enable Context Aware Commercial Areas," *IEEE Sensors Journal*, vol. 16, no. 13, July 2016.

- *International Conference Papers:*

1. "Analysis of Topological impact in Wireless Indoor Sensor Networks," (2011 *IEEE AP-S International Symposium on Antennas and Propagation and 2011 USNC/URSI National Radio Science Meeting*).
2. "Radio Characterization for ISM 2.4 GHz Wireless Sensor Networks for Judo Applications," (In *Proceedings of the 1st Int. Elec. Conf. on Sens. and App.*, 1-16 June 2014; *Sciforum Electronic Conference Series*).
3. "Analysis of Vehicular Connectivity in Smart Health Service Provision Scenarios," (*The 7th International Conference on Information, Intelligence, Systems and Applications - IISA 2016*).
4. "Deterministic Radio Propagation Estimations in Judo venues for WSN deployment by 3D Ray Launching Method," accepted in (2017 *IEEE International Symposium on Antennas and Propagation and USNC-URSI National Radio Science Meeting*).

- *National Conference Papers:*
  1. “Análisis del comportamiento de redes de sensores inalámbricos en entornos interiores heterogéneos,” (2011 *URSI XXVI National Symposium*).
  2. “Haririk Gabeko Komunikazio Sistemen Azterketa Ingurune Konplexuetan 3D Ray Launching Metodo Deterministaren bidez,” (*Ikertzaile Euskaldunen I. Nazioarteko Kongresua-IkerGazte* 2015).
  3. “Caracterización de la Banda ISM 2.4 GHz para Aplicaciones de Redes de Sensores Inalámbricas en Entornos de Judo,” (2015 *URSI XXX National Symposium*).
  4. “Sistemas Inalámbricos Heterogéneos como Facilitadores de Entornos Contextuales,” (2015 *URSI XXX National Symposium*).
  5. “Caracterización de Redes de Sensores en Entornos Contextuales Ferroviarios,” (2016 *URSI XXXI National Symposium*).

# Chapter 4

## Deterministic Interference Analysis

**T**HE previous chapter shows the accurate radio propagation results that can be obtained by the aid of the in-house 3D Ray Launching algorithm for many different environments. The presented radio propagation results, mainly the RF power distribution, within specific scenarios are very relevant in terms of the radio planning of WSNs. In fact, the traditional objective of all radio propagation models discussed in Chapter 2 is the estimation of the RF power distribution (or at least at specific points) within a scenario in order to know if a potential receiver would receive enough power to establish a wireless communication with the emitter, which is determined by the sensitivity level of the receiver. Specifically for Ray Launching and Ray Tracing methods, the estimation of RF power level [Ber95][Moy00][Ros02][Deb08][Roc10][Cho13][Shi15a] and equivalent Power Delay Profile channel [Ata13] are calculated. But what happens to the overall performance of a wireless network when other wireless communication systems are operating at the same place and interfere

with each other? This is a problem that is usually overlooked, but extremely important for the upcoming Smart City environments due to the high quantity of wireless communications systems and devices that are expected, such as the advent of IoT and 5G. For this reason, a new point of view regarding the use of radio propagation models is presented in this chapter: Instead of only predicting the received RF power and see if it is higher than the sensitivity level of the wireless devices, the 3D Ray Launching tool has been used for determining optimum device deployment regarding energy consumption, as well as for analyzing the coverage and capacity of the wireless systems. For that purpose, assessing interference levels within the scenarios is a key issue, which has been also carried out with the aid of the 3D Ray Launching tool. Section 4.1 shows the different interference analysis results obtained by means of the 3D Ray Launching method. In Section 4.2 the main contributions to the state of the art regarding those results are cited.

## 4.1 Interference Analysis Results

For a first approximation to the problem, a single interfering source has been placed on an adjacent room of a scenario that had been previously studied (shown in Figure 3.10). The interfering source has been defined just like the transmitter antennas are defined for the 3D Ray Launching simulations. Once the RF power distribution of the interfering source has been obtained, SNR values for the whole volume of the scenario have been calculated, being the Signal level those results obtained for the transmitter antenna (see Figure 3.13) and the Noise level the results obtained for the interfering source. The SNR results for two different heights can be seen in Figure 4.1. As it happens with the RF power distribution, significant variations of SNR value as a function of the position are observed.

The RF power level distribution results give valuable information about the radio propagation in specific and unique scenarios, and allow knowing if the received power level will be above the sensitivity level

of the receivers, which will depend on the specific devices used for the deployment of the WSN. The interference analysis and results presented in this Chapter lead to new assessments in terms of SNR levels, and therefore, achievable data rates, energy consumption and BER values.

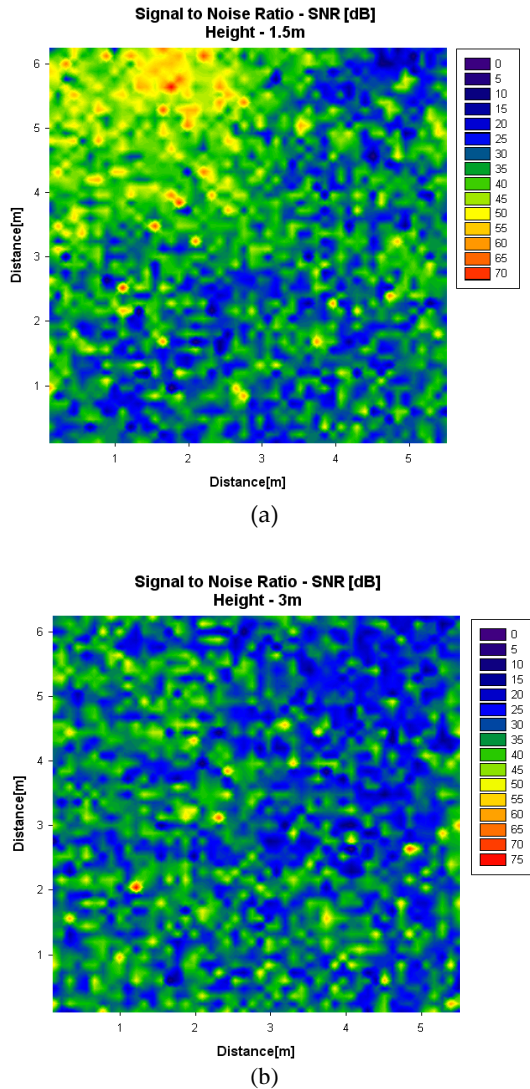


**Figure 4.1.** Spatial distribution of Signal to Noise Ratio estimations for different heights in the indoor scenario of Figure 3.10.

Among these radio planning parameters, minimizing energy consumption has become one of the main goals for the deployment of WSNs, driven by international Green policies. In this context, radio channel features of indoor environments pose a challenge to energy consumption, due to the fact that the complexity of the scenario increases losses due to strong multipath propagation and diffraction, as well as absorption due to lossy dispersive media of the obstacles within it. The existence of interference sources in these complex environments also affects the deployment strategies and the overall power consumption of the WSN.

In order to show how the presented 3D Ray Launching method can aid in this regard, the topological influence of a layout of in-house developed CyFi based wireless sensors have been analyzed in terms of power consumption and radio coverage. For that purpose, a system based on a set of wireless motes has been designed in house by the University of Valencia. Each mote includes sensor/actuator elements, a PSoC processor core, expansion ports and power, and a CyFi transceiver. Depending on the role that the nodes play in the protocol, the motes can be configured as a master or as a slave.

The basic network topology is a star configuration, in which a master node manages a certain number of peripheral slave nodes. Following a hierarchical scheme, different master nodes can be connected at slave-type stages to form a second layer around a master node that is responsible for monitoring the platform. Each mote has two parts: a main card which contains the microcontroller, and an additional one that contains the radio frequency part. The main board consists of different blocks, as shown schematically in Figure 4.2. The real implementation can be seen in Figure 4.3.

The microcontroller is the Cypress CY8C24894 PSoC. It incorporates an 8-bit microcontroller M8C and up to 4 MIPS. As reconfigurable elements, it contains 4 digital blocks and 6 analog blocks, in addition to 1KB of SRAM and 16KB of Flash. Also, the device has the possibility to communicate via USB without requiring any additional items. The humidity and temperature sensor used is an SHT75 model. This is calibrated at the factory, controlled digitally, has high resolution and

accuracy, with an operating range of 0-100% relative humidity and a temperature range between -40°C and 123°C.

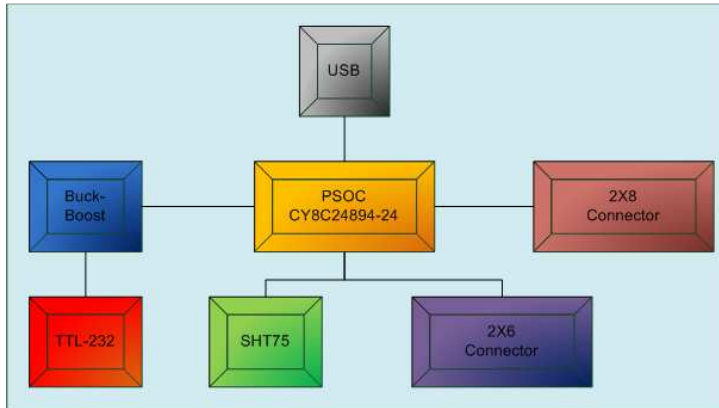


**Figure 4.2.** Block diagram for the implemented mote device.



**Figure 4.3.** Image of the main board (left) and the radio frequency module (right) of the mote device.

The used CyFi technology is a cost effective low-power wireless solution developed by Cypress Semiconductor that operates in the unlicensed 2.4 GHz ISM band, with active link and power management features. The network topology consists in a simple star network

controlled by a central hub. Due to the lightweight network protocol stack of CyFi nodes, a bidirectional communication to up to 250 nodes is provided. CyFi output maximum power is 4 dBm and the receiver sensitivity -97 dBm, with a typical range in a line of sight, interference-free environment between 50 m and 70 m.

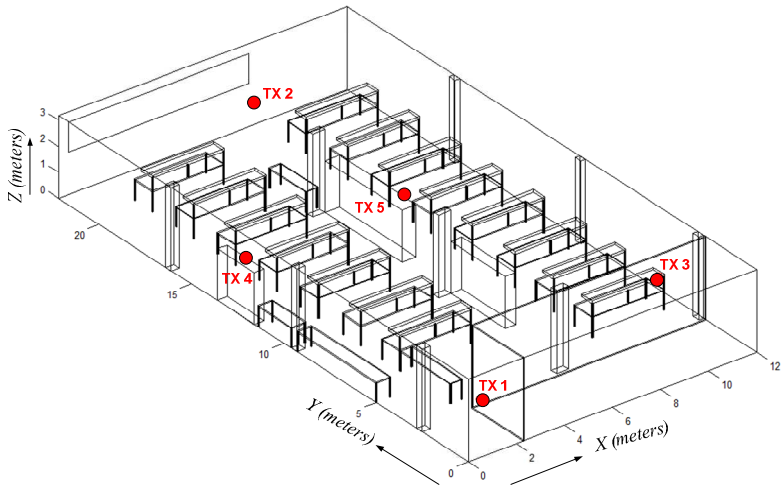
The mentioned active link and power management provide interesting dynamic functionalities. For more robustness, the transmitter changes the modulation and data rates dynamically between 1 Mbps and 250 Kbps depending on the environment's interference. If the interference increases, then the power output level is dynamically increased to overcome that interference. Besides, if a node detects that its power output is excessive, it will dynamically reduce it, reducing power consumption. Also, to ensure that the central hub of the network receives packets correctly, an interference free channel is selected whenever possible. If the hub detects a noisy channel, a CyFi network will look for a clean channel and settle there. The dynamic power handling capability, in terms of coverage/capacity estimation, will lead to smaller coverage radius as overall transmission speed increases, as will be shown in the following paragraphs.

The scenario where the CyFi nodes have been analyzed is the Radio Communication Laboratory, placed in the Electric and Electronic Engineering Department of the Public University of Navarre. The scenario has the inherent complexity of an indoor scenario, as it has interior columns, many furniture elements, different types of instruments and walls made of different materials (wood, concrete, bricks, metal and glass). The scenario can be seen in Figure 4.4a and its schematic representation for the ray launching software can be seen in Figure 4.4b. Red points in Figure 4.4b represent the different points where the wireless nodes have been placed. These positions have been chosen in order to simulate a possible morphology of a real wireless network. For that reason, the nodes have been placed at different heights. The exact coordinates for the nodes are shown in Table 4.1.





(a)



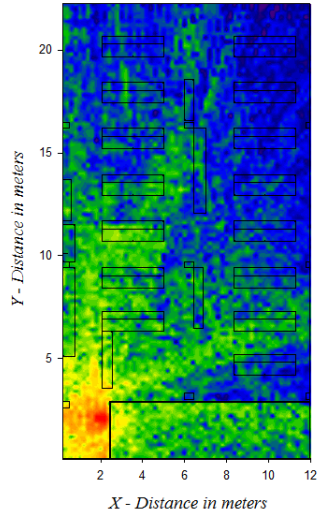
(b)

**Figure 4.4.** (a) Indoor scenario under analysis, corresponding to Radio Communication Laboratory, UPNA. (b) Schematic representation of the scenario in the 3D Ray Launching software.

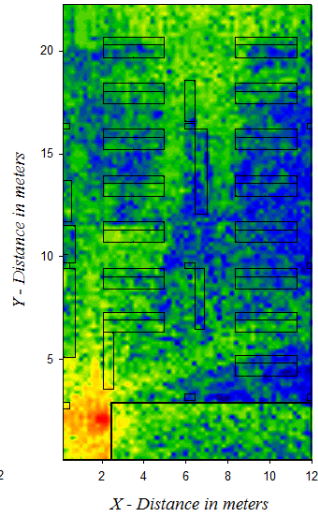
Transmitter	Coordinates
TX1	(2, 2, 0.81)m
TX2	(6.5, 21, 2.7)m
TX3	(11, 4, 1.5)m
TX4	(0.3, 12.5, 2.1)m
TX5	(7, 12.5, 2.1)m

**Table 4.1.** Coordinates where the wireless notes have been placed within the indoor scenario.

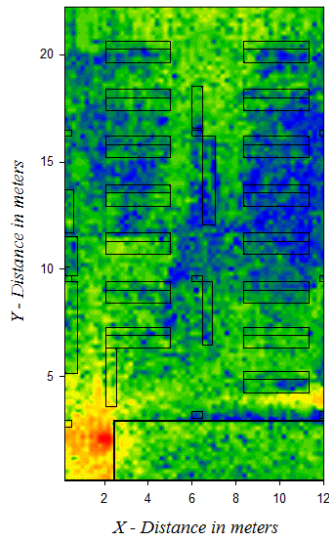
Simulation results have been obtained for the whole volume of the scenario. The parameters used for the simulation have been the following: uniform cuboids resolution of 20cm, vertical plane angle resolution  $\Delta\theta=\pi/180$ , horizontal plane angle resolution  $\Delta\Phi=\pi/180$ , maximum number of tolerated reflections  $N=5$ , frequency of operation 2.4GHz and transmission power of 4dBm (the maximum level achievable by the CyFi notes). The considered parameters regarding the transmitters are equivalent to those of the CyFi mote system. Figure 4.5 shows the obtained received power levels for the same bi-dimensional plane at height 0.81m (the same height of the tables within the laboratory) for different number of transmitters. For each of the represented planes (from Figure 4.5a to Figure 4.5e), a new transmitter has been added consecutively, starting with a single transmitter (Figure 4.5a) and finishing with a wireless network composed by five transmitters (Figure 4.5e).



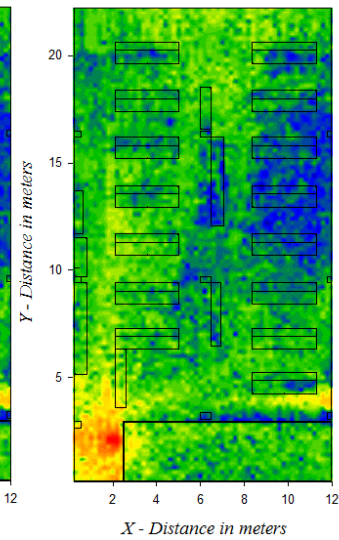
(a)



(b)



(c)



(d)

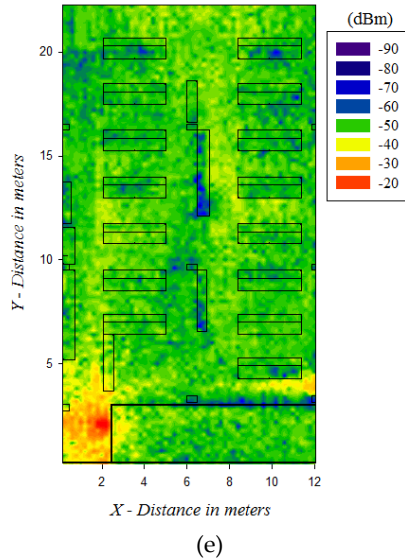


**Figure 4.5.** RF power distribution results obtained at a bi-dimensional plane at a height of 0.81m for different number of transmitters (a) TX1, (b) TX1 and TX2, (c) TX1, TX2 and TX3, (d) TX1, TX2, TX3 and TX4, (e) TX1, TX2, TX3, TX4 and TX5.

As it can be seen from the previous figures, received power level is strongly dependent on the position of the potential receiver element and the morphology of the wireless network. Variations can be in order of 10 dB within 1 meter when the number of transmitters is low, which has a strong impact on the performance of the sensors, not only in terms of receiver sensitivity limits but also on overall system capacity, which is dependent on signal level as well as on signal to noise ratio. As it is shown in Figure 4.5, this received power variations can be strongly mitigated changing the morphology (e.g. adding wireless nodes) of the wireless network, thus obtaining a reasonable received power level for every position of the complete indoor scenario.

The multipath propagation is the strongest phenomenon in this type of complex indoor environments, hence, to appreciate the variability of estimated received power level more precisely, Figure 4.6 shows this variability within a given line path for a fixed value of X for two

different heights in the indoor scenario. The X value has been set to 3.5 m randomly, since this phenomenon happens all alike within the whole scenario. As stated above, the signal variation is driven by strong multipath components, as can be seen from the short term variation component within the received power level. For a more thorough analysis of the impact of the multipath propagation in the scenario, in Figure 4.7 and Figure 4.8 time domain results are shown. Specifically, power delay profiles are presented for the locations of TX2 and TX3 respectively, when TX1 transmits. A red line has been depicted in both graphics to delimit the sensitivity level of the CyFi motes (i.e. -97dBm). As expected, a lot of components reached the TX2 and TX3 points due to the multipath propagation, but in Figure 4.7, which corresponds to the farthest mode of the network (from TX1), there are a lot of components under the sensitivity level, due mainly the distance. On the other hand, in Figure 4.8 most of the components are above the sensitivity level, as it corresponds to the nearest node of the network. In order to complete the time domain results, the delay spread for a plane of 0.81 m height (the height of the tables and TX1) is presented in Figure 4.9.

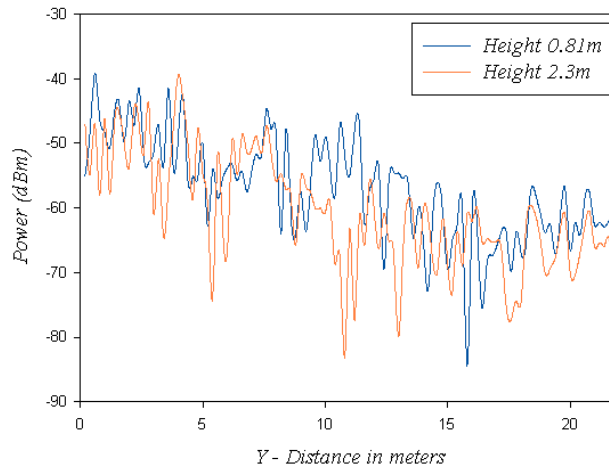


**Figure 4.6.** Simulation results for height 0.81m and height 2.3m, for X=3.5m, along the Y-axis of the indoor scenario under analysis (see Figure 4.4).

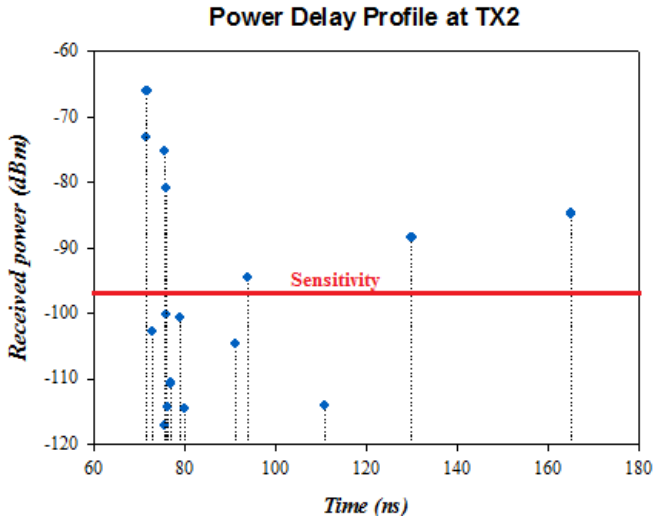


Figure 4.7. Power Delay Profile at location of TX2 (the farthest node), when TX1 is transmitting.

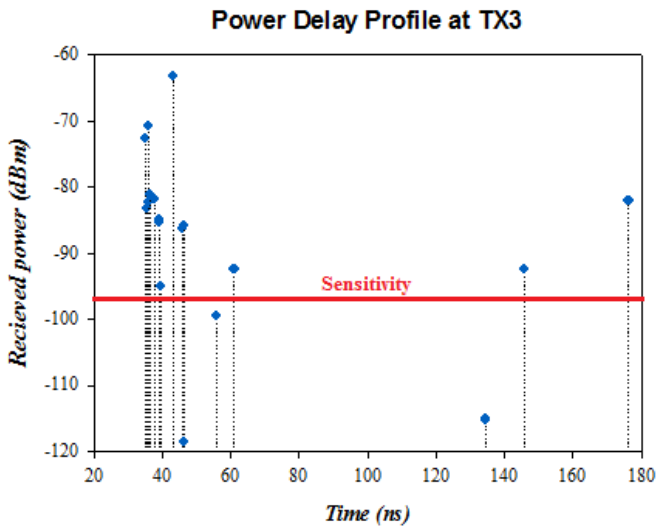
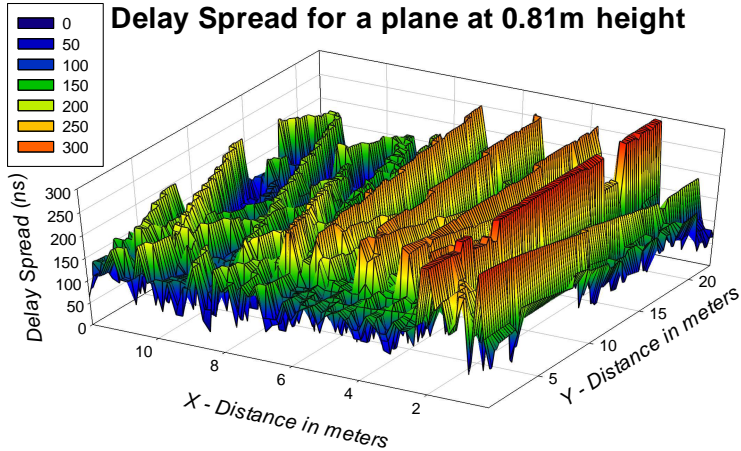


Figure 4.8. Power Delay Profile at location of TX3 (the nearest node), when TX1 is transmitting.



**Figure 4.9.** Delay Spread values for a plane at 0.81 meters height (i.e. the height of TX1 within the scenario).

The obtained simulation results and mainly the estimated values of received power can lead to the analysis of the performance of the wireless system. As an example, Figure 4.11 represents the signal to noise ratio (SNR) for two different heights in the same scenario, which could be used to consider the most adequate deployment strategy of a set of wireless sensor networks within the indoor scenario. Specifically, SNR planes depicted in Figure 4.11 have been calculated taking into account that the whole CyFi network is deployed and as noise sources, an interfering WiFi network (an access point and 3 laptops) operating at the same frequency band of the CyFi motes has been simulated. The simulation parameters have been the same than those used for the simulation of the CyFi motes, but the transmitted power of WiFi nodes has been set to 20 dBm, which corresponds to a typical maximum transmitted power of a commercial device. In Figure 4.10 the schematic configuration of the wireless networks within the scenario is shown. Table 4.2 shows the position within the scenario of the WiFi nodes.

Transmitter	Coordinates
WiFi access point	(3, 3, 2.5)m
Laptop 1	(4.5, 6.9, 0.9)m
Laptop 2	(2, 13.5, 0.9)m
Laptop 3	(8.5, 17.7, 0.9)m

**Table 4.2.** Coordinates where WiFi devices have been placed within the scenario.

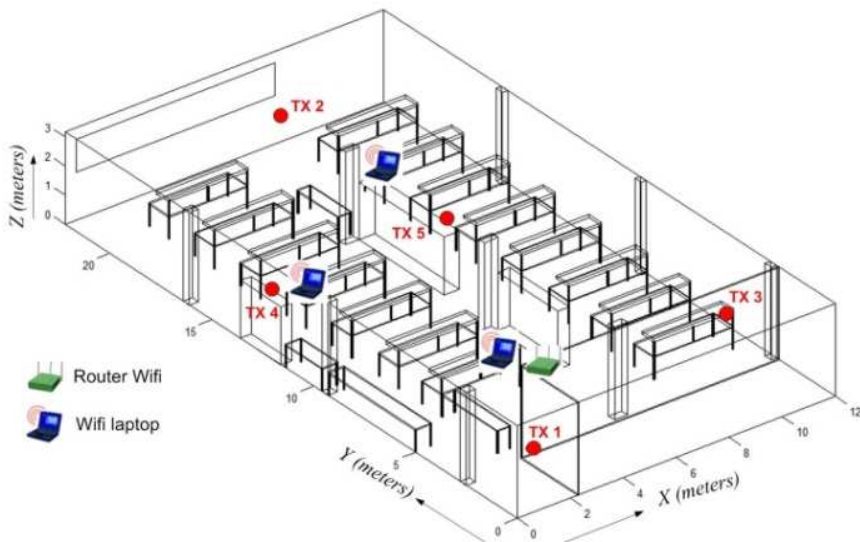


**Figure 4.10.** Schematic representation of the scenario used to calculate the SNR planes of Figure 4.11.



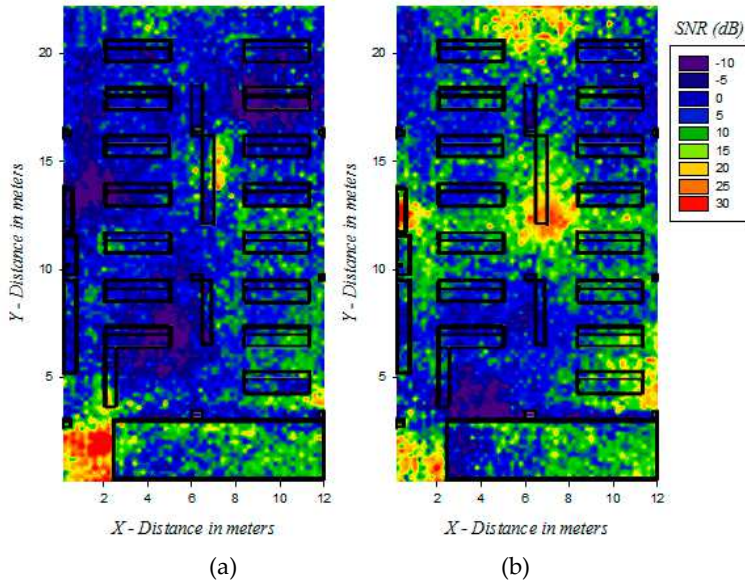


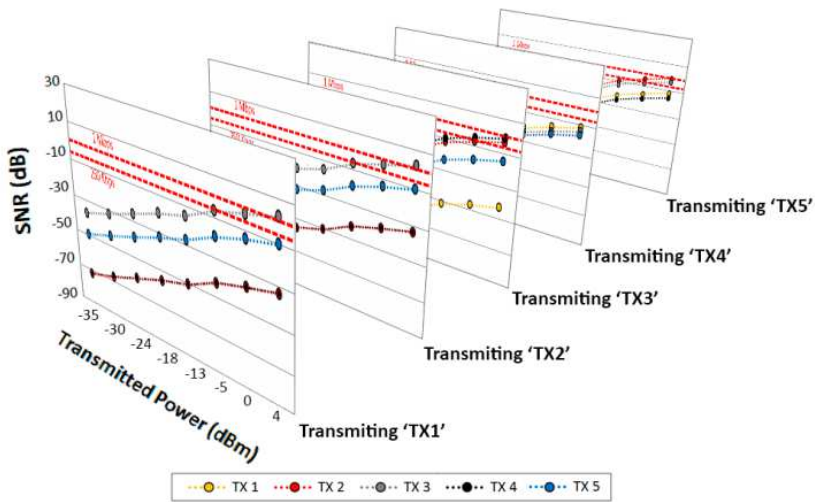
**Figure 4.11.** Spatial distribution of SNR within the indoor scenario for two different heights (a) 0.81 meters, (b) 2.3 meters.

Thus, the SNR value is obtained for each point within the room, giving valuable information about the zones and points where the placement of a mote will be better in terms of received signal quality, whilst maintaining the optimal wireless power transmission (and hence energy consumption) of the system. As can be clearly seen in Figure 4.11, the zones where interfering devices have been placed are the zones with lower SNR, as expected. For a more in-depth analysis of the proposed CyFi network in terms of SNR, in Figure 4.12 the SNR at each receiver CyFi mote is depicted, when a single mote is transmitting. In Table 4.3 the preset transmission power levels for the CyFi motes are shown, which have been used for the calculation of the SNR, in order to show how it affects the SNR at the receiver motes. As the CyFi motes can change dynamically the transmission rate between 1 Mbps and 250 Kbps, the minimum SNR needed has been calculated for both data rates, and these limits have been depicted by red dashed lines (0 dB for 1 Mbps, and -7.23 dB for 250 Kbps). Figure 4.12a shows the results for

the worst noise case, i.e. when the WiFi devices transmit 20 dBm, whilst Figure 4.12b shows the results for WiFi devices transmitting 0 dBm. These results show how the presented method can aid in an adequate deployment strategy within a harsh indoor scenario, which has a direct impact on the network efficiency.

Defined internal level	Transmitted power (dBm)
7	4
6	0
5	-5
4	-13
3	-18
2	-24
1	-30
0	-35

Table 4.3. CyFi motes’ preset levels and their correspondent transmission power level.



(a)

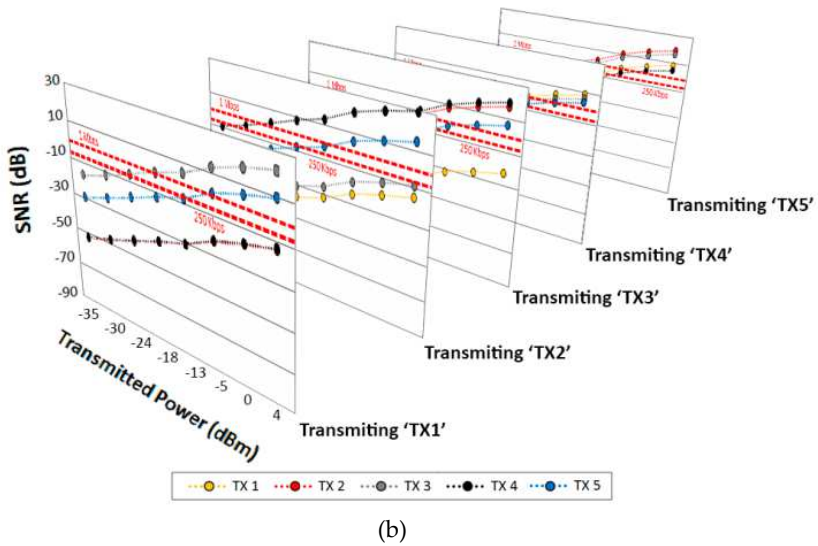
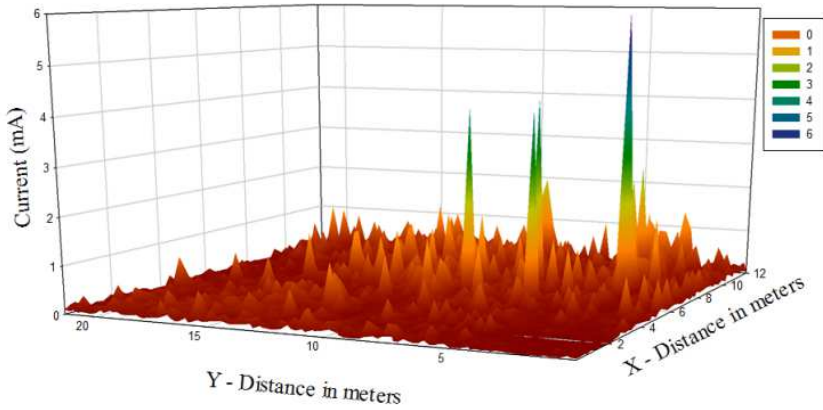


**Figure 4.12.** SNR values at each CyFi mote position for a single transmitting mote, while WiFi-interference sources are transmitting (a) 20 dBm and (b) 0 dBm.

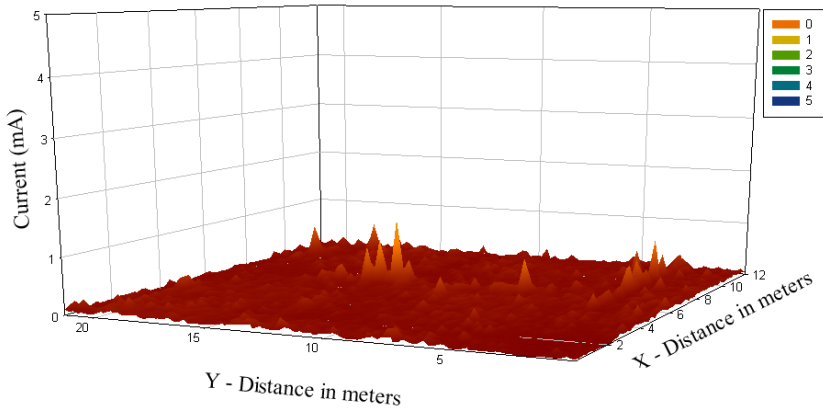
Considering the overall power consumption of the deployed motes is also a highly important issue in radio planning strategies. As it has been shown previously, the location of the transceiver has a significant role in terms of the variations of the expected value of received power within the scenario, which has a great impact on the power consumption of transmitting motes. This is given by the fact that as the received power varies, the link balance within the sensitivity threshold limit also varies, modifying the required current for the transceiver to operate. Therefore, it is possible to estimate energy consumption of the transmitter as a function of the receiver location. In order to gain insight on the effect of topology and morphology on energy consumption in the previous scenario, Figure 4.13 shows the consumption increase maps for two cases (always considering a fixed transmitted power level of 4 dBm): first when only two motes are operating (TX1 and TX2) and afterwards when the whole wireless network is operating (5 transmitters), which corresponds to the optimal

configuration of the network for the presented indoor scenario. These maps represent the overall increase of current consumption of the transmitting nodes placed at the scenario for each possible receiver location. From the real measurements explained later, it is shown that the lowest measured consumption of a node when transmitting is 40.5mA (distance between transmitter and receiver of 5 cm). So, as it can be seen in the consumption maps for the first case (Figure 4.13a), a maximum current consumption increase of 6.03 mA is reached for a specific location (this maximum peak seems not to reach that value, but it is due to the perspective of the graph). This corresponds to the worst location for a receiver to be placed in terms of current consumption. This means that for that receiver location, the overall current consumption for the transmitters will increase in 6.03 mA due to the power level received at that location, which is equal to 14.8% more consumption. On the other hand, for the optimal case of 5 transmitters deployed (Figure 4.13b), the worst receiver location implies an increase of 3.11% of the total consumption of the five transmitting nodes of the network. This lower increase of consumption is expected as the received power level for the whole scenario is higher due to the higher amount of deployed transmitting nodes.

All these results can be really useful in order to plan the design of the optimal network, taking into account the number of employed nodes, the required transmission bandwidth and the sensitivity level. Moreover, as it is shown in Figure 4.13, the density of the nodes within the network has a clear impact on energy consumption, due to the fact that link balance limitations are lower when the whole network is operating. Nevertheless, it is important to achieve a commitment between the density of nodes and interference levels, because a larger number of nodes could lead to increased interference levels, which could degrade system performance.



(a)



(b)

**Figure 4.13.** Estimation of Energy Consumption in terms of current values in mA for different locations of the scenario depicted in Figure 4.4: (a) TX1 and TX2, (b) The 5 transmitters.

After showing simulation estimations, in which the morphological dependence of the network performance in terms of received signal is observed, wireless CyFi motes have been configured and measured. For that purpose, power distribution and current consumption measurement results are presented. In Figure 4.14, a layout of the tested setup is shown. The laboratory has two zones, separated by

several metallic shelves. For the purpose of the study, the left hand zone has been measured, due to the fact that this is a zone of interaction with students and collaborators, leading to a realistic situation for the deployment and use of a wireless sensor network. The measurements have been performed by programming a test setup among the motes, given by a coordinator element and a wireless sensor.

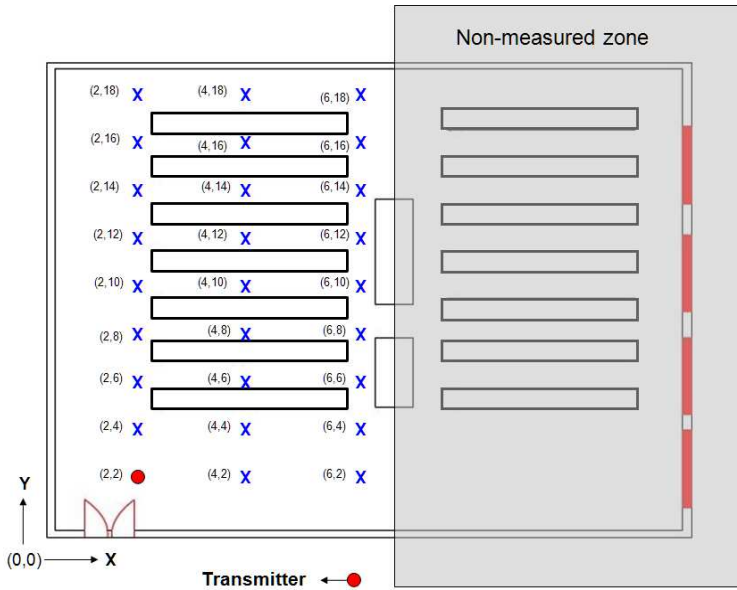


**Figure 4.14.** Schematic upper view of the indoor scenario (Figure 4.4).

Initially, the RSSI values in different points of the scenario (Figure 4.14) have been measured: The transmitter is located in coordinates (2, 2) and it is represented by a red point. The receiver has been placed in different points, which are represented by blue X marks in the figure. Both the transmitter and receiver have been placed at the same height of 81 cm, which is the height of the tables located in the scenario. The same antenna orientation in all the measurements has been carefully maintained in order to minimize variations due to the radiation pattern of the receiving antenna. The motes have been programmed to transmit at low data rate of 1 packet every 20 seconds, emulating a possible

wireless sensor network application linked to Ambient Intelligence or Smart Homes. The RSSI values have been read directly from the data provided by the motes. The obtained values are shown in Figure 4.15. The scale has been set up to -100 dBm in order to account for the sensitivity value of the motes (-97 dBm). As expected, due to the CyFi's active link and power management, signal level does not clearly decrease with the distance as it happens in a common radio wave transmission (with a transmitter transmitting a fixed power level). The signal level is maintained quite well within the scenario, although variations on received power can be seen due probably to the multipath radio propagation effects (mainly diffraction and reflection), very significant in an indoor complex scenario like this.

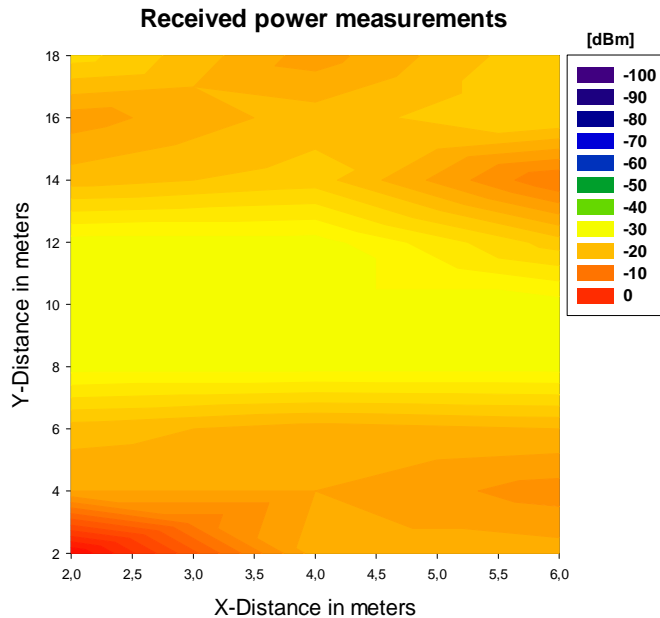


**Figure 4.15.** Measured power levels in dBm for a pair of mote coordinator/sensor in the indoor scenario.

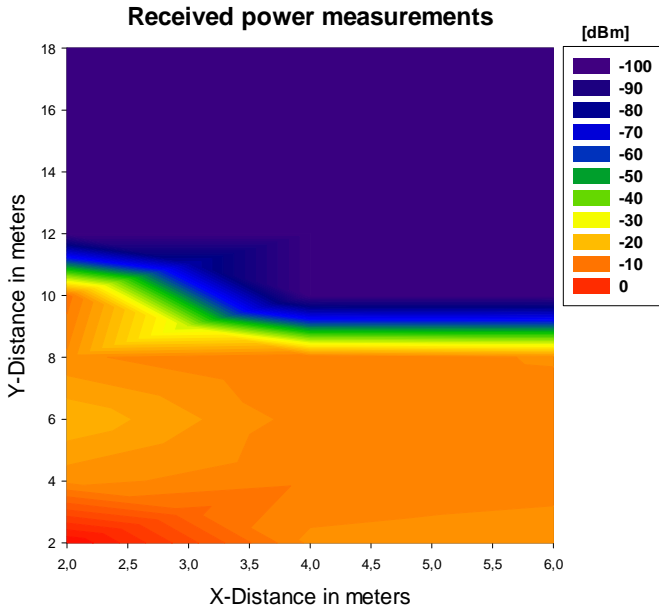


**Figure 4.16.** Measured power levels in dBm for a pair of mote coordinator/sensor in the indoor scenario at highest transmission data rate.

To gain more insight in the operation of the sensor motes and the influence of the topology and morphology of the scenario, current consumption has been measured for several positions. For that purpose, the motes have been programmed to transmit at their highest packet transmission rate (1 packet per 15 ms) and initially at the highest transmission power level (4 dBm) in order to increase the current demand of the motes. As in the previous case, both the transmitter and receiver have been placed at the same height of 81 cm. With this new approach, unlike the previous case, at certain distance from the coordinator no packets are received. The RSSI values shown in Figure 4.16 are the mean values of the RSSI data of the packets received in a 2 second duration time slot, which correspond approximately to 130 packets as long as the communication has been correctly done. When the distance is higher, the communication has problems and the number of received packets decreases up to 10 packets in 2 seconds due



to the approach of the received power to the sensitivity level of the motes. Figure 4.16 shows how the received power level near the transmitter is quite constant as well as the sensitivity level zone, in which no packets are received. This is due, once again, to the automatic regulation of transmit power that is embedded in the motes. But, despite of that, variations on received power level could be measured (on a smaller extent than in a case without transmitter power regulation), once again, due to the particularities of radio propagation within a heterogeneous scenario with a complex morphology like this (a lot of furniture composed of different materials). As an example, although coordinates (6,6) are located further from the transmitter than coordinates (2,6), and the transmitter tries to maintain the received power level throughout the scenario, the zone corresponding to coordinates (2,6) has lower received power level. It is worth noting how the increase in the overall transmission rate leads to lower coverage zones, as clearly observable from Figure 4.16. As an example, a PER (Packet Error Rate) measurement has been made between a transmitter in (2,2) and a receiver in (2,6). As mentioned previously, a low received power zone is detected surrounding the coordinate (2,6). This zone has the same characteristics as the zone near the sensitivity level, in which the number of received packets decreases abruptly. This is clearly shown in the PER value obtained for the transmission of 100,000 packets: only 1,363 packets arrived (PER = 98.637 %).

In order to see the evolution of the current consumption of the transmitter in this scenario, the receiver has been placed at different distances from the transmitter. A Tektronix DPO 3014 oscilloscope has been used to obtain the current consumption measurements. For this purpose, a 1 ohm resistor has been introduced in series in the feeding circuit of the mote. In this way, by measuring the voltage difference in the resistor, an estimation of the current value is obtained. The obtained results are shown in Figure 4.17 and Figure 4.18.

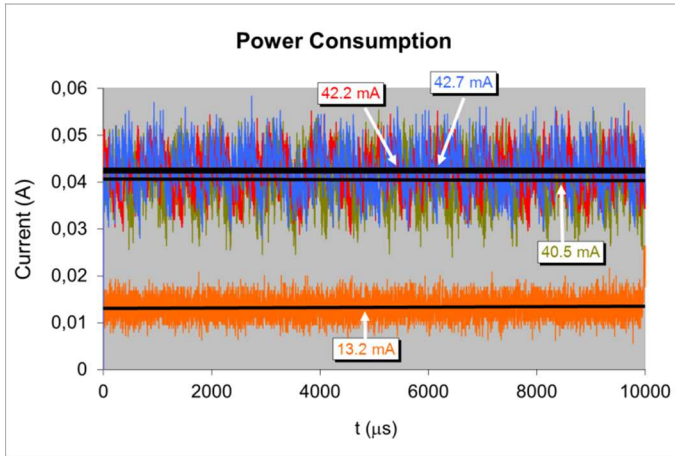


**Figure 4.17.** Power consumption variation as a function of time for different positions. The bottom curve (13.2 mA) is for standby, whereas as the rest of the curves span from the closest to the farthest mote within the scenario.

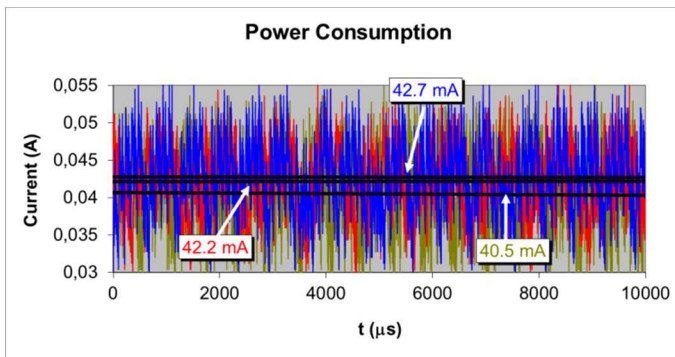


**Figure 4.18.** Detail of the power consumption for the designed mote device within the indoor scenario. The mean values for different currents are proportional to the separation between motes.

As it can be seen in Figure 4.17, a clear difference exists between the standby (orange curve) and the transmit mode (the rest of the curves), which is expected due to the normal operational procedure in the wireless transceiver. In Figure 4.18, a detail of the different transmit mode current values can be seen, given for different positions of the sensor within the scenario. These distances have been 0.05 m, 2 m and

4.2 m, respectively. The last distance corresponds to the point in which the sensitivity level has been almost reached, in which few packets are received. This sensitivity point varies between 4 and 6 m depending on the environment and the objects surrounding the motes. From the measured values of the current consumption from the motes in operating mode at different distances, an increase in current consumption in the order of 4.2% in the case of 2 m and 5.4% in the case of 4.2 m is observed. Therefore, by considering the pre-existent levels of interference as well as the expected fading losses of the scenario, the optimal location of the motes can be planned prior to real network deployment.

As the distance increases, the power consumption level also increases, which is in accordance to the operation of the power management of CyFi motes: By increasing the distance between motes, the received power decreases. But due to the power management features of the motes, the transmitted power level increases in order to maintain the received power level in each position, leading to higher power demands of the transmitter.

Following this way, the analysis of SNR values and current consumption has been carried out for bigger and more complex scenarios. In addition, the quality of service (QoS) of the wireless link in terms of BER (Bit Error Rate) by the aid of the 3D Ray Launching algorithm is introduced, which provides new and very valuable information about the feasibility of deploying a WSN within such complex indoor scenarios.

The scenario under analysis, depicted in Figure 4.19, represents the entire ground floor of a department building of the Public University of Navarre. Note that the furniture as chairs, tables and air ducts has been taken into account. The dimensions of the scenario are 55.3 m × 27.85 m × 3.8 m. A WiFi hotspot (blue dot) and six ZigBee-based devices have been distributed throughout the scenario (red dots). A summary of the parameters used for the simulations is given in Table 4.4. The ZigBee parameters are equivalent to those of well-known and previously shown XBee devices. As can be seen, the transmitted power of the WiFi

hotspot is significantly higher. The frequency channel of both wireless systems has been chosen overlapped in order to interfere each other.

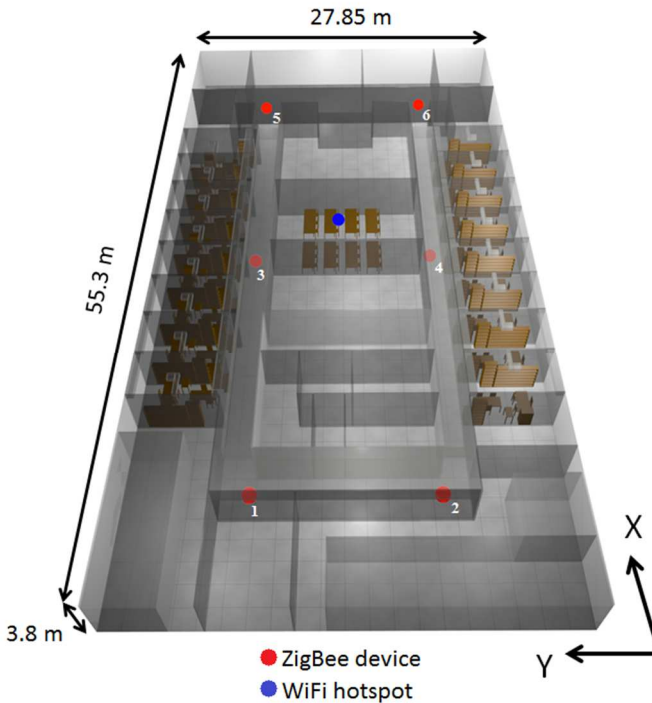
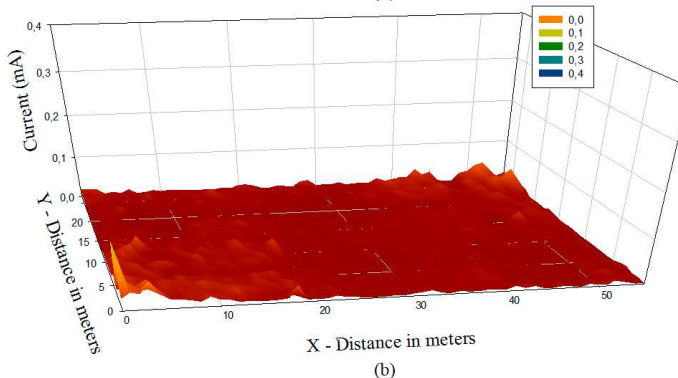
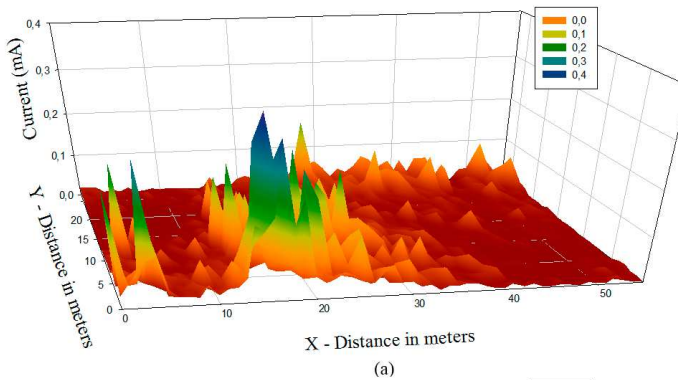


**Figure 4.19.** The ground floor of the Mathematics department created for 3D Ray Launching simulations.

Parameter	ZigBee	WiFi
Cuboid Resolution	1 × 1 × 1 m	1 × 1 × 1 m
Launched Ray Resolution	1°	1°
Permitted Reflections	5	5
Transmitted Power	0 dBm	20 dBm
Channel Frequency	2.41 GHz	2.412 GHz

**Table 4.4.** Summary of 3D Ray Launching parameters.

In order to show the impact of the deployment of WSNs, three different wireless network configurations have been analyzed, for two, four and six ZigBee devices. The two device configuration corresponds to the antenna number 1 and 6; and the four device network to number 1, 2, 5 and 6. In Figure 4.20, bi-dimensional planes at height of 2 m for each of the mentioned network configurations are presented, in which the overall increase of current consumption of the transmitting devices placed at the scenario for each possible receiver location is represented. The typical short term variations of the received power due mainly to the multipath propagation lead also to a significant variation of the current consumption, which can be clearly seen in Figure 4.20. Also, as expected, when the number of devices in the network increases, the consumption of the transceivers decreases, as the coverage within the scenario is better.



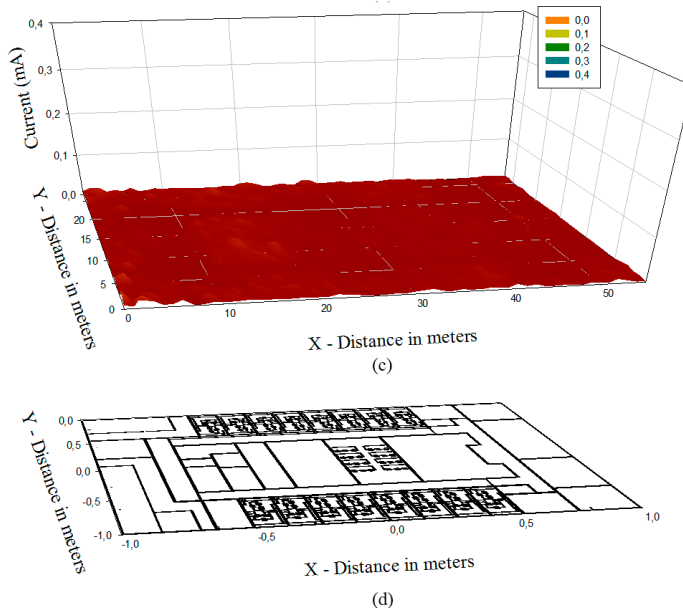


**Figure 4.20.** Estimated overall current consumption increase, based on simulation results for different network configurations, (a) two devices (1 and 6), (b) four devices (1, 2, 5 and 6), and (c) six devices. (d) upper view of the scenario.

A significant parameter that is used in assessing systems that transmit digital data in a wireless link is the BER. As previously stated, the inclusion of this parameter estimated by the 3D Ray Launching algorithm provides valuable information in order to deploy a wireless communication system within complex scenarios. As an example, the BER values for this scenario have been estimated assuming QPSK modulation scheme, which can be obtained by the following expression:

$$BER_{QPSK} = Q(\sqrt{2E_b/N_0})$$

where  $E_b = PRX/R_b$ . The received power (PRX) has been estimated with the aid of the 3D Ray Launching algorithm for each spatial sample in the considered scenario. With these values, the BER has been calculated

for different values of data rate ( $R_b$ ) (in this example 9.6 Kbps and 250 Kbps) and different interference source configurations operating within the scenario. With this method, both intra-system and inter-system interferences can be analyzed. As an illustrative example, the configuration of the ZigBee network plus the WiFi hotspot is presented, as shown in Figure 4.19. For that purpose, the device 1 has been set as transmitter, and the WiFi hotspot has been considered noise, as it transmits overlapping the ZigBee frequency channel (see Table 4.4). Figure 4.21 shows the estimated BER results for this particular configuration. As the considered transmitted interference level (20 dBm) is very high comparing to the transmitting signal power (0 dBm), very high BER values are obtained throughout the scenario, even more for higher transmission data rates (Figure 4.21). When possible, changing the frequency channel of some of the wireless communication systems present within the environment is the most effective way to avoid interferences. But in many cases the source of the interference is unknown or its configuration cannot be changed. In these cases, the transmitted power plays a key role. Increasing the signal output power or reducing the interference level lead to better BER results. In order to show the effect of changing these values, Figure 4.22 shows the new BER estimations, when the WiFi hotspot operates at an upper frequency channel, i.e. reducing the noise level at 2.41 GHz band due to the lower degree of overlapping between the operating frequency channels of WiFi and ZigBee. The depicted results of Figure 4.22 show how the BER values have been reduced for the new configuration. These kinds of results can be obtained for each particular scenario, taking into account variable parameters like transmitted power level, data rate, modulation scheme and noise level.

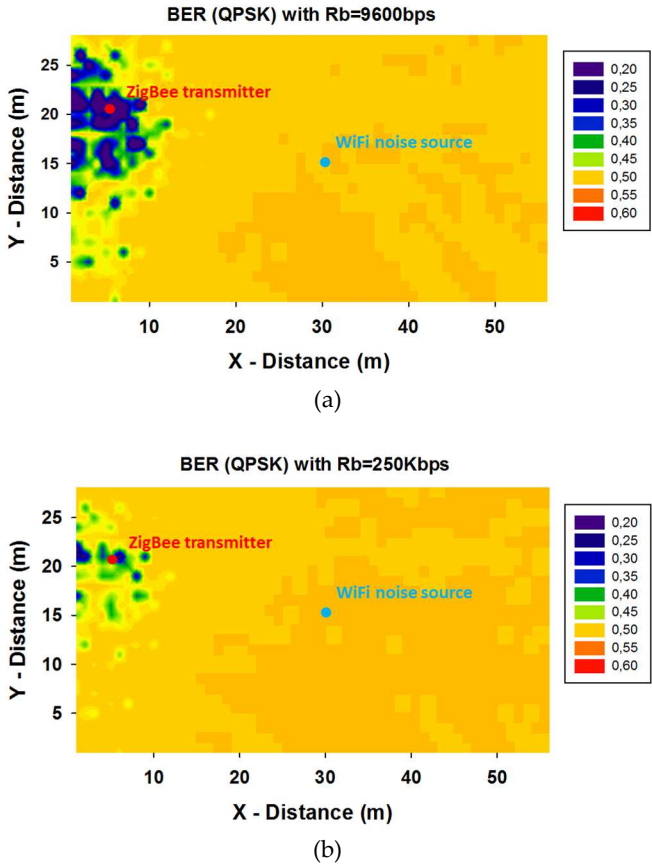
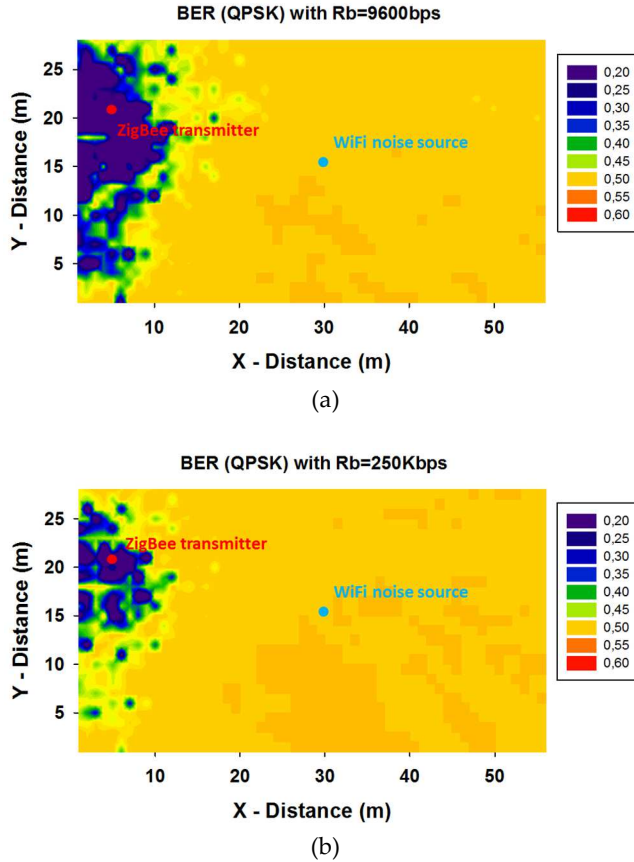


Figure 4.21. Estimated BER for different transmission data rates, (a) 9.6 Kbps, and (b) 250 Kbps.





**Figure 4.22.** Estimated BER when noise level decreases for different transmission data rates, (a) 9.6 Kbps, and (b) 250 Kbps.

Finally, as it has been previously shown for smaller scenarios, estimated SNR values can be obtained for the bigger scenario of Figure 4.19. For the estimations shown in Figure 4.23, the device 1 has been considered as transmitter and the WiFi hotspot as noise. The obtained SNR values at positions of device 2 and device 3 are represented, for different transmitted power levels of a real XBee device (x-axis).

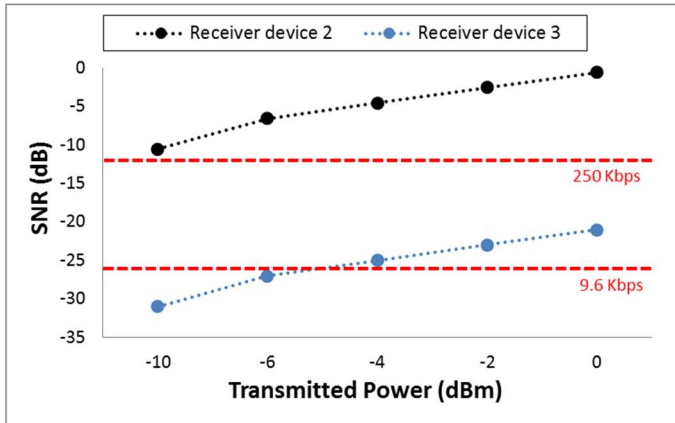
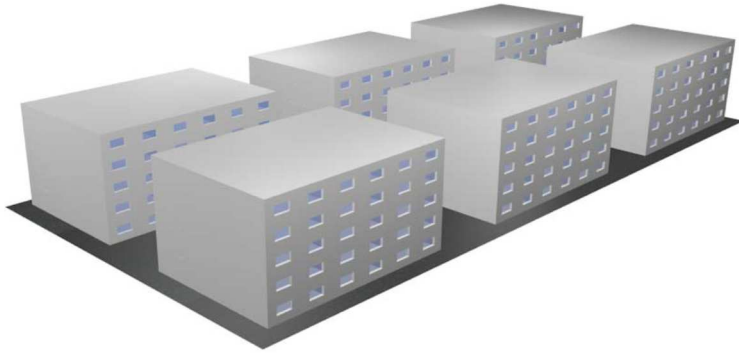


Figure 4.23. Estimated SNR values at the positions of device 2 and 3 when transceiver 1 is emitting.

Following the same methodology, urban environments have been also analyzed. Due to the intensive use of the wireless spectrum and the large density of multiple types of users that are expected to be present within this kind of environments, interference must be carefully controlled in order to optimize the performance of the deployed transceivers. With the advent of IoT and the concept of Smart Cities, in a typical zone of a dense urban area, a set of such transceivers of different technologies will be deployed: indoor, outdoor, static and in movement. This leads to a heterogeneous wireless environment, in which multiple types of traffic, with different bit rate, bandwidth and quality of service requirements will be deployed.

In order to perform the analysis of wireless channel performance within a dense urban environment, the scenario of Figure 4.24 has been implemented. The scenario represents a sub-set of a dense urban area, and consists of 6 buildings of 5 stories. The main simulation parameters used for the scenario are summarized in Table 4.5. Within the scenario, several sources, which are equivalent to wireless transceivers, have been placed in order to generate wireless traffic (useful traffic or interference, depending on the required analysis). The number of sources employed for this study has been 6, although there is no formal restriction in order to increase and hence, provide scalability in the

obtained results. All the 6 sources have been placed within the buildings, as can be seen in Figure 4.25.



**Figure 4.24.** Simulation Scenario corresponding to a section of buildings within the context of a city.

Parameter	Value
Launched Ray Resolution	1°
Permitted Reflections	6
Transmitted Power	30 dBm
Channel Frequency	2.4 GHz

**Table 4.5.** Summary of main 3D Ray Launching parameters.

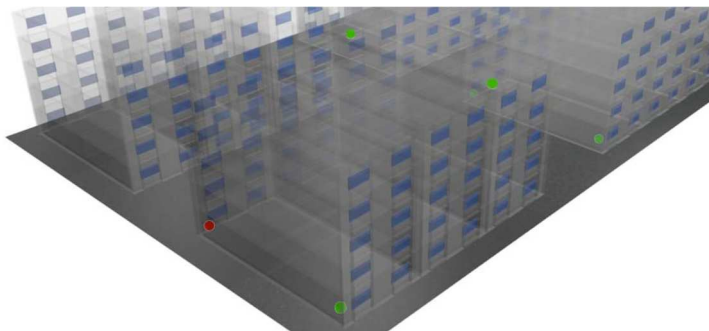


**Figure 4.25.** Detail of wireless sources' location within the scenario.

As an example, the estimated RF power distribution for the source represented by a red dot in Figure 4.25 is shown in Figure 4.26. The presented results correspond to a plane at height 1.5m. Based on these results, as it has been done for the previous cases, the current consumption (Figure 4.27) and SNR graphs (Figure 4.28) can be obtained.

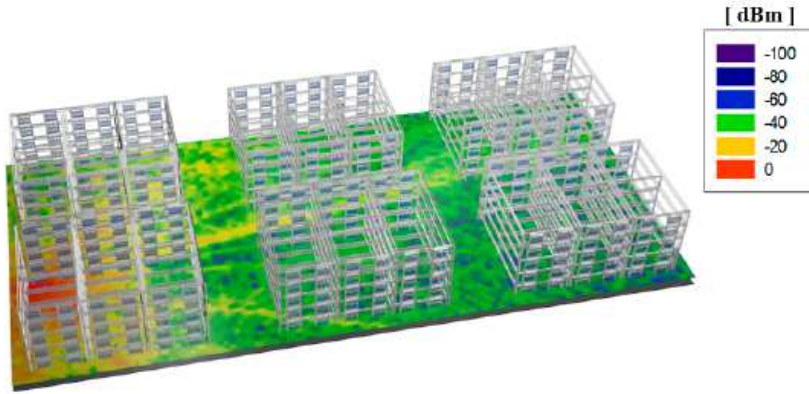


Figure 4.26. RF power distribution for a plane of 1.5m height.

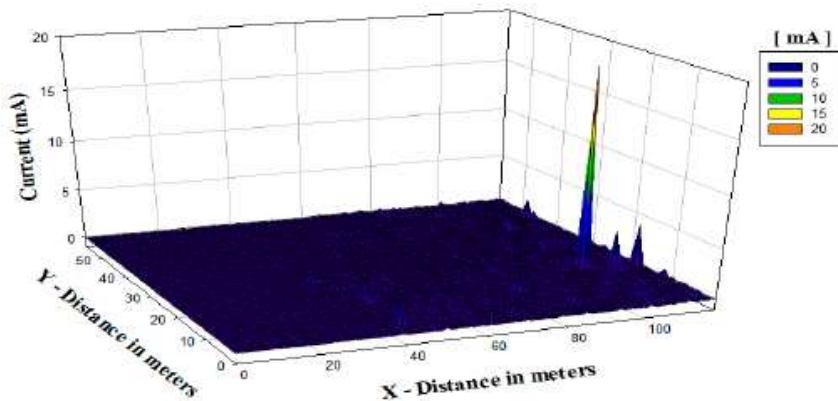
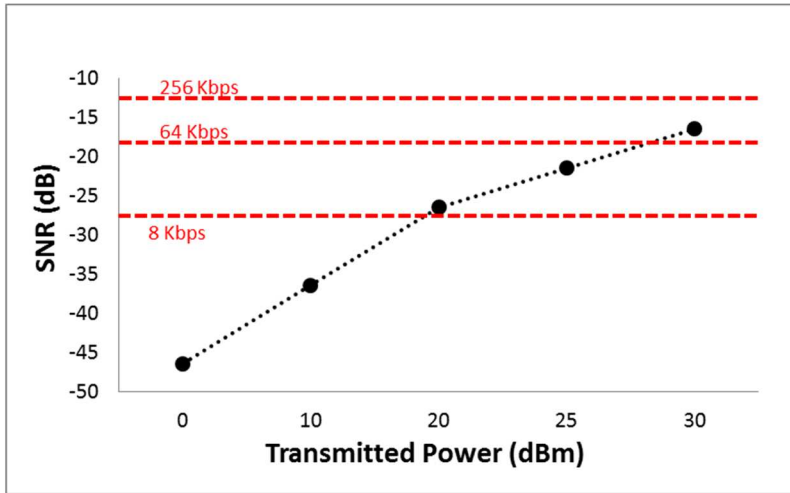


Figure 4.27. Current consumption increase depending on receiver position for the results of Figure 4.26.



**Figure 4.28.** Estimation of SNR values as a function of transmitted power at a specific point within the scenario, compared to different bit rate thresholds.

The results shown in this section are specific examples of how the 3D Ray Launching radio propagation model can be used to obtain extra valuable data for environments where the coexistence of different wireless systems is a requirement. Typically, ray launching algorithms are used in the literature for obtaining received power level values within different kind of scenarios. In this work, in addition to this kind of results, the in-house developed 3D Ray Launching algorithm has been used in order to obtain channel quality estimations, with the aim of improving radio planning duties. For that purpose, estimations of current consumption, BER and SNR values are presented. The obtained results can aid in the identification of the optimal location for the deployment of wireless transceivers, in order to minimize power consumption and increase the overall service performance of wireless networks, taking into account variable parameters like transmitted power level, data rate, modulation scheme and noise/interference level. The proposed method will gain interest for the analysis of dense transceiver scenarios with complex topologies, typical of Context Aware applications, Smart City environments and within the IoT frame.

### 4.1.1 Human Body Effect

Some of the most promising wireless systems that are expected to grow in the near future are the WPANs (Wireless Personal Area Network) and WBANs (Wireless Body Area Network). A key element in this kind of wireless networks is the presence of human body and its effect on the transceivers placed on the body (wearable devices) as well as on the radio propagation within the environment, including the known Body Shadow Effect [Sch14]. Although the human body itself is not a noise source at the frequencies of operation that interest us, the presence of human beings within the environment (which is the most common situation in the framework of Context Aware scenarios) can affect significantly the radio propagation, changing the RF power distribution throughout the scenario, which in turn it can affect the overall performance of a deployed wireless communication system. For such analysis, a human body model developed by Dr. Erik Aguirre has been included in the 3D Ray Launching simulations [Agu12].

One of the environments that can take more advantage of the implementation of wearable and the deployment of WBANs is the health environment, where an efficient patient monitoring could be carried out, among other applications. This leads to the concept of e-Health, which is defined as the recollection and interchange of medical information through electronic devices and digital communication networks to provide essential information to doctors or users for the achievement of a best diagnosis and a fast action in case of emergency. To make this possible, a significant amount of technologies must work together to offer a transparent, or at least, the less obstructive possible service for the end user. This ease in usability must be reached in different levels, starting from the development of small-scale devices, enabling straightforward integration with user apparel. In this sense, wireless technologies which enable freedom of movements to users are essential. Taking this into consideration, energy usage profiles must be as efficient as possible to use small batteries and to reduce recharge times.

Based on these premises, some research prototypes have been

already developed and implemented on textile or on conventional materials. These prototypes are capable of measuring and monitoring a wide variety of physiological parameters. As an example, in [Lop10] a device uses textile sensors to obtain information about location, ECG, heart rate and body temperature in hospital environments. In [Mel11] a textile device is also used for monitoring sleep movements and detecting neurodegenerative diseases as Alzheimer or Parkinson. Regarding the transmission of the medical data acquired by those sensors, the most important wireless systems are WBANs [Seu13][Chi13][Lup13], where different wireless technologies are employed to transfer the sensed data to portable devices such as a tablet or a mobile phone, where the data will be stored and could be analyzed by a specific software capable of processing and showing all this information in the best way depending on the kind of information and end user. ZigBee [Roc14], Bluetooth [Won13] or RFID [Mal08] are the most widely used communication technologies in this application area, being essential the flexibility and energy autonomy offered by some of them. But standalone WBANs are suitable for remote monitoring applications and usually require other devices as gateways between them and other wireless networks, in order to have access to databases that will work with the data acquired by the sensors belonging to the WBANs. In this sense, the proliferation of smartphones has solved partially this issue, since most users have a device with multiple connectivity possibilities (Bluetooth, WiFi, HSPA, etc.). In fact, nowadays the most widely extended schema is the one that uses mobile phones as gateways [Mar09][Rah09].

All these wireless technologies and e-Health devices proposed for patient remote monitoring usually operate in complex indoor scenarios in terms of radio propagation, like hospital rooms and areas, or a patient home [Ara11][Pau09]. In these scenarios, the placement of the different devices that integrate the wireless communication system can determine the correct performance of the entire system. The fact that the human body is necessarily involved in the scenarios increases the complexity of the communication system analysis. Therefore, the theoretical study of WBANs using simulation tools, aids to determine

their feasibility as well as to improve the performance of the wireless system. In fact, the deployment of WBANs in indoor scenarios has been studied from different points of view in several works. In [Rob11] several WBAN indoor scenarios are studied through the measurement of Power Delay Profile (PDP). In [Abu12] empirical Path-loss model and measurement results are compared for different human parts and postures considering a ZigBee sensor network. Finally, in [Rob15] statistical WBAN channel characterization is carried out using a complete homogeneous body phantom.

In this work, a first approximation of how wearable devices position on the human body affect the radio propagation within a hospital environment is presented. A brief WBAN-based wireless channel analysis with the presence of people is also presented. Since hospital environment are complex and the performance of the systems depends strongly on the performance of the WBAN interacting with human bodies, the 3D Ray Launching simulation tool has been employed with the aim of studying the behavior of potential wireless e-Health devices of a WBAN, deployed on the mentioned in-house developed human body model.

Simulations have been carried out in different areas of the Emergency-department of the Hospital of Navarre, located in the city of Pamplona. In Figure 4.29 the outdoor view of the building is shown, where three different areas that have been studied are highlighted. On the one hand, within the smaller area (Figure 4.29a) the operation of a WBAN communication system attached to the human body and the behavior among different possible placements of the wearable device have been analyzed. On the other hand, the other two areas (Figure 4.29b and 4.29c) have been used for studying the radio propagation of a WBAN within the complete ground floor of the building. All these three scenarios contain concrete pillars, plasterboard walls, glass walls and glass windows, among other elements. Two different ISM band frequencies have been used in simulations based on the characteristics of typical WBAN technologies. In Table 4.6, the main parameters used in simulations are shown.



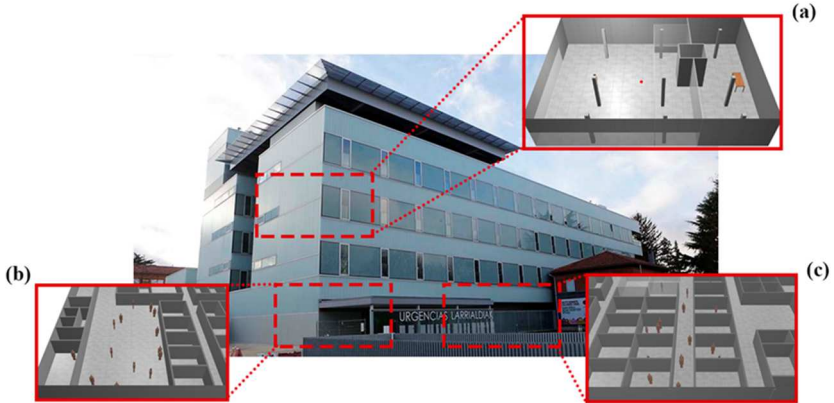


**Figure 4.29.** Outdoor view of the emergency building of the Hospital of Navarre: (a) First floor, (b) Entrance hall and (c) Medical boxes.

Parameter	ZigBee
Launched Ray Resolution	1°
Permitted Reflections	6
Transmitted Power	10 dBm / 18 dBm
Frequency	2.4 GHz / 868 MHz

**Table 4.6.** 3D Ray Launching simulation parameters.

In Figure 4.30 the scenario corresponding to Figure 4.29a is depicted. The dimensions are 19.6 m × 16.6 m × 3.8 m and it has been divided into two different resolution areas in order to obtain more accurate results surrounding the human body and in turn to avoid possible divergence problems in the rest of the scenario, as well as not increasing the calculation time due to very small cuboids. The high resolution area (cuboids of 3cm) shown in Figure 4.30 has the dimensions of 0.55 m × 0.55 m × 3.8 m. The low resolution area (cuboids of 20cm) corresponds to the rest of the scenario. In order to study different communication configurations, antennas have been placed on the human body model as well as in the center of the scenario at a height of 0.7 m (see red points represented in Figure 4.30).

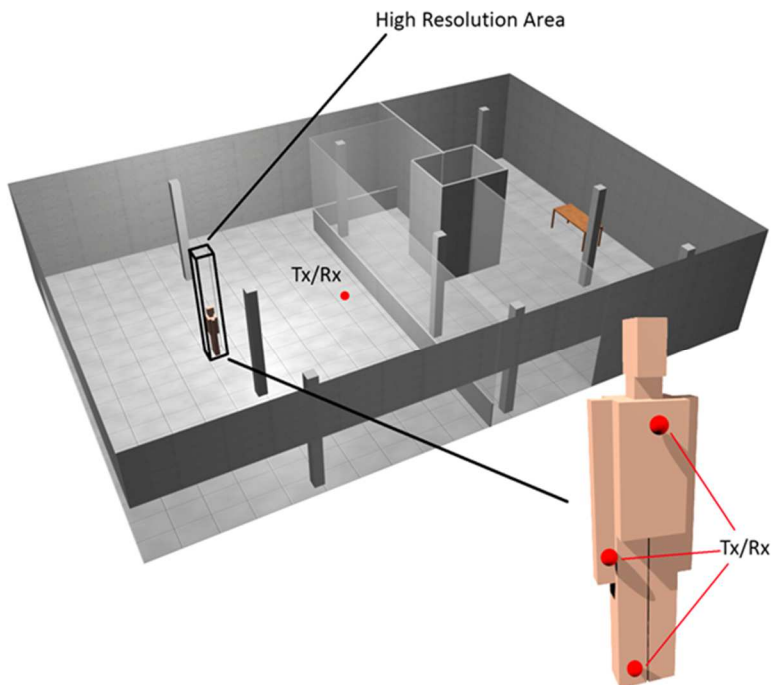


**Figure 4.30.** Schematic view of the scenario corresponding to Figure 4.29a, where the placements of the used antennas are represented (red points). The high-resolution area around the human body model is also highlighted.

In Figure 4.31 estimated RF power distribution is shown for the case of the antenna in the center of the scenario transmitting 10 dBm at 2.41 GHz. In order to see clearer the influence of the multipath propagation and the RF power variations that creates, in Figure 4.32 the received power in the linear paths between the transmitter and the three antennas placed on the human body are depicted. Note that human body position corresponds to x-axis value 4 m and the antenna placement corresponds to x-axis value 8.5 m (corresponding to the deployment shown in Figure 4.30). The multipath behavior of the propagated electromagnetic waves is more noticeable since the decrease of power does not exhibit a monotonically decreasing trend. The faster variations near the human body are due to the high resolution area.

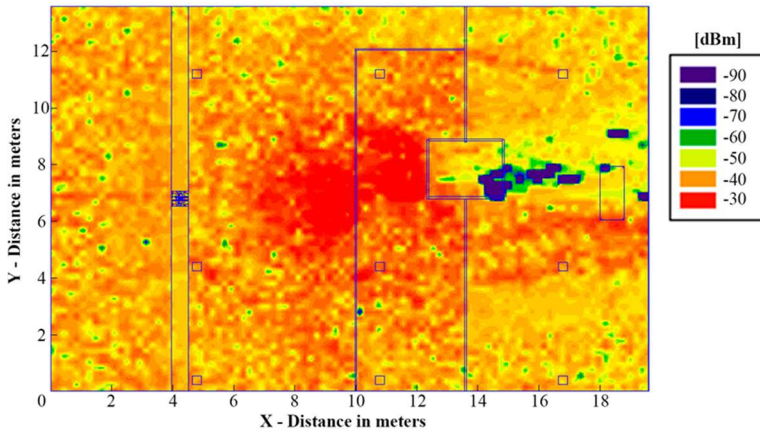


**Figure 4.31.** Bi-dimensional RF power distribution when the antenna in front of the human body is emitting.

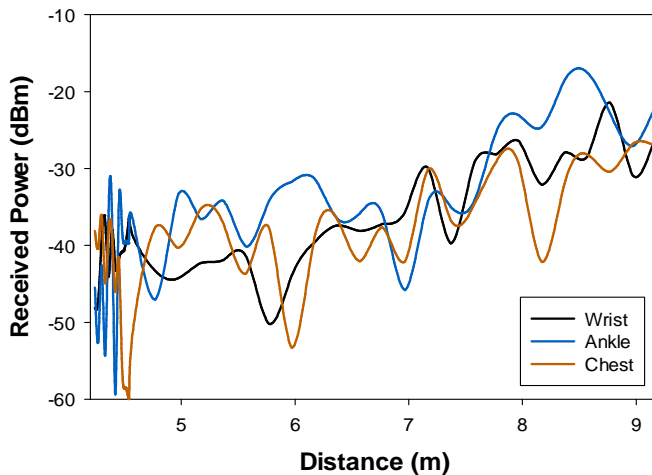


**Figure 4.32.** Received power vs. linear distance for the paths between the transmitter antenna and the antennas on the human body model (see Figure 4.30).

An easy way to see the previously mentioned Body Shadow Effect is to depict the PDP of a point between the transmitter antenna and the human body, and other point behind the human body, i.e. placing the body between the transmitter and the point under analysis. The PDPs

for these both points are represented in Figure 4.33. As expected, the influence of the human body is visible as fewer rays reach the point behind the human body, due to its dispersive nature and the high absorption rate of the human body, avoiding the arrival of many rays to the back area of the person.

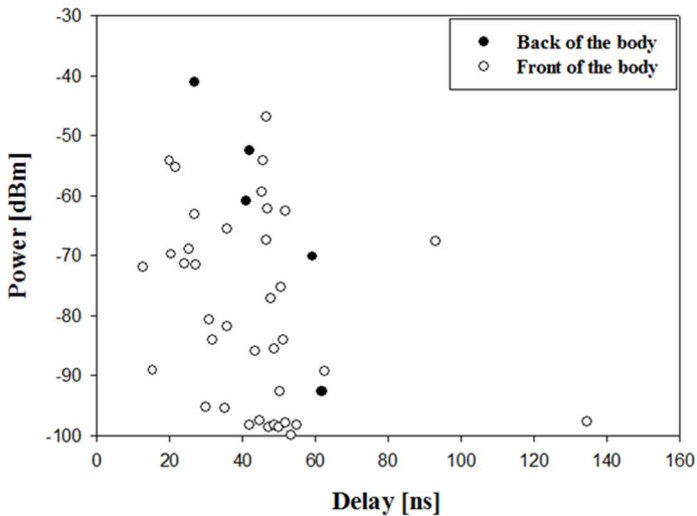


**Figure 4.33.** Power Delay Profile estimations considering two points located in front and behind the human body model.

The same analysis has been carried out, but now considering the three antennas on the human body (wrist, ankle and chest) as transmitters. Figure 4.34 shows the obtained RF power distributions at height of 1.27 m for the three cases. These results and the previous ones show that the location of the wearable device as well as the WBAN gateways that could be placed on the infrastructure affects how the signal will propagate within the scenario, and hence, the performance of the wireless communication. These facts should be taken into account for the design of potential applications where wearable devices are required. Even more important for the development of potential medical applications where patients or medical staff have to adopt a specific body position and orientation.

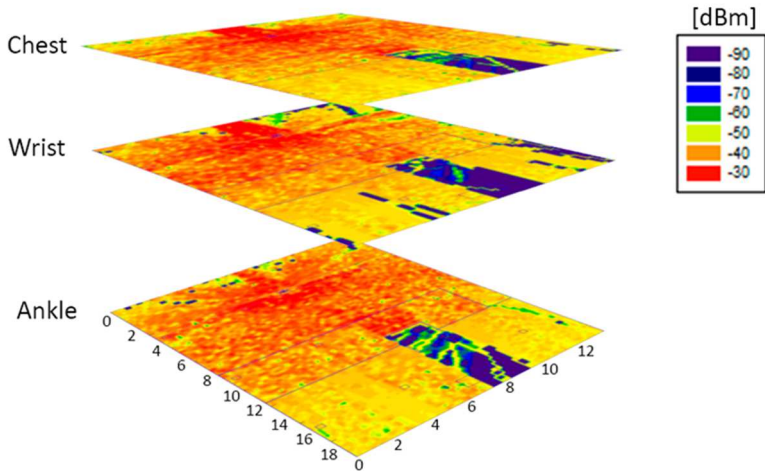


**Figure 4.34.** Bi-dimensional RF power distribution at height 1.27 m when antennas placed on the chest, ankle and wrist are emitting.

Now, the bigger scenarios of Figure 4.29b and Figure 4.29c have been simulated in order to study the link quality between a wearable device and a gateway device fixed on the infrastructure. The detailed schematic view of the scenarios is shown in Figure 4.35. Although the complete ground floor of the Emergency building has been created with all the 90 rooms and the real constitutive materials of walls, ceiling and floor, no furniture has been implemented since the building was new and empty when these simulations were performed. Instead, human body models have been randomly included in both simulation areas (see Figure 4.35). Two antennas have been placed emulating a wireless gateway: In the center of entrance hall (Tx 1 in Figure 4.35b) and in the aisle (Tx 2 in Figure 4.35c), both placed on the ceiling. In addition, two more antennas have been placed on the wrist of two human models (Tx 3 and Tx 4 in Figure 4.35c) emulating wearable devices. Note that Tx 3 is placed in the aisle and Tx 4 within a medical box. The gateways have been configured to transmit 18 dBm and wearable devices 10 dBm.

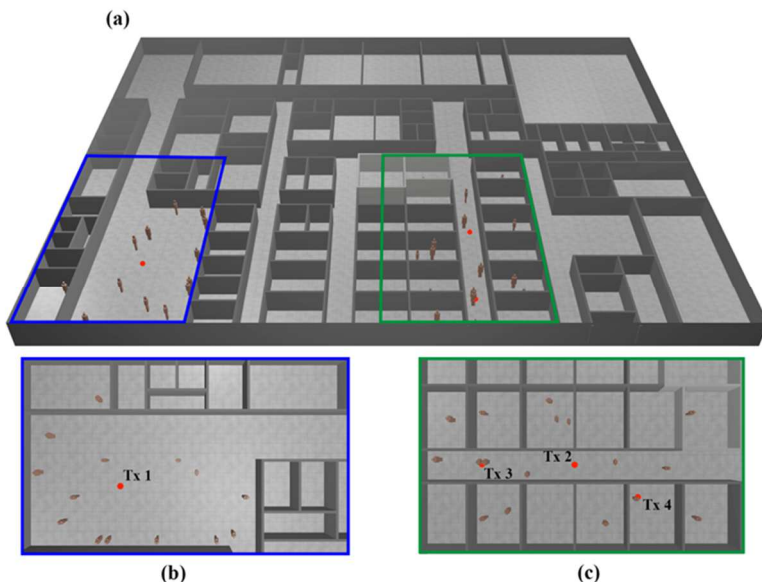


**Figure 4.35.** (a) Ground floor of the Emergency building of the Hospital of Navarre, (b) entrance hall and (c) medical boxes.

Once the received power distribution from the proposed transceiver locations has been obtained, the performance of the wireless links can be assessed in terms of Signal to Noise Ratio (SNR). As an example, the two wearable transceivers placed on the wrists of the patients as well as the node placed on the ceiling of the medical boxes zone have been evaluated (see Figure 4.35c). Both the uplink (from wearable mote to fixed node) and the downlink (from fixed node to wearable mote) communications have been analyzed. In Figure 4.36 the SNR values for the wireless communication link between the node placed on the ceiling and the patient within the aisle are shown. Figure 4.37 represents the same, but for the case of the patient within the medical box. The red dashed lines show the minimum SNR required for a successful communication at the indicated bit rates. Although the data rate for ZigBee communications is 250Kbps, other data rates have been taken into account in the study in order to gain insight in the effect of the noise on different configurations operating at different data rates.

These required minimum SNR values have been calculated by the following well-known Shannon's equation:

$$C = BW \times \text{Log}_2\left(1 + \frac{S}{N}\right) \quad (4.1)$$

where  $C$  is the capacity of the channel in bps,  $BW$  the channel bandwidth (3 MHz for ZigBee) and  $S$  and  $N$  the received signal and noise power levels respectively. Firstly, it is worth noting how the SNR values of the uplink are lower than the values of the downlink for both Figure 4.36 and Figure 4.37. This is mainly due to the transmitted power differences between the wearable device and the fixed node at the ceiling. This fixed node has been configured to transmit 18 dBm, but the wearable has been configured to transmit 10 dBm since reducing the power consumption of devices powered by batteries is a desirable fact. Besides, the maximum transmitted power level for this kind of communications in some countries (e.g. in Europe) is 10dBm.

As it can be also observed in the figures, the influence of noise (i.e. electromagnetic interferences) present in the scenario is very relevant, which will have a great impact on the performance of the deployed WSN: Depending on the data rate required by the application running over the WSN, a minimum SNR value will be required, which could not be achieved if the noise level is high enough. For example, for the case of -40 dBm of background noise shown in Figure 4.36, if the wireless network needs to transmit at 250 Kbps, the downlink will do it successfully, but the uplink will fail, as it will scarcely transmit successfully at 125 Kbps. A solution for this situation is increasing the transmitted power, but it will lead to higher consumptions of the wireless motes, as well as increasing the electromagnetic noise level of the environment. Related to this, Figure 4.38 shows the effect of varying the transmitted power level for the mentioned case of -40 dBm of noise level from Figure 4.36. The graph shows how the obtained SNR values can be improved by increasing the transmitted power of the wireless motes, being decisive in many cases in order to achieve specific bit rates.

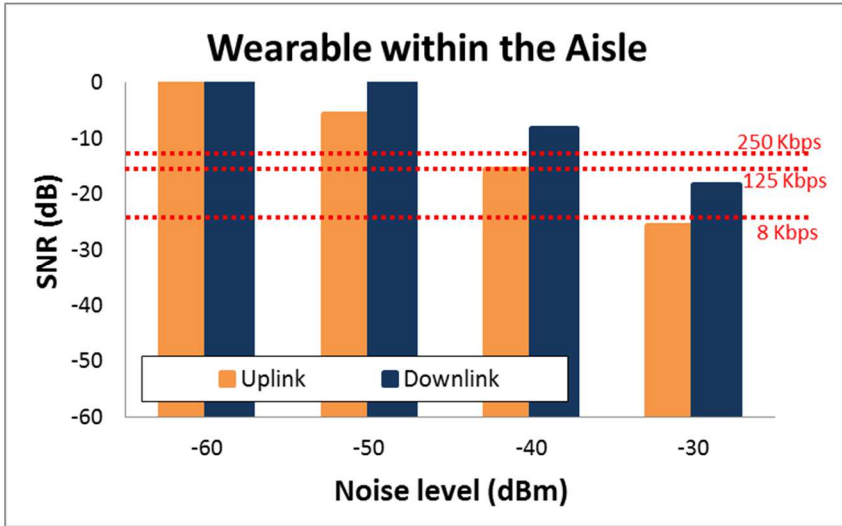


Figure 4.36. SNR values for the case of the patient within the aisle for different noise levels.

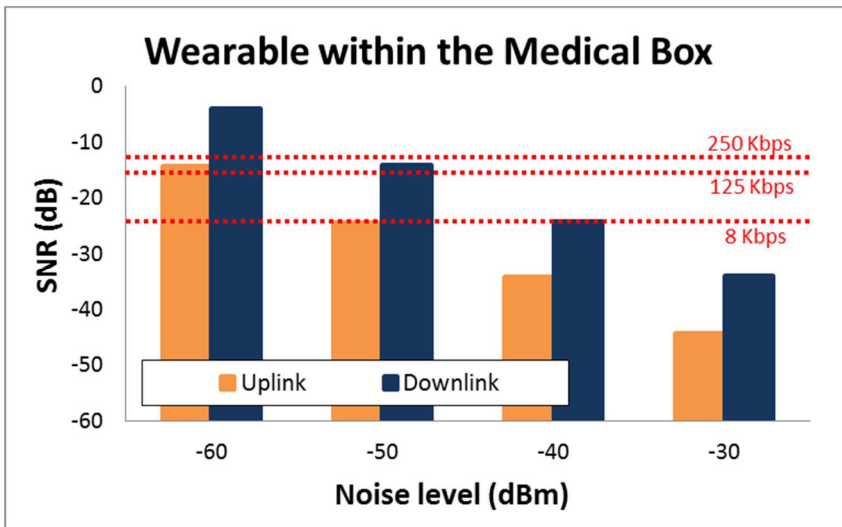
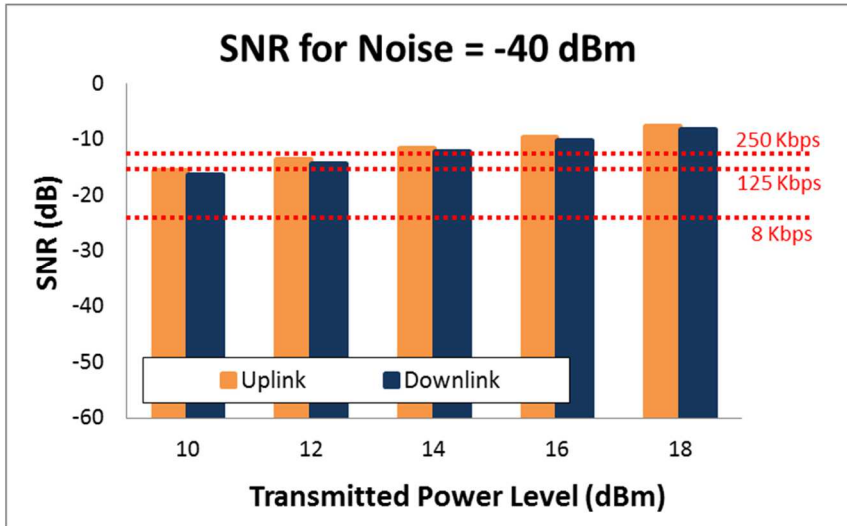


Figure 4.37. SNR values for the case of the patient within the medical box for different background noise levels.





**Figure 4.38.** SNR values for different transmitted power levels for the case of the patient within the aisle and a noise level of -40 dBm.

Summarizing, this study has shown how the position of the wearable device affects the radio propagation and how it can influence the performance of the wireless link. Now, a new case study is presented in order to gain insight in how the presence of people within a specific scenario where a WSN is operating can affect the radio propagation, and hence the overall performance of the WSN. The scenario chosen for performing this study is a Judo training venue, since it is a complex environment where different density of human beings can be present. Besides, it is an interesting and novel environment for the development of potential wireless systems where wearable devices could have a major importance.

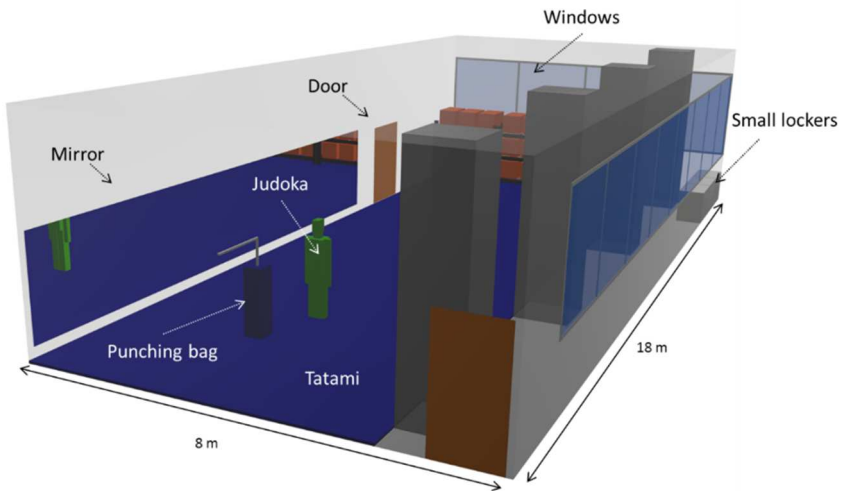
As Judo is one of the most spread martial arts in the world, there is a huge variety of different training venues where judo is practiced. All these venues usually have some common aspects (such as having a tatami), but in general, each training venue has specific morphological aspects, making them unique complex indoor scenarios in terms of radio propagation due to the size of the venue itself and the presence of different furniture elements (e.g., cupboards, benches, chairs), columns, pads and other elements and equipment that can be found within

training gyms, which will have a strong influence in the propagation of the electromagnetic waves as they generate phenomena such as reflection, refraction and diffraction. Therefore, the deployment of WSNs in such environments requires a previous radio planning work, especially considering that electromagnetic interferences created by other wireless sources such as personal portable devices and other wireless systems such as WiFi or other WSNs are likely to happen, making the coexistence in such indoor environments a complex task. Furthermore, in addition to the morphology of the training venues and the potential interferences, the presence of human beings within the scenario is a major issue in terms of radio propagation, especially taking into account that the person density in this kind of scenarios can be high as many judokas can be practicing and exercising at the same time.

The scenario where the study has been carried out is a gym located in the facilities of the Public University of Navarre. The dimensions of the scenario are 18 m (long)  $\times$  8 m (wide)  $\times$  4.8 m (height) and it contains a tatami of 17.5 m  $\times$  6 m, where judo is practiced. As happens in many judo training venues, other sports and physical activities are also practiced, therefore, the scenario contains typical elements easily found in many indoor training environments, such as a punching bag, big foam balls, doors, columns, a mirror and some furniture elements such as small lockers and shelves. All these elements make the scenario a complex indoor environment in terms of radio propagation, as the number of reflections, refractions and diffractions will be increased, making the multipath propagation the main phenomenon within the scenario, much more when persons are present. Figure 4.39 shows the real scenario and the schematic view of the scenario created for the 3D Ray Launching simulations.



(a)



(b)

**Figure 4.39.** (a) Real scenario under analysis; (b) Schematic view of the created scenario for 3D ray launching simulations.

Apart from the real size of the different elements of the scenario, the materials of all the objects within the scenario have been carefully chosen in order to obtain an electromagnetic behavior as closer as possible to the real materials. Table 4.7 shows the main materials used for the definition of the objects within the scenario, which both their relative permittivity and conductivity at the frequency of operation of the wireless system have been obtained from [Kom12]. As the main objective of this work is to analyze the effect of the presence of persons

on the radio wave propagation, the definition of the scenario has been completed with the inclusion of the in-house developed human body computational model presented previously. Thus, in addition to analyzing the effect of the presence of people on the radio propagation, the inclusion of the human body model permits the propagation study of wearable devices.

Material	$\epsilon_r$	Conductivity (S/m)
Tatami	3	0.2
Concrete	25	0.02
Aluminum	2.2	$37.8 \times 10^6$
Polypropylene	3	0.11
Foam	1.4	0.021
Brick	4.44	0.11
Door	5.84	0.06
Glass	6.06	$10^{-12}$
Plasterboard	2.02	0

**Table 4.7.** Material properties defined for the 3D ray launching simulations. Data obtained from [Kom12].

Once the scenario for the 3D ray launching has been created, the simulation parameters regarding the launching of rays and the wireless communication such as frequency of operation, antenna gain or cuboids size have to be defined. In Table 4.8 the main parameters are shown, which have been the same for all the simulations performed in this work. It is worth noting that the parameters have been chosen in order to match those of the real ZigBee-based devices and antennas used for the measurement campaign shown in the following paragraphs.

Parameter	Value
Launched Ray Resolution	1°
Permitted Reflections	5
Transmitted Power	10 dBm
Frequency	2.41 GHz
Transmitter/Receiver Antenna type	Monopole
Transmitter Antenna Gain	1.5 dBi
Receiver Antenna Gain	7 dBi
Cuboids size	10 × 10 × 10 cm

**Table 4.8.** 3D Ray Launching simulation parameters.

Firstly, the validation of the 3D Ray Launching simulations for its use in the presented scenario has been carried out. For that purpose, a measurement campaign within the real scenario has been made in order to compare these measurement results with those obtained by the 3D Ray Launching. On one hand, a ZigBee-compliant XBee-Pro module with a 1.5 dBi gain monopole antenna mounted on an Arduino board has been used as a transmitter (see Figure 4.40a). It has been connected to a laptop via USB cable and placed on a standing judoka's chest, at 1.35 m height. The wireless mote has been configured to operate at 2.41 GHz, which corresponds to the channel 12 of the IEEE 802.15.4 standard. The transmitted power level has been set to 10 dBm and the bitrate to 250 Kbps, with the 'Serial Interface Data Rate' set to 125 Kbps (bauds per second). On the other hand, an OAN-1070 monopole 7 dBi gain antenna for ISM 2.4 GHz band operation connected to an Agilent FieldFox N9912A portable spectrum analyzer has been used as receiver. Figure 4.40 shows both the transmitter mote and the receiving antenna. Before the measurement campaign, a spectrogram has been measured in the center of the scenario under analysis in order to evaluate if any interference could affect the transmission over the chosen wireless channel. It has been measured with the antenna shown in Figure 4.40b connected to the Agilent FieldFox N9912A portable spectrum analyzer. Figure 4.41 illustrates the obtained spectrogram. As

can be seen, there is not any signal interfering the wireless channel 12, which is centered at 2.41 GHz with a bandwidth of 3 MHz.

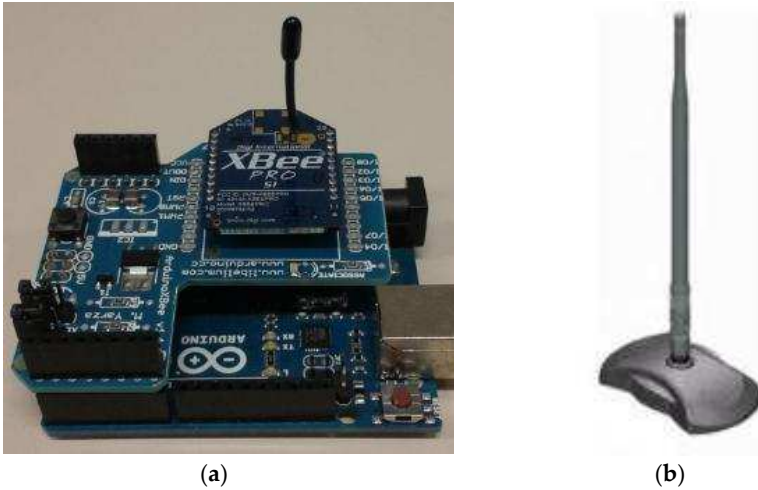


Figure 4.40. (a) XBee-Pro module used as transmitter; (b) 2.4–2.5 GHz band monopole antenna used as receiver.

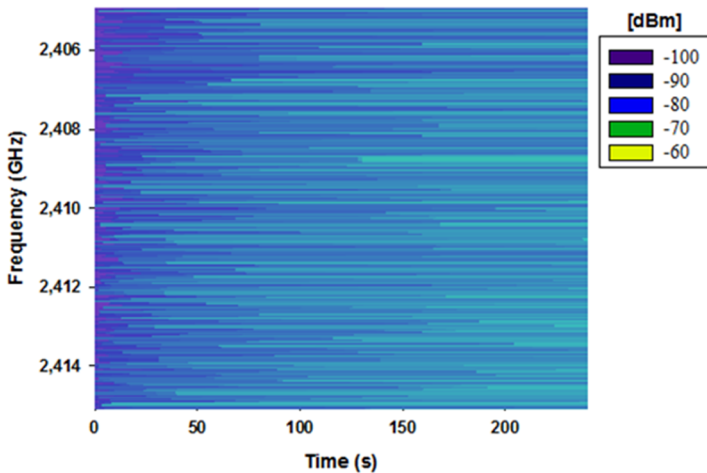


Figure 4.41. Measured spectrogram within the scenario under analysis for the ZigBee channel 12.

The configuration of the scenario for the radio propagation measurements is represented in Figure 4.42, where the standing judoka with the transmitter on the chest can be seen. The white dashed lines represent the linear distance where the measurements have been taken. The height is 1.35 m, the same height of the transmitter on the chest. The measured power level values are depicted in Figure 4.43, where the comparison with the estimations obtained by the 3D Ray Launching method is shown. Besides, estimations by traditional empirical models such as COST-231 and ITU-R P.1238 are included in the graph in order to compare them with the in-house 3D Ray Launching simulation tool. As can be clearly seen in Figure 4.43, the empirical models follow the tendency of the measurements curve, but they do not fit it properly due to the rapid variations of the received power, which is due to the multipath propagation. Besides, the empirical models do not take into account the effect of the presence of the judoka. Thus, the estimated power levels for  $x$ -axis negative values (i.e., behind the judoka) obtained by the Cost-231 Multiwall and ITU-R F.1236 empirical models are worse since the losses due to the human body are not taken into account (see Figure 4.43b,c). On the contrary, the 3D ray launching algorithm takes into account all the elements within the scenario, including the judoka, and its estimations fit very well the variations observed in measurements. In fact, taken into account the 100 measurement points represented in Figure 4.43, the mean error between measurements and 3D Ray Launching estimations is 0.76 dB, with a standard deviation of 2.07 dB.

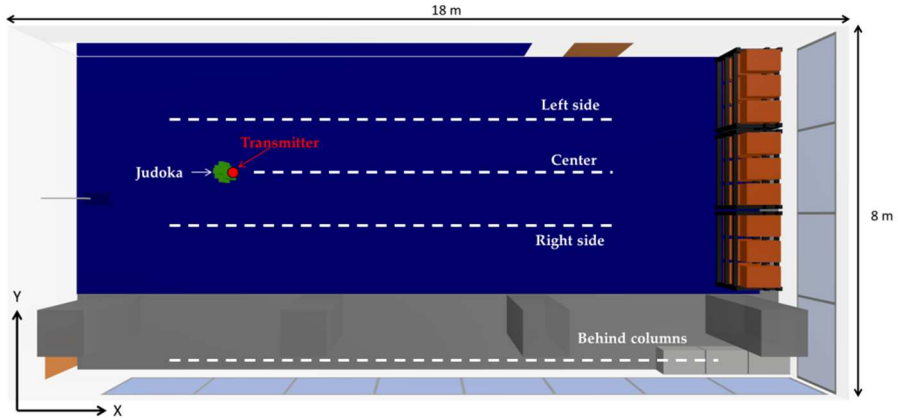
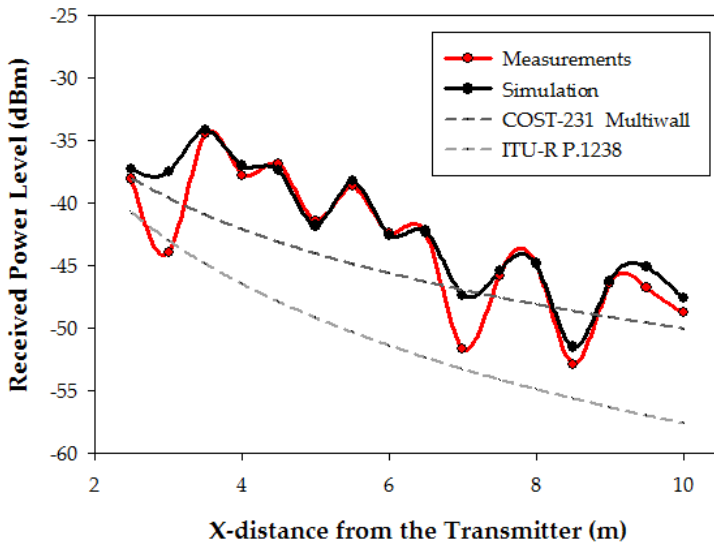


Figure 4.42. Upper view of the scenario presented in Figure 3 with the position of the transmitter element and the linear distances where the measurements have been taken (white dashed lines).

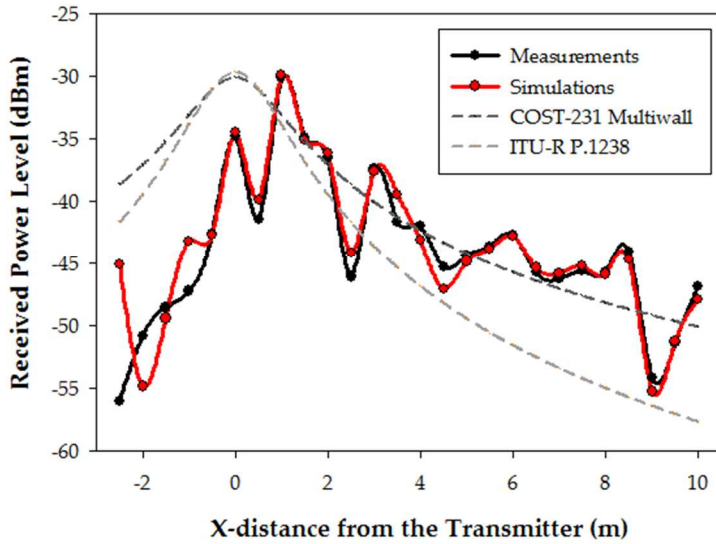
### Center Linear Distance vs. Received Power



(a)

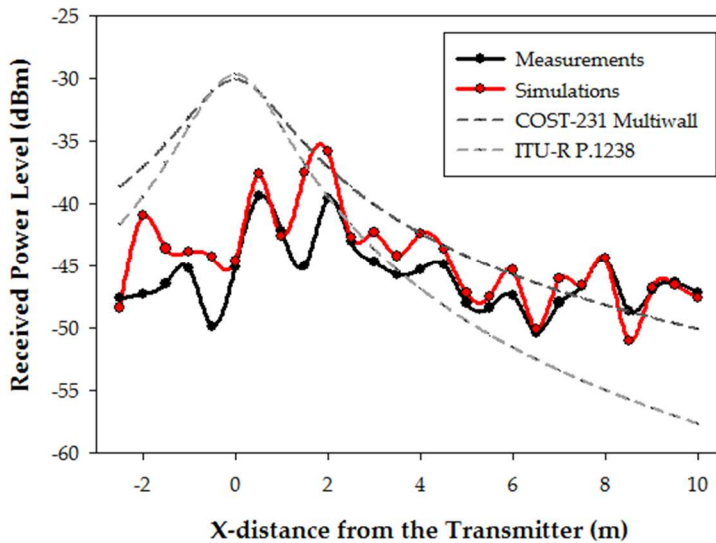


### Right side Linear Distance vs. Received Power



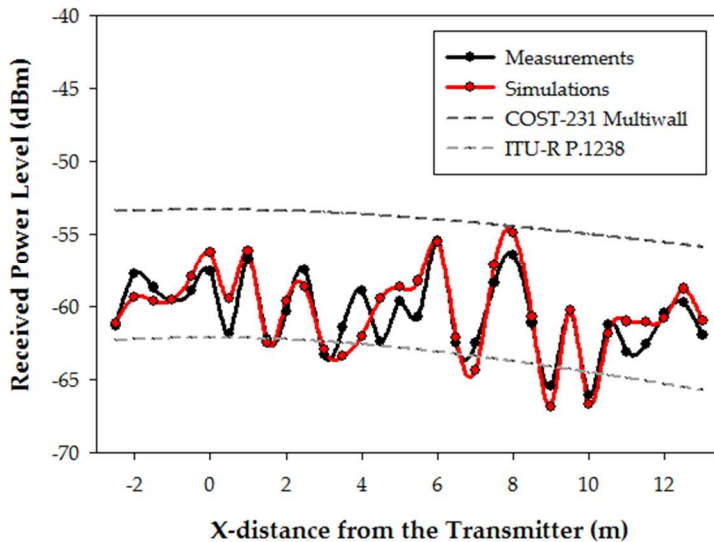
(b)

### Left side Linear Distance vs. Received Power



(c)

### Behind Columns Linear Distance vs. Received Power



(d)

**Figure 4.43.** Linear distance vs. received power level corresponding to the dashed lines depicted in Figure 4.42: (a) Center; (b) Right side; (c) Left side; (d) Behind columns.

As the aim of this work is to assess the impact of the presence of persons within this kind of scenario, once the validity of the results obtained by means of the 3D Ray Launching algorithm for the scenario without people (except the judoka with the transmitter) has been made, new measurements and simulations with the inclusion of an extra human being (placed 2 m in front of the judoka with the transmitter) have been performed in order to validate the inclusion of the in-house developed human body model. Figure 4.44 shows the position of the persons and the new measurement points, represented by white numbers (from 1 to 12). The measurement points are at the height of 1.35 m. Figure 4.45 shows the comparison between measurements and 3D Ray Launching simulations. In addition to the results with the inclusion of the person in front of the transmitter, the results without that person are also shown. Thus, besides the accuracy of the obtained

estimations, the effect of introducing a person can be seen. As expected, the received power level is lower when the extra person is included in the scenario. It can be also seen that the accuracy of the estimations is also high when the human model is included in the simulated scenario.

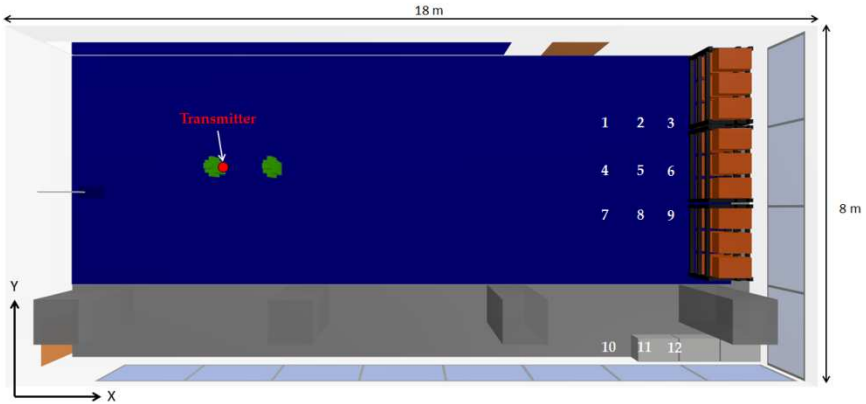


**Figure 4.44.** Upper view of the scenario with the new measurement configuration. The white numbers represent the measurement points.

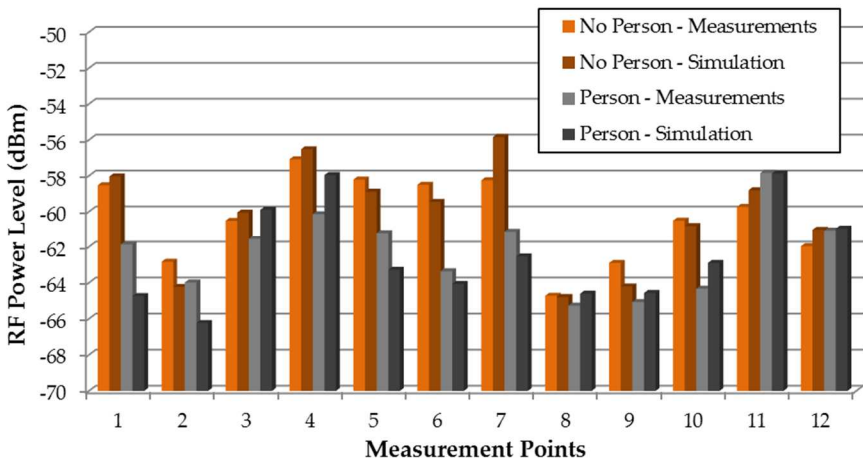
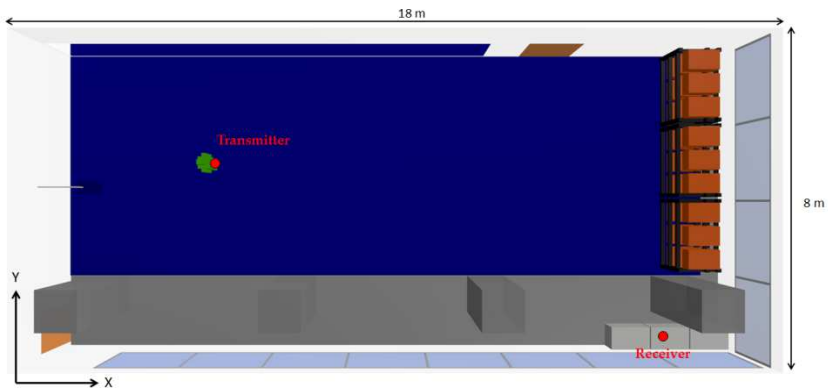


**Figure 4.45.** Measurements vs. 3D Ray Launching simulation results, both for the presence of an extra person and without the person. The measurement points correspond to those shown in Figure 4.44.

In order to gain insight on the assessment of the impact of the presence of persons within the scenario, further simulations have been performed. For that purpose, a XBee-Pro transmitter has been placed on the chest of a judoka (represented by a red dot in Figure 4.46), at 1.35 m height, and a receiver has been placed on the small lockers at height of 0.8 m (represented by a red dot in Figure 4.46), emulating a wireless link between a wearable wireless sensor and a laptop acting as a sink, receiving the information of the deployed WSN.

Three different cases have been simulated, maintaining both the transmitter and the receiver in the same place, but changing the person density within the scenario. The three cases are with the only presence of the person who has the transmitter, the presence of 10 persons and the presence of 30 persons. All simulations are static. The distribution of the persons throughout the scenario has been chosen randomly, but taken into account that some of them represent training Judokas (placed on the tatami) and others represent people outside the tatami. Figure 4.46 shows the upper view of the scenario with the three different simulated cases. The simulations with persons have been carried out with the aid of the previously mentioned in-house developed human body model.



(a)

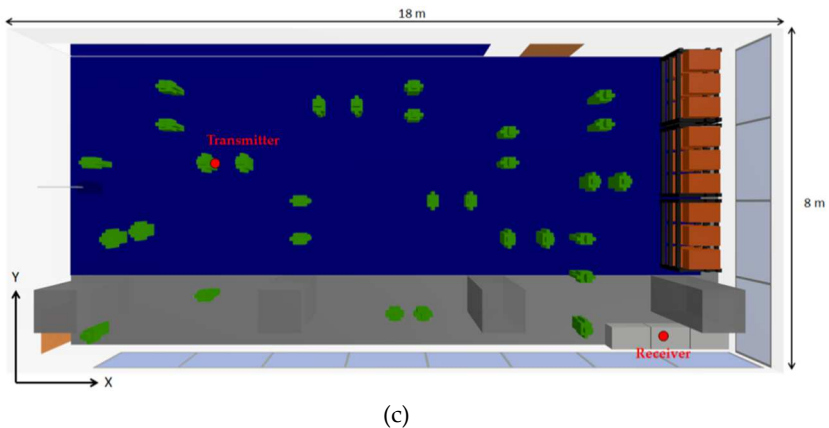
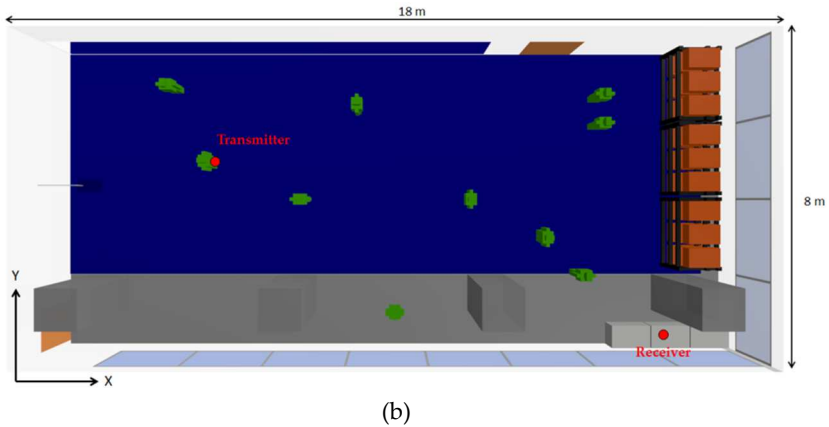


**Figure 4.46.** Upper view of the scenario under analysis with the position of the transmitter and the receiver devices (red dots) for the three cases of human being density: (a) Without persons; (b) With 10 persons; (c) With 30 persons.

As it is previously stated, the parameters used for the 3D Ray Launching simulations have been chosen to match the characteristics of ZigBee-compliant XBee-Pro devices operating at ISM 2.4 GHz band. Figure 4.47 shows the bidimensional plane of the estimated received power level at 0.8 m height (i.e., the height of the receiver) for the three cases under analysis. Both the position of the transmitter and the receiver are represented by white dots with the text 'TX' and 'RX'

respectively. Note that the position of the transmitter has been drawn although its real position is at height 1.35 m. The short term variation of the received power due to multipath propagation seen in Figure 4.43 can be also seen throughout the scenario. As the multipath propagation has a strong impact on the received power level, even more in the zones where the surrounding obstacles affect the LoS, two power delay profiles (PDP) are presented in Figure 4.48 for the case without persons in order to gain insight in this matter. Specifically, one PDP corresponds to a point just in front of the transmitter on the Judoka's chest at a distance of 10 m. The second one corresponds to the point where the receiver is placed (see Figure 4.46). It can be clearly seen how the first components arrive earlier to the position in front of the transmitter due to the LoS and the shorter distance. Besides, less multipath components and with lower power level arrive to the receiver location, as it is expected due to the surrounding obstacles. In addition, a dashed red line is depicted to show which components have a power level lower than the sensitivity of the used XBee-Pro modules.

Regarding the effect of the presence of persons, the difference between the case without persons and with 30 persons can be clearly seen, as the received power decreases at higher distances. On the contrary, the difference between the case without persons and with 10 persons is hard to note with a naked eye. In order to gain insight in the effect of the presence of persons, in Figure 4.49 the difference between the received power plane for the case without persons and the cases with persons is represented. As expected, the difference for the case of 30 persons is much bigger than for the case of 10 persons. Even so, the differences for the case of 10 persons are significant in terms of wireless channel quality for many points in the scenario, as the decrement of few dB in the received power can lead to a failure in the wireless communication due to either a received power level lower than the sensibility of the receiver device or an insufficient SNR value.

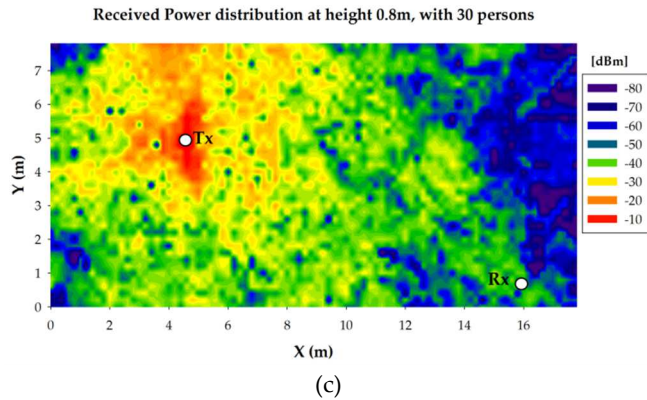
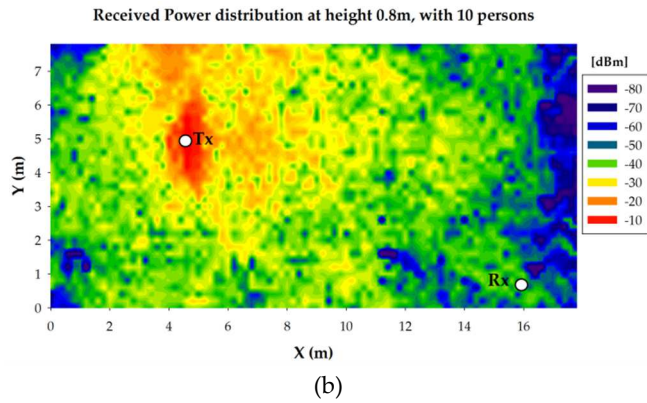
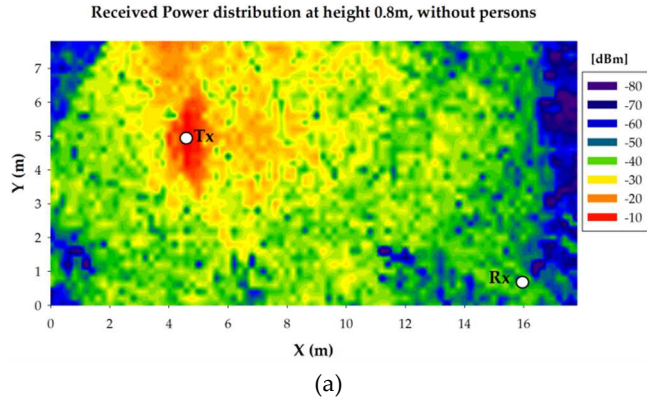


**Figure 4.47.** Estimated RF power distribution planes for the transmitter on the Judoka’s chest, (a) without persons; (b) with 10 persons; (c) with 30 persons.

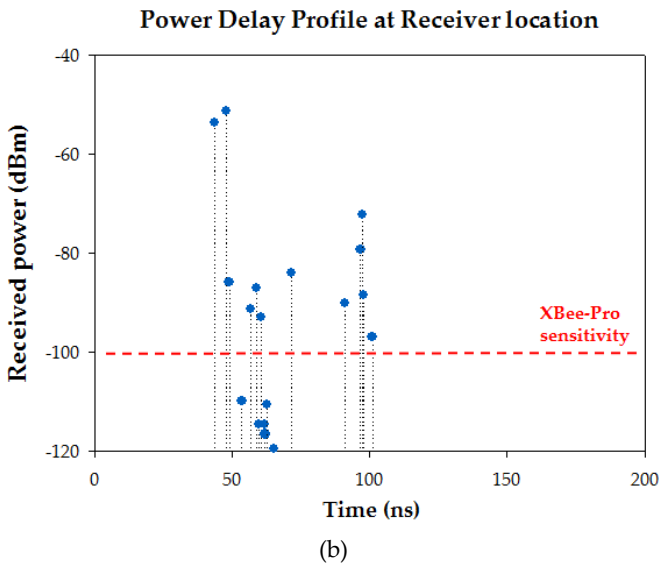
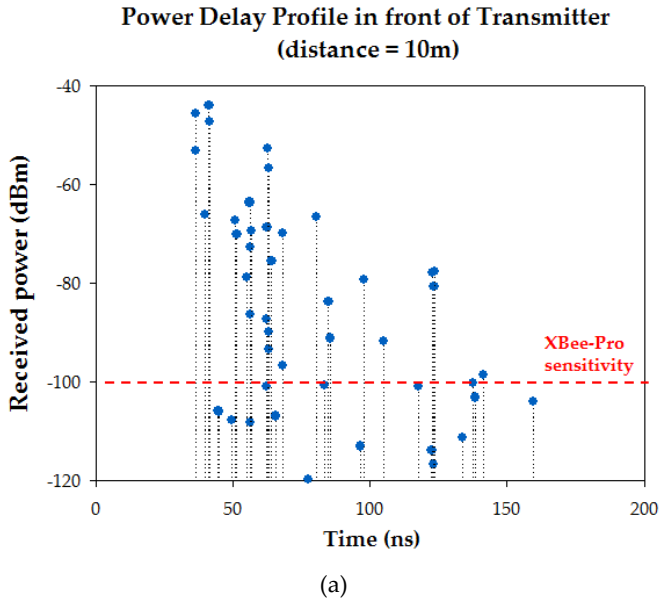


**Figure 4.48.** Power delay profiles at two different positions: (a) In front of the transmitter on the judoka’s chest at a distance of 10 m; (b) At the receiver location.



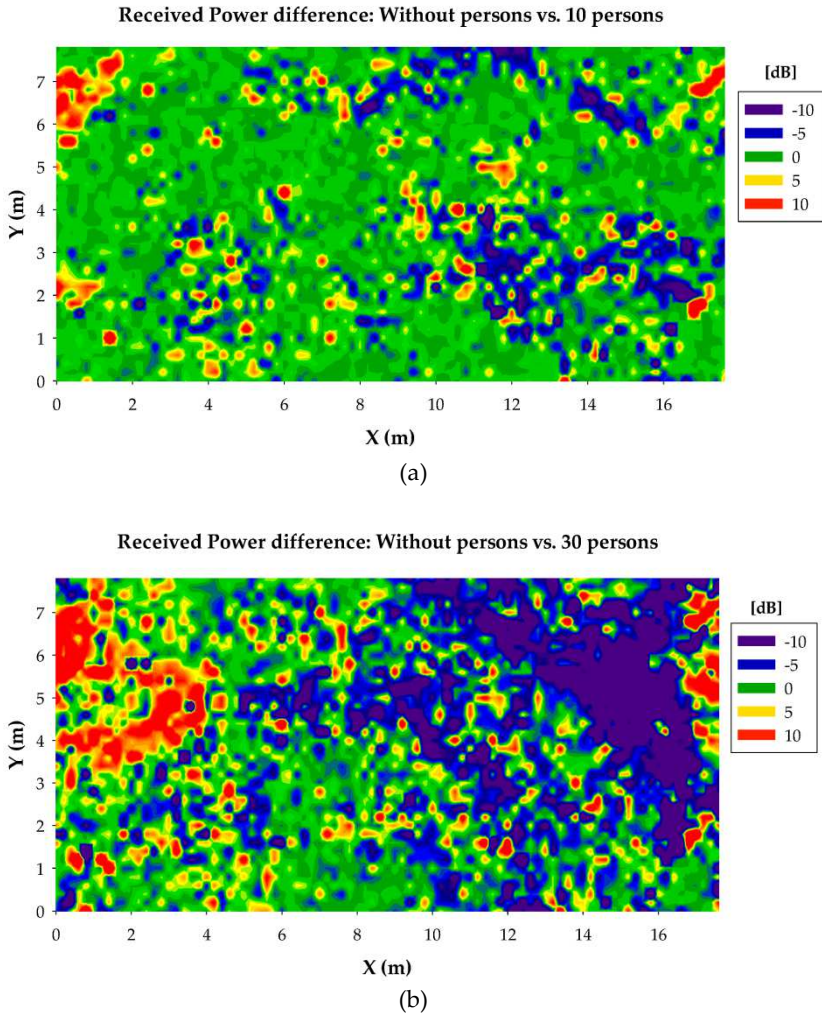


**Figure 4.49.** Received power level difference for the bidimensional plane at 0.8 m height between the results without persons and (a) with 10 persons; (b) with 30 persons.

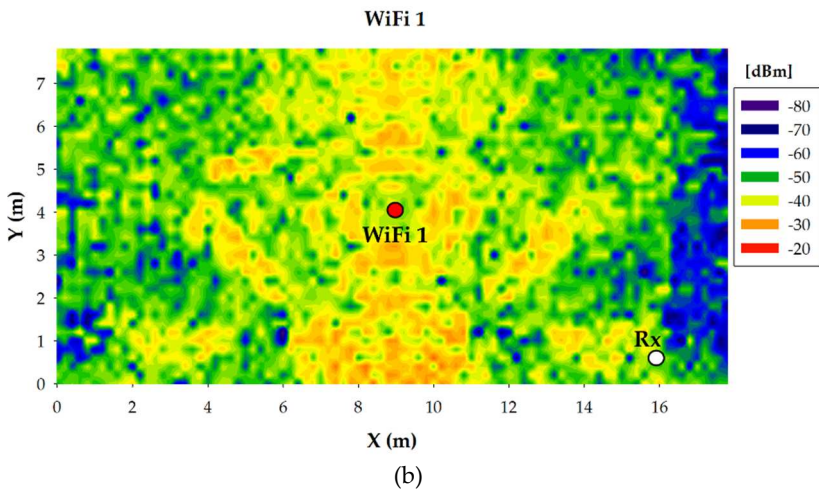
Once the effect of the presence of persons within the scenario under analysis in terms of received power level has been performed, how these results can affect the deployment of wireless transceivers in terms of data rate and energy consumption is presented. Firstly, the estimated

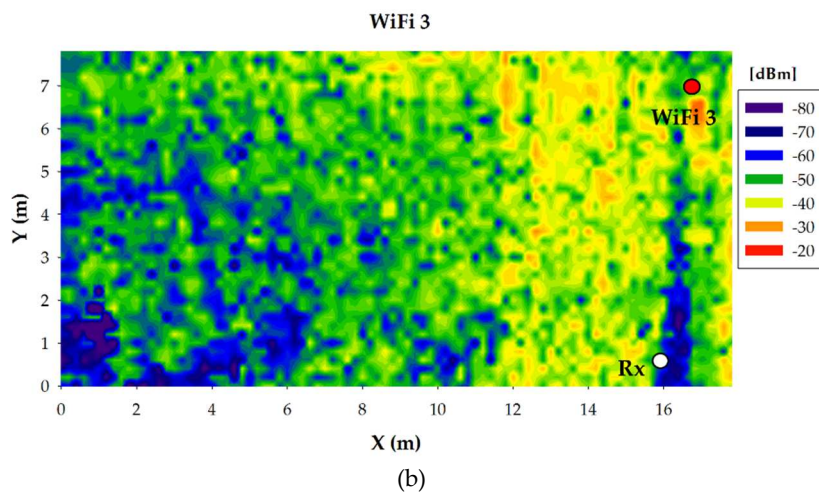
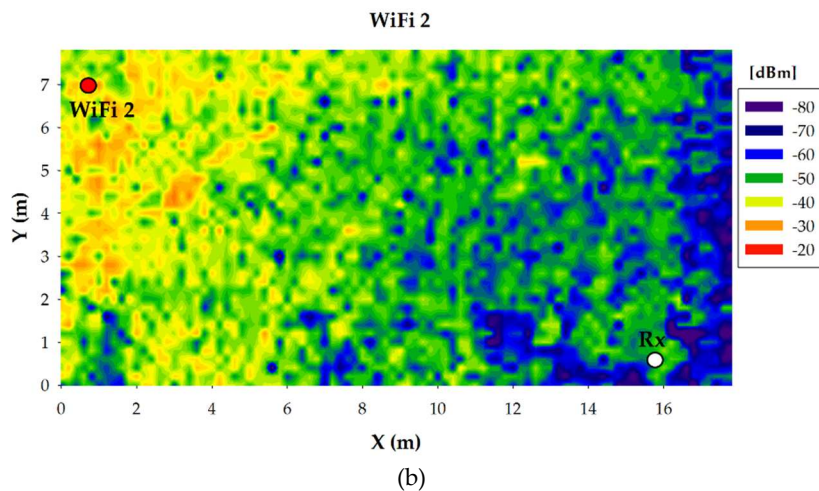
received power values give the information needed in order to know if a specific wireless transceiver will receive the required minimum signal power to have a successful communication with the transmitter. This minimum signal power is given by the sensitivity of the transceivers. In this case, the XBee-Pro modules have a sensitivity of  $-100$  dBm, which is surpassed by the received power for almost all the points throughout the whole scenario. But this is not enough to have a successful wireless communication between the transmitter and the potential receiver, as electromagnetic interference is likely to be present in such a scenario, even more in a future context aware scenario framed by the IoT and Smart City environments. In order to show the impact that interferences could have on the wireless communication within judo training environments, as an example, four WiFi access points have been placed in the scenario, fixed to the ceiling (height of 3.9 m), emitting 20 dBm at the same frequency of operation of the ZigBee nodes. The ZigBee transmitted power level has been set to 10 dBm. The location of the WiFi access points as well as the estimated WiFi power distribution at the height of 0.8 m for each access point is presented in Figure 4.50, for the case without persons. In order to assess if the ZigBee communication can be successfully achieved when those WiFi access points are transmitting, the relation between the received ZigBee signal power and the interference produced by the WiFi access points has been calculated, i.e., the SNR. Note that both the WiFi access points and the ZigBee nodes usually transmit traffic burst, not continuously. Therefore, the interference between those two wireless systems happens when both systems transmit at the same time, i.e., when collision of both signals happen. For this particular case, the required minimum SNR for a successful ZigBee communication is  $-12.26$  dB, calculated by equation 4.1. Table 4.9 shows the simulation results of the received ZigBee signal power level as well as WiFi interference levels at the receiver location (Rx), and in Figure 4.51 the estimated SNR values at receiver position for the different WiFi access point positions are depicted. The dashed red line represents the previously calculated minimum SNR value of  $-12.26$  dB. As can be seen, the potential positions of the wireless transceivers, both the nodes of our network

and the interfering devices, have a great impact on the performance, which at the same time will depend strongly on the morphology of the scenario.

WiFi Location	ZigBee Signal level (dBm)	WiFi Interference level (dBm)
WiFi 1	-64.12	-51.16
WiFi 2	-64.12	-71.11
WiFi 3	-64.12	-68.99
WiFi 4	-64.12	-48.91

**Table 4.9.** Simulation results at receiver point (Rx) for ZigBee transmitting 10 dBm and WiFi transmitting 20 dBm.





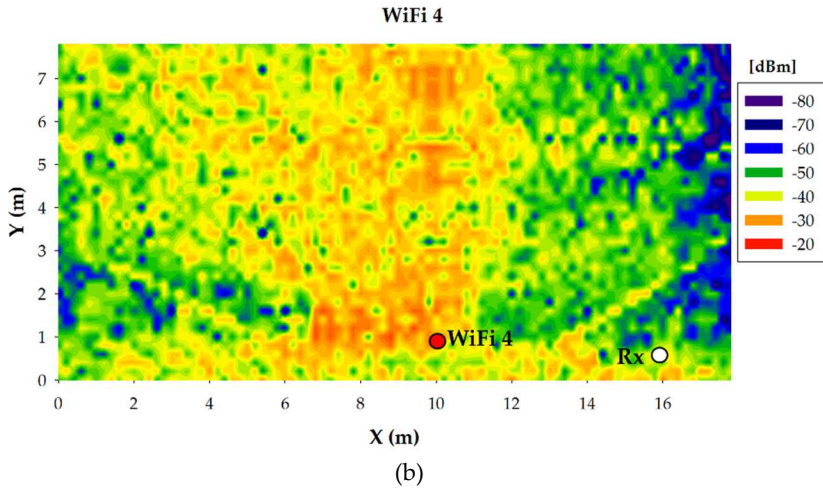


**Figure 4.50.** WiFi power distribution for the bidimensional plane at 0.8 m height for the case without persons. The red dots represent the WiFi access point locations.

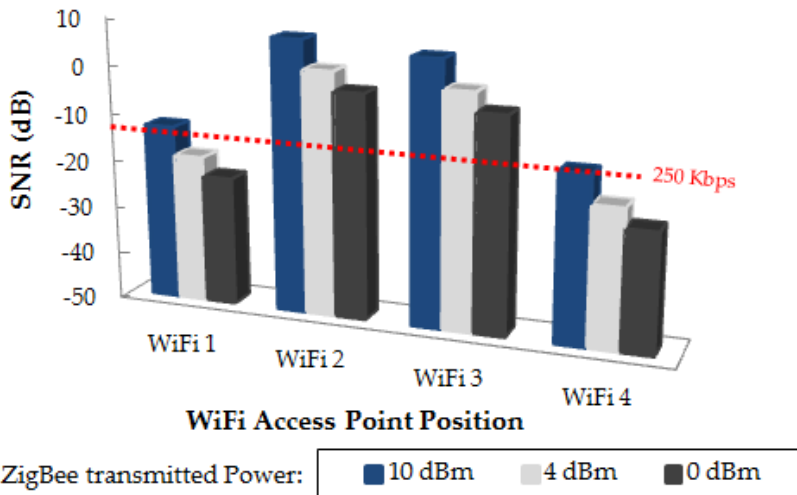


**Figure 4.51.** Estimated SNR values at receiver position for different WiFi access point positions, for different ZigBee transmitted power levels.

In order to gain insight in how the presence of human beings affects the performance of a ZigBee communication in terms of SNR, the WiFi 4 position has been taken as an example and in Figure 4.52 the SNR calculated at the receiver position (Rx) for the three cases without persons, with 10 persons and with 30 persons is presented. The x-axis indicates different transmission power levels for the ZigBee sensor of the judoka's chest. Note that although the European regulations allow transmitting up to 10 dBm, the inclusion of higher transmitting power levels in the analysis is due to the limitations are different in some other parts of the world and there are commercial devices which can transmit higher power level (e.g., the XBee-Pro modules used in this work, which transmit up to 18 dBm). Table 4.10 shows the simulation results of the received signal power levels as well as WiFi interference levels at the receiver location (Rx) when ZigBee transmits 10 dBm. As can be seen, for the WiFi 4 position, the received WiFi signal is not affected by the inclusion of persons, which is mainly due to the shorter distance between the WiFi access point and the receiver. But the received ZigBee signal is affected significantly, which is expected as in the case under analysis the included persons are in the path between the ZigBee transmitter and the receiver. Back to Figure 4.52, the difference between the cases without persons and including persons is due mainly to the lower ZigBee signal power received at the Rx point, which lead to a lower SNR value. As expected, the SNR increases when the transmitting power levels are higher. But it is worth noting that the 250 Kbps data rate is not achievable transmitting 10 dBm or less when collision between the WiFi and ZigBee happens. Increasing the transmitting power level above 10 dBm will avoid that problem, but at the expense of a higher energy consumption of the transmitter, which is likely to be powered by batteries. Instead, the proposed method based on the 3D Ray Launching algorithm can aid in finding an optimized WSN deployment, in order to obtain optimized transceiver placement in terms of achievable data rate as well as energy consumption.



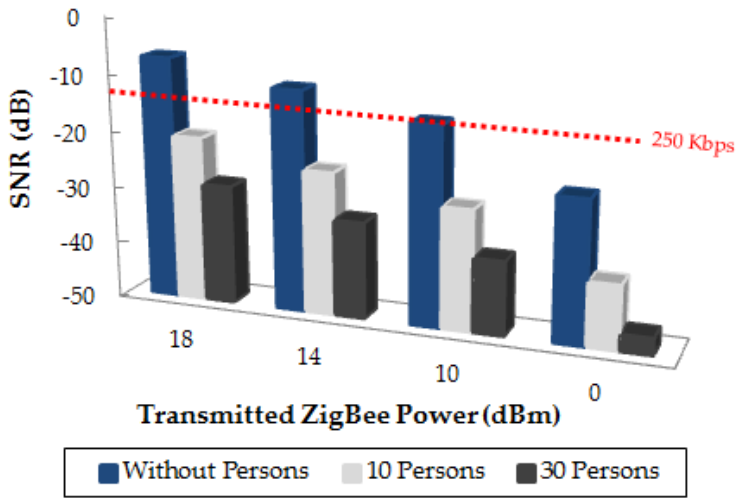


**Figure 4.52.** Estimated SNR values for different configurations of the Tx-Rx wireless link when the WiFi 4 access point is interfering.

Human Density Case	ZigBee Signal level (dBm)	WiFi Interference level (dBm)
Without Persons	-64.12	-48.91
10 Persons	-77.85	-48.91
30 Persons	-86.08	-49.02

**Table 4.10.** Simulation results at receiver point (Rx) for ZigBee transmitting 10 dBm and WiFi transmitting 20 dBm.

The presented results show that in addition to the placement of the wireless transceivers (transmitters as well as receivers), which has a great impact on the power distribution throughout the scenario, the presence of persons is an important factor that has to be taken into account in order to obtain an optimized deployment of a ZigBee WSN. In fact, the high density of persons that can be found in this kind of scenarios can be a determining factor in the performance of the deployed ZigBee-based WSN in terms of achievable data rate and energy consumption.

### 4.1.2 Acceleration Technique

At this point of the work, it has been shown how accurate and valid the in-house developed 3D Ray Launching algorithm is. Although this simulation technique obtains results in a reasonable amount of time comparing to other deterministic methods, the computational cost could be quite high in some scenarios (e.g. a few days).

Searching for a way that could reduce the computational time and which maintains the accuracy of this 3D Ray Launching algorithm, a novel hybrid simulation method based on the combination of the in-house developed 3D Ray Launching algorithm and a Collaborative Filtering (CF) technique has been developed with the collaboration of the Universitat de Rovira i Virgili. The following presented methodology gains importance when dense wireless networks are deployed within complex scenarios, which will be very common in the frame of IoT and Context Aware environments.

In this section of the manuscript, this novel approximation based on the combination of the in-house developed 3D Ray Launching code and a Collaborative Filtering (CF) technique is used to analyze the performance of wireless systems emulating a Context Aware scenario. The application of the presented method, in combination with new optimizing algorithms [Ahm15][Cam15][Jai15], will enhance the WSNs performance in Context-Aware environments.

The first step for developing the hybrid method has been to set two different 3D Ray Launching simulation configurations in order to fit the CF method with results: High Definition (HD) simulations and Low Definition (LD) simulations. HD simulations use parameters usually set to obtain accurate estimations in indoor environments. On the contrary, LD simulations provide less accurate estimations, but the computational cost is much lower. The main parameters that have been used for both LD and HD simulations are summarized in Table 4.11.



Parameter	LD	HD
Frequency	2.4 GHz	2.4 GHz
ZigBee Transmitted Power	0 dBm	0 dBm
WiFi Transmitted Power	20 dBm	20 dBm
Antenna Gain	1.5 dBi	1.5 dBi
Diffraction enabled	No	Yes
Horizontal plane angle resolution ( $\Delta\Phi$ )	2°	1°
Vertical plane angle resolution ( $\Delta\theta$ )	2°	1°
Maximum permitted reflections	3	7
Cuboids Resolution	10cm	10cm

**Table 4.11.** Parameters for the 3D Ray Launching HD and LD simulations.

The CF technique is a kind of Recommender System (RS) [Gol92]. RS are a family of techniques used to manage and understand the information created by users in Web 2.0 websites and to allow them to obtain recommendations about products and services [Res97]. RS help users to distinguish between noise and profitable information, hence achieving their goals more efficiently. Moreover, thanks to RS, companies increase their revenue, reduce their costs and provide better services to their customers.

Regarding the CF technique, its aim is to make suggestions on a set of items ( $I$ ) (e.g. books, music, films or routes), based on the preferences of a set of users ( $U$ ) that have already acquired and/or rated some of those items. In order to make recommendations (i.e. to predict whether an item would please a given user) CF methods rely on large databases with information on the relationships between sets of users and items.

These data take the form of matrices composed by  $n$  users and  $m$  items, and each matrix cell  $(i,j)$  stores the evaluation of user  $i$  on item  $j$ . Recommendations provided by CF methods make the assumption that similar users are interested in the same items. Hence,  $u_a$ 's high rated items could be recommended to user  $u_b$  if  $u_a$  and  $u_b$  are similar. CF methods are classified into three main categories according to the data they use: (i) memory-based methods, which use the data matrix with all entries, ratings and relationships, (ii) model-based methods, which

estimate statistical models and functions based on the data matrix, and (iii) hybrid methods, which combine the previous methods with content-based recommendation [Su09].

In this work a memory-based approach has been used in order to finely tune (recommend) the results obtained by LD simulations and produce better values that resemble HD simulations in much less time. This CF approach is divided in two steps: neighborhood search and recommendation/prediction computation. In the Neighborhood search phase, given a user  $u_a \in U$ , similarity functions are used to determine the users that are most similar to  $u_a$  (i.e., the neighborhood of  $u_a$ ). In the Recommendation/Prediction computation phase, the neighborhood of  $u_a$  is determined and a recommendation is made using well-known methods such as the ones proposed in [Su09].

#### Applying Collaborative Filtering on 3D Ray Launching simulations:

The RF power distribution results obtained by the 3D Ray Launching technique are represented as matrices with dimensions  $n \times m$ . Without loss of generality, each matrix  $M_{n \times m}$  is represented as a row vector  $V$  that results from the concatenation of all rows of  $M$ . Each scenario may contain different sets of obstacles and materials. The goal is to predict (recommend) values that LD simulations are unable to compute properly due to their low resolution. In order to do so, a memory-based CF method with two stages was suggested. Those stages are: (i) knowledge database creation and (ii) values prediction.

**Knowledge database creation:** This stage consists in the creation of a database that will be later used to predict missing values in LD simulations (in the second stage). For each scenario represented by a vector  $V = (v_1, v_2, \dots, v_{L_V})$ , with length  $L_V$ , a collection of sub-vectors is created, with fixed length  $L_{SV}$ ,  $SV = \{sv_1, sv_2, \dots, sv_{(L_V - L_{SV} + 1)}\}$  so that  $sv_i = (v_i, v_{i+1}, \dots, v_{L_{SV} + i - 1}) \forall i \mid L_V - L_{SV} + i \geq 0$ . Figure 4.53 shows how sub-vectors with  $L_{SV} = 3$  are generated from a given vector scenario  $V$ . This process results in a database comprising fixed-length sub-vectors that are used as patterns representing a variety of scenarios. Note that several databases with different sub-vector lengths containing as much

scenarios as wanted can be created. Also, it is worth noting that this procedure has been applied to vectors of LD simulations and their corresponding HD counterparts. As a result, the databases contain LD patterns/vectors that are correlated/associated with their corresponding HD counterparts.

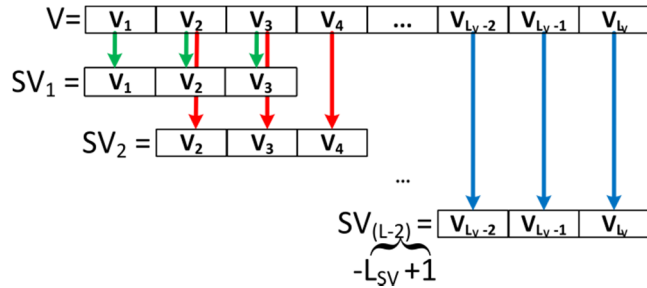


**Figure 4.53.** Graphical scheme of sub-vectors generation.

**Values prediction:** Given a LD simulation  $S$  with missing/null values, the goal is to predict them so that they are as similar as possible to the values that would have been obtained in a HD simulation. First,  $S$  is divided in sub-vectors of a chosen length  $L_{sv}$  (like in the previous step). For each sub-vector containing missing values, the  $k$  most similar sub-vectors in the LD knowledge database (created in the previous step) are found. Then, their corresponding HD sub-vectors are retrieved and the missing values in  $S$  are replaced by the average of those HD values.

In order to compute the similarity between sub-vectors, the Euclidean distance over non-missing values has been used. A graphical representation of this procedure is depicted in Figure 4.54. The prediction procedure is first applied by rows and then by columns and the average of the outputs is computed. It is worth mentioning that the prediction procedure is applied for each sub-vector length. Hence, different outcomes depending on  $L_{sv}$  are obtained.

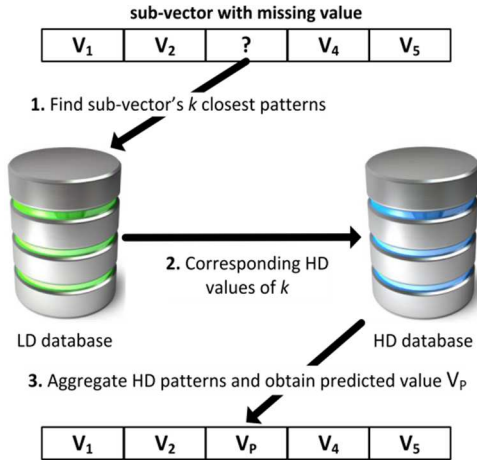


Figure 4.54. Illustration of the procedure of predicting missing values .

Now, a scenario has been chosen in order to apply the novel 3D Ray Launching – CF hybrid method. The scenario is shown in Figure 4.55, which is the same scenario of Figure 3.22, where the results obtained by the 3D Ray Launching have been already presented and validated in section 3.2.2 of this work.

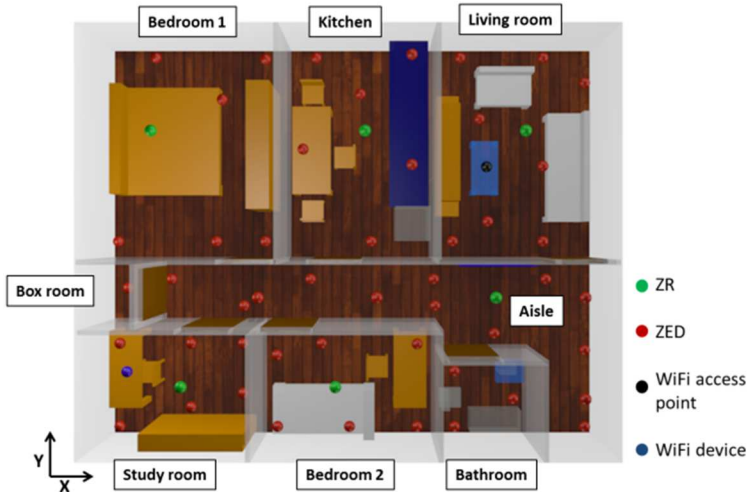


Figure 4.55. Top view of the scenario under analysis.

Due to the increasing number of wireless systems and applications based on CA environments, scenarios like the apartment studied in this work are expected to need a large number of wireless devices deployed in quite small areas. In order to emulate a dense wireless network, a 56-device ZigBee network has been distributed throughout the apartment. Those devices could be either static or mobile and wearable devices. In Figure 4.55 the distribution of the devices can be seen: ZigBee End Devices (ZED) are represented by red dots and ZigBee Routers (ZR) by green dots, which emulate the devices that will receive the information transmitted by the ZEDs included in their own network.

A WiFi access point (black dot) and a WiFi device (blue dot) have been also deployed within the scenario. In the real scenario, there is a WiFi access point in the same place. These wireless elements, which are very common in real scenarios, could interfere with a ZigBee network. In order to gain insight into this issue, two spectrograms have been measured in the aisle of the real scenario. First, a spectrogram with only the WiFi access point operating has been measured. Then, an operating XBee Pro mote has been measured, with the WiFi access point off. Figure 4.56 shows both spectrograms. The XBee Pro module is operating at the lowest frequency band allowed for these devices, and it can be seen how its spectrum overlaps the WiFi signal. Both the WiFi and ZigBee can be configured to operate at other frequency bands, but taking into account that the bandwidth of the WiFi signal is wider than the ZigBee signal and in an AAL environments a lot of ZigBee-based network could be deployed, each one operating at different frequency band, it is likely that overlapping between wireless systems in this kind of scenarios occur.

Therefore, in addition to the performance of a WSN in CA environments in terms of received power distribution, the assessment of the non-desired interferences is a major issue, especially in complex indoor environments where many wireless networks coexist and where radio propagation phenomena like diffraction and fast fading are very strong. The effect of these phenomena, as well as the topology and morphology of the scenario under analysis, can be studied with the previously presented simulation method. The deployment of ZigBee-

based WSNs is versatile and allows several topology configurations such as star, mesh or tree. Besides, due to the wireless inherent properties and the size of the nodes, their position as well as the network topology itself can be easily changed and reconfigured. Thus, very different networks and sub-networks can be found in a single CA environment.

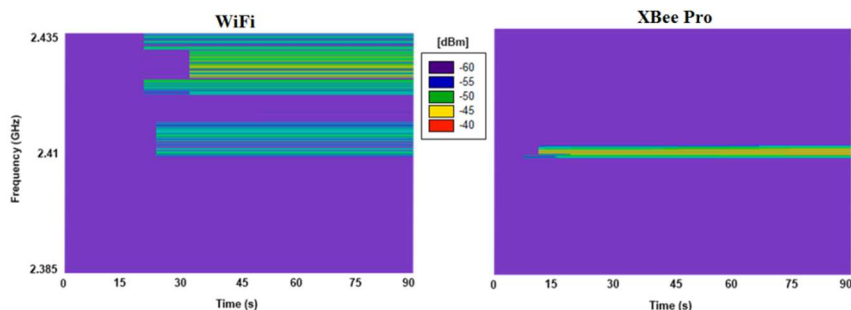


**Figure 4.56.** Spectrograms in the real scenario: (left) WiFi access point only, (right) XBee Pro module only.

On the other hand, the undesirable interference received by those wireless nodes could have different sources such as electromagnetic noise produced by electric appliances, but it is mainly generated by other wireless communication systems and devices, as it is shown in Figure 4.56. With the aim to show the usefulness of the presented hybrid simulation method for the analysis of interferences, 3 different situations for the wireless communication between a ZED and a ZR deployed in the scenario under analysis have been analyzed, namely an intrasystem interference case, a ZigBee intersystem case and a WiFi intersystem case. The interference level produced by the correspondent sources of the 3 case studies is respectively shown in Figure 4.57, Figure 4.58 and Figure 4.59, where the estimations obtained by both the HD Ray Launching simulations and the hybrid LD Ray Launching + Collaborative Filtering (LD+CF) method are shown. Note that in all the cases, the interference will occur only when the valid ZED and the interference sources transmit simultaneously and the frequency bands overlap. For the intrasystem interference case (Figure 4.57), a ZED

within the same network of the valid ZED-ZR devices has been chosen to act as interference source (cf. Figure 14). For the intersystem interference analysis, two different configurations have been studied. On the one hand, 4 ZigBee modules of another network deployed within the scenario act as interference sources: Figure 4.58 shows the interference level when the 4 ZEDs (at 1m. height) transmit simultaneously. On the other hand, 2 WiFi devices, placed at  $(X=7, Y=5, Z=0.8)$  and  $(X=0.5, Y=1.3, Z=1.1)$ , act as interference sources: It can be observed in Figure 4.59 that the interference level is significantly higher than in the previous cases. This is due to the transmission power of the WiFi devices, which has been set to 20dBm (i.e., the maximum value for 802.11 b/g/n 2.4GHz), while the ZED's has been set to 0dBm. In all the cases, the morphology of the scenario has a great impact in the interference level that will reach the ZR. The number of interfering devices and their transmission power level will also be key issues in terms of received interference power. Once more, it can be seen that an adequate and exhaustive radio planning analysis is fundamental to obtain optimized WSN deployments. Not only in the traditional way of calculating the RF power distribution of the deployed devices, but also analyzing the interference level within the environment.

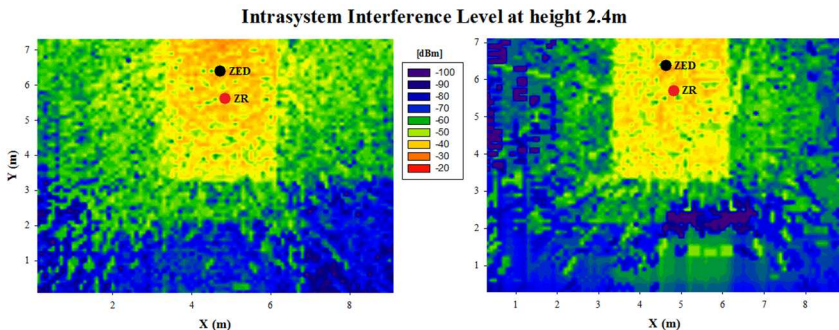


**Figure 4.57.** Received intrasystem interference level at 2.4m height when a second ZED in the kitchen ( $X=4.7\text{m}$ ,  $Y=6.3\text{m}$ ,  $Z=1\text{m}$ ) is transmitting: (a) HD results and (b) LD+CF estimations.



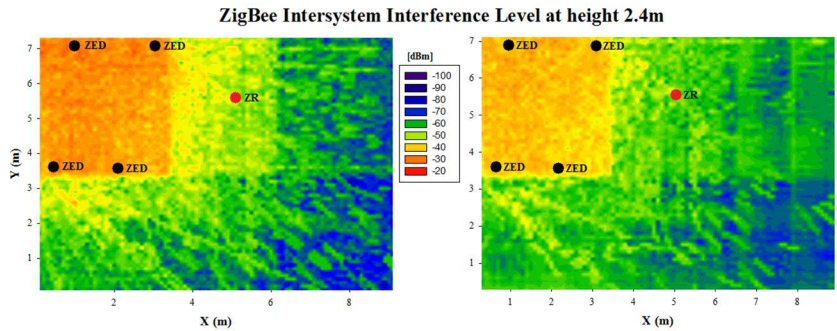


**Figure 4.58.** Received ZigBee intersystem interference level at 2.4m height when four ZEDs belonging to a network in the Bedroom1 are transmitting: (a) HD results and (b) LD+CF estimations.

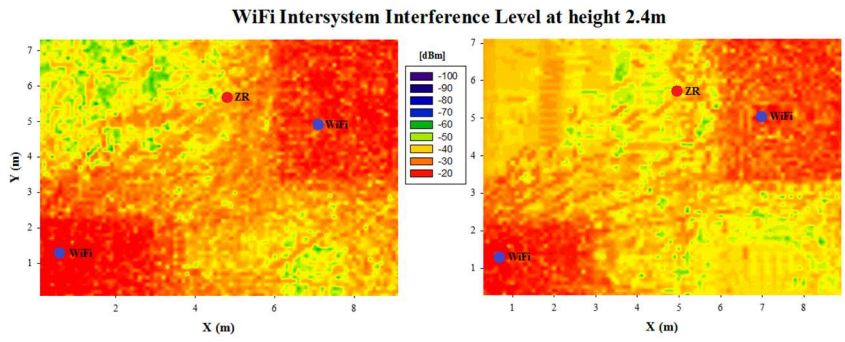


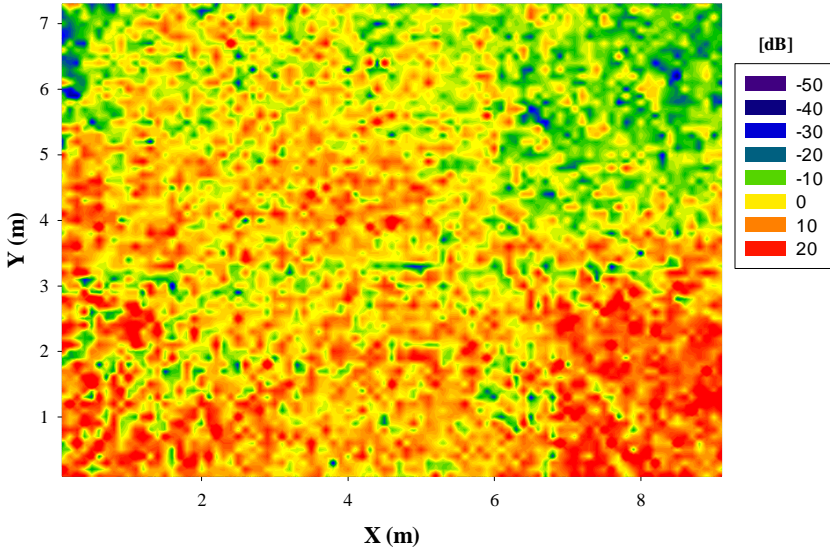
**Figure 4.59.** Received WiFi interference level at 2.4m height: (a) HD results and (b) LD+CF estimations.

Based on the previous results, SNR (Signal to Noise Rate) maps have been obtained. The SNR maps provide very useful information about how the interfering sources affect the communication between two elements, making easier to identify zones where the SNR is higher, and hence, better to deploy a potential receiver. Figure 4.60 shows SNR maps for the analyzed 3 interference cases. For some applications, it might not be possible to choose the receiver’s position, nor the position of other wireless emitters. In those cases, instead of using SNR maps, estimations of SNR level at the specific point where the receiver is placed are calculated. Figure 4.61 shows the SNR value at the position of the ZR for the studied cases. Note that the x-axis represents possible



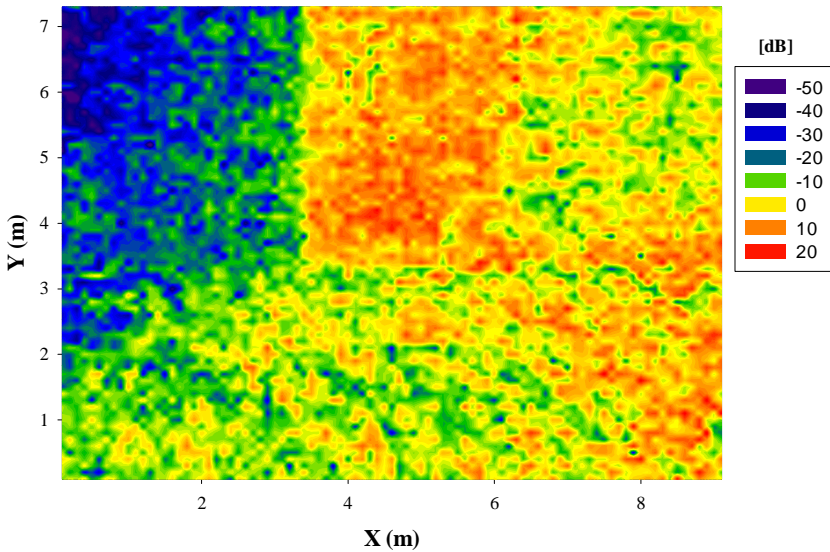
transmission power levels of the valid ZED. Again, the estimations by the HD ray launching as well as estimated values by LD+CF are shown in order to show the similarity between both methods in terms of predicted values. The red dashed lines in the figure represent the minimum required SNR value for a correct transmission between the valid ZED and the ZR at 256 Kbps and 32 Kbps. As it can be seen in Figure 18, for the analyzed ZigBee intersystem interference case (green curve), estimations show that it is likely to have no problem and the transmission will be done at the highest data rate (256 Kbps), even for a transmission power level of -10dBm. For the intrasystem case (black curve), a communication could fail when the transmitted power decay to -10dBm, where the SNR value is not enough to transmit at 256 Kbps, while the transmission will be successful at lower data rates. Finally, under the conditions of the 2 WiFi devices interfering the ZED-ZR link, the communication viability depends strongly on the transmission power level of the valid ZED, even for quite low data rates, as the noise level produced by the WiFi devices transmitting at 20dBm is high. It is important to note that these SNR results have been calculated for a specific case with specific transmission power levels of the involved devices. Due to the large variability in the possible combinations of the previous factors (number, position and transmission power of interfering sources as well as valid communicating devices, the required data rates, the morphology of the scenario, etc.), the design procedure is site-specific, and therefore, the estimated SNR will vary if the configuration of the wireless networks present in the scenario change. Therefore, the presented simulation method can help estimating the SNR values at each point of the scenario for any WSN configuration, allowing the designer to make the correct decision in order to deploy and configure the wireless devices in an energy-efficient way.

### SNR for Intrasystem Interference



(a)

### SNR for ZigBee Intersystem Interference



(b)

### SNR for WiFi Intersystem Interference

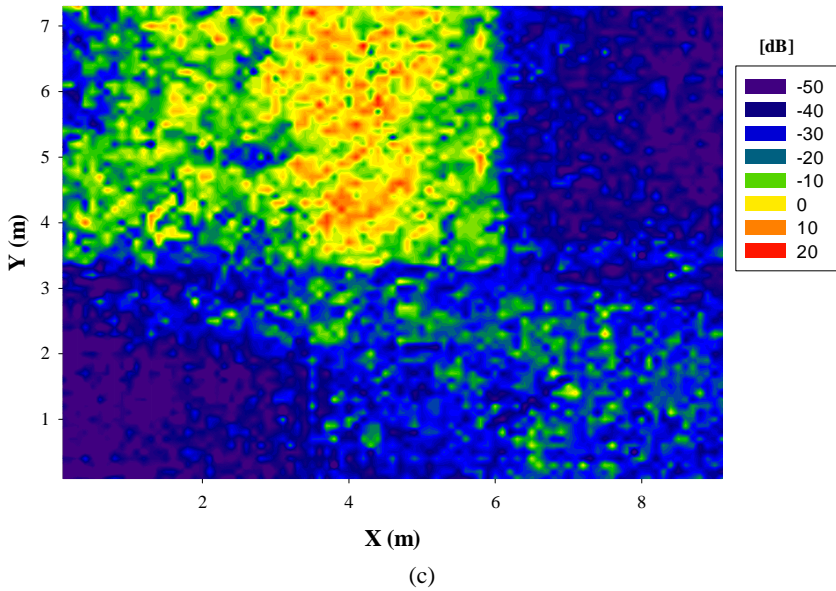


Figure 4.60. SNR maps for the 3 different interference sources acting over the valid ZED: (a) Intrasytem, (b) ZigBee intersystem, and (c) WiFi.

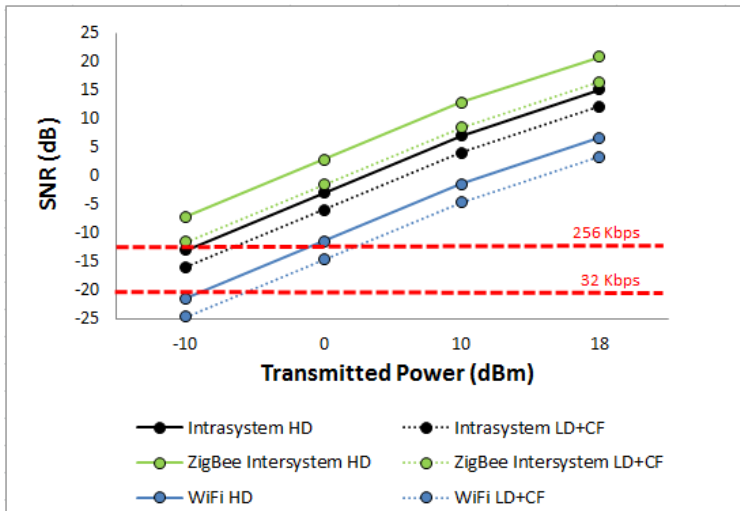


Figure 4.61. Estimated SNR values at ZR for 3 different interference cases.

## LD+CF PREDICTION QUALITY ANALYSIS

The previous results have shown that the estimations of the hybrid LD+CF proposal are similar to those obtained with 3D Ray Launching HD simulations. Next, we summarize how these results have been obtained and we evaluate, in detail, the difference between the computationally cost HD simulation and the fast LD+CF approach.

**Knowledge Database Creation:** In order to create the knowledge databases used by the LD+CF method, 16 different scenarios have been simulated with 30 to 40 layers, each containing a variety of features (i.e. corridors, columns, walls, doors and furniture). Each scenario has been simulated in LD and HD. With these simulations results, five LD knowledge databases with  $L_{sv}$  11, 9, 7, 5 and 3, and their five HD counterparts have been created. Each knowledge database contains approximately one million patterns/sub-vectors. In this study, the scenario under analysis has similar characteristics than those used for the creation of the databases. The dimensions and density of obstacles of the scenario under analysis are summarized in Table 4.12. Rows and Columns refer to the planar dimensions of the scenario (i.e., the dimensions  $(x, y)$  of the matrices analyzed/used by the CF method). The Layers row indicates the number of matrixes, i.e., the height  $(z)$  of the scenario. Finally, the Density row shows the percentage of the volume of the scenario occupied by obstacles.

	Rows	Cols	Layers	Density %
Scenario	91	73	27	9.497

**Table 4.12.** Dimensions and characteristics of the scenario under analysis.

**Accuracy and benefits of the Collaborative Filtering approach:** With the aim of analyzing the accuracy and performance of the LD+CF approach, different prediction strategies have been applied for the scenario under analysis (see Table 4.13). For instance, Strategy 1 uses the previously created knowledge database with  $L_{sv} = 11$  to compute predictions, in Strategy 2  $L_{sv} = 9$  and so on. In all cases, an aggregator value  $k=25$  is used. Hence, for each missing value of an LD simulation,

the CF approach finds the  $k=25$  most similar sub-vectors and compute their average to predict the missing value. Although the CF approach significantly helps to improve the quality of the LD simulation, it does not always predict the exact same value of the HD simulation. In order to compute this discrepancy the well-known mean absolute error 'MAE' has been used, defined as follows:

$$\text{MAE} = \frac{\sum_{i=1}^n |p_i - r_i|}{n} \quad (4.2)$$

where  $n$  is the number of missing values predicted,  $p_i$  is the predicted value for a missing element  $i$ , and  $r_i$  is the real value of  $i$  in the HD simulation. Note that the HD simulation is only used to compute the error but it is not involved in the prediction process of the CF method.

Strategy	Details
1	$L_{SV} = 11, k=25$
2	$L_{SV} = 9, k=25$
3	$L_{SV} = 7, k=25$
4	$L_{SV} = 5, k=25$
5	$L_{SV} = 3, k=25$

**Table 4.13.** Simulation strategies: Sub-vector length  $L_{SV}$  and aggregator value  $k$ .

Without loss of generality and for the sake of brevity, 24 sensors have been randomly selected from the studied scenario and the comparison between the simulation results obtained by HD simulations and the hybrid approach LD+CF has been made. Table 4.14 reports the obtained results: Sparseness is the % of empty values in the LD simulation; Time HD, LD, CF and LD+CF are the time in seconds of each method (for LD+CF the worst time of the strategies is reported); Best Strategy is the strategy that performed better;  $MAE_R$  represents the mean absolute error considering that null cells are kept empty (i.e., LD vs. HD);  $MAE_P$  represents the mean absolute error considering that null cells are replaced by the values predicted by the CF method (i.e.,

LD+CF vs. HD); and  $\sigma_P$  is the standard deviation of  $MAE_P$ . Note that for the MAE, the lower the values the better the result. Hence, it is apparent that the results obtained by the hybrid LD+CF method ( $MAE_P$ ) clearly outperform those of the LD simulation alone ( $MAE_R$ ). In addition, the low values of  $\sigma_P$  indicate that predictions are stable and reliable. It can be also observed that the hybrid LD+CF approach requires 10 to 20 times less time than HD simulations and that the cost of the CF method is almost negligible comparing to HD and LD times. In Figure 4.62 the time comparison is represented graphically.

	Sparseness %	Time HD	Time LD	Time CF	Time LD+CF	Best Strategy	MAE <sub>R</sub>	MAE <sub>P</sub>	$\sigma_P$
1	47.221	90650	2981	112	3116	1	74.707	11.825	9.05
2	49.933	52309	3543	187	2783	4	75.181	13.252	10.22
3	30.291	64959	2953	55	3302	1	73.091	9.796	7.47
4	49.071	53709	3168	106	2948	1	72.737	10.812	8.36
5	41.458	58763	3197	116	3053	3	75.051	10.52	8.56
6	42.722	83949	3004	88	2730	1	72.509	10.281	7.57
7	33.574	90189	2596	84	3362	1	72.439	9.88	7.12
8	34.711	76368	3247	102	3211	2	73.408	9.914	7.49
9	39.952	94287	2842	103	3153	1	74.996	9.814	7.82
10	20.03	69627	2937	79	2889	2	78.893	7.797	6.25
11	24.915	80113	3315	99	2947	3	78.38	9.72	7.67
12	35.317	79136	2882	98	3246	1	70.076	13.394	8.92
13	35.266	56627	2608	101	2982	1	72.139	12.021	8.83
14	43.428	59785	2906	115	2776	1	73.255	14.092	10.1
15	43.154	46410	2870	138	2558	4	76.506	12.005	9.11
16	38.066	67031	2642	95	2971	1	72.24	13.756	9.94
17	45.551	50729	3278	123	2509	2	76.485	13.294	9.89
18	42.902	83750	3109	120	3106	1	69.985	14.618	10.73
19	55.942	50423	3050	168	2761	2	74.522	12.073	8.91
20	54.066	58216	2810	186	3109	3	72.824	11.724	8.8
21	57.699	55179	3183	201	2985	3	74.018	10.716	8.29
22	44.755	74635	2606	99	2869	1	71.712	14.338	10.88
23	38.979	59727	2877	56	2983	1	64.586	16.998	11.45
24	48.459	75307	3245	79	2794	1	74.443	10.435	7.86

**Table 4.14.** Average results (over all layers of the scenario) of the hybrid LD+CF vs. the HD approach.

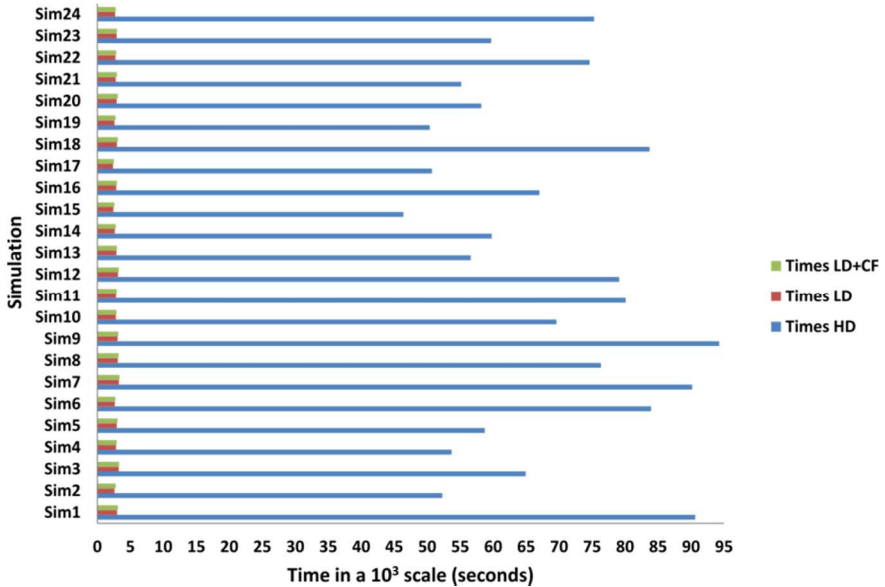


**Figure 4.62.** Time comparison of the different approaches (i.e. LD, LD+CF, HD) for each simulation.

Finally, the relationship between the MAE of each approach and simulation/prediction time is depicted in Figure 4.63. LD predictions (in red) correspond to the MAE<sub>R</sub> values from Table 4.14. LD+CF results (in green) show that the computational time is slightly increased with respect to LD simulations. Notwithstanding, the MAE is reduced between 8 and 10 times. Finally, the values of HD simulations (in blue) clearly show that the time required is 10 to 20 times higher than the other approaches. Clearly, the best tradeoff between MAE and time is obtained by the proposed hybrid LD+CF method. Therefore, it can be concluded that the proposed novel method outperforms the others when both accuracy and computational cost are considered.

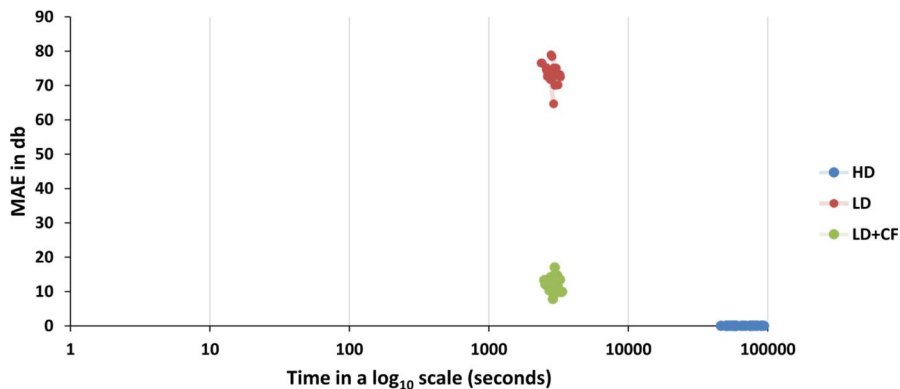


**Figure 4.63.** Relationship between MAE and execution time for LD, LD+CF and HD approaches.

Summarizing, the use of Ray Launching simulations in High Definition (HD) and Low Definition (LD) and Collaborative Filtering (CF) techniques have been compared in terms of accuracy and required computational time. A complex indoor scenario with multiple transceiver elements has been analyzed with those techniques and the obtained results show that the proposed hybrid LD+CF approach outperforms LD and HD approaches in terms of error/time ratio.

Results also show that the presented hybrid calculation approach enables to enlarge the scenario size without increasing computational complexity, or what is the same, to reduce drastically the simulation time consumption, while the error of the estimations remains low. The proposed approach to perform wireless channel estimations and analysis provides valuable insight in the network design phases of complex wireless systems, which derives in optimal network deployment, reducing overall interference levels and increasing overall system performance in terms of cost reduction, transmission rates and energy efficiency.



## 4.2 Main Contributions

In this last section of Chapter 4, as it has been previously done in Chapter 3, I list only my main contributions (i.e. the articles and conference papers in which I am the first author) regarding the topic covered in this chapter. The rest of works regarding this topic where I contributed can be consulted in the List of Publications section.

As the published works have been carried out together with other co-authors, I would like to point explicitly what has been my work regarding those published works: My main contributions to the list of publications shown below have been the study of the state of the art, the performance of measurements within the scenarios under analysis, the creation of the scenario for the 3D Ray Launching simulations and the corresponding simulations, the post-processing of the obtained data and the writing of the most of the text of the manuscripts.

Note that all the research articles have been published in JCR (Journal Citation Reports) indexed journals.

- *Research Articles:*
  1. "Analysis of Energy Consumption Performance towards Optimal Radioplanning of Wireless Sensor Networks in Heterogeneous Indoor Environments," *Radioengineering*, vol. 23, no. 3, September 2014.
  2. "Performance Analysis of ZigBee Wireless Networks for AAL through Hybrid Ray Launching and Collaborative Filtering," *Journal of Sensors*, vol. 2016, Article ID 2424101, 2016.
  3. "Implementation and Analysis of ISM 2.4 GHz Wireless Sensor Network System in Judo Training Venues," *Sensors*, vol. 16, p. 1247, 2016.

- *Book Chapters:*
  1. “Chapter 13. Wireless performance in dense-transceiver scenarios to enable context-aware scenarios,” *The World of Applied Electromagnetics in Appreciation of Magdy Fahmy Iskander*, (to be published by Springer).
  
- *International Conference Papers:*
  1. “Analysis of Efficient Dense Wireless Sensor Network Deployment in Smart City Environments,” (*IEEE Sensors 2014*).
  2. “Performance Analysis of Heterogeneous Wireless Networks in Complex Indoor Scenarios,” (*2015 IEEE International Symposium on Antennas and Propagation and USNC-URSI National Radio Science Meeting*).
  3. “Assessment of ISM 2.4 GHz Wireless Sensor Networks Performance in Judo Training Venues,” (*2nd International Electronic Conference on Sensors and Applications-ECSA 2015*).
  4. “Radiofrequency Interference Analysis for s-Health and Context Aware scenarios in Hospital Environments,” (*2016 IEEE International Symposium on Antennas and Propagation and USNC-URSI National Radio Science Meeting*).
  5. “Analysis of Bluetooth-based Wireless Sensor Networks Performance in Hospital Environments,” (*In Proceedings of the 3th Int. Elec. Conf. on Sens. and App., 15-30 Nov. 2016; Sciforum Electronic Conference Series*).
  6. “Hybrid Ray Launching-Collaborative Filtering Approach for Wireless Propagation in Indoor Environments,” accepted in (*2017 IEEE International Symposium on Antennas and Propagation and USNC-URSI National Radio Science Meeting*).

# Chapter 5

## Modeling of Wireless Interference Sources

**T**HE validity of the in-house 3D Ray Launching simulation tool for radio propagation analysis within different kinds of complex scenarios has been widely discussed and demonstrated in the previous sections of this work. Besides, a novel point of view regarding radio planning duties in terms of interferences has been also developed, obtaining results such as SNR and BER values by simulating other wireless communication systems present within the environment under analysis, which is expected to be a key issue in a near future due to the advent of IoT and 5G systems. The radio propagation estimations of these interfering wireless systems are quite easy to perform as long as the RF characteristics of the wireless systems are known. Except some particular cases, the frequency of operation, power level, bit rate and antenna characteristics of such communication systems are usually obtainable, and therefore, susceptible to be simulated by the presented 3D Ray Launching method. But, what happens with the great amount of devices that generate

electromagnetic noise such as electronic devices, engines or power transformers? All these elements could interfere wireless communication systems, but contrary to them, estimate the electromagnetic propagation of noise sources within a scenario is an extreme difficult task to carry out. In fact, there are not reported works that estimate it. Trying to fill this gap, in this section of the work, a novel method for modeling electromagnetic interference sources for radio propagation estimations by the in-house 3D Ray Launching algorithm is presented. Section 5.1 focuses on the analysis of the interference created by one of the most known electromagnetic noise sources: a common microwave oven. Section 5.2 describes in detail the proposed modeling of electromagnetic sources for the inclusion in the 3D Ray Launching tool, particularized to the microwave oven. Finally, in Section 5.3 an application of the created model for dosimetric studies is presented.

## 5.1 Microwave Oven Interference on WSNs

Nowadays microwave ovens are very popular and can be found in almost every home and building. The heating source of these residential microwave ovens is based on a magnetron tube. The entire generated electromagnetic field does not remain in the oven's cavity, due to the fact that there are losses due mainly to power leakage from around the microwave oven's front door [Wen02][Kus02][Wen03][Mat03]. This leakage can be considered in practical terms as an interference source in the 2.4 GHz Industrial Scientific Medical (ISM) band [Mat05][Sol11].

In parallel, there is a wide variety of communication systems and protocols, such as digital radio communication systems, Bluetooth, 802.11 and ZigBee that operate in the 2.4 GHz ISM band which can be potentially interfered by the power leakage of microwave ovens [Min02][Ron04][Sim11][Tah12]. Due to the existence of this leakage power, it is important to analyze the performance of these devices operating in the 2.4 GHz ISM in the presence of microwave ovens, since

this interference can completely block services provided by such wireless systems. This effect is becoming more relevant due to fact that the number of existing applications based mainly on ZigBee WSNs operating in the 2.4 GHz band in indoor scenarios is rapidly growing (e.g., home automation and monitoring, energy management, health monitoring and lighting) [Zua09][Yan10][Han11][Bel12].

The negative impact that microwave oven power leakage has on the quality of a ZigBee communication in buildings has been demonstrated in the literature [Huo09][Guo10][Guo12]. It is worth noting that even though it is a known interference source, characterization of such interference and adequate radio planning analysis within an environment with wireless systems under operation has not been reported. In this work the coexistence between a ZigBee wireless sensor network, implemented with Digi XBee Pro devices, operating at 2.4 GHz and a real domestic microwave oven has been analyzed. For that purpose, a real scenario has been set up to perform measurements of leakage radiated power and its impact on transmission quality of ZigBee channels of operating wireless sensor nodes.

The scenario where the measurements have been performed is depicted in Figure 5.1. It is located in one of the R&D laboratories at the Public University of Navarre. The microwave oven has been located on a wooden table at a height of 0.7 m, in the location shown in Figure 5.1. The behavior of the microwave oven radiated electromagnetic power leakage has been characterized in first place. Once the nature of the interference has been analyzed, the impact that this interference has on the quality of the ZigBee channels of a set of operating wireless sensors has been measured. The value of PER (Packet Error Rate) has been used as the quality parameter. Due to the spectral width of the microwave oven frequency spectrum, all the ZigBee channels supported by the XBee Pro device have been analyzed (channels 12 to 23 of the 802.15.4 standard). A portable spectrum analyzer (Agilent FieldFox N9912A) with a LevelOne OAN-1070 omnidirectional antenna has been used to perform measurements of radiated power. The first measurement performed was the power spectrum when the microwave oven is heating an object. Figure 5.2 shows the measured spectrum of the

microwave oven operating at maximum power (the oven has three operating power levels), in which the interference level will be the highest. The distance from the receiving antenna coupled to the spectrum analyzer to the microwave oven front door is 10 cm and both are placed at the same height. It can be seen that the microwave oven radiates with significant power levels in almost all the 2.4 GHz ISM band, becoming this leakage a significant source of interference to wireless networks [Zha05].

Secondly, Figure 5.3 shows the frequency spectrum corresponding to ZigBee channel number 12 alongside the oven leakage power spectrum. As it can be seen, the leakage power level can be higher than the received ZigBee power within the operating range of the sensors. Therefore, the quality of ZigBee channels will be affected when both RF emissions (Wireless Sensor Network and microwave interference spectrum) overlap. This occurs in practically all the ZigBee channels measured in this paper (channels 12 to 23 of the 802.15.4 standard).



**Figure 5.1.** Real scenario where measurements have been carried out.

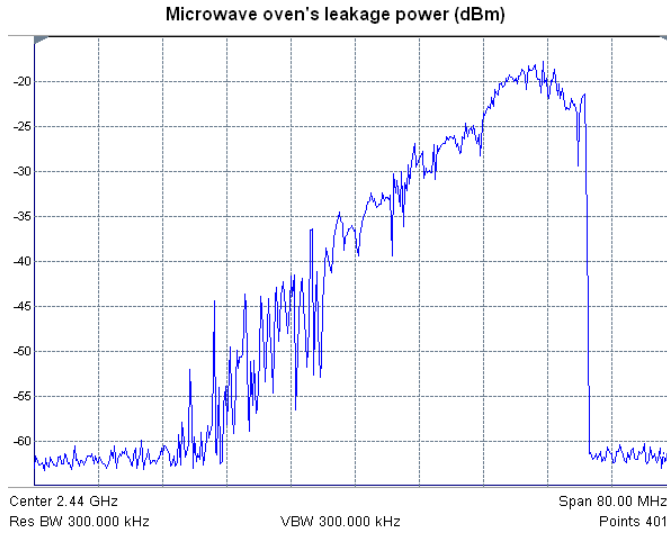


**Figure 5.2.** Measurement of the microwave oven leakage power spectrum in 2.36 GHz–2.52 GHz band, obtained from direct spectrum measurement within the indoor scenario.

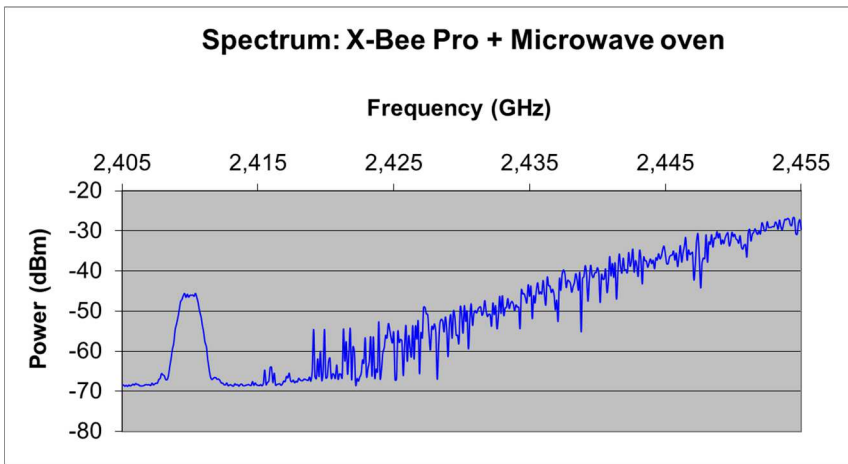


**Figure 5.3.** Measurement of ZigBee channel 12 (given by the peak visible on the left hand side) and microwave oven leakage spectrum.

Another aspect to consider is the fact that the microwave oven leakage spectrum has a time dependent power distribution. Taking this time dependent nature into account, a spectrogram using the max hold method (i.e., storing the maximum detected power level in the measurement time span) has been obtained (depicted in Figure 5.4) to gain insight in the power leakage process. The receiver antenna coupled to the portable spectrum analyzer has been placed at the same height of 0.7 m and separated 10 cm from the microwave oven front door. The spectrogram has been obtained by performing measurements in 5 minute intervals once the oven starts heating. The result presented in Figure 5.4 depicts how the highest frequencies are the first to appear and how the lowest ones need more time to be observed. Therefore, the interference that each ZigBee channel suffers depends on the microwave oven leakage power level and the time that the microwave oven has been operating.

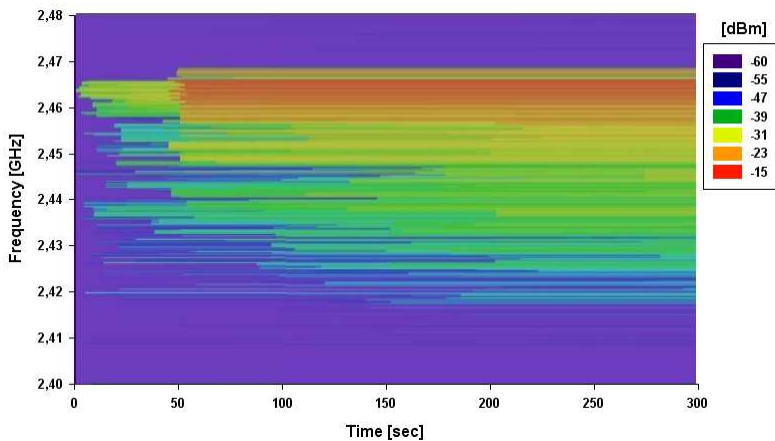


**Figure 5.4.** Measured Spectrogram in 2.4 GHz ISM band, corresponding to detected leakage power within the measurement scenario.



Once the interference levels have been characterized, the performance of the radio links between wireless sensors have been analyzed, in the same scenario previously described. The RF modules employed have been Digi XBee Pro models, which can operate using channels 12 to 23 of the IEEE 802.15.4 standard.

In order to determine the radio link quality, two Java-based applications have been developed specifically for this purpose. The first one, the transmitter application, sends the number of packets set by the user. Each one of these packets is identified by a sequence number. The receiver application reads the sequence number of the received packets and determines how many packets have been lost in order to calculate the PER. A receiver ZigBee device has been placed at the same height as the microwave oven and 50 cm away in front of the front door. The transmitter device is placed also at the same height and in front of the microwave oven, but 12 meters away. Because of the irregular radiation diagram of the integrated antennas of XBee Pro modules, care has been taken in maintaining the same antenna orientation in all measurements that have been performed.

The PER value has been calculated considering 50,000 transmitted packets for each of the 802.15.4 channels (12 to 23) and each of the available transmission power levels (18, 16, 14, 12 and 10 dBm). Figure 5.5 shows the measured values of PER for channels 12, 18, 20 and 22, considering different transmitted power levels. As expected, PER increases as the transmitted power level is reduced, due to decrease in SNR derived from lower available TX power. Channel 12, as can be seen in Figure 5.3, does not overlap with the microwave oven leakage power spectrum and the measured PER value is very low in this case. For channels located at higher frequencies, an increase of PER can be seen. This is due to higher power level of the microwave oven leakage in those frequencies (depicted in Figure 5.2). It is worth noting, however, that due to the time dependent nature of the interference, there are intermediate cases, e.g., channel 20 where overall interference levels seem to be lower.

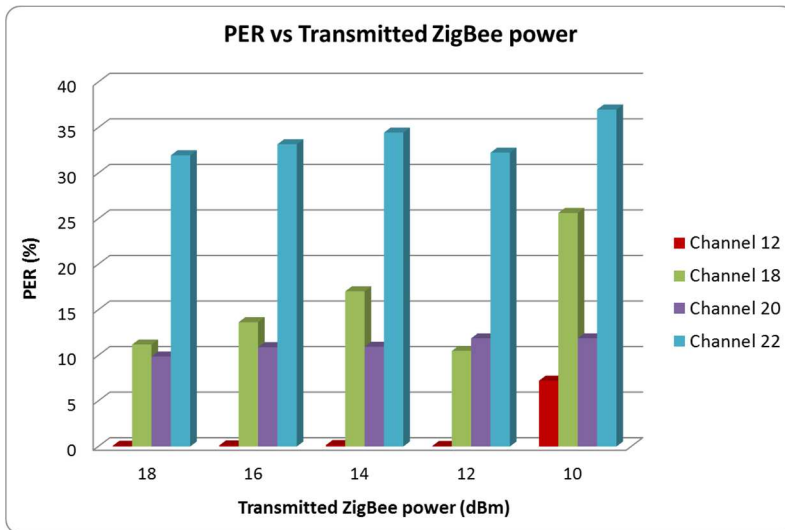


**Figure 5.5.** Measured PER values versus transmitted power for ZigBee channel 12, 18, 20 and 22.

Figure 5.6 shows the dependence of PER levels on the selected ZigBee channel when the interference due to microwave oven power leakage appears. The measured values have been taken with the maximum transmission power level of the XBee Pro modules (18 dBm). The same measurements have been taken for all the transmission power levels and the results are channel dependent in all cases, as can be graphically stated in Figure 5.7. Due to the fact that interference levels due to leakage increase as the channel frequency increases, the SNR will decrease for the same level of transmit power. Therefore, the direct consequence is an increase of the PER as the channel number is increased (i.e. frequency increases), leading to lower radio link quality.

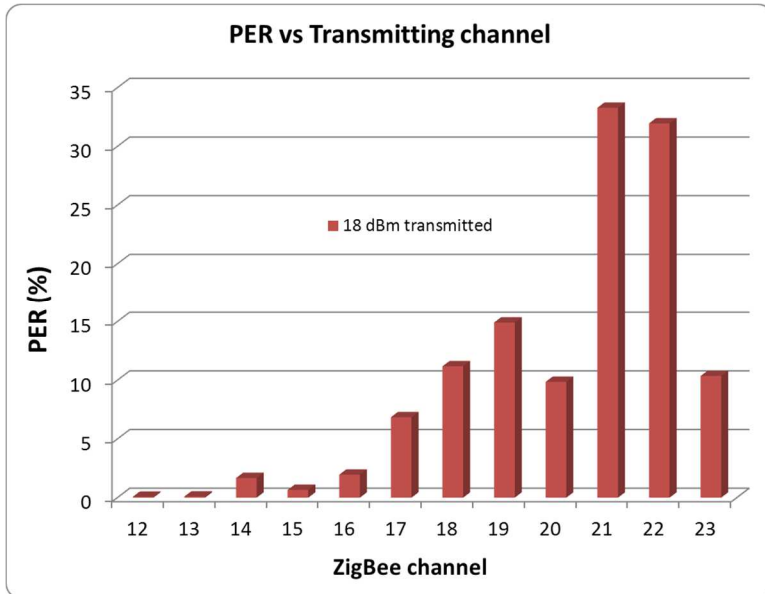


Figure 5.6. Measured PER for each ZigBee channel, transmitting 18 dBm.

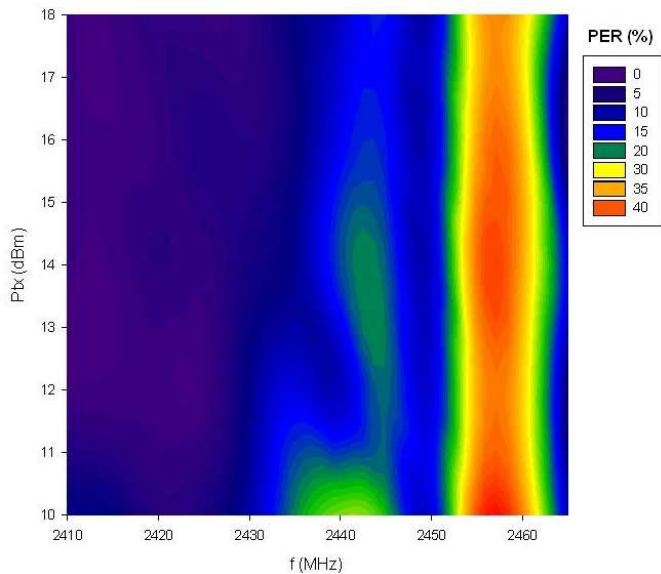


Figure 5.7. Packet Error Rate measurements (%) as a function of frequency and transmission power.

## 5.2 Deterministic Estimation of Radiated Emissions of Electric Appliances: The Microwave Oven

After the demonstration of how important could be the effect of electromagnetic noise sources on the deployment of WSNs, in this section a novel hybrid Equivalent Source – 3D Ray Launching simulation technique for deterministic estimation of radiated emissions of electric appliances is presented, particularized for the microwave oven. A detailed description of the proposed modeling of electromagnetic sources for the inclusion in the 3D Ray Launching simulation tool is shown.

Most of the used techniques to simulate the electromagnetic behavior of a microwave oven, as finite-difference time-domain method (FDTD) or finite element approach, allow obtaining estimations within the cavity or the vicinity of the oven [Iwa96][Sun01]. In addition, there is a work which presents a time-domain noise model based on a simple and general expression of the noise waveform in terms of six parameters that can be determined from measurements [Mat03b]. But in the literature there are not found microwave oven models or methods for estimating the interference caused by a microwave oven in the whole volume of real environments.

The aim of this work is to fill this gap, and to obtain an efficient as well as accurate microwave oven model (which could be generalized to any other electromagnetic noise source) to estimate the behavior of its leaked power within complex indoor scenarios. For that purpose, there are several interesting works in the literature in which this study has been based on, e.g. the approach for radiated emission prediction based on amplitude-only near-field measurements [Wei12], the transmission through subwavelength holes [Pen04], an hybrid ray-launching/full-wave method for site-specific indoor radio wave propagation [Yin00], and how virtual equivalent sources can be obtained to model radio propagation through a leaky medium, as a Frequency Selective Surface (FSS) (i.e. a structure like the oven door metallic mesh) [Min10b] are presented in the literature.

Since the Equivalence Principle was first formulated [Sch36], the

radiation produced by any object in a homogeneous environment can be described by equivalent sources, and it has become a widely spread method to obtain those equivalent radiating sources (i.e. current distributions or antenna arrays) of different elements and radiating surfaces [Sch04][Top07][Alv07][Sar10][Moh13][Pin13c]. Furthermore, the Huygens principle for calculating equivalent sources has been also widely used in order to characterize the electromagnetic field in the near-field zone of a source to estimate its far-field radiation [Bus90][Pot01][Leu05][Ber09][Eib09][Aio10]. Among the applications of the mentioned principles can be found antenna diagnosis [Alv10][Fog12], Specific Absorption Rate (SAR) evaluation [Aio10b], and different equivalent sources approaches for near-field to far-field transformations such as using magnetic currents [Pet92][Taa96], electric currents [Sar99][Wei12b] and arrays of dipole probes [Pet02], among others [Shi04][Yan09][Pin11][Qur13].

One of the goals of obtaining the equivalent sources for an arbitrary radiating element is the study of the EMI (Electromagnetic Interference) or the EMC (Electromagnetic Compatibility) [Can05][Bau07][Pin11]. Traditionally, the emitted electromagnetic fields from PCB (Printed Circuit Board) environments have been emulated by means of these techniques in order to analyze the EMC of electronic devices [Reg01][Jin08][Ada09][Hai11][Li13]. The EMI produced by the leaked power from electric machines has been also studied [Gon87][Ant99][Nis01][Yam04][Bar11][Sar12]. The frequency of the EMIs presented in the mentioned literature is at most in the range of MHz [Pay12], although a novel method for broadband radiators has been rather recently presented [Pin13b]. The device analyzed in this work, a domestic microwave oven, represents a complex radiating source due to its nature, and unlike the devices analyzed in the literature, the oven radiates at higher frequencies (2.4 GHz ISM band). Due to the great amount of emitting systems that can be found nowadays at this frequency, the motivating application of this study is obtaining the equivalent sources in order to emulate the EMI generated by the oven leakage.

Following, the specific and complex method used to model the oven

leakage by equivalent radiation sources in the 3D Ray Launching software is presented. The first step of this method consists in obtaining full wave electromagnetic results with the aid of CST Microwave Studio™ (CST MWS) in order to simulate the behavior of the microwave oven leakage in the vicinity of the oven. For that purpose, an equivalent model of the oven has been created, including the homogenization of the oven door's metallic mesh using a retrieval process, in order to model it as an equivalent surface impedance. Finally, equivalent radiation sources have been calculated by means of the obtained electric field amplitude-only values, and have been incorporated in a proprietary ray launching simulation software. This simulation method allows the estimation of the interference in a complete volume of an indoor scenario with a reduction in computational complexity and hence, simulation time. To validate the method, a real scenario has been set to perform measurements of the oven's radiated leakage in order to compare them with the simulation results.

### **FULL-WAVE SIMULATION OF THE MICROWAVE OVEN**

As it has been mentioned, there are a variety of techniques which can be used to simulate the electromagnetic behavior of a microwave oven, based on finite element approach, finite-difference time-domain method (FDTD) or other 3D electromagnetic approaches [Iwa96][Sun01][Han09][Mon11]. These techniques allow one to characterize the behavior of the microwave oven, in terms of efficiency in heating process as well as to analyze power leakage, within close vicinity of the microwave oven device. However, none of these previous approaches is employed in order to simulate how this leakage power is propagated in an indoor scenario, thus becoming an effective interference source. In this work, CST Microwave Studio, based on Finite Integration Time Domain full wave simulation, has been used for modeling the microwave oven, as an initial step in order to identify the equivalent interference source within the complete scenario. Due to the fact that full wave simulation techniques are computationally

demanding, the goal is to obtain information on the equivalent radiation sources in order to combine these results with the efficient deterministic 3D Ray Launching algorithm. By following this approach, the overall result is to reduce the computational complexity of the simulation scenario, speeding the simulation process and enabling the analysis of the full simulation scenario.

The microwave oven that has been used in this work is a BMG20-4 model of the Bluesky brand. It is a common domestic oven with the following dimensions:  $w = 455$  mm,  $h = 277$  mm and  $d = 310$  mm, with a cavity of  $285$  mm  $\times$   $205$  mm  $\times$   $270$  mm. The maximum power level of operation of the oven is 800 Watt, which is the value used for simulations and experiments throughout this work. The created model for simulations by CST MWS is shown in Figure 5.8, in which a porcelain bowl filled with water (which will be used as the object to heat) above the turntable has also been included. Due to the significant influence that the objects inside the cavity have on the results [Mon11], their electromagnetic properties have been carefully selected to match with the actual components used in the experimental measurements (see Table 5.1). In this work non-magnetic materials have been used, which is the normal case in real microwave oven enclosing elements. The material of the cavity walls, the waveguide and the external box are defined as Perfect Electric Conductors (PEC), a valid approximation given the frequency of operation under consideration. The bowl is porcelain, filled with normal water and the turntable is made of lossy glass. The external part of the microwave oven front door is Plexiglas. The perforated metal walls inside the cavity can be replaced by solid PEC sheets in the model [Kil11].

The microwave oven heating source is a magnetron, which has been modeled by a rectangular waveguide, fed by a rectangular waveguide port. In Figure 5.8 the waveguide coupled in the microwave oven cavity wall can be seen. The dimensions of the waveguide have been calculated to propagate the fundamental  $TE_{10}$  mode at 2.45 GHz, which are length  $a = 612$  mm and height  $b = 20$  mm. The oven has three power levels of operation, with a maximum level of 800 Watt. In the simulations that have been performed, the power of the port that feeds

the waveguide has been set at 1Watt in order to have the possibility of normalizing it to the microwave oven power level. This consideration has been taken into account later on, when these results are employed in the 3D Ray Launching simulation of the complete indoor scenario.

In order to characterize the power leakage mechanism, the front door and its metallic mesh are the key elements, due to the fact that non-metallic elements and physical gaps can be present. In this work, the structure of the metallic mesh embedded in the microwave oven front door has been simulated independently, as a Frequency Selective Surface unit cell. This approach has been followed in order to give a valid description of the effect of the oven front door (which is one of the main contributors to RF leakage), while allowing reduction in computational complexity and hence simulation time.

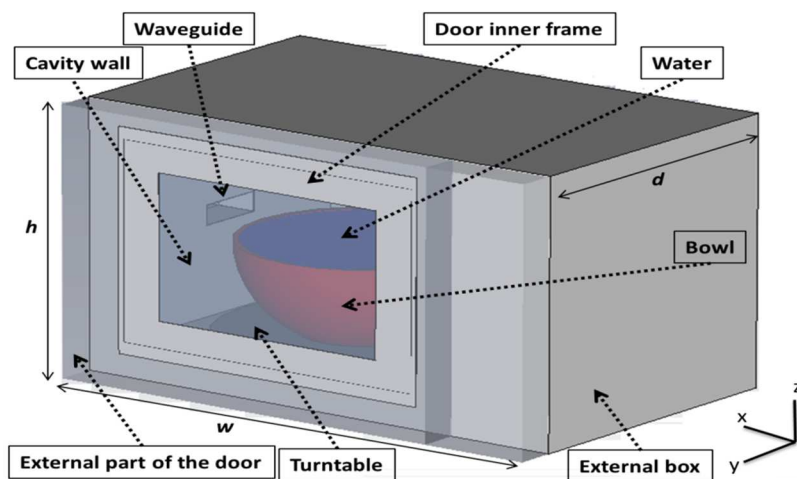


**Figure 5.8.** Schematic view of the microwave oven simulation model. The different objects and parts of the oven are highlighted.



Object	Material	Relative Permittivity
Bowl	Porcelain	6
Water	Water	81
Turntable	Glass (Pyrex) (Lossy)	4.82
External part of the door	Plexiglass	3.6

**Table 5.1.** Material properties for schematic objects.

To characterize the mesh, a unit cell (i.e. infinite periodic structure) analysis has been carried out. Figure 5.9 shows the created unit cell for the analysis, replicated. Thus, a homogenization is done to model the mesh as an equivalent surface impedance, which will be used in simulation of the whole oven, thereby reducing greatly the computational load since the mesh needed to model the holes of the metallic mesh (diameter  $D = 1.2$  mm, i.e.  $0.0098\lambda$ ) should be excessively small. The unit cell material has been considered as Perfect Electric Conductor (PEC), which is a valid approximation for the operation frequency, with a thickness of  $t = 0.5$  mm and lattice constant for x axis periodicity of 4.25 mm, y axis periodicity of 2.463385 mm and grid angle of 30.46555 degrees.

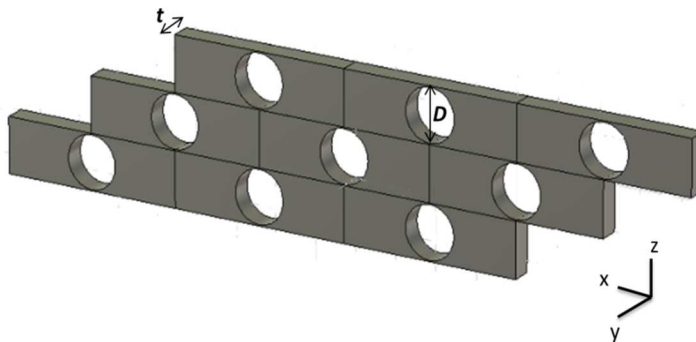


**Figure 5.9.** CST screenshot of the simulated unit cell (replicated) for the characterization of the door's metallic mesh.

The S-parameters of the metallic mesh have been obtained from the previous simulation. Then, an equivalent medium retrieval algorithm based on the inversion of S-parameters is launched to obtain the equivalent surface impedance. This approximation is valid, since the thickness is much smaller than the working wavelength. This procedure has been historically used for experimental characterization of unknown materials [Nic70][Bar10] and has been revived and extended ultimately for determination of effective parameters in metamaterial structures [Che04]. The equivalent surface impedance can be obtained from S-parameters from the following formula:

$$Z = \pm \sqrt{\frac{(1 + S_{11})^2 - S_{21}^2}{(1 - S_{11})^2 - S_{21}^2}} \tag{5.1}$$

In Figure 5.10 the obtained equivalent surface impedance is depicted. As can be seen, the mesh behaves almost as a short circuit (magnitude values near 0).

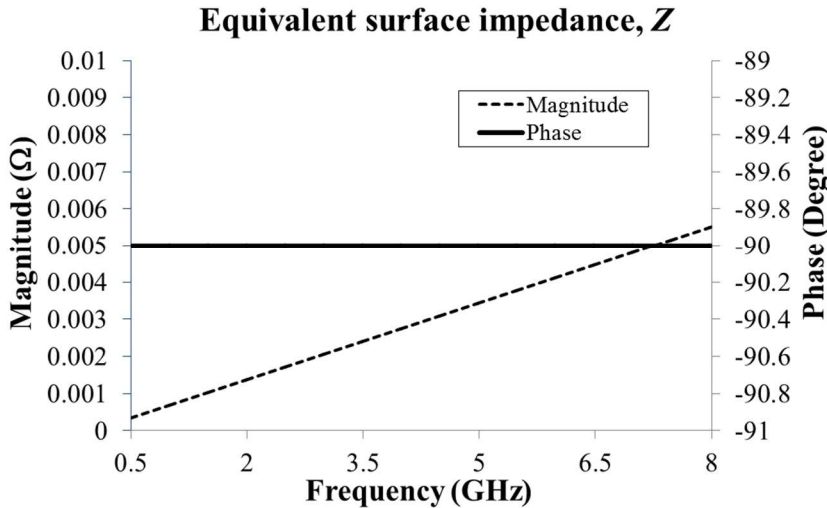
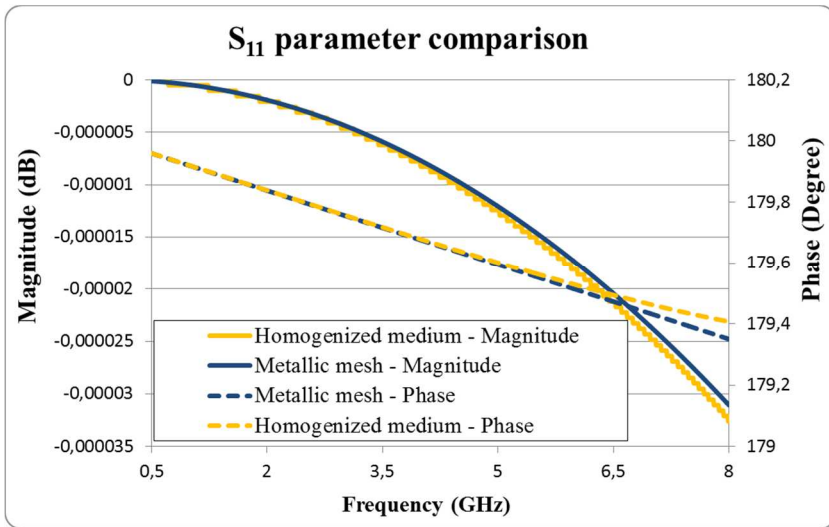
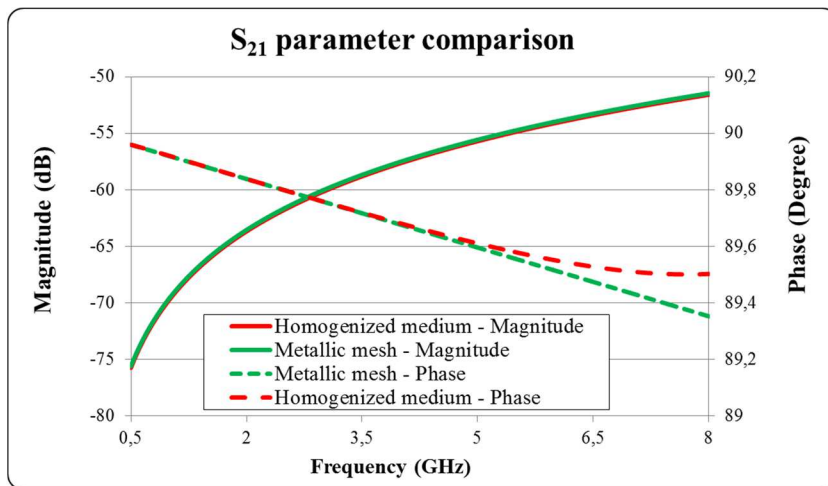


Figure 5.10. Retrieved equivalent surface impedance for the homogenized material.

To validate the homogenization, further simulations have been performed with a surface impedance slab as unit cell (with the same dimensions and thickness as the metallic mesh unit cell) to compare the S-parameters of the new effective material with the previous ones. A negligible difference between the metallic mesh and the equivalent medium parameters is obtained, as can be seen in Figure 5.11, where the magnitude of the S-parameters is represented by continuous lines and the phase by dashed lines. The  $S_{21}$  parameter shows that some transmission exists through the oven door, which is the responsible for the leakage. In the same way, the  $S_{11}$  parameter shows how the most of the power remains in the oven cavity. It is worth noting that the agreement between the metallic mesh and the homogenized medium is very good even beyond the frequency of interest, up to 8 GHz.



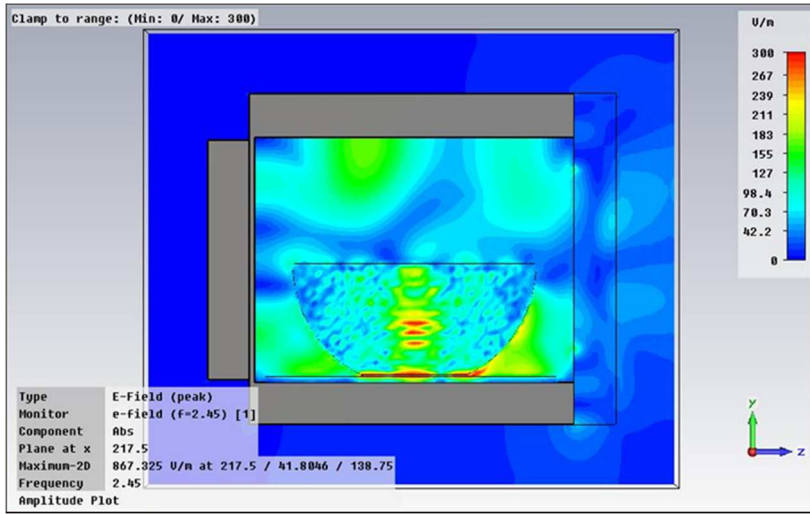
(a)



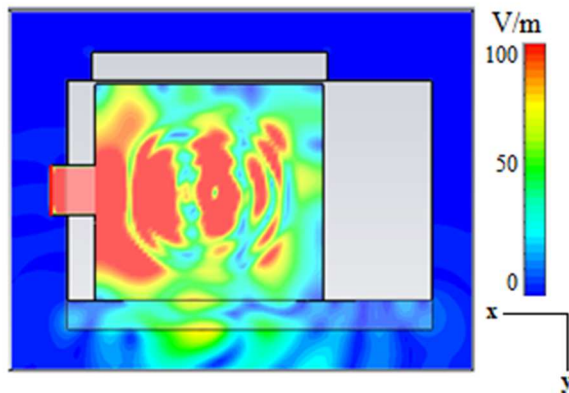
(b)

**Figure 5.11.** Comparison between the S-parameters of the metallic mesh and the obtained equivalent homogenized medium: (a) S<sub>11</sub> and (b) S<sub>21</sub>.

Finally, the oven with the homogenized material substituting the door mesh has been simulated using the transient solver of CST MWS. The complexity of the oven and the shape of the bowl lead to a computationally intensive calculation of 12,188,160 mesh-cells. Figure 5.12a shows the amplitude of the electric field in V/m from a lateral cut taken from the simulated system, in which the power leakage at the oven door can be seen. In Figure 5.12b the upper cross-section at half the height of the waveguide is represented. The leakage through the front door is also observed (down side of the picture), and as expected, significantly higher electric field values can be found near the waveguide and in the water. For an in-depth understanding of how the oven radiates, in Figure 5.13 the obtained radiation pattern of the whole oven is shown. It can be clearly seen how the oven radiates mainly forward due to the leakage through the door, and how radiated power is much lower backwards and laterally, as expected. For the sake of completeness, the 3D radiation pattern is shown in the inset.



(a)



(b)

**Figure 5.12.** (a) A lateral cut taken from the simulation of the microwave oven. The amplitude of the electric field is represented, in which the oven front door is located on the right hand side of the figure. (b) Upper cut of the simulated system, where the leakage through the door is clearly seen.

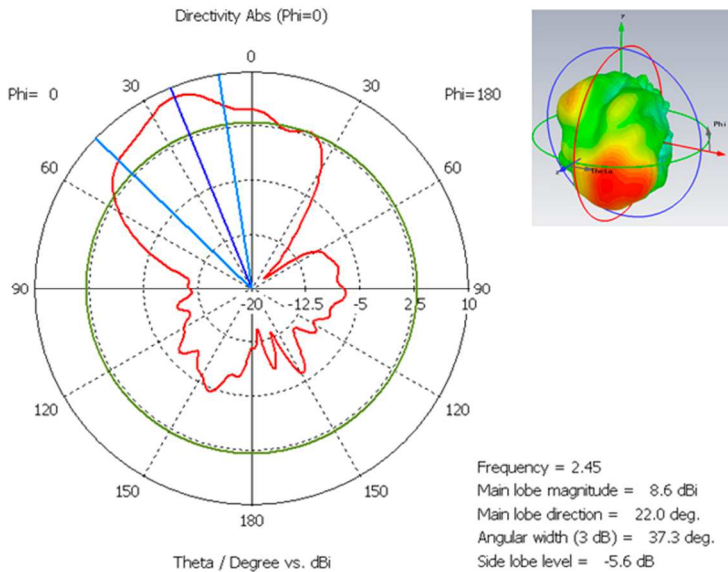


**Figure 5.13.** Radiation pattern of the microwave oven.

The electromagnetic field distribution calculated outside the oven is necessary for obtaining equivalent sources for the 3D Ray Launching simulations, which will allow the estimation of interference effect within the complete simulation scenario.

### **OBTAINING EQUIVALENT SOURCES**

The previous simulation results show the values of power leakage in the close vicinity of the microwave oven. However, for radio planning purposes it is necessary to estimate interference levels within an indoor scenario, such as a household or office location, in which one or more Wireless Sensor Networks can be deployed. Application of 3D full wave electromagnetic techniques is not feasible, due to the large computational effort they require, given the size of the proposed scenario. It is necessary therefore to apply alternative simulation methods to finally obtain interference estimations within the complete indoor scenario.

Taking as a basis the numerical simulations of the previous section, equivalent sources have been modeled as arrays of isotropic sources (an array for each face of the oven) in order to model the microwave oven leakage. Although in the literature the most used radiating element for that purpose is the elementary dipole [Lop09][Ada09][Wei12b][Sar12][Mik12], isotropic sources have been chosen primarily for simplicity. The obtained arrays of sources have been included in the 3D Ray Launching simulation tool with the aim of simulating the radio propagation of the oven leakage within a complete volume of an indoor scenario. Table 5.2 shows the parameters set for the simulations. The employed values of maximum reflections considered until extinction, launched rays angular resolution and cuboid dimensions have been chosen as a compromise between accuracy and computational cost, given by preliminary convergence analysis of the 3D Ray Launching algorithm in this kind of scenarios.

Parameter	Value
Frequency	2.45 GHz
Source type	Isotropic
Resolution (cuboids size)	5 cm x 5 cm x 5 cm
Maximum reflections permitted	5
Launched rays resolution	1°

**Table 5.2.** Material properties for schematic objects.

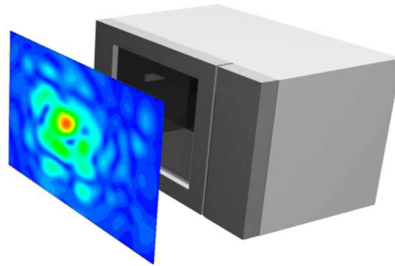
A study has been carried out in order to obtain an accurate and computationally efficient model of source arrays for the 3D Ray Launching algorithm. The elements of the arrays have been defined in the simulator as isotropic sources (point sources with directivity = 1 and efficiency = 1) transmitting only in a half-space out of the oven with vertical polarization. Considerations as the size of the planes where the arrays have been set, the size of the cuboids defined for the 3D Ray Launching simulations and the wavelength of the simulated frequency have been taken into account to obtain source arrays

compatible with the mesh resolution, since not all combinations are feasible. For example, a distance between sources of  $\lambda/4$  (3.06 cm) is not feasible because only an emitting source can be placed within a simulation cuboid (5 cm). The performed procedure is explained in the remaining part of this section, specified for the front plane of the oven as it is the most significant of the oven faces.

Firstly, in order to obtain the transmitted power level for the equivalent sources, the electric field amplitude-only values just outside the oven obtained by the previous CST full wave simulation have been used [Sch36]. A projection of the electric field distribution for the front plane of the oven can be seen in Figure 5.14a. Then, the mean electric field value of the whole plane has been calculated, and from here the transmitted power level ( $P$ , in Watts) has been obtained by means of the following formula [Bal05]:

$$P = \frac{|E|^2 \lambda^2}{120\pi 4\pi} \quad (5.2)$$

where  $\lambda$  is the operation wavelength (12.245 cm at 2.45 GHz) and  $E$  is the electric field in V/m.



(a)



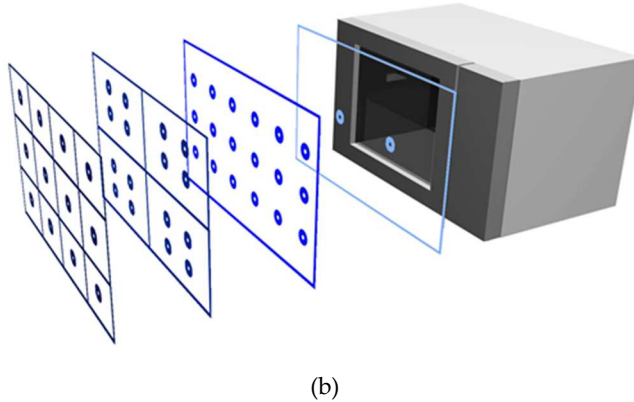


**Figure 5.14.** (a) Electric field distribution for the front plane obtained by means of CST full wave simulation, and (b) Schematic representation of different source array distributions used for the 3D Ray Launching simulations.

For defining the source arrays for the 3D Ray Launching simulations, the array size (amount of sources), the radiating power distribution among the sources and the distance between sources, basic arrays of in-phase point sources with uniform and non-uniform amplitude distributions have been applied [Kra02]. Once the arrays have been defined, the power obtained using formula (5.2) has been distributed among the sources, using uniform, binomial or triangular distributions.

The simulated cases are shown in the left side of Table 5.3. The ‘Power distribution’ column indicates how the calculated power has been distributed among the sources of the array. The ‘Source array size’ indicates the number of elements on the array and their distribution: ‘2×4’ is a 2 rows and 4 columns array. The ‘Distance between sources’ refers to an equal spacing distribution (both within a row and between columns). Note that the distance between sources determines the biggest size of the array (front plane size: 45.5 cm × 27.7 cm, i.e.  $3.71\lambda \times 2.26\lambda$ ). All the feasible largest arrays are included in Table 5.3. Finally, the last column shows the mean error between the simulation results and measurements (the measurement methodology is discussed later), which shows the accuracy of each proposed equivalent sources array model. The two planes closer to the oven depicted in Figure 5.14b

show, as an example and with the aim of clarifying, the 1×2 and 3×6 size arrays. The meaning of the other two planes is explained later. As can be seen in the obtained results, neither the power distribution, neither the array size, nor the distance between sources has a significant impact on the error (apart from the case 1.1 and 2.1, where an array of only 2 elements is used and the error is significantly higher). The mean error is around 12 dB for these cases, which is not acceptable. In Figure 5.15 the leaked power distribution estimated by the 3D Ray Launching simulation tool corresponding to cases 1.1 to 1.4 of Table 5.3 are shown. The resulting planes show the leaked RF power level for a plane of 5×5 meters just in front of the microwave oven [the oven is placed at coordinates (0,0), on a wooden table as shown in Figure 5.1]. In addition, Figure 5.16 the same results but in terms of electric field level are depicted, as in many EMI and EMC standards the electric field level is the reference measurement.

Case	Power distribution	Source array size	Distance between sources	Mean Error (vs. measurements) (dB)
1.1	Uniform	1×2	0.5λ	21.65
1.2	Uniform	2×2	0.5λ	12.11
1.3	Uniform	2×4	0.5λ	11.95
1.4	Uniform	5×8	0.5λ	11.38
2.1	Uniform	1×2	0.7λ	22.07
2.2	Uniform	2×2	0.7λ	13.07
2.3	Uniform	2×3	0.7λ	12.69
2.4	Uniform	3×6	0.7λ	11.99
3.1	Binom./Triang.	1×3	0.7λ	13.19
3.2	Binom./Triang.	2×3	0.7λ	12.78
3.3	Binomial	3×4	0.7λ	12.21
3.4	Binomial	3×6	0.7λ	12.13
4.1	Triangular	1×5	0.7λ	12.98
4.2	Triangular	2×5	0.7λ	12.58
4.3	Triangular	3×5	0.7λ	12.00

**Table 5.3.** Parameters of equivalent sources arrays.

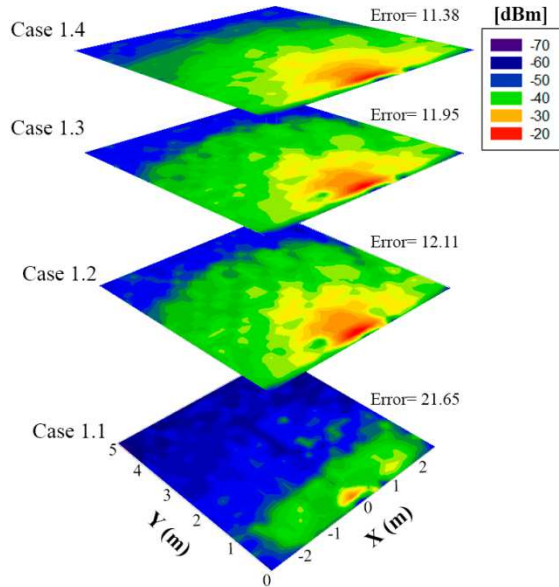


Figure 5.15. 3D Ray Launching power distribution results for some cases shown in Table 5.3.

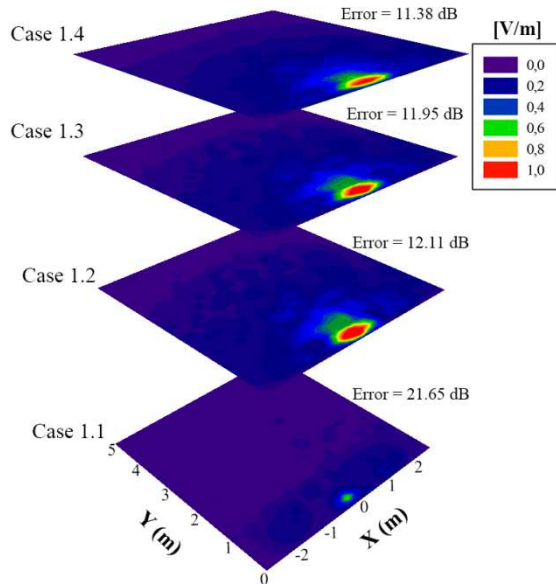


Figure 5.16. Same results of Figure 5.15 but in terms of electric field strength.

In order to obtain more accurate simulation results, the electric field plane obtained by full wave simulation has been divided into 4 equal-size rectangles. For each rectangle, using again equation (5.2), the overall transmitted power level has been calculated. The power level has been applied to the corresponding array (named sub-arrays) following the same power distribution methodology explained previously for cases in Table 5.3. As an illustrative example, in Figure 5.14b, the third plane closer to the oven represents the plane divided in 4 rectangles with a 2×2 sub-array for each one. The sub-arrays are centered in each rectangle, so the distance between sources refers to the distance between sources in the same sub-array. Table 5.4 shows the new simulated cases, followed by Figure 5.17, where the simulation results of some selected cases are depicted. The results show that a significant improvement has been obtained, as the error has been reduced from around 12 dB to around 6 dB. Again, the radiated power level distribution, the distance between sources and array size have no significant impact on the obtained mean error. Again, in addition the same cases of Figure 5.17 are depicted in Figure 5.18, but in terms of electric field strength.

Following this methodology, a precise front plane model has been obtained, with a low mean error (1.06 dB) and an acceptable number of sources for the 3D Ray Launching simulation method. This model consists in a division of the CST electric field plane into 12 equal-size rectangles (3 rows × 4 columns), with a unique source placed on each rectangle (the farthest plane of Figure 5.), transmitting the power level corresponding to the electric field value calculated by equation (2) for each rectangle. This case corresponds to the case 7 of Table 5.4. This is due to the fact that the proposed distribution of equivalent sources consistently maps the field distributions that can be observed in the surface of the microwave oven. As the distribution grid of the equivalent sources is made smaller, higher accuracy in the field mapping potentially is obtained, leading to a compromise between the grid size and the required computational cost, which in the limiting case would be in the order of full wave simulation results. The 3D Ray Launching simulation results for the configuration of case 7 can be seen

in Figure 5.19 in terms of leaked power distribution and in Figure 5.20 in terms of electric field level.

Case	Power distribution	Source array (sub-array) size	Distance between sources	Mean Error (vs. measurements) (dB)
5.1	Binom./Triang.	2×6 (1×3)	0.7λ	6.19
5.2	Uniform	2×6 (1×3)	0.7λ	6.16
6.1	Uniform	2×8 (1×4)	0.5λ	5.79
6.2	Uniform	4×4 (2×2)	0.5λ	6.10
6.3	Uniform	4×8 (2×4)	0.5λ	6.00
6.4	Binomial	2×8 (1×4)	0.5λ	5.81
6.5	Binom./Triang.	2×6 (1×3)	0.5λ	5.91
6.6	Binom./Triang.	4×6 (2×3)	0.5λ	6.13
7	-----	3×4 (1×1)	-----	1.06

**Table 5.4.** Parameters of equivalent sources arrays (with sub-arrays).

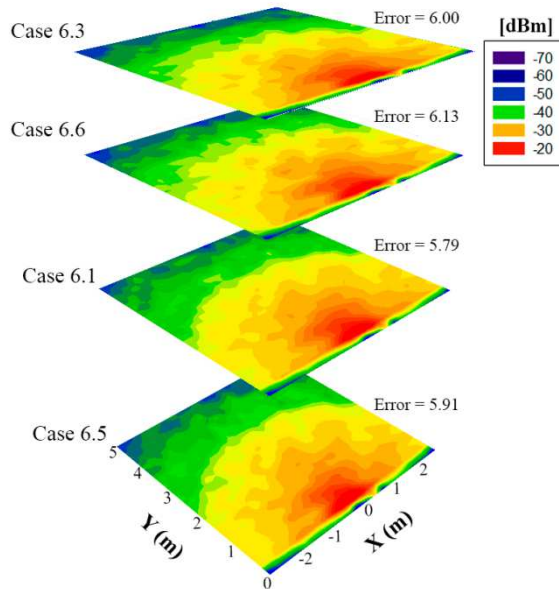


**Figure 5.17.** 3D Ray Launching power distribution results for some cases from Table 5.4.

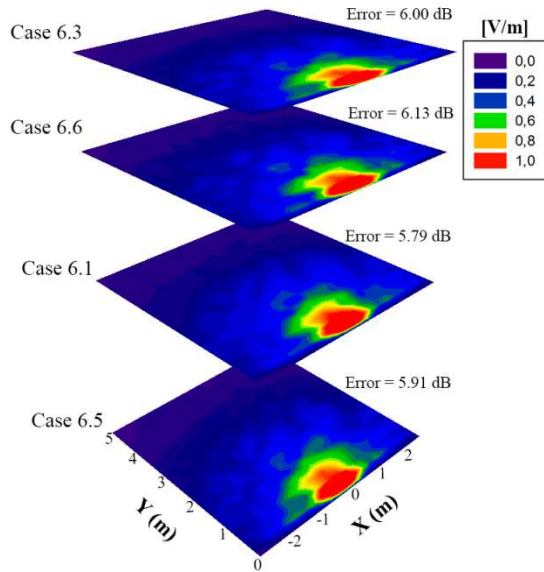


Figure 5.18. Same results of Figure 5.17 but in terms of electric field strength.

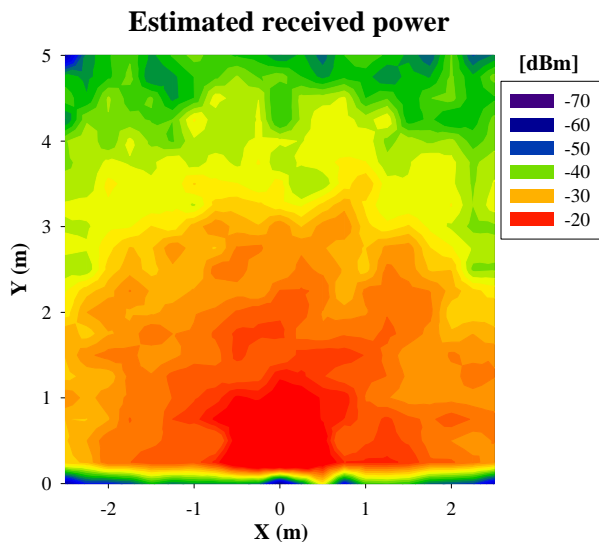
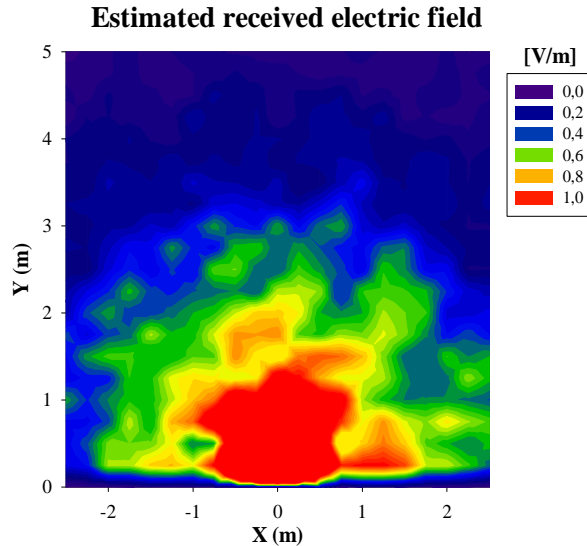


Figure 5.19. 3D Ray Launching leaked power distribution results for the final 12-source front plane model.



**Figure 5.20.** 3D Ray Launching leaked power distribution results in terms of electric field strength for the final 12-source front plane model.

Once an adequate equivalent source array has been obtained for the front plane of the oven, the same methodology has been followed for the rest of the oven planes (i.e. left side, right side, upper and back), in order to create a complete microwave oven model. Top and back planes consist of arrays of 12 sources like the front plane, and lateral planes consist of arrays of 9 sources ( $3 \times 3$ ) due to the smaller size of the plane. The distance between rows for both cases is 113.75 mm and the distance between columns is 69.25 mm for 12-source arrays and 68.75 mm for 9-source arrays. The bottom plane has not been taken into account due to the negligible radiated power level and the fact that for both simulation and measurements the oven has been placed on a wooden table (see Figure 5.1).

Due to the fact that all the leakage sources cannot be considered in the simulation (e.g., microwave racks in the oven, inner joints and bolts, etc.), a calibration to fit simulated and measured data has been performed in order to model this extra leakage power. Taking into account the measured values and path losses, the transmitted power level has been recalculated for 3 of the 9 sources of the left plane array.

These 3 sources correspond to location of the microwave ventilation grating. Figure 5.21a shows the leaked power distribution results obtained by the 3D Ray Launching algorithm for a plane of 5×5 meters using the proposed microwave oven model. The oven and the door are represented in the middle part of the plane, in order to show not only the results in front of the oven, but to show the complete power distribution around the oven. In addition, Figure 5.21b shows the same results in terms of electric field strength.

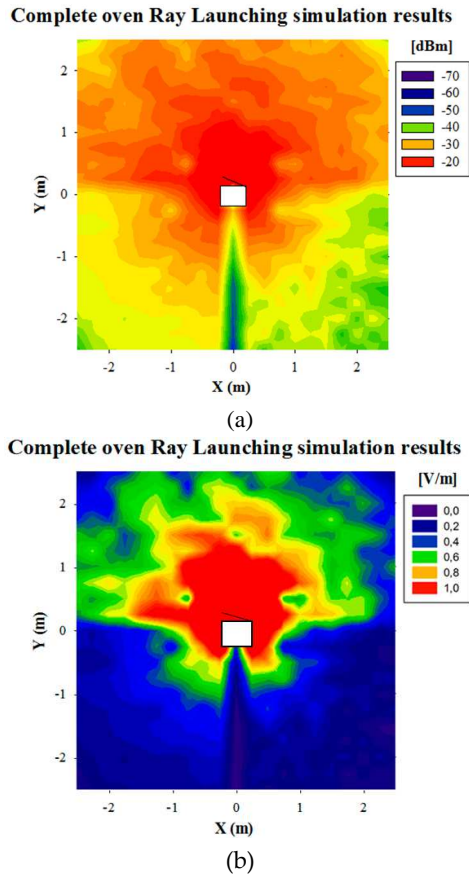


**Figure 5.21.** (a) 3D Ray Launching power distribution results around the oven using the complete equivalent sources model of the oven, (b) in terms of electric field strength.



## MEASUREMENT METHODOLOGY

In this section, the performance of the measurement procedure used to validate the simulation results is presented. The measurements have been done in a real indoor scenario, placed at the Research and Development Building of the Public University of Navarre. A non-ideal and non-anechoic environment has been chosen, as it is the typical environment where domestic microwave ovens can be found. In order to obtain valid simulation vs. measurements comparisons, the scenario for the 3D Ray Launching simulation software has been generated, shown in Figure 5.22. The microwave oven has been placed on a wooden table, and the leaked power was measured by means of an Agilent N9912A spectrum analyzer with the aid of an omni-directional 7dBi indoor antenna (which corresponds to an antenna model OAN-1070 from LevelOne). The measurement area has been delimited to 5 meters wide and 7.5 meters long, with 650 total measurement points distributed uniformly (0.25 m distance between points) in a plane at 0.7 m height (i.e. the height where the oven has been placed). Figure 5.23 shows the measured leaked power in front of the oven [placed at coordinates (0,0)] and Figure 5.24 represents the same measurements in terms of electric field level.

In order to gain insight into the accuracy of the created oven model, leaked power level and electric field level versus linear distance are represented in Figure 5.25 and Figure 5.26 respectively, showing good agreement between simulation results and measurements. The shown linear distributions of received electric field correspond to the dashed lines depicted immediately in front, left and right sides of the microwave oven in Figure 5.23 and Figure 5.24. The obtained mean error between measurements and the 3D Ray Launching simulation results is 0.15 dB with standard deviation of 0.35 (0.049 V/m in terms of electric field level, with a standard deviation of 0.126), taking into account a total of 650 different measurement points distributed within the plane.

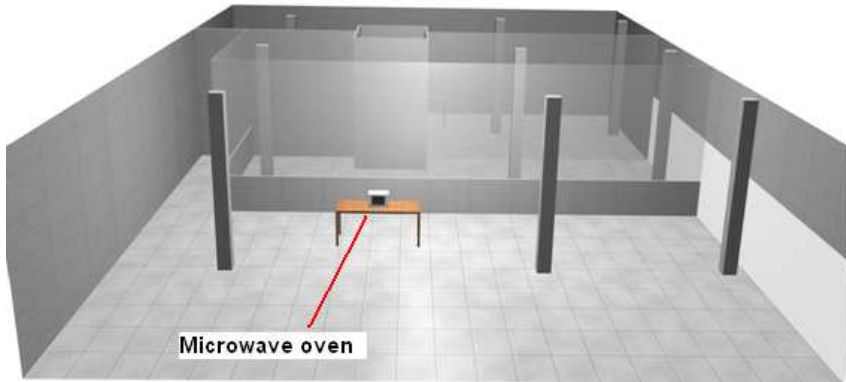


**Figure 5.22.** Schematic view of the scenario created for 3D Ray Launching simulations, which represents the real scenario.

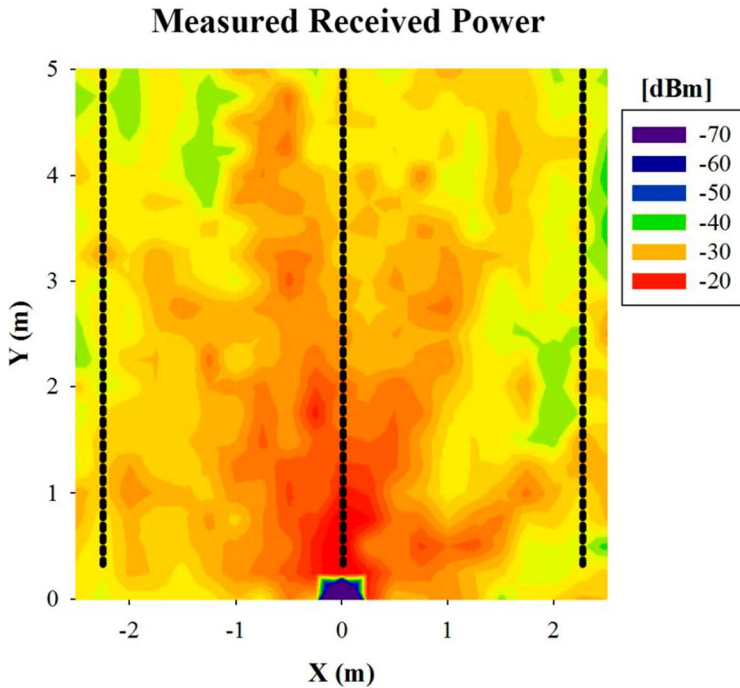


**Figure 5.23.** Leaked power measurements for a plane at 0.7 m height in front of the oven. Dashed lines correspond to Figure 5.25 graphs.

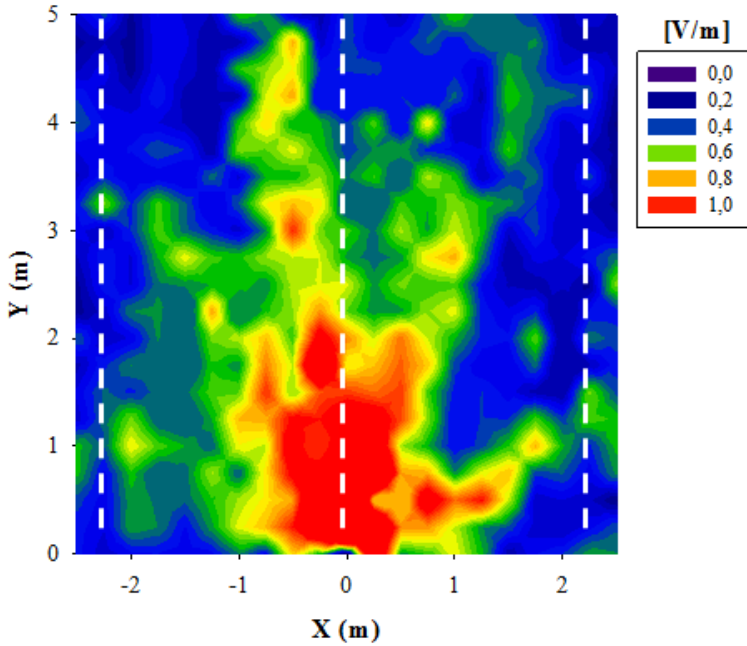
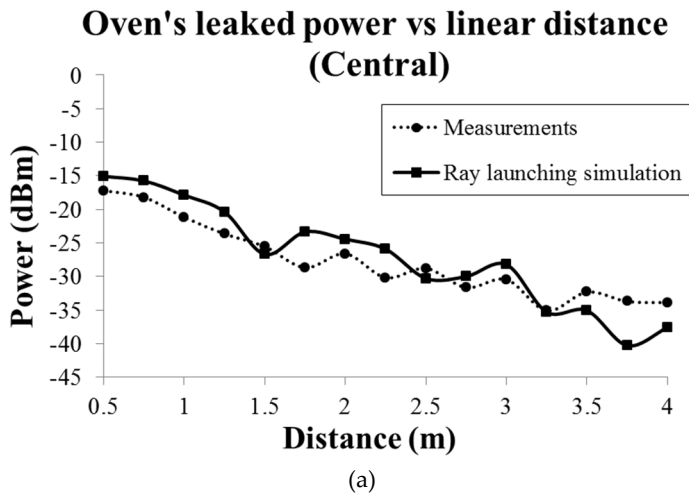
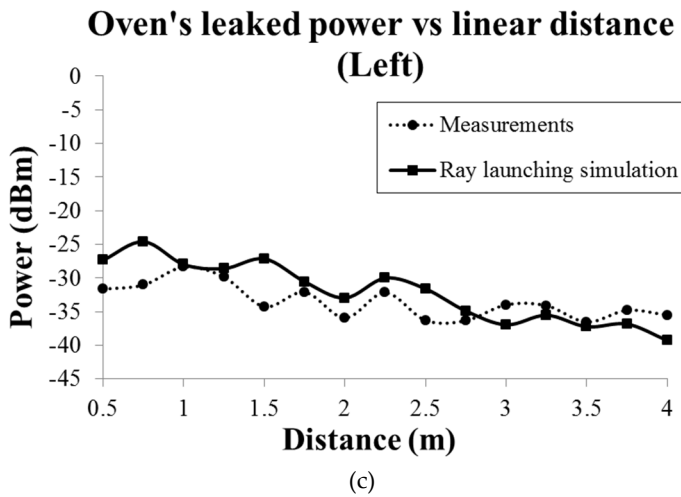
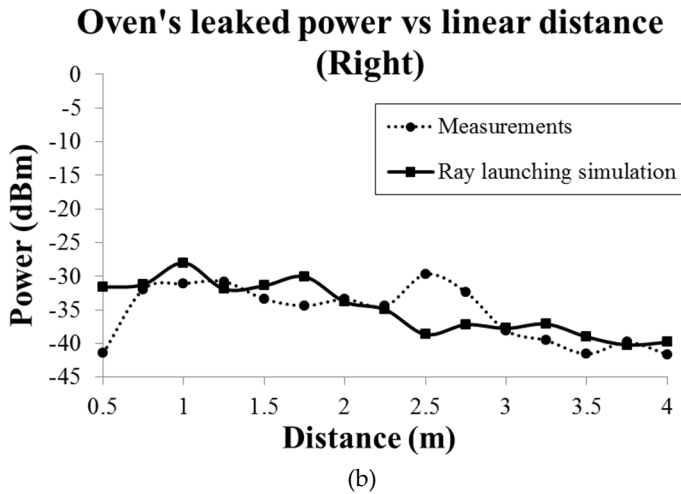


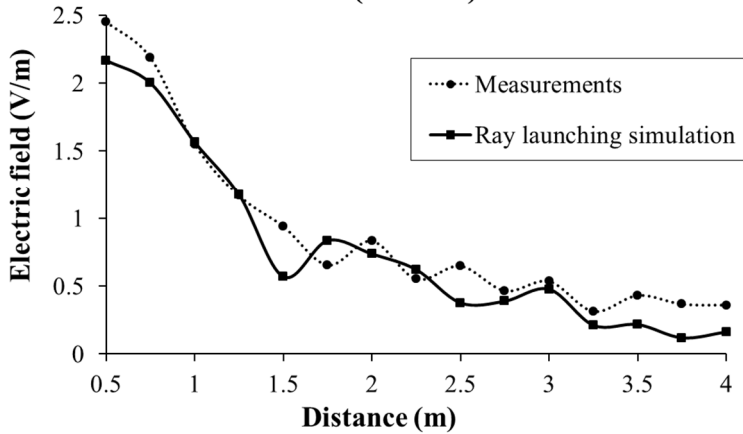
Figure 5.24. Leaked power measurements in terms of electric field strength for a plane at 0.7 m height in front of the oven. Dashed lines correspond to Figure 5.26 graphs.





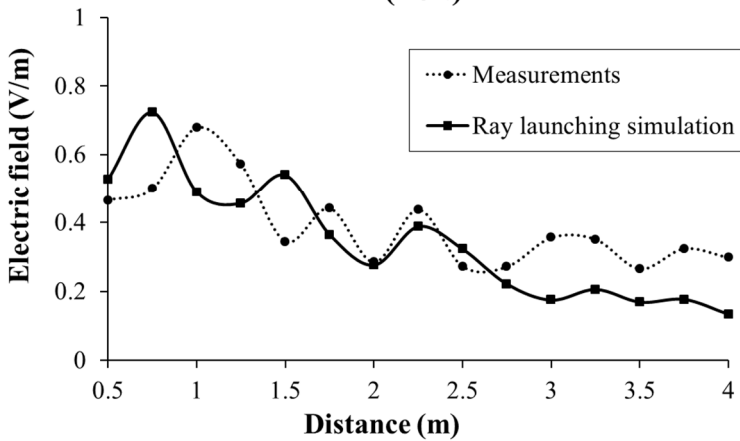
**Figure 5.25.** Evolution of the oven's leaked power in straight linear distance, (a) in front of the microwave oven, (b) right side, and (c) left side.

### Oven's leaked electric field vs linear distance (Central)



(a)

### Oven's leaked electric field vs linear distance (Left)



(b)

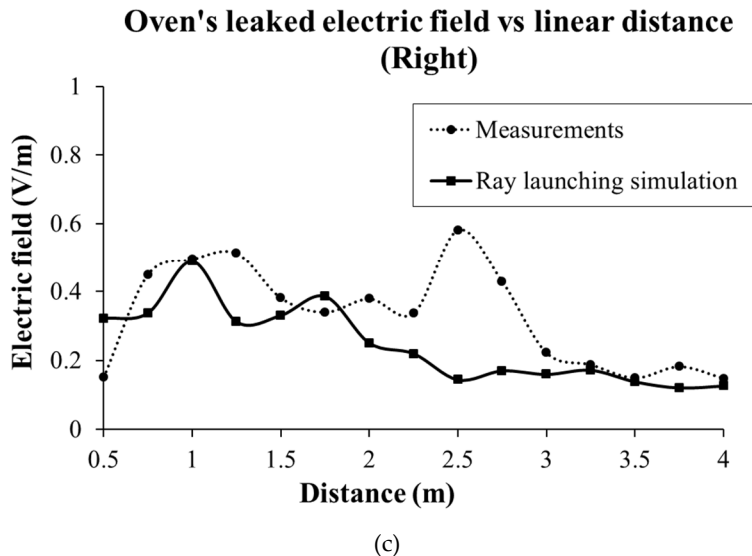


**Figure 5.26.** Evolution of the oven's leaked in terms of electric field strength in straight linear distance, (a) in front of the microwave oven, (b) right side, and (c) left side.

Summarizing, in this study a method to model and characterize the microwave radiation leakage from a domestic microwave oven has been described. This characterization allows simulating the behavior of the oven's radiated power in an indoor scenario, where the leakage can be a potential source of interference for wireless networks operating at ISM 2.4 GHz band. For that characterization, a detailed model of an oven has been implemented for full wave simulations. To enhance the simulation process and reduce computational cost, a parameter retrieval procedure has been applied in order to characterize the metallic mesh embedded in the microwave oven door as an equivalent surface impedance. Based on these results, a study of equivalent radiation sources has been performed, obtaining an accurate model ready to employ in the in-house 3D Ray Launching algorithm. The comparison between measurements and simulation results shows good agreement (mean error value of 0.15 dB with standard deviation of 0.35 regarding power level distribution and 0.049 V/m in terms of electric

field level, with a standard deviation of 0.126.

Further simulations could be carried out, studying e.g. other kind of equivalent sources, other power distributions among the equivalent sources (e.g. Dolph-Tschebyscheff), and how the phase of the equivalent sources could affect the model, but the presented model is simpler and the obtained accuracy is a good enough approximation to a real domestic microwave oven.

The proposed technique seems to be a good method for obtaining estimations of RF leakage from high power sources in general, such as microwave ovens, which can aid in radio planning considerations prior to the deployment of wireless systems in complex indoor scenarios, while the estimated electric field values can be very useful in order to determine the compliance with radiation limits, as in the case of commercial electronic devices or the ICNIRP exposure levels.

### 5.3 Application on Dosimetric Studies

Once the modeling of interference sources has been described for its application on the 3D Ray Launching simulation algorithm and a successful model of a domestic microwave oven has been developed, in this section an application based on the obtained simulation model is presented. Taking into account that the microwave oven is a very common appliance at which human beings are usually exposed to, a dosimetric study in collaboration with the Health Institute Carlos III has been carried out.

The analysis of the leaked electric field has been performed taking measurements in an indoor scenario and comparing them to the simulation results obtained by the previously presented novel hybrid method. Once the prediction and measurements of the leaked electric field have been obtained, these values have been compared with the ICNIRP (International Commission on Nonionizing Radiation Protection) scale in order to see if they comply with the corresponding human exposure level. In addition, for a more in-depth study of the human exposure to an operating microwave oven, SAR values on a human body have been estimated.

Due to the different operation modes that microwave ovens support, several cases of maximum output power values have been considered in this study, in the range of 750 W (low power model) to 1800 W (heavy duty model). Figure 5.27 shows the results obtained for the simulation of the complete scenario by the 3D Ray Launching method, for 4 different operating power levels. The microwave oven is located at coordinates (0, 0), with the door orientated facing the positive values of the  $Y$ -axis. As expected, the highest electric field values can be found in the nearest zone of the oven, particularly in front of the door, as the radiated power is mainly due to the leakage through the door. It is worth noticing that, although in lesser extent, the leaked power also affects the zone behind the oven. The radiated electric field can easily reach more than 3 meters, which is a significant distance considering indoor scenarios as home environments. In order to provide insight in relation to the expected leaked E-field values as a function of the



operating power of the oven, Figure 5.28 depicts the region (in grey) where those expected E-field values will be, as a function of distance. It can be seen how the power decreases rapidly with the distance, as expected, and how in the vicinity of the oven the leaked E-field strength difference between operation powers is bigger.

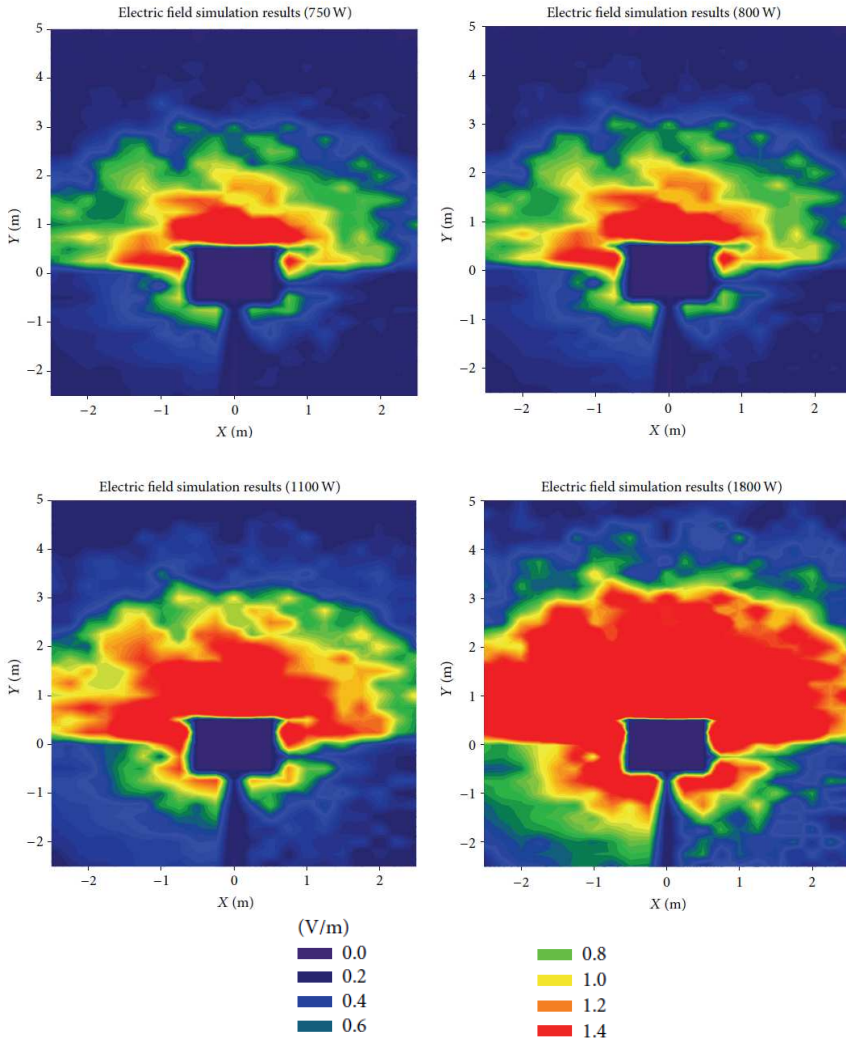


**Figure 5.27.** 3D Ray Launching electric field results for a height of 0.7m, considering different oven's operation power values.

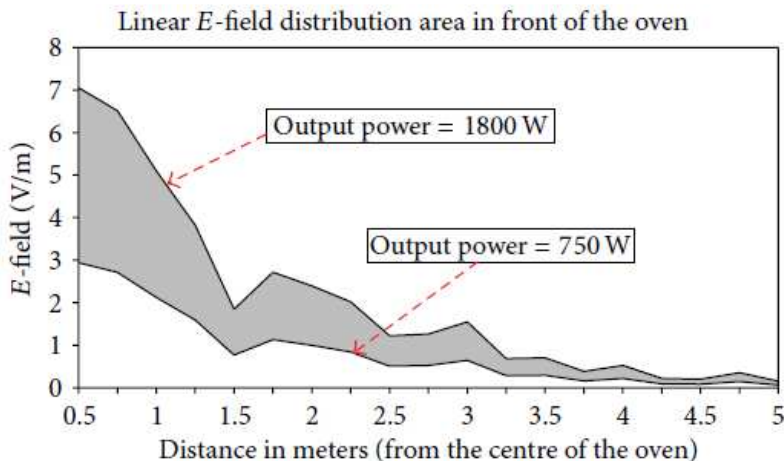


**Figure 5.28.** Linear E-field distribution in front of the oven as a function of operation power level of the oven.

The scenario where the measurements have been taken and the simulations have been performed is placed in the ground floor of the Research and Development building of the Public University of Navarre, and it is the same test bed proposed in the previous section, shown in Figure 5.22. On one hand, measurements with an Agilent Field Fox N9912A spectrum analyzer have been taken (see Figure 5.23 and Figure 5.24). On the other hand, the same measurements have been performed, but with an EME Spy 121 personal dosimeter (see Figure 5.29). This type of dosimeter is specifically designed to make selective measurements of the level of personal exposure (in terms of electric field strength in V/m). Although most regulations require gathering data at a rate of one sample per second for a measurement time of six minutes, the shortest sample rate available for the EME Spy 121 dosimeter device is one sample per 4 seconds, which has been the sample rate used for the measurements in this study. The overall measurement time for each measurement point has been set to 3 minutes instead of 6 minutes due to the big quantity of measurement points proposed for this study (i.e. 650 points). Besides, the purpose of these measurements is to validate the measurement data obtained by the spectrum analyzer as well as the simulation results, proving that

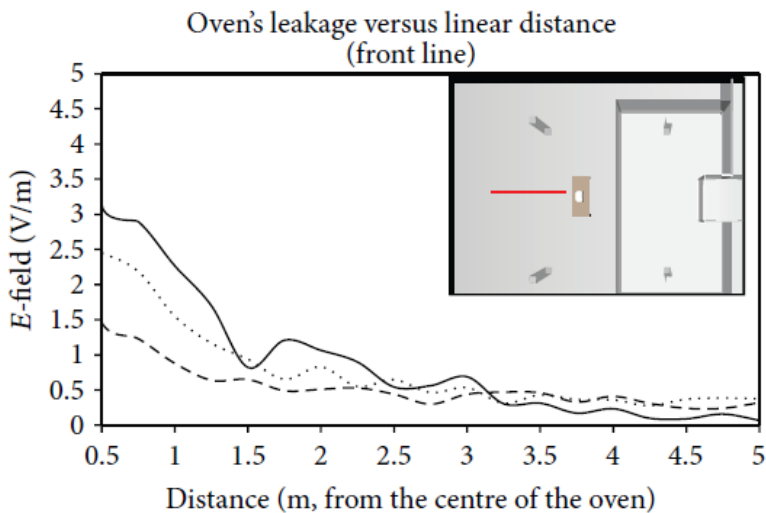
the presented 3D Ray Launching algorithm can be also used for dosimetric assessment duties.



**Figure 5.29.** The EME Spy 121 dosimeter used to obtain electric field values of the leakage of the microwave oven.

In order to show the comparison between simulation results and measurements, three different linear power distributions with transmitter-receiver distance have been analyzed from the measurement/simulation zone. Figure 5.30a represents the radiated oven leakage versus linear distance for a central line, which corresponds to a straight line just in front of the microwave oven, as can be seen in the inset of the figure. Figures 5.30b and Figure 5.30c represent the comparison for left side and right side lines. As can be seen, the electric field values obtained with the spectrum analyzer and dosimeter are heavily similar, as expected. If measurements are compared to simulation results, a high accuracy is also observed. Taking into account the 650 points distributed within the scenario where the measurements have been taken, a total error mean of 0.059V/m is obtained between simulation results and spectrum analyzer measurements. Those values and the values obtained by means of the dosimeter are also close. Specifically, the mean error

between simulation results and dosimeter values is  $0.147\text{V/m}$ , higher than the error obtained by the spectrum analyzer measurements, probably due to the loss of information derived from the method employed by the dosimeter to extract electric field samples (i.e., a sample every 4 seconds). It is worth noting how important it is to use a well-developed and detailed microwave oven for simulations in order to obtain accurate dosimetric values throughout a scenario: although the lateral lines used to show the comparison between simulation results and measurements (see Figures 5.30b and Figure 5.30c) are symmetric with respect to the oven’s cavity, the simulation results are different for both lines, as it also happens to the measurement results. The main reason for that phenomenon is that the power leaked through the oven’s door is not uniformly distributed on the oven’s surface, and, consequently, the radiation pattern of the whole oven is not symmetric (see Figure 5.13). Besides, the scenario itself is not symmetric (see Figure 5.22), making the propagated multipath components different for both sides of the oven. The nonsymmetrical radiation characteristics exhibited by the microwave oven can be clearly observed in the results depicted in Figure 5.27.



(a)

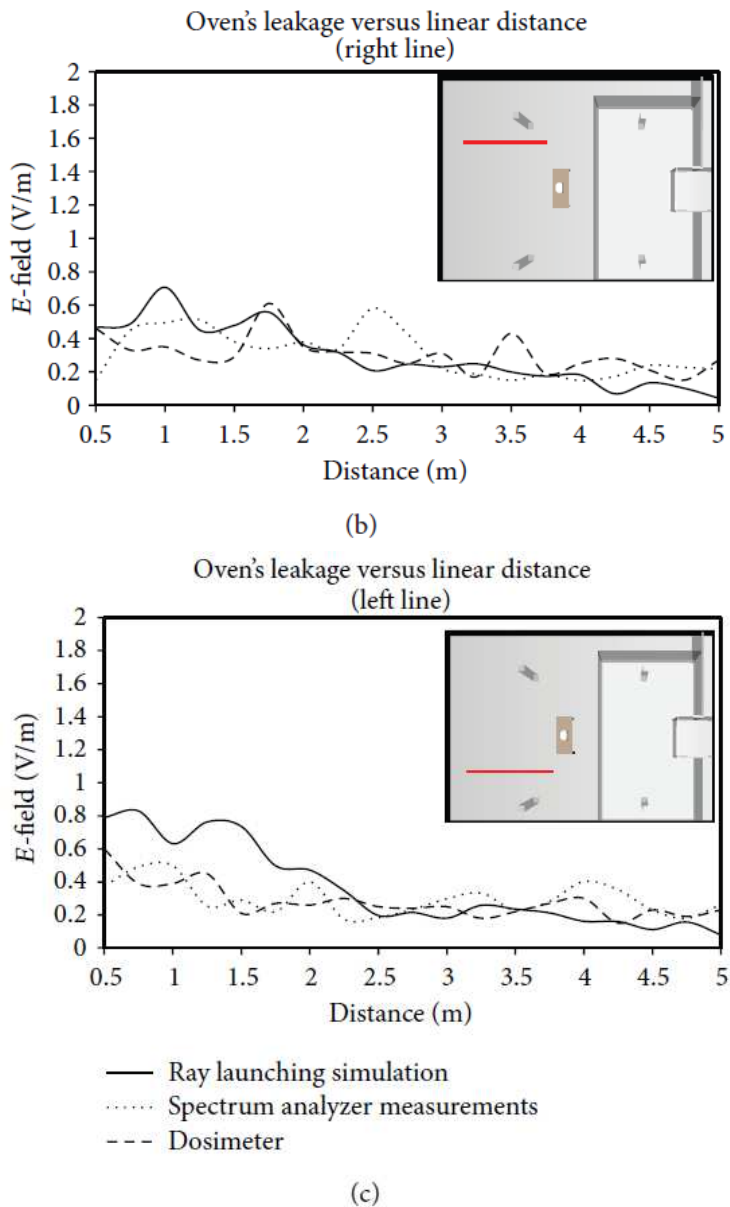


**Figure 5.30.** Received electric field distribution versus distance for 3 different linear paths ((a) front, (b) right and (c) left). Simulation as well as measurement results from spectrum analyzer and EME Spy personal dosimeter are represented, with good agreement among them.

**EXPOSURE LEVEL ANALYSIS**

Studies on the impact of electromagnetic wave exposure on humans and different kinds of animals have led to the specification of different standards, which have been designed to set a nonionizing radiation exposure level compatible with human health. The most authoritative guidelines at international level have been developed by the ICNIRP. The ICNIRP criteria and guidelines specify limit values for occupational exposure as well as for general public exposure. At the frequency of operation of the current work (around 2.45GHz), the ICNIRP general public exposure limit is 61.492 V/m, and occupational exposure limit is 137 V/m. As can be seen throughout this work, the obtained electric field values are lower than 4V/m, so far lower than the ICNIRP limit levels. Figure 5.31 shows the E-field exposure reference levels recommended by the ICNIRP.

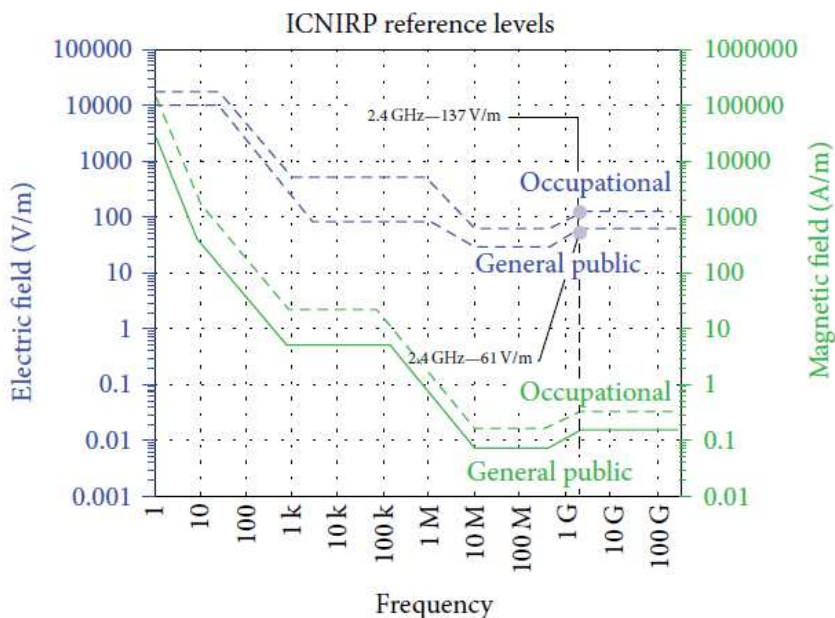


**Figure 5.31.** ICNIRP reference levels of E-field exposure for occupational and general public exposure. The specific level for the working frequency of 2.4 GHz has been indicated.

In order to get the specific absorption rate (SAR) for the human body, the in-house developed human body model has been used and situated in three different locations in front of the oven: at a distance of 1 m, 1.5 m, and 2 m from the microwave oven, as seen in Figure 5.32.

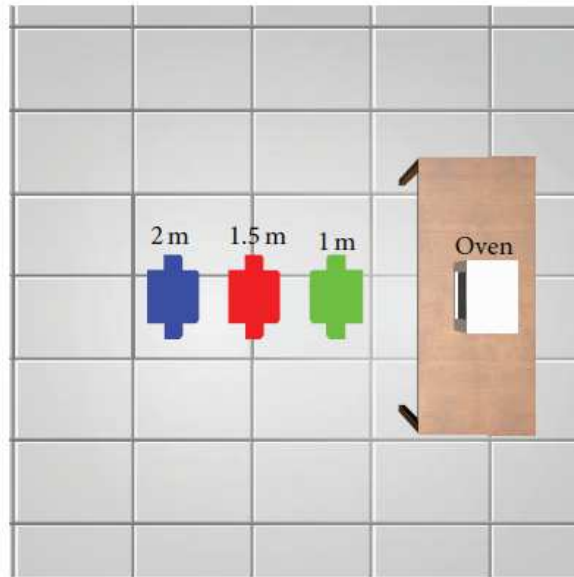


**Figure 5.32.** Upper view of the three positions for calculating the SAR, 1m (Green), 1.5m (Red) and 2m (Blue) from the microwave oven.

The SAR values have been obtained using the following expression:

$$SAR = \frac{\sigma}{\rho} |\vec{E}|^2 \quad (5.3)$$

where conductivity ( $\sigma$ ), tissue density ( $\rho$ ) and electric field are considered. This SAR calculation method has been extracted from [San09] and has been previously implemented in other works [Kin08][Wat10][Loa12]. The human body model parameters used in this study, as the age (35-39 years old), the height (1.80 m) and the fat percentage (26.9%) have been chosen taken into account previously

published works, as well as conductivity of the skin (10.18 S/m) [Agu12], and the human body density (1043 Kg/m<sup>3</sup>) [Krz67].

In Figure 5.33 the 3D Ray Launching simulation results of the RF power distribution within the scenario under analysis are depicted. The scenario has been simplified in order to show only the interest zone, i.e. in front of the microwave oven, where the human body model is located. The influence of the presence of the human body model in the overall radiated power distribution within the complete scenario can be clearly seen, as lower power levels appear in the regions behind the human body model (shadow effect).

In Figure 5.34 obtained SAR results for the three different simulation cases are depicted, for a microwave oven operating at 1800W, which corresponds to a heavy duty model, not a common domestic microwave oven. As expected, higher absorption has been produced when the human body is closer to the microwave oven.

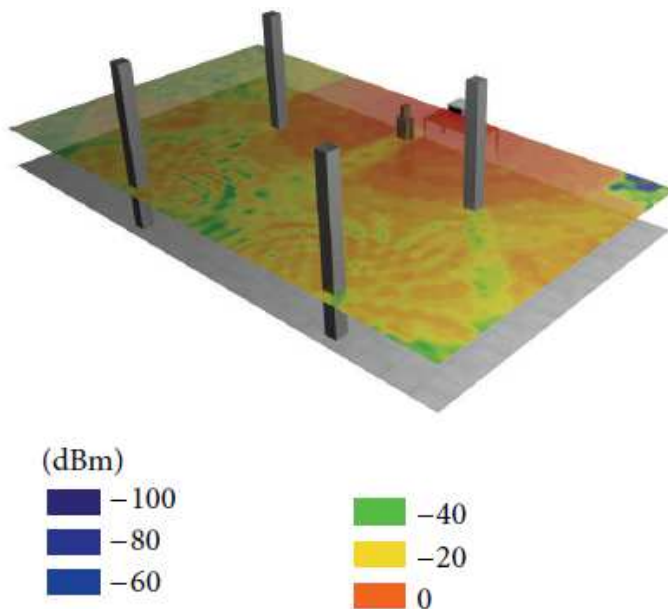


**Figure 5.33.** Power distribution for the zone of the scenario where human body model is placed at 1.5m distance from the microwave oven.



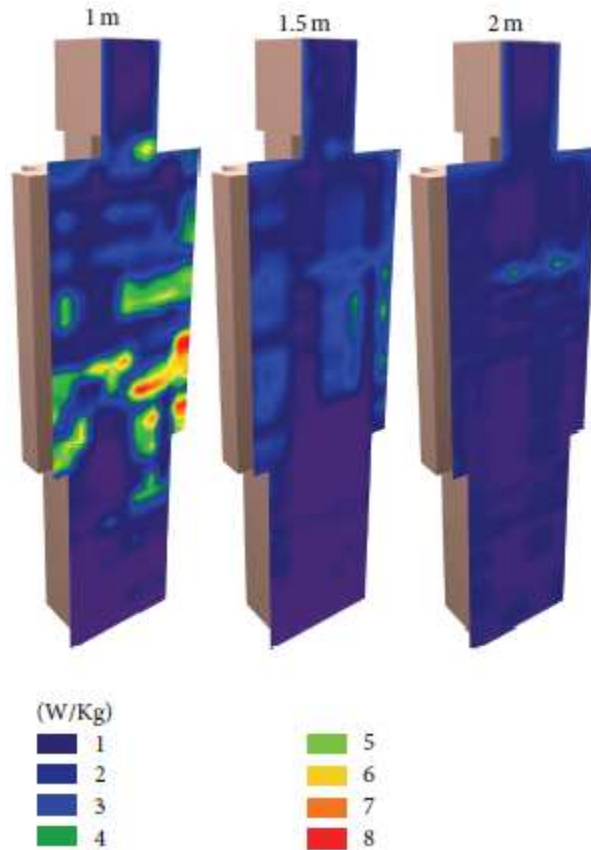


**Figure 5.34.** SAR values for human body model situated at 1 m, 1.5 m and 2 m in front of the microwave oven.

In order to protect people from EMF (Electromagnetic Fields) overexposure, the ICNIRP and the IEEE have defined SAR limits that have been established in the great majority of countries in the world. The restrictions in these guidelines were based on scientific data alone. Currently available knowledge, however, indicates that these restrictions provide an adequate level of protection from exposure to time-varying EMF. Two classes of guidance are presented in ICNIRP, which is the most widespread and used standard [ICN98]:

- **Basic restrictions:** Restrictions are based directly on established health effects. Some of the physical quantities used to specify these restrictions are the SAR, expressed in W/Kg, and the power density (S), in W/m<sup>2</sup>.
- **Reference levels:** These levels are provided for practical exposure assessment purposes to determine whether the basic restrictions are likely to be exceeded. Some reference levels are derived from relevant basic restrictions using measurement and/or computational techniques, and some address perception and adverse indirect effects of exposure to EMF. One of the derived quantities is the electric field strength.

The basic restrictions provided by ICNIRP for whole-body average SAR and localized SAR for frequencies between 10 MHz and 10 GHz are presented in Table 5.5:

Exposure Characteristics	Whole-body average SAR (W/kg)	Localized SAR (head and trunk) (W/kg)	Localized SAR (limbs) (W/kg)
Occupational Exposure	0.4	10	20
General Public Exposure	0.08	2	5

**Table 5.5.** Basic restrictions of SAR for frequencies from 10 MHz to 10 GHz.

The frequency of 2.45 GHz, where microwave ovens operate at, belongs to the range of 10 MHz to 10GHz shown in Table 5.5. After analyzing Figure 5.34, it follows that at the distance of 1 meter, the SAR reaches the value of 8 W/kg in localized areas above the legs. This value is between the levels for occupational and general public of localized SAR. Therefore, the basic restrictions of the SAR values for the general public are exceeded (but the domestic ovens operate at a maximum power level much lower than the level used in this case), although the obtained values are under the levels for occupational exposure.

It can be concluded that although the microwave oven’s leakage can degrade the quality of a wireless communication, as can be seen in the

bibliography, the obtained electric field values are well below the limit values specified by ICNIRP. Diversity in the models of microwave ovens has been taken into account as a function of maximum output power, in the range of 750W to 1800W, obtaining estimations of leakage field exposure within this range. By considering the introduction of the human body model, modification in overall E-field levels can be assessed, as well as initial estimations of SAR values, which can be employed in order to analyze compliance with different regulations. Moreover, the obtained values are compared with these regulations, showing compliance for the complete scenario under analysis in the case of using a conventional microwave oven operating with a maximum output power of 800W.

This technique allows performing assessment of exposure levels in complete scenarios, with feasible computational cost, aiding in the adoption of exposure reduction measurements, such as the identification of the optimal location of potential radiofrequency emitting sources, such as microwave ovens. This analysis in the future can be extended to other types of devices, such as household appliances or industrial equipment.

## 5.4 Main Contributions

This section presents the list with my main contributions (i.e. the articles and conference papers in which I am the first author) regarding the work presented in this chapter. The rest of works regarding this topic where I contributed can be consulted in the List of Publications section.

Specifically, my main contributions to the list of publications shown below have been the study of the state of the art, the performance of measurements within the scenarios under analysis, the creation of the scenario for the 3D Ray Launching simulations and the corresponding simulations, the post-processing of the obtained data, the writing of the most of the text of the manuscripts, and the development of the hybrid method for the modeling of electromagnetic noise sources, in this case a microwave oven.

Note that all the research articles have been published in JCR (Journal Citation Reports) indexed journals.

- *Research Articles:*

1. "Impact of High Power Interference Sources in Planning and Deployment of Wireless Sensor Networks and Devices in the 2.4 GHz Frequency Band in Heterogeneous Environments," *Sensors*, vol. 12, issue 11, pp. 15689-15708, 2012.
2. "Hybrid Equivalent Source – 3D Ray Launching Simulation Technique for Deterministic Estimation of Radiated Emissions of Electrical Appliances," *Journal of Electromagnetic Waves and Applications*, vol. 30, issue 4, 2016.
3. "Estimation of Radiofrequency Power Leakage from Microwave Ovens for Dosimetric Assessment at Non Ionizing Radiation Exposure Levels," *BioMed Research International*, Hindawi Publishing Corporation, Article ID 603260, 2015.

- *International Conference Papers:*
  1. "Impact and Characterization of the Microwave Oven Power Leakage on 802.15.4 Networks," (2013 *IEEE AP-S International Symposium*).
  2. "Impact of the microwave oven power leakage on 802.15.4 networks," (2013 *EuCAP International Symposium*).
  3. "Assessment of Electromagnetic Dosimetric values from Non-Ionizing Radiofrequency Sources in a Conventional Road Vehicle," (2014 *IEEE International Symposium on Antennas and Propagation and USNC-URSI National Radio Science Meeting*).
  4. "Dosimetric Assessment of Radiofrequency Power Leakage from Microwave Ovens in Complex Scenarios," (2015 *IEEE International Symposium on Antennas and Propagation and USNC-URSI National Radio Science Meeting*).
  5. "Hybrid Method for Deterministic Estimation of Radiated Emissions of Electrical Appliances," (2016 *EuCAP. 10th European Conference on Antennas and Propagation*).
  
- *National Conference Papers:*
  1. "Impacto de la potencia de fuga de hornos microondas en redes 802.15.4," (2012 *URSI XXVII National Symposium*).
  2. "Análisis Dosimétrico de las Fugas de Hornos Microondas," (2013 *URSI XXVIII National Symposium*).
  3. "Gailu Elektrikoek sortutako Erradiazioaren Estimazio Determinista Metodo Hibrido berri baten bidez," (Ikertzaile Euskaldunen II. Nazioarteko Kongresua- IkerGazte 2017).

# Chapter 6

## Conclusions and Future Work

**T**HIS last chapter presents the conclusions as well as the future research lines derived from the research work presented in this thesis document. First, Section 6.1 provides a summary of the obtained results and the conclusions, in order to verify the achievement of the initial objectives proposed in Chapter 1. Then, future research lines and trends are shown in Section 6.2.

### 6.1 Conclusions

As mentioned in Chapter 1, the presented Ph.D. thesis was motivated by the expected exponential growth of wireless device deployment due to the advent of the IoT and the new 5G communication systems, which will lead to extremely dense radio environments. For the development of the work, the in-house implemented 3D Ray Launching algorithm has been the starting point since it is a valuable tool for radio propagation analysis. Figure 6.1 presents schematically the main contributions of this thesis, and the conclusions of the obtained results

are listed in the following points:

- The first conclusion derives from the application of the 3D Ray Launching tool for radio propagation analysis within different scenarios, all of them being framed in the Smart City environment: The simulation methodology has been validated for Home, Office, Sport, Commercial area, Vehicular and Hospital environments, providing a good trade-off between the accuracy of the estimated results (i.e. RF power distribution) and the required computational time.
- Obtained RF power distribution results show that the morphology and the topology of these complex environments play a relevant role in electromagnetic propagation, due mainly to multipath propagation. Therefore, site specific radio planning is required in this kind of scenarios. For that reason, the presented 3D Ray Launching simulation method is an adequate tool to carry out radio planning tasks.
- The importance of analyzing interferences for optimized radio planning tasks has been highlighted and demonstrated, especially when dense wireless networks and the coexistence of different wireless communication systems are considered. For that purpose, a novel point of view regarding the use of propagation models has been presented in this thesis: The use of the in-house 3D Ray Launching algorithm for analyzing the interference effect on wireless communication links, obtaining SNR, Current consumption and BER estimations.
- It is well known that human bodies create the Shadow Effect in radio propagation. In this thesis, this effect has been analyzed and estimated deterministically by the 3D Ray Launching method, allowing the assessment of the performance of

wireless communication systems for different densities of human beings within Smart City environments.

- Due to the high quantity of wireless nodes that could be present in dense WSNs, 5G communications systems and IoT-based networks, the computational cost for the simulation of such scenarios by the 3D Ray Launching algorithm will be very high. In order to alleviate this problem, an acceleration hybrid 3D Ray Launching-Collaborative Filtering technique has been developed during this thesis work. This new technique reduces the simulation time drastically while the accuracy of the results worsens very little.
- In addition to the interferences generated by other wireless communication systems, electronic devices and appliances also emit electromagnetic noise, becoming a potential source of interferences to wireless communication links. In this thesis the impact of the electromagnetic noise generated by domestic microwave ovens on ZigBee communication links has been studied. This study has led to one of the most important results of this thesis: a novel method for modeling electromagnetic noise sources has been developed, based on equivalent sources theory and 3D Ray Launching simulations. Thus, the radiated power distribution of this kind of sources can be determined within the complete volume of different environments.
- Finally, the modeling of radiating sources has led to its application in dosimetric studies. As the obtained methodology provides deterministic estimations of the radiated power of electronic devices and appliances, these results have been used to obtain SAR levels. Due to the possibilities provided by the 3D Ray Launching tool, this methodology can be used for any scenario where the radiating sources are placed.



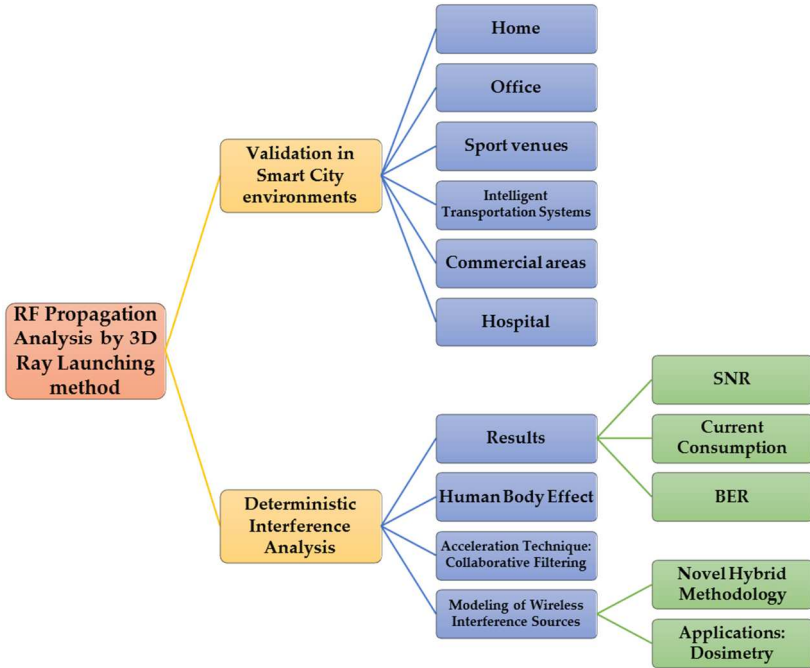


**Figure 6.1.** Summary of the work presented in this thesis.

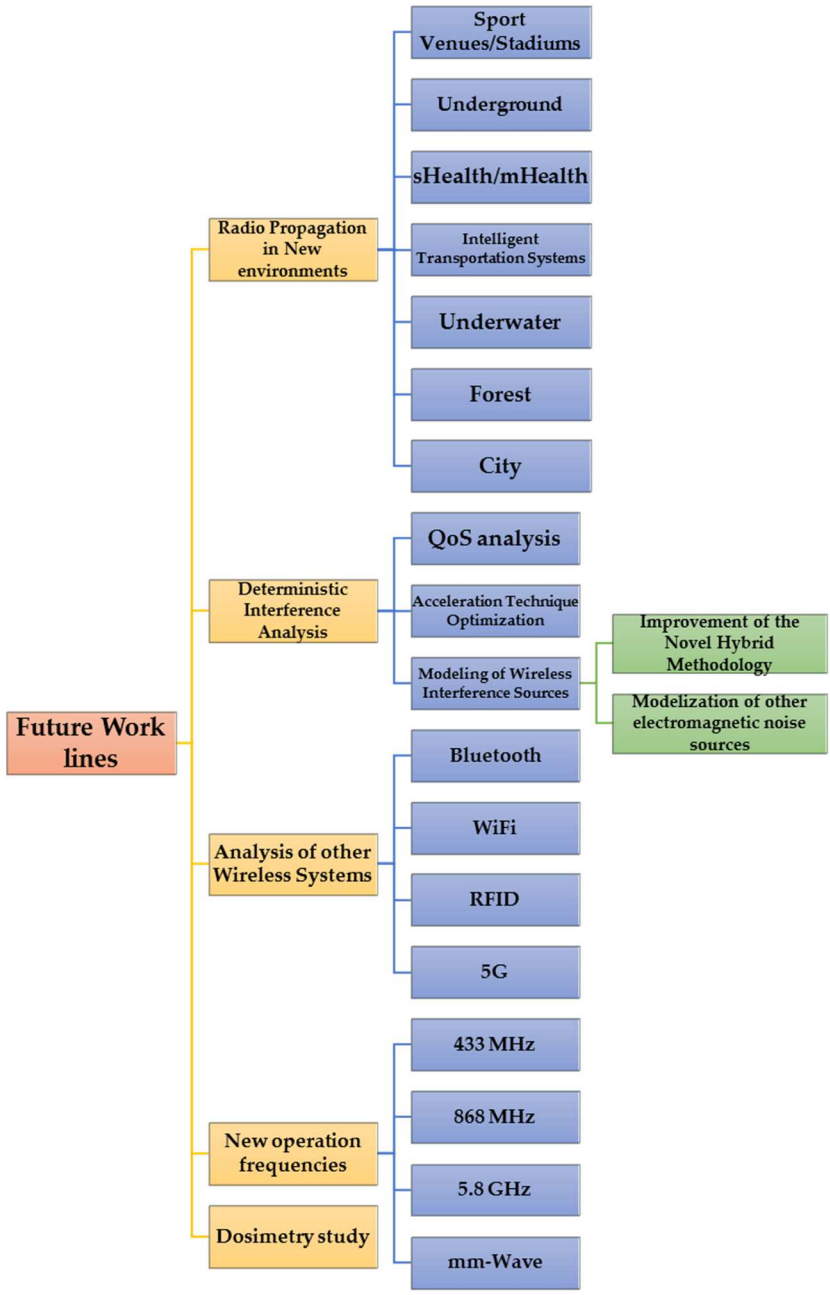
Based on the results presented in this manuscript, which are backed by its publication in international journals, it can be stated that the objectives of this thesis have been fulfilled satisfactorily. The importance of the interference analysis on the deployment and performance of the upcoming dense WSNs, 5G communication systems and IoT networks has been highlighted. Besides, it has been demonstrated that the in-house developed 3D Ray Launching algorithm is an accurate and efficient simulation tool to carry out site-specific radio propagation and radio planning tasks within the scenarios where these wireless systems will be deployed (including interference sources), obtaining estimations of the optimal positions for the transceivers, minimizing power consumption, increasing overall system capacity and improving the overall performance of the system.

## 6.2 Future Work

The study presented in this thesis document can lead to different work lines. These potential research lines are listed below, which most of them are currently being developed:

- Radio propagation within new environments can be analyzed by the presented 3D Ray Launching method: Sport environments such as stadiums and runner-to-infrastructure communications; Hospital-health environments for the provision of sHealth and mHealth services; Delve into city environments; Intelligent transportation systems; Underwater communications; Forest and vegetation environments; Underground environments.
- Due to the relevance that interference analysis will have with the advent of IoT and the implementations of Context-Aware scenarios, the study of very dense WSNs in different environments by the 3D Ray Launching algorithm is an interesting line of work, where more in-depth analysis regarding QoS parameters of wireless communication systems is required.
- The work developed in this thesis is focused on ZigBee devices due to their appropriate characteristics for the deployment of WSNs applied to Context-Aware scenarios. But another research line is to extend the presented analysis to other wireless systems based on Bluetooth, RFID and WiFi devices.
- In the same way, the study of different frequency bands such as 433 MHz, 868 MHz and higher frequencies (GHz and mm-Wave) is an interesting research field mainly due to the advent of the new 5G networks.

- The hybrid Ray Launching + Collaborative Filtering acceleration technique is being evolved and several improvements are being developed.
- The presented novel hybrid method based on equivalent sources has been applied successfully to a common microwave oven. The method is being improved and its application to other types of electrical devices is a fundamental task in order to validate it: Household appliances such as the wireless devices employed to watch babies (which have been observed that can greatly affect ZigBee and WiFi communications); Industrial equipment such as engines and transformers; Wireless Power Transfer systems; radiated emissions from PCB boards; Urban noise sources such as Smart meters, streetlights (there are specific bulbs that can interfere wireless communications), etc.
- The novel hybrid method itself is being improved with the inclusion of different methodologies to define the equivalent source arrays in the 3D Ray Launching tool.
- The dosimetry line of research is being developed by using the microwave oven model to calculate other dosimetric quantity parameters such as SA (Specific Absorption) and obtaining the dosimetry levels within different and potentially more hazardous environments such as passenger aircrafts.



# Bibliography

## A

- [Abd11] A. Y. Abd-Fatah, R. M. Yusuff, F. A. Aziz, N. Zulkifli, "Simulation of time-based versus sensor- based traffic light system," *In Proceedings of the IEEE 3rd International Conference on Communication Software and Networks (ICCSN)*, Xi'an, China, 27-29 May 2011.
- [Abd12] A. H. Abdul Razak, A. Zayegh, R. K. Begg, Y. Wahab, "Foot Plantar Pressure Measurement System: A Review," *Sensors*, 12, pp. 9884-9912, 2012.
- [Abr00] F. Abrishamkar, J. Irvine, "Comparison of Current Solutions for the Provision of Voice Service to Passengers on High Speed Trains," *Vehicular Technology Conference (VTC 2000)*, Tokyo, Japan, 15-18 May, 2000.
- [Abu12] N. AbuAli, M. Hayajneh, "Performance Evaluation of Channel Models of ZigBee Sensor Networks," *International Wireless Communications and Mobile Computing Conference*, Limassol, pp.860-865, Aug. 2012.
- [Ada09] F. S. de Adana, M. F. Catedra, J. M. Gomez, R. Mittra, J. B. Renuncio, F. Gutierrez, M. A. Prieto, "An Effective Technique for System-Level Prediction of the Radiated Emissions of Unknown Sources Inside Low- Q Cavities Using Unit-Level Measurements," *IEEE Trans. Electromagnetic Compatibility*, vol. 51, no. 2, pp. 181 – 191, 2009.
- [Agg40] C. V. Aggers, "Methods of Controlling Radio Interference," *Transactions of the American Institute of Electrical Engineers*, vol. 59, no. 4, pp. 193-201, 1940.
- [Agu12] E. Aguirre, J. Arpon, L. Azpilicueta, S. De Miguel Bilbao, V. Ramos, F. Falcone, "Evaluation of electromagnetic dosimetry of wireless systems in complex indoor scenarios with human body interaction," *Progress In Electromagnetics Research B*, vol. 43, pp. 189-209, 2012.
- [Ahm07] M. Ahmed, C. U. Saraydar, T. ElBatt, Jijun Yin, T. Talty, M. Ames, "Intra-Vehicular Wireless Networks," *IEEE Globecom Workshops*, Washington, DC, USA, November 26-30, 2007.
- [Ahm15] A. Ahmad, M. M. Rathore, A. Paul, B.-W. Chen, "Data Transmission Scheme Using Mobile Sink in Static Wireless Sensor Network," *Journal of Sensors*, vol. 2015, Article ID 279304.
- [Aio10] O. Aiouaz, D. Lautru, M. F. Wong, A. Gati, J. Wiart, V. F. Hanna, "Near-field modal decomposition using Huygens' principle and equivalent sources," *European Microwave Conference (EuMC)*, Paris, France, 28-30 Sept. 2010.
- [Aio10b] O. Aiouaz, D. Lautru, M. F. Wong, A. Gati, J. Wiart, V. F. Hanna, "SAR evaluation by modal decomposition using induced near-field of equivalent

- current sources," *URSI International Symposium on Electromagnetic Theory (EMTS)*, Berlin, Deutschland, 16-19 Aug. 2010.
- [Ais14] R. Aissaoui, H. Menouar, A. Dhraief, F. Filali, A. Belghith, A. Abu-Dayya, "Advanced real-time traffic monitoring system based on V2X communications," *In Proceedings of the IEEE International Conference on Communications (ICC)*, Sydney, Australia, 10-14 June 2014.
- [Aky02] I. F. Akyildiz, W. Su, Y. Sankarasubramaniam, E. Cayirci, "Wireless sensor networks: A survey," *Comput. Netw.*, vol. 38, no. 4, pp. 393-422, Mar. 2002.
- [AlK08] K. Al-Khateeb, J. A. Y. Johari, "Intelligent dynamic traffic light sequence using RFID," *In Proceedings of the International Conference on Computer and Communication Engineering, ICCCE 2008*, Kuala Lumpur, Malaysia, 13-15 May 2008.
- [AlK17] M. O. Al Kalaa, W. Balid, H. H. Refai, N. J. LaSorte, S. J. Seidman, H. I. Bassen, J. L. Silberberg, D. Witters, "Characterizing the 2.4 GHz Spectrum in a Hospital Environment: Modeling and Applicability to Coexistence Testing of Medical Devices," *IEEE Transactions on Electromagnetic Compatibility*, vol. 59, no. 1, pp. 58-66, 2017.
- [Alv07] Y. Alvarez, F. Las-Heras, M. R. Pino, "Reconstruction of Equivalent Currents Distribution Over Arbitrary Three-Dimensional Surfaces Based on Integral Equation Algorithms," *IEEE Trans. Antennas and Prop.*, vol. 55, no. 12, pp. 3460 - 3468, Dec. 2007.
- [Alv10] Y. Alvarez, F. Las-Heras, M. R. Pino, "Antenna characterization using the Sources Reconstruction Method," *Proceedings of the Fourth European Conference on Antennas and Propagation (EuCAP)*, Barcelona, Spain, 12-16 April 2010.
- [Amb13] D. Ambekar, Z. Al-Deneh, T. Dao, A. L. Dziech, V. Subbian, F. R. Beyette, "Development of a Point-of-Care Medical Device to Measure Head Impact in Contact Sports," *35th Annual International Conference of the IEEE Engineering in Medicine and Biology Society*, Osaka, Japan, 2013.
- [Ant99] G. Antonini, S. Cristina, A. Orlandi, "A prediction model for electromagnetic interferences radiated by an industrial power drive system," *IEEE Trans. Industry Applications*, vol. 35, no. 4, pp. 870 - 876, 1999.
- [Ara11] A. Aragues, J. Escayola, I. Martínez, P. del Valle, P. Munoz, J. D. Trigo, J. Garcia, "Trends and Challenges of the Emerging Technologies toward Interoperability and Standardization in e-Health Communications," *IEEE Trans. Veh. Technol.*, vol. 49(11), pp. 182-184, Nov. 2011.
- [Ata13] M. Atamanesh, F. Farzaneh, "A Proposed Equivalent Channel Power Delay Profile for a Millimeter WaveWireless OFDM System and Optimum Guard Interval Evaluation in a Built-Up Area Propagation Scenario," *Wireless Personal Communications*, 69, pp. 1223-1239, 2013.
- [Aus98] B. A. Austin, K. P. Murray, "The Application of Characteristic-Mode Techniques to Vehicle-Mounted NVIS Antennas," *IEEE Antennas and Propagation Magazine*, vol. 40, Issue 1, pp. 7-21, 1998.

- [Azi08] M. Aziz, B. Raouf, N. Riad, R. M. Daoud, H. M. Elsayed, "The use of Ethernet for single on-board train network," *Proceedings of the IEEE International Conference on Networking, Sensing and Control ICNSC*, Sanya, China, 2008.
- [Azm14] N. Azmi, L. M. Kamarudin, M. Mahmuddin, A. Zakaria, A. Y. M. Shakaff, S. Khatun, K. Kamarudin, M. N. Morshed, "Interference Issues and Mitigation Method in WSN 2.4GHz ISM Band: A Survey," *2nd International Conference on Electronic Design (ICED)*, pp. 404-408, 2014.
- [Azp12] L. Azpilicueta, F. Falcone, J. J. Astráin, J. Villadangos, I. J. García Zuazola, H. Landaluce, I. Angulo, A. Perallos, "Measurement and Modeling of a UHF-RFID System in a Metallic Closed Vehicle," *Microwave and Optical Technology Letters*, vol. 54, Issue 9, pp. 2126-2130, 2012.
- [Azp14] L. Azpilicueta, M. Rawat, K. Rawat, F. Ghannouchi, F. Falcone, "Convergence Analysis in Deterministic 3D Ray Launching Radio Channel Estimation in Complex Environments," *ACES Journal*, vol. 29, pp. 256-270, 2014.
- [Azp14b] L. Azpilicueta, P. López-Iturri, E. Aguirre, I. Mateo, J. Astrain, J. Villadangos, F. Falcone, "Analysis of radio wave propagation for ISM 2.4 GHz wireless sensor networks in inhomogeneous vegetation environment," *Sensors*, vol. 14, pp. 23650-23672, 2014.

## B

- [Baa14] A. A. Baaddi, M. D. El Oudghiri, "Hybrid Wireless Sensor-based system for chaotic traffic," *In Proceedings of the Fifth International Conference on Next Generation Networks and Services (NGNS)*, Casablanca, Morocco, 28-30 May 2014.
- [Bac10] B. Bach, D. Wilhelmer, P. Palensky, "Smart buildings, smart cities and governing innovation in the new millennium," *8th IEEE International Conference on Industrial Informatics (INDIN)*, 2010.
- [Bal05] C. Balanis, "Antenna Theory: Analysis and Design," *Wiley-Interscience*, 3rd Edition, 2005.
- [Ban14] B. Bangerter, S. Talwar, R. Arefi, K. Stewart, "Networks and Devices for the 5G Era," *IEEE Communications Magazine*, vol. 52, no. 2, pp. 90-96, Feb. 2014.
- [Bar10] J. J. Barroso, A. L. de Paula, "Retrieval of permittivity and permeability of homogeneous materials from scattering parameters," *Journal of Electromagnetic Waves and Applications*, vol. 24, pp. 1563-1574, 2010.
- [Bar11] M. R. Barzegaran, A. Sarikhani, O. A. Mohammed, "An equivalent source model for the study of radiated electromagnetic fields in multi-machine electric drive systems," *IEEE International Symposium on Electromagnetic Compatibility (EMC)*, Rome, Italy, 14-19 Aug. 2011.
- [Bas13] C. U. Bas, S. C. Ergen, "Ultra-wideband Channel Model for Intra-vehicular Wireless Sensor Networks Beneath the Chassis: From Statistical Model to

- Simulations," *IEEE Transactions on Vehicular Technology*, 62, 1, pp. 14-25, January 2013.
- [Bau07] D. Baudry, C. Arcambal, A. Louis, B. Mazari, P. Eudeline, "Applications of the Near-Field Techniques in EMC Investigations," *IEEE Trans. Electromagnetic Compatibility*, vol. 49, no. 3, pp. 485 - 493, 2007.
- [Bel09] F. Bellens, F. Quitin, F. Horlin, P. De Doncker, "Channel Measurements and MB-OFDM Performance Inside a Driving Car," *International Conference on Electromagnetics in Advanced Applications*, Torino, Italy, September 14-18, 2009.
- [Bel12] F. J. Bellido-Outeirino, J. M. Flores-Arias, F. Domingo-Perez, A. Gil-de-Castro, A. Moreno-Munoz, "Building lighting automation through the integration of DALI with wireless sensor networks," *IEEE Trans. Consum. Electron.*, vol. 58, pp. 47-52, 2012.
- [Bel13] P. Bellavista, G. Cardone, A. Corradi and L. Foschini, "Convergence of MANET and WSN in IoT Urban Scenarios," *IEEE Sens. Jour.*, vol. 13, no. 10, pp. 3558 - 3567, 2013.
- [Ber95] P. Bergholm, M. Honkanen, S. -G. Haggman, "Simulation of a microcellular DS-CDMA radio network," *Fourth IEEE International Conference on Universal Personal Communications*, pp. 838 - 842, 1995.
- [Ber09] J. -P. Berenger, "Extension of the FDTD Huygens Subgridding Algorithm to Two Dimensions," *IEEE Trans. Antennas and Prop.*, vol. 57, no. 12, pp. 3860 - 3867, 2009.
- [Ber15] L. Bernado, T. Zemen, F. Tufvesson, A. F. Molisch, C. F. Mecklenbrauker, "Time- and frequency-varying k-factor of non-stationary vehicular channels for safety-relevant scenarios," *IEEE Transactions on Intelligent Transportation Systems*, vol. 16, pp. 1007-1017, 2015.
- [Bol06] C. A. M. Bolzani, C. Montagnoli, M. L. Netto, "Domotics Over IEEE 802.15.4 - A Spread Spectrum Home Automation Application," *IEEE Ninth International Symposium on Spread Spectrum Techniques and Applications*, 2006.
- [Bon10] D. D. Bona, G. S. Ferreira, L. Schwarz, "Sensoriamento remoto em pranchas de surfe utilizando tecnologia ZigBee," *Proc. of the 9th IEEE/IAS INDUSCON*, Sao Paulo, Brazil, 2010.
- [Bor13] A. Borhani, M. Pätzold, "Correlation and spectral properties of vehicle-to-vehicle channels in the presence of moving scatterers," *IEEE Transactions on Vehicular Technology*, vol. 62, pp. 4228-4239, 2013.
- [Bud12] H. Buddendick, T. F. Eibert, "Incoherent Scattering-center Representations and Parameterizations for Automobiles," *IEEE Antennas and Propagation Magazine*, vol. 54, Issue 1, pp. 140 - 148, 2012.
- [Bur07] R. Burda, C. Wietfeld, "Multimedia over 802.15.4 and ZigBee Networks for Ambient Environment Control," *IEEE 65th Vehicular Technology Conference*, Dublin, Ireland, April 22-25, 2007.
- [Bus90] K. B. Bush, "A method for the transformation of arbitrary electromagnetic fields



based on Huygens principle," *Proceedings of the IEEE Southern Tier Technical Conference*, Binghamton, NY, USA, 25 April 1990.

## C

- [Cam15] N. G. S. Campos, D. G. Gomes, F. C. Delicato, A. J. V. Neto, L. Pirmez, J. Neuman de Souza, "Autonomic Context-Aware Wireless Sensor Networks," *Journal of Sensors*, vol. 2015, Article ID 621326.
- [Can05] A. Canova, F. Freschi, M. Repetto, M. Tartaglia, "Identification of Equivalent Source System for electromagnetic field pollution evaluation," *18th International Conference and Exhibition on Electricity Distribution (CIRED)*, Turin, Italy, 6-9 June 2005.
- [Car93] A. Cardama, "Antenas," *Editions UPC*, 1993.
- [Cha13] N. Chakravorti, T. Le Sage, S. E. Slawson, P. P. Conway, A. A. West, "Design and Implementation of an Integrated Performance Monitoring Tool for Swimming to Extract Stroke Information at Real Time," *IEEE Transactions on Human-Machine Systems*, vol. 43, 2, 199-213, 2013.
- [Cha14] P. Chandrasekar, T. Sangeetha, "Smart Shopping Cart with Automatic Billing System through RFID and ZigBee," *International Conference on Information Communication and Embedded Systems (ICICES)*, Chennai, Feb. 2014.
- [Che04] X. Chen, T. M. Grzegorzczuk, Bae-Ian Wy, J. Pacheco Jr., J. A. Kong, "Robust method to retrieve constitutive effective parameters of metamaterials," *Phys. Rev. E* 70, 016608, 2004.
- [Che08] L. Cheng, S. Hailes, "Analysis of Wireless Inertial Sensing for Athlete Coaching Support," *IEEE Global Telecommunications Conference*, New Orleans, LO, USA, 2008.
- [Che11] Chen Changjiang, Wei Biao, Zhang Fengying, "Design and realization of wireless environmental monitoring system based on ZigBee for stadium," *IEEE International Conference on Future Computer Science and Education (ICFCSE)*, Xi'an, China, pp. 149 – 151, 2011.
- [Chi05] E. H. Chi, "Introducing wearable force sensors in martial arts," *IEEE Pervasive Computing*, vol. 4, 3, 47 – 53, 2005.
- [Chi13] C. A. Chin, G. V. Crosby, T. Ghosh, R. Murimi, "Advances and Challenges of Wireless Body Area Networks for Healthcare Applications," *Int. Conf. Comp. Net. Comm.*, Maui, HI, pp. 99- 103, Jan. 2013.
- [Cho13] B. Choudhury, H. Singh, J. P. Bommer, R. M. Jha, "RF Field Mapping Inside a Large Passenger-Aircraft Cabin Using a Refined Ray-Tracing Algorithm," *IEEE Antennas and Propagation Magazine*, vol. 55, no. 1, February 2013.
- [Chu10] S. Chumkamon, P. Tuvaphanthaphiphat, P. Keeratiwintakorn, "The Vertical Handoff between GSM and Zigbee Networks for Vehicular Communication," *International Conference on Electrical Engineering/Electronics Computer*

- Telecommunications and Information Technology (ECTI-CON)*, Chiang Mai, Thailand, pp. 603 – 606, May 19-21, 2010.
- [Chu12] W. Chung, H. Kim, Y. Yoo, C.-B. Moon, J. Park, "The Detection and Following of Human Legs Through Inductive Approaches for a Mobile Robot With a Single Laser Range Finder," *IEEE Transactions On Industrial Electronics*, vol. 59, no. 8, pp. 3156-3166, Aug. 2012.
- [Cla11] J. Clarhaut, S. Hayat, H. Tahiri, "Integration of communication systems for a railroad smart wagon", *IEEE International Conference on Logistics*, pp. 19-24, 2011.
- [Coc14] J. Cockcroft, J. M. Muller, C. Scheffer, "A Novel Complimentary Filter for Tracking Hip Angles During Cycling Using Wireless Inertial Sensors and Dynamic Acceleration Estimation," *IEEE Sensors Journal*, vol. 14, 8, pp. 2864 – 2871, 2014.

## D

- [Dae10] Dae-Man Han, Jae-Hyun Lim, "Smart Home Energy Management System using IEEE 802.15.4 and ZigBee," *IEEE Transactions on Consumer Electronics*, vol. 56, 2010.
- [Deb08] C. J. Debono, R. A. Farrugia, "Optimization of the UMTS Network Radio Coverage On-board an Aircraft," *IEEE Aerospace Conference*, pp. 1-7, 2008.
- [deF09] R. de Francisco, Li Huang, G. Dolmans, H. de Groot, "Coexistence of ZigBee Wireless Sensor Networks and Bluetooth inside a Vehicle," *IEEE 20th International Symposium on Personal, Indoor and Mobile Radio Communications*, Tokyo, Japan, September 13-16, 2009.
- [Dia04] N. R. Diaz, J. E. J. Esquitino, "Wideband channel characterization for wireless communications inside a short haul aircraft," *IEEE 59th Vehicular Technology Conference (VTC)*, vol.1, 17-19 May, 2004.
- [Din14] Y. Ding, J. Sun, X. Wang, "Sea surface reflection and power attenuation analysis of radio wave in UHF satellite communications," *TELKOMNIKA Indonesian Journal of Electrical Engineering*, vol. 12, no.4, pp. 3168-3176, April 2014.
- [Dis08] S. D. Dissanayake, P. P. C. R. Karunasekara, D. D. Lakmanarachchi, A. J. D. Rathnayaka, A. T. L. K. Samarasinghe, "Zigbee Wireless Vehicular Identification and Authentication System," *4th International Conference on Information and Automation for Sustainability*, Colombo, Sri Lanka, December 12-14, 2008.
- [Don10] W. Dong, G. Liu, L. Yu, H. Ding, J. Zhang, "Channel Properties of indoor part for high-speed train based on wideband channel measurement," *5th International ICST Conference on Communications and Networking in China (CHINACOM)*, pp. 1-4, 2010.

## E

- [Eam08] P. Eamsomboon, P. Keeratiwintakorn, C. Mitrpant, "The performance of Wi-Fi and Zigbee Networks for Inter-Vehicle Communication in Bangkok Metropolitan Area," *8th International Conference on ITS Telecommunications*, Phuket, Thailand, pp. 408 – 411, October 24, 2008.
- [Eib09] T. F. Eibert, C. H. Schmidt, "Multilevel Fast Multipole Accelerated Inverse Equivalent Current Method Employing Rao–Wilton–Glisson Discretization of Electric and Magnetic Surface Currents," *IEEE Trans. Antennas and Prop.*, vol. 57, no. 4, pp. 1178 – 1185, 2009.
- [Ere13] H. Eren, H. M. Pakka, A. S. AlGhamdi, Y. Yizuo, "Instrumentation for safe vehicular flow in intelligent traffic control systems using wireless networks," *In Proceedings of the IEEE International Instrumentation and Measurement Technology Conference (I2MTC)*, Minneapolis, MN, USA, 6–9 May 2013.
- [Eva06] C. Evans, Bin Hu, "E-commerce to U-business: A Model for Ubiquitous Shopping Mall," *in Proc. ISPCA*, Urumqi, 2006, pp. 427 – 432.

## F

- [Far08] S. Farahani, "ZigBee Wireless Networks and Transceivers," Newnes (2008), ISBN: 978-0-7506-8393-7.
- [Fla10] F. Flamini, A. Gaglione, F. Ottello, A. Pappalardo, C. Pragliola, A. Tedesco, "Towards Wireless Sensor Networks for railway infrastructure monitoring," *IEEE Electrical Systems for Aircraft, Railway and Ship Propulsion (ESARS)*, pp. 1-6, 2010.
- [Fin09] J. Fink, N. Michael, A. Kushleyev, V. Kumar, "Experimental characterization of radio signal propagation in indoor environments with application to estimation and control," *in Proceedings of IEEE/RSJ International Conference on Intelligent Robots and Systems (IROS '09)*, pp. 2834–2839, St. Louis, Mo, USA, October 2009.
- [Fog12] L. J. Foged, L. Scialacqua, F. Saccardi, J. L. A. Quijano, G. Vecchi, M. Sabbadini, "Practical Application of the Equivalent Source Method as an Antenna Diagnostics Tool," *IEEE Antennas and Propagation Magazine*, vol. 54, no. 5, pp. 243 – 249, 2012.
- [Foi09] A. G. Foina, A. El-Deeb, J. Ramirez-Fernandez, "PeSoV - Pervasive Software-Oriented Vehicles," *IEEE EUROCON*, St.-Petersburg, Russia, pp. 1117 – 1122, May 18-23, 2009.
- [Frä09] K. Främling, I. Oliver, J. Honkola, J. Nyman, "Smart Spaces for Ubiquitously Smart Buildings," *IEEE Third International Conference on Mobile Ubiquitous Computing, Systems, Services and Technologies*, 2009.
- [Fuj10] K. Fujita, H. Sawada, S. Kato, "Intra-Car Communications System using Radio Hose," *Asia-Pacific Microwave Conference Proceedings (APMC)*, Yokohama, Japan,

December 7-10, 2010.

- [Fuq09] Z. Fuqiang, Y. Bo, C. Yitao, "Traffic light control for a single intersection based on wireless sensor network," *In Proceedings of the 9th International Conference on Electronic Measurement & Instruments (ICEMI 2009)*, Beijing, China, 16–19 August 2009.

## G

- [Gao11] C. Gao, X. Hu, B. Wang, L. Guo, W. Wang, "Design of train ride quality testing system based on wireless sensor network", *IEEE International Conference on Electronic and Mechanical Engineering and Information Technology (EMEIT)*, vol. 5, pp. 2636- 2639, 2011.
- [Gil15] G. Gil, M. Goyeneche, L. Azpilicueta, J. J. Astrain, J. Villadangos, F. Falcone, "Analysis of Topo-Morphological Influence of Vineyards in the Design of Wireless Sensor Networks for Smart Viticultural Management", *International Journal of Sensor Networks*, vol. 19, Issue 2, pp. 78 – 90, 2015.
- [Gis] D. Gislason, "ZigBee Wireless Networking," Newnes. [www.newnespress.com](http://www.newnespress.com).
- [Gol92] D. Goldberg, D. Nichols, B. M. Oki, D. Terry, "Using collaborative filtering to weave an information tapestry," *Communications of the ACM*, vol. 35, no. 12, pp. 61–70, 1992.
- [Gon87] Gong Lian, Yao Ruoping, Chen Pizhang, "An Equivalent Magnetization Surface Current Approach of Calculation 3-Dimensional Leakage Fields of a Transformer," *IEEE Trans. Power Delivery*, vol. 2, no. 3, pp. 817 – 822, 1987.
- [Gon12] M. Gong, L. Zhang, Z. Ding, F. Dong, L. Wang, "Research and development of swimming training information system based on zigbee technology," *Proc. of The ICSAI*, 2012.
- [Goo13] B. Goodhart, V. Yerneni, A. Brodsky, V. Rudraraju, N. Egge, "SmartCart: A consolidated shopping cart for pareto-optimal sourcing and fair discount distribution," *IEEE 29th International Conference on Data Engineering Workshops (ICDEW)*, Brisbane, April 2013, pp. 163-172.
- [Gra07] V. Gradinescu, C. Gorgorin, R. Diaconescu, V. Cristea, L. Iftode, "Adaptive traffic lights using car-to-car communication," *In Proceedings of the IEEE 65th Vehicular Technology Conference-VTC2007-Spring*, Dublin, Ireland, 22–25 April 2007.
- [Gru09] M. Grudén, A. Westman, J. Platbardis, P. Hallbjorner, A. Rydberg, "Reliability experiments for Wireless Sensor Networks in train environment," *IEEE European Wireless Technology Conference EuWIT*, pp. 37-40, 2009.
- [Gsc03] E. Gschwendtner, W. Wiesbeck, "Ultra-Broadband Car Antennas for Communications and Navigation Applications," *IEEE Transactions on Antennas and Propagation*, vol. 51, Issue 8, pp. 2020-2027, August 2003.
- [Gua16] Guangjie Han, Zhangbing Zhou, Longjun Dong, J. J. P. C. Rodrigues, K. Namuduri, "Mobility Support for Next-Generation Wireless Sensor

- Networks," *International Journal of Distributed Sensor Networks*, vol. 2016, Article ID 2462754, 2016.
- [Guo10] W. Guo, W. M. Healy, M. Zhou, "An Experimental Study of Interference Impacts on ZigBee-Based Wireless Communication inside Buildings," *In Proceedings of IEEE International Conference on Mechatronics and Automation*, Xi'an, China, pp. 1982–1987, 4–7 August 2010.
- [Guo11] Guo Chen, Huang Xuejun, Hongbo Zhu, "A new IVC based on Ad Hoc and its Design Simulations," *International Conference on Wireless Communications and Signal Processing (WCSP)*, Nanjing, China, pp. 1-4, November 9-11, 2011.
- [Guo12] W. Guo, W. M. Healy, M. Zhou, "Impacts of 2.4-GHz ISM band interference on IEEE 802.15.4 wireless sensor network reliability in buildings," *IEEE Tran. Instrum. Meas.*, vol. 61, pp. 2533–2544, 2012.

## H

- [Hai06] Haibo Xie, Yidong Cui, Huimin Xu, "A New MAC Mechanism for Priority Differentiation in Multi-hop IVC Networks," *6th International Conference on Telecommunications Proceedings*, Chengdu, China, June 2006.
- [Hai11] Haixiao Weng, D. G. Beetner, R. E. DuBroff, "Prediction of Radiated Emissions Using Near-Field Measurements," *IEEE Trans. Electromagnetic Compatibility*, vol. 53, no. 4, pp. 891 - 899, 2011.
- [Hal12] P.S. Hall, Y. Hao, "Antennas and Propagation for Body Centric Wireless Communications," *Artech House*, Norwood Massachusetts, 2012.
- [Han09] J. Han, Z. Qing, "Simulation and experimental method for microwave oven," *Journal of Electronic Science Technology*, vol. 7, 188–191, 2009.
- [Han11] J. Han, C. Choi, I. Lee, "More efficient home energy management system based on ZigBee communication and infrared remote controls," *IEEE Trans. Consum. Electron.* vol. 57, pp. 85–89, 2011.
- [Has08] M. Hassan, S. Gamal, S. Louis, G. F. Zaki, H. H. Amer, "Fault Tolerant Ethernet network model for control and entertainment in railway transportation systems," *Proceeding of the Canadian Conference on Electrical and Computer Engineering CCECE*, Niagara Falls, Canada, May 2008.
- [Has01] F. D. Hastings, J. B. Schneider, S. L. Broschat, E. I. Thorsos, "An FDTD method for analysis of scattering from rough fluid–fluid interfaces," *IEEE JOE*, vol. 26, no. 1, pp. 94-101, Jan. 2001.
- [Hei06] E. A. Heinz, K. S. Kunze, M. Gruber, D. Bannach, P. Lukowicz, "Using Wearable Sensors for Real-Time Recognition Tasks in Games of Martial Arts - An Initial Experiment," *IEEE Symposium on Computational Intelligence and Games*, Reno, NV, USA, 2006.
- [Hri00] H. D. Hristov, "Fresnel Zones in Wireless links, Zone Plate Lenses and Antennas," *Artech House, Inc.* 2000.

- [Hsi07] Hsin-Mu Tsai, C. Saraydar, T. Talty, M. Ames, A. Macdonald, O. K. Tonguz, "ZigBee-based Intra-car Wireless Sensor Network," *IEEE International Conference on Communications*, Glasgow, Scotland, June 24-28, 2007.
- [Hua08] Huaqun Guo, Lek Heng Ngoh, Yongdong Wu, Lian Hwa Liow, Choon Hwee Kwek, Feng Tao, Jun Jie Ang, "Embedded Info-Security Solutions for Vehicular Networks," *Third International Conference on Communications and Networking in China (ChinaCom)*, pp. 29 – 33, August 25-27, 2008.
- [Hua12] Hua Zeng, T. H. Hubing, "The Effect of the Vehicle Body on EM Propagation in Tire Pressure Monitoring Systems," *IEEE Transactions on Antennas and Propagation*, 60, 8, pp. 3941 – 3949, 2012.
- [Hua15] G. Huang, D. Chen, X. Liu, "A node deployment strategy for blindness avoiding in wireless sensor networks," *IEEE Communications Letters*, vol. 19, pp. 1005–1008, 2015.
- [Huo09] H. Huo, Y. Xu, C. C. Bilen, H. Zhang, "Coexistence Issues of 2.4GHz Sensor Networks with other RF Devices at Home," *In Proceedings of Third International Conference on Sensor Technologies and Applications*, Athens/Glyfada, Greece, pp. 200–205, 18–23 June 2009.
- [Hyn12] O. Hyncica, P. Honzik, P. Kucera, K. Pavlata, "Urban Vehicle-to-Infrastructure Wireless Communications Range Evaluation," *15th International IEEE Conference on Intelligent Transportation Systems (ITSC)*, Anchorage, Alaska, USA, pp. 915 – 920, September 16-19, 2012.

## I

- [ICN98] International Commission on Non-Ionizing Radiation (ICNIRP), "Guidelines for limiting exposure to protection time-varying electric, magnetic and electromagnetic fields (up to 300 GHz)," *Health Phys.*, vol. 74, no. 4, pp: 494–522, 1998.
- [Isk02] M. F. Iskander, Z. Yun, "Propagation prediction models for wireless communication systems," *IEEE Transactions on Microwave Theory and Techniques*, vol. 50, no. 3, pp. 662–673, 2002.
- [Iwa96] K. Iwabuchi, T. Kubota, T. Kashiwa, "Analysis of electromagnetic fields in a mass-produced microwave oven using the finite-difference time-domain method," *Journal of Microwave Power and Electromagnetic Energy*, vol. 31, no. 3, pp. 188-196, 1996.

## J

- [Jai15] T. K. Jain, D. S. Saini, S. V. Bhooshan, "Lifetime Optimization of a Multiple Sink Wireless Sensor Network through Energy Balancing," *Journal of Sensors*, vol. 2015, Article ID 921250.
- [Jam10] D. A. James, A. Galehar, D. V. Thiel, "Mobile sensor communications in aquatic

- environments for sporting applications," *Proc. of the 8th Conference of the ISEA*, 2010.
- [Jia09] M. Jiang, Z. Guo, F. Hong, Y. Ma, H. Luo, "OceanSense: A practical wireless sensor network on the surface of the sea," *Proc. of the IEEE PerCom*, Galveston, USA, 2009.
- [Jin08] Jin Shi, Jiangqi He, E. Chan, K. Slattery, J. Zhao, J. Fejfar, F. Zanella, "Equivalent radiation source extraction method for system level EMI and RFI prediction," *IEEE International Symposium on Electromagnetic Compatibility (EMC)*, Detroit, MI, USA, 18-22 Aug. 2008.
- [Jiu11] Jiun-Ren Lin, T. Talty, O. K. Tonguz, "Feasibility of Safety Applications Based on Intra-Car Wireless Sensor Networks: A Case Study," *IEEE Vehicular Technology Conference (VTC Fall)*, San Francisco, CA, USA, September 5-8, 2011.

## K

- [Kin08] K. Kininami, T. Iyama, T. Onishi, S. Uebayashi, "Evaluation of an optical electric field sensor for measurement of specific absorption rate (SAR) during magnetic resonance imaging," *IEEE Transaction on Electromagnetic Compatibility*, vol. 50, no. 4, pp. 828-836. Nov. 2008.
- [Kil11] E. M. Kiley, V. V. Yakovlev, "Modeling of Microwave Ovens with Perforated Metal Walls," *In Proceedings of IEEE MTT-S International Symposium Digest* Baltimore, MD, USA, 5-10 June 2011.
- [Kom12] K. K. Komarov, "Handbook of Dielectric and Thermal Properties of Materials at Microwave Frequencies," Artech House: Boston, MA, USA; London, UK, 2012.
- [Kom14] R. D. Komguem, R. Stanica, M. Tchuente, F. Valois, "WARIM: Wireless sensor networks architecture for a reliable intersection monitoring," *In Proceedings of the IEEE 17th International Conference on Intelligent Transportation Systems (ITSC)*, Qingdao, China, 8-11 October 2014.
- [Kra02] J. D. Kraus, R. J. Marhefka, "Antennas For All Applications," *McGraw-Hill*, 2002.
- [Krz67] H. J. Krzywicli, K. S. K. Chinn, "Human Body Density and Fat of an Adult Male Population as Measured by Water Displacement," *The American Journal of Clinical Nutrition*, vol. 20, no. 4, pp. 305-310. Apr. 1967.
- [Kus02] Y. Kusama, O. Hashimoto, M. Makida, "Analysis of door seal structure of microwave oven with consideration of higher modes by the FDTD method," *Electron. Comm. Jpn.*, doi:10.1002/ecjb.10040, 2002.
- [Kuz12] A. Kuznietsov, D. Neubauer, "A wireless framework for movement activity monitoring of sprinters," *9th International Multi-Conference on Systems, Signals and Devices*, Chemnitz, Germany, 2012.

## L

- [Lam11] K. L. Lam, K. T. Ko, H. Y. Tung, H. C. Tung, K. F. Tsang, L. L. Lai, "ZigBee Electric Vehicle Charging System," *IEEE International Conference on Consumer*

- Electronics (ICCE)*, Las Vegas, Nevada, USA, January 9-12, 2011.
- [Laz16] M. Lazarus, "The troubled past and uncertain future of radio interference," *IEEE Spectrum*, vol. 53, no. 8, 2016.
- [Led13] S. Led, L. Azpilicueta, E. Aguirre, M. Martínez de Espronceda, L. Serrano, F. Falcone, "Analysis and Description of HOLTIN Service Provision for AECG monitoring in Complex Indoor Environments," *Sensors*, vol. 13, Issue 4, pp. 4947-4960, 2013.
- [Lee09] H. Lee, Hsin-Mu Tsai, O. K. Tonguz, "On the Security of Intra-Car Wireless Sensor Networks," *IEEE 70th Vehicular Technology Conference Fall (VTC 2009-Fall)*, Anchorage, Alaska, USA, September 20-23, 2009.
- [Lee11] G. Leen, D. Heffernan, "Vehicles Without Wires," *Computing and Control Engineering Journal*, vol. 12, Issue 5, pp. 205-211, 2011.
- [Lee13] J. B. Lee, R. B. Mellifont, B. J. Burkett, D. A. James, "Detection of Illegal Race Walking: A Tool to Assist Coaching and Judging," *Sensors*, 13, 16065-16074, 2013.
- [Lei10] Leilei Liu, Yuanqing Wang, Nianzu Zhang, Yan Zhang, "UWB Channel Measurement and Modeling for the Intra-Vehicle Environments," *12th IEEE International Conference on Communication Technology*, Nanjing, China, November 11-14, 2010.
- [Leo13] A. Leone, G. Diraco, P. Siciliano, "Context-Aware AAL Services through a 3D Sensor-Based Platform," *Journal of Sensors*, vol. 2013, Article ID 792978.
- [Leu05] D. Leugner, H. -D. Bruns, H. Singer, "Use of Huygens source excitation in a MoM surface-current EFIE formulation," *IEEE International Symposium on Electromagnetic Compatibility (EMC)*, vol. 3, 8-12 Aug. 2005.
- [Li13] P. Li, L. J. Jiang, "Source Reconstruction Method-Based Radiated Emission Characterization for PCBs," *IEEE Trans. Electromagnetic Compatibility*, vol. 55, no. 5, pp. 933 – 940, 2013.
- [Lin15] C.-C. Lin, D. J. Deng, "Optimal two-lane placement for hybrid VANET-sensor networks," *IEEE Transactions on Industrial Electronics*, vol. 62, pp. 7883–7891, 2015.
- [Loa12] B. Loader, A. Gregory, D. Bownds, F. Seifert, "Evaluation of an optical electric field sensor for measurement of specific absorption rate (SAR) during magnetic resonance imaging," *International Symposium on Electromagnetic Compatibility*, pp. 1-4. Sept. 2012.
- [Lop09] P. F. Lopez, A. Ramanujan, Y. V. Gilabert, C. Arcambal, A. Louis, B. Mazari, "A Radiated Emission Model Compatible to a Commercial Electromagnetic Simulation Tool," *20th International Zurich Symposium on Electromagnetic Compatibility*, Zurich, Switzerland, 12-16 Jan. 2009.
- [Lop10] G. Lopez, V. Custodio, J. I. Moreno, "Location-Aware System for Wearable Physiological Monitoring within Hospital Facilities," *IEEE 21st International Symposium on Personal Indoor and Mobile Radio Communications*, Istanbul, Turkey, pp. 2609- 2614, Sept. 2010.



- [Lue88] R. J. Luebbers, "Comparison of Lossy Wedge Diffraction Coefficients with Application to Mixed Path Propagation Loss Prediction," *IEEE Transactions on Antennas and Propagation*, vol. 36, pp. 1031-1034, 1988.
- [Lue89] R. J. Luebbers, "A Heuristic UTD Slope Diffraction Coefficient for Rough Lossy Wedges," *IEEE Transactions on Antennas and Propagation*, vol. 37, pp. 206-211, 1989.
- [Lup13] C. Lupu, M. Cosmin-Constantin, "Actual portable devices as base for telemedicine and e-health: Research and case study application," *E-Health and Bioengineering Conference (EHB)*, Iasi, pp.1-4, Nov. 2013.

## M

- [Mal08] P. Malison, S. Promwong, N. Sukutamantanti, T. Banpotjit, "Indoor Measurement and Modeling of RFID Transmission Loss at 5.8 GHz with Human Body," *Proceedings of the 5<sup>th</sup> international conference on electrical engineering/electronics, computer, telecommunications and information technology*, Krabi, Thailand, pp. 421-424, May 2008.
- [Mar09] M. Martínez-Espronedada, I. Martínez, S. Led, J. D. Trigo, I. Oses, J. Escayola, L. Serrano, J. García, A. Garcia, "INTENSA: Heart Failure Patient's Follow-up System Using the ISO/IEEE 11073 Standard," *9th Int. Conf. Inf. Tech. App. Biomed.*, Larnaca, pp. 1-4, Nov. 2009.
- [Mar16] A. Marinčić, A. Kerner, D. Šimunić "Interoperability of IoT wireless technologies in ambient assisted living environments," *Wireless Telecommunications Symposium (WTS)*, pp. 1-6, 2016.
- [Mat03] K. Matsumoto, O. Hashimoto, K. Wada, "An Efficient Analysis on Door Structure of a Microwave Oven Using Combined Waves of Higher Order Modes," *In Proceedings of 33rd European Microwave Conference*, Munich, Germany, vol. 3, pp. 1171–1174, 7–9 October 2003.
- [Mat03b] Y. Matsumoto, M. Takeuchi, K. Fujii, A. Sugiura, Y. Yamanaka, "A time-domain microwave oven noise model for the 2.4 GHz band," *IEEE Transactions on Electromagnetic Compatibility*, vol. 45, no. 3, pp. 561-565, 2003.
- [Mat05] Y. Matsumoto, M. Takeuchi, K. Fujii, A. Sugiura, Y. Yamanaka, "Performance analysis of interference problems involving DS-SS WLAN systems and microwave ovens," *IEEE Trans. Electromagn. Compat.*, vol. 47, pp. 45–53, 2005.
- [Mat08] D. W. Matolak, A. Chandrasekaran, "Aircraft intra-vehicular channel characterization in the 5 GHz band," *Integrated Communications, Navigation and Surveillance Conference*, Bethesda, USA, 5-7 May, 2008.
- [Maz12] O. Mazumder, A. S. Kundu, S. Bhaumik, "Development of wireless insole foot pressure data acquisition device," *International Conference on Communications, Devices and Intelligent Systems*, Kolkata, India, 2012.
- [McG99] T. McGuffog, "E-commerce and the value chain," *Manufacturing Engineer*, pp.

- 157-160, Aug. 1999.
- [Mel11] M. Melo Tavares, N.J. Ramos Belino, M.A. Vaz Patto, M.J.O. Gerales, "Development of an electroactive textil system for the objective assessment of sleep movements and neurodegenerative diseases," *1st Portuguese Meeting in Bioengineering (ENBENG)*, Lisbon, Portugal, pp. 1-4, March 2011.
- [Mie11] F. Mieveville, Wan Du, I. Daikh, D. Navarro, "Wireless Sensor Networks for Active Control Noise Reduction in Automotive Domain," *14th International Symposium on Wireless Personal Multimedia Communications (WPMC)*, Brest, France, October 3-7, 2011.
- [Mik12] S. M. Mikki, Y. M. M. Antar, "Near-Field Analysis of Electromagnetic Interactions in Antenna Arrays Through Equivalent Dipole Models," *IEEE Transactions on Antennas and Propagation*, vol. 60, no. 3, march 2012.
- [Min02] N. Mingxin, L. Ling, "Simulation of Microwave Oven Interference on Digital Radio Communication Systems," *In Proceedings of 3rd International Symposium Electromagnetic Compatibility*, Beijing, China, pp. 513–516, 21–24 May 2002.
- [Min10] Mingke Fang, Lei Li, Wei Huang, "Research of Hybrid Positioning Based Vehicle Interactive Navigation System," *International Conference on Multimedia Information Networking and Security (MINES)*, Nanjing, Jiangsu, China, pp. 974 – 978, November 4-6, 2010.
- [Min10b] Ming Yang, A. K. Brown, "A Hybrid Model for Radio Wave Propagation Through Frequency Selective Structures (FSS)," *IEEE Trans. Antennas and Prop.*, vol. 58, no. 9, pp. 2961-2968, 2010.
- [Min12] Mingxin Gong, Lei Zhang, Zicheng Ding, Fei Dong, Lejun Wang, "Research and development of swimming training information system based on ZigBee technology," *International Conference on Systems and Informatics*, Yantai, China, 2012.
- [Mir06] S. A. Mirtaheri, S. Salimpoor, "HEV (Hybrid Electric Vehicles) and the Wiring Reduction Methods," *IEEE Vehicle Power and Propulsion Conference*, Windsor, pp. 1-5, September 6-8, 2006.
- [Miy13] M. Miyu, H. Shinsuke, "A Cooperative Relaying Scheme for Real-Time Vital Data Gathering in a Wearable Wireless Body Area Network," *7th International Symposium on Medical Information and Communication Technology*, Tokyo, Japan, 2013.
- [Mog09] A. R. Moghimi, Hsin-Mu Tsai, C. U. Saraydar, O. K. Tonguz, "Characterizing Intra-Car Wireless Channels," *IEEE Transactions on Vehicular Technology*, 58, 9, pp. 5299 - 5305, November, 2009.
- [Moh13] M. A. Moharram, A. A. Kishk, "Electromagnetic scattering from 2D dielectric objects using randomly distributed sources," *7th European Conference on Antennas and Propagation (EuCAP)*, Gothenburg, Sweden, 8-12 April 2013.
- [Mon11] J. Monteiro, L. C. Costa, M. A. Valente, T. Santos, J. Sousa, "Simulating the electromagnetic field in microwave ovens," *IEEE MTT-S International Microwave*

*& Optoelectronics Conference*, Natal, Brazil, Oct. 2011.

- [Mor08] N. Moraitis, P. Constantinou, "Radio Channel Measurements and Characterization inside Aircrafts for In-Cabin Wireless Networks," *IEEE 68th Vehicular Technology Conf.*, Calgary, Canada, 21-24 Sept. 2008.
- [Mor12] A. Moreno, I. Angulo, A. Perallos, H. Landaluce, I. J. G. Zuazola, L. Azpilicueta, J. J. Astráin, F. Falcone, J. Villadangos," IVAN: Intelligent Van for the Distribution of Pharmaceutical Drugs," *Sensors*, vol. 12, pp. 6587-6609, 2012.
- [Moy00] M. Moya, V. Almenar, S. J. Flores, J. L. Corral, "Analysis and Simulation of Smart Antennas for GSM and DECT in Indoor Environments based on Ray Launching Modeling Techniques," *Proceedings of the 2000 IEEE Sensor Array and Multichannel Signal Processing Workshop (SAM 2000)*, pp. 403-407, 2000.

## N

- [Nec10] Y. I. Nechayev, P.S. Hall, Z.H. Hu, "Characterization of Narrowband Communication Channels on the Human Body at 2.45GHz," *IET Microwaves Antennas and Propagation*, vol. 4, no.6, pp. 722-732, 2010.
- [Nic70] A. M. Nicolson, G. Ross, "Measurement of the intrinsic properties of materials by time domain techniques," *IEEE Trans. Instrumentation and Measurement*, IM-19, pp. 377-382, 1970.
- [Nis01] S. Nishizawa, W. Spreitzer, H. -O. Ruo, F. M. Landstorfer, O. Hashimoto, "Equivalent Source Model for Electrical Appliances emitting low Frequency Magnetic Fields," *31st European Microwave Conference*, London, UK, 24-26 Sept. 2001.
- [Nou08] F. Nouvel, P. Maziero, "X-by-Wire and Intra-Car Communications: Power Line and/or Wireless Solutions," *8th International Conference on ITS Telecommunications*, Phuket, Thailand, October 24, 2008.
- [Nou09] F. Nouvel, P. Tanguy, "What is about future High Speed Power Line Communication Systems for In-Vehicles Networks?," *7th International Conference on Information, Communications and Signal Processing*, Macau, December 8-10, 2009.

## O

- [Ost07] F. Osterlind, E. Pramsten, D. Roberthson, J. Eriksson, N. Finne, T. Voigt, "Integrating Building Automation Systems and Wireless Sensor Networks," *IEEE Conference on Emerging Technologies and Factory Automation*, 2007.

## P

- [Pal13] F. Palumbo, P. Barsocchi, F. Furfari, E. Ferro, "AAL Middleware Infrastructure for Green Bed Activity Monitoring," *Journal of Sensors*, vol. 2013, Article ID 510126.

- [Pat14] M. Pätzold, A. Borhani, "A non-stationary multipath fading channel model incorporating the effect of velocity variations of the mobile station," *In Proceedings of the Wireless Communication and Network Conference, WCNC 2014*, Istanbul, Turkey, pp. 194–199, 2014.
- [Pau09] I. Pau, F. Seoane, K. Lindecrantz, M. A. Valero, J. Carracedo, "Home e-health system integration in the Smart Home through a common media server," *Ann. Int. Conf. Eng. Med. Bio. Soc.*, Minneapolis, USA, pp. 6171–6174, Sept. 2009.
- [Pay12] N. Payet, M. Darces, J. –L. Montmagnon, M. Hélier, F. Jangal, "Near field to far field transformation by using equivalent sources in HF band," *15th International Symposium on Antenna Technology and Applied Electromagnetics (ANTEM)*, Toulouse, France, 25–28 June 2012.
- [Pen04] J. B. Pendry, L. Martín-Moreno, F. J. Garcia-Vidal, "Mimicking Surface Plasmons with Structured Surfaces," *Science*, vol. 305, no. 5685, pp. 847–848, 2004.
- [Pet92] P. Petre, T. K. Sarkar, "A planar near-field to far-field transformation using an equivalent magnetic current approach," *IEEE Antennas and Propagation Society International Symposium (AP-S/URSI)*, Chicago, IL, USA, 18–25 June 1992.
- [Pet02] P. Petre, T. K. Sarkar, "Planar near-field to far-field transformation using an array of dipole probes," *IEEE Trans. Antennas and Prop.*, vol. 42, no. 4, pp. 534 – 537, 2002.
- [Pin11] Ping Li, Lijun Jiang, "A novel characterization method of the radiation emission for electromagnetic compatibility," *IEEE International Symposium on Electromagnetic Compatibility (EMC)*, Rome, Italy, 14–19 Aug. 2011.
- [Pin13] Pinghung Wei, B. Morey, T. Dyson, N. McMahon, Yung-Yu Hsu, S. Gazman, L. Klinker, B. Ives, K. Dowling, C. Rafferty, "A conformal sensor for wireless sweat level monitoring," *IEEE Sensors*, Baltimore, MD, USA, 2013.
- [Pin13b] Ping Li, Li Jun Jiang, Jun Hu, Sheng Sun, "A novel broadband equivalent source reconstruction method for broadband radiators," *International Conference on Electromagnetics in Advanced Applications (ICEAA)*, Turin, Italy, 9–13 Sept. 2013.
- [Pin13c] Ping Li, Li Jun Jiang, "Modeling Radiated Emissions Through Shielding Boxes Based on the Tangential Electrical Field Samplings Over Openings," *IEEE Trans. Electromagnetic Compatibility*, vol. 55, no. 6, pp. 1140 - 1146, 2013.
- [Pop09] D. C. Popescu, D. Treeumnuk, S. Olariu, "Requirements for the Physical Layer of the NOTICE System for Vehicular Communications," *IEEE GLOBECOM Workshops*, Honolulu, HI, USA, pp. 1–5, November 30–December 4, 2009.
- [Pot01] M. E. Potter, M. A. Stuchly, M. Okoniewski, "Modeling of near-field sources in the finite-difference time-domain (FDTD)," *IEEE International Symposium Antennas and Propagation Society*, vol. 1, Boston, MA, USA, 8–13 July 2001.

## Q

- [Qur13] M. A. Qureshi, C. H. Schmidt, T. F. Eibert, "Efficient Near-Field Far-Field Transformation for Nonredundant Sampling Representation on Arbitrary Surfaces in Near-Field Antenna Measurements," *IEEE Trans. Antennas and*

*Prop.*, vol. 61, no. 4, pp. 2025 – 2033, 2013.

## R

- [Rab95] J. M. Hernando Rábanos, "Transmisión por radio," Editorial Centro de Estudios Ramón Areces, S.A. (1995). ISBN: 84-8004-146-3.
- [Rah09] M. A. Rahman, M. F. Alhamid, A. El Saddik, W. Gueaieb, "A Framework to Bridge Social Network and Body Sensor Network: an E-Health Perspective," *IEEE Int. Conf. Mult. Expo.*, New York, pp. 1724-1727, Jul. 2009.
- [Rao12] T. R. Rao, D. Balachander, P. Sathish, N. Tiwari, "Intra-Vehicular RF Propagation Measurements at UHF for Wireless Sensor Networks," *International Conference on Recent Advances in Computing and Software Systems (RACSS)*, Chennai, India, April 25-27, 2012.
- [Rec09] Recomendation UIT-R P. 526-11, s.l.: "Propagación por difracción. Serie P. Propagación de las ondas radioeléctricas, 10/2009".
- [Reg01] J. –R. Regue, M. Ribo, J. –M. Garrell, A. Martin, "A genetic algorithm based method for source identification and far-field radiated emissions prediction from near-field measurements for PCB characterization," *IEEE Trans. Electromagnetic Compatibility*, vol. 43, no. 4, pp. 520 - 530, 2001.
- [Res97] P. Resnick, H. Varian, "Recommender systems," *Communications of the ACM*, vol. 40, no. 3, pp. 56–58, 1997.
- [Rez10] A.W. Reza, M. S. Sarker, K. Dimyati, "A novel integrated mathematical approach of ray-tracing and genetic algorithm for optimizing indoor wireless coverage," *Progress in Electromagnetics Research*, vol. 110, pp. 147–162, 2010.
- [Rob11] C. Roblin, "Analysis of the Channel Power Delay Profile of WBAN Scenarios in Various Indoor Environments," *IEEE International Conference on Ultra-Wideband*, Bologna, Italy, pp. 545-549, Sept. 2011.
- [Rob15] C. Roblin, Y. Wei, "Scenario-based WBAN channel characterization in various indoor premises," *9<sup>th</sup> European Conference on Antennas and Propagation*, Lisbon, Portugal, pp. 1-3, May 2015.
- [Roc10] G. de la Roche, P. Flipo, Z. Lai, G. Villemaud, Jie Zhang, J. –M. Gorce, "Implementation and Validation of a New Combined Model for Outdoor to Indoor Radio Coverage Predictions," *EURASIP Journal on Wireless Communications and Networking*, vol. 2010, Article ID 215352, 2010.
- [Roc14] M. P. Rocu, "Implementation for a WBAN-ECG Monitoring System (Preliminary results)," *Int. Conf. Opt. Electr. Equip.*, Bran, pp. 823-826, May 2014.
- [Rod13] J. Rodríguez-Molina, J.-F. Martínez, P. Castillejo, L. López, "Combining Wireless Sensor Networks and Semantic Middleware for an Internet of Things-Based Sportsman/Woman Monitoring Application," *Sensors*, 13, pp. 1787-1835, 2013.
- [Ron04] T. W. Rondeau, M. F. D'Souza, D. G. Sweeney, "Residential microwave oven interference on Bluetooth data performance," *IEEE Trans. Consum. Electron.*, vol. 50, pp. 856–863, 2004.

- [Ros02] J.-P. Rossi, Y. Gabillet, "A Mixed Ray Launching/Tracing Method for Full 3-D UHF Propagation Modeling and Comparison With Wide-Band Measurements," *IEEE Transactions on Antennas and Propagation*, vol. 50, no. 4, 2002.
- [Rou06] G. Roussos, "Enabling RFID in Retail," *Computer*, vol. 39, no. 3, pp. 25-30, Mar. 2006.
- [Row12] D. D. Rowlands, T. McNab, L. Laakso, D. A. James, "Cloud based activity monitoring system for health and sport," *International Joint Conference on Neural Networks*, Brisbane, Australia, 2012.
- [Rui12] Rui Yang, Lingfeng Wang, "Multi-objective optimization for decision-making of energy and comfort management in building automation and control," *Sustainable Cities and Society*, vol. 2, pp. 1-7, 2012.
- [Rup15] S.R Rupanagudi, F. Jabeen, K R Savarni, S. Adinarayana, V.K. Bharadwaj, R. Karishma, V.G. Bhat, "A Novel Video Processing based Cost Effective Smart Trolley System for Supermarkets using FPGA," *2015 International Conference on Communication, Information & Computing Technology (ICCICT)*, Mumbai, India, Jan. 2015, pp. 1-6.

## S

- [Sal14] I. Salaberria, A. Perallos, L. Azpilicueta, F. Falcone, R. Carballedo, I. Angulo, P. Elejoste, A. Bahillo, J. J. Astrain, J. Villadangos, "Ubiquitous Connected Train Based on Train-To-Ground and Intra-Wagon Communications Capable of Providing on Trip Customized Digital Services for Passengers," *Sensors*, pp. 8003-8025, 2014.
- [Sam97] V. Sampath, C. Despins, B. Sultana, W. Lippler, G. Y. Delisle, "Comparison of statistical and deterministic indoor propagation prediction techniques with field measurements," in *IEEE VTC*, Phoenix, USA, 1997, 1138 – 1142.
- [San09] D. A. Sánchez-Hernández, High Frequency Electromagnetic Dosimetry, Artech House, Inc., 2009.
- [Sar99] T. K. Sarkar, A. Taaghoul, "Near-field to near/far-field transformation for arbitrary near-field geometry utilizing an equivalent electric current and MoM," *IEEE Trans. Antennas and Prop.*, vol. 47, no. 3, pp. 566 – 573, 1999.
- [Sar10] T. K. Sarkar, "A super-resolution source reconstruction method using free space Green's function," *IEEE International Conference on Wireless Information Technology and Systems (ICWITS)*, Honolulu, HI, USA, August 2010.
- [Sar12] A. Sarikhani, M. Barzegaran, O. A. Mohammed, "Optimum Equivalent Models of Multi-Source Systems for the Study of Electromagnetic Signatures and Radiated Emissions From Electric Drives," *IEEE Trans. Magnetics*, vol. 48, no. 2, pp. 1011 – 1014, 2012.

- [Saw09] H. Sawada, T. Tomatsu, G. Ozaki, H. Nakase, S. Kato, K. Sato, H. Harada, "A Sixty GHz Intra-Car Multi-Media Communications System," *IEEE 69th Vehicular Technology Conference*, Barcelona, Spain, April 26-29, 2009.
- [Sch36] S. A. Schelkunoff, "Some equivalence theorems of electromagnetics and their application to radiation problems," *Bell System Technical Journal*, vol. 15, pp. 92-112, 1936.
- [Sch86] M. Schulkin, "Sea surface loss in surface ducts and shallow water: A historical perspective," in *Proc. of the IEEE Oceans Conference*, Washington DC, USA, 1986.
- [Sch04] I. Scherbatko, R. Diaz, "A new hybrid FDTD field-teleportation approach for modeling radiating/scattering structures," *10th International Conference on Mathematical Methods in Electromagnetic Theory*, Dnepropetrovsk, Ukraine, 14-17 Sept. 2004.
- [Sch14] S. Schmitt, S. Adler, M. Kyas, "The effects of human body shadowing in RF-based indoor localization," in *Proc. of 2014 International Conference on Indoor Positioning and Indoor Navigation (IPIN)*, Busan, Korea, 2014.
- [Sen11] S. Sendra, J. V. Lamparero, J. Lloret, M. Ardid, "Underwater communications in wireless sensor networks using WLAN at 2.4 GHz," *Proc. of the 8th IEEE MASS*, 2011.
- [Sen12] S. Sendra, J. Lloret, J. J. P. C. Rodrigues, J. M. Aguiar, "Underwater wireless communications in freshwater at 2.4 GHz," *IEEE Communications Letters*, vol. 17, no. 9, pp. 1794- 1797, Sep. 2013.
- [Seu13] Seulki Lee, Hoi-Jun Yoo, "Low Power and Self-Reconfigurable WBAN Controller for Continuous Bio-Signal Monitoring System," *IEEE Trans. Biomedical Circuits and Systems*, vol. 7(2), pp. 178-185, April 2013.
- [Sha07] G. M. Shafiullah, A. Gyasi-Agyei, P. Wolfs, "Survey of wireless communications applications in the railway industry," *The 2nd International Conference on Wireless Broadband and Ultra Wideband Communications*, pp. 65-65, 2007.
- [She14] Shengnan Gai Eui-Jung Jung, Byung-Ju Yi, "Localization Algorithm Based on Zigbee Wireless Sensor Network with Application to an Active Shopping Cart," *2014 IEEE/RSJ International Conference on Intelligent Robots and Systems (IROS 2014)*, Chicago, IL, USA, Sep. 2014, pp. 4571-4576.
- [Shi04] J. Shi, M. A. Cracraft, J. Zhang, R. E. DuBroff, K. Slattery, "Using near-field scanning to predict radiated fields," *International Symposium on Electromagnetic Compatibility (EMC)*, vol. 1, 9-13 Aug. 2004.
- [Shi10] Shichao Cai, M. Becherif, M. Wack, "Context System using Pervasive Controller Area Network Bus System to improve Driving Safety," *IEEE/ASME International Conference on Mechatronics and Embedded Systems and Applications (MESA)*, Qingdao, ShanDong, China, July 15-17, 2010.
- [Shi15] J. Shi, C. Peng, Q. Zhu, P. Duan, Y. Bao, M. Xie, "There is a will, there is a way: A new mechanism for traffic control based on VTL and VANET," *In Proceedings of*

- the IEEE 16th International Symposium on High Assurance Systems Engineering (HASE)*, Daytona Beach Shores, FL, USA, 8–10 January 2015.
- [Shi15a] D. Shi, J. Bi, Z. L. Tan, Y. G. Gao, "Site-specific wave propagation prediction with improved shooting and bouncing ray tracing method," *URSI AT-RASC 2015 Conference*, ISBN: 9789090086286, 2015.
- [Shu09] Shu-Chiung Hu, You-Chiun Wang, Chiuan-Yu Huang, Yu-Chee Tseng, "A Vehicular Wireless Sensor Network for CO<sub>2</sub> Monitoring," *IEEE Sensors*, Christchurch, New Zealand, pp. 1498 – 1501, October 25–28, 2009.
- [Sim11] M. Simek, M. Fuchs, L. Mraz, P. Moravek, M. Botta, "Measurement of lowPAN Network Coexistence with Home Microwave Appliances in Laboratory and Home Environments," *In Proceedings of International Conference on Broadband and Wireless Computing, Communication and Applications*, Barcelona, Spain, pp. 292–299, 26–28 October 2011.
- [Sin13] S. Singh, S. Chand, R. Kumar, B. Kumar, "Optimal sensor deployment for WSNs in grid environment," *Electron. Letters*, vol. 49, pp. 1040–1041, 2013.
- [Skr11] A. Skrebtsov, A. Burnic, Dong Xu, A. Waadt, P. Jung, "UWB applications in public transport," *International Conference on Communications, Computing and Control Applications (CCCA)*, Hammamet, Tunisia, 3–5 March, 2011.
- [Sol11] M. Soltysiak, M. Celuch, U. Erle, "Measured and Simulated Frequency Spectra of the Household Microwave Oven," *In Proceedings of IEEE MTT-S International Microwave Symposium Digest*, Baltimore, MD, USA, pp. 1–4, 5–10 June 2011.
- [Sol14] A. Solanas, C. Patsakis, M. Conti, I. S. Vlachos, V. Ramos, F. Falcone, O. Postolache, P. A. Perez-Martinez, R. Di Pietro, D. N. Perrea, A. Martinez-Balleste, "Smart Health: A Context-Aware Health Paradigm within Smart Cities," *IEEE Communication Magazine*, vol. 52, Issue 8, pp. 74–81, 2014.
- [Son06] H. J. Song, J. S. Colburn, H. P. Hsu, R. W. Wiese, "Development of Reduced Order Model for Modeling Performance of Tire Pressure Monitoring System," *IEEE 64th Vehicular Technology Conference*, Montreal, Canada, September 25–28, 2006.
- [Soo14] Sooyoung Hur, Yeon-Jea Cho, JungAun Lee, Noh-Gyoung Kang, Jeong Ho Park, H. Benn, "Synchronous channel sounder using horn antenna and indoor measurements on 28 GHz," *in Proc. IEEE IBSCCN (BlackSeaCom)*, Odessa, 2014, pp. 83 – 87.
- [Sta12] A. Stamm, D. A. James, R. M. Hagem, D. V. Thiel, "Investigating arm symmetry in swimming using inertial sensors," *IEEE Sensors*, Taipei, China, 2012.
- [Su09] X. Su, T. M. Khoshgoftaar, "A Survey of Collaborative Filtering Techniques," *Advances in Artificial Intelligence*, vol. 2009, Section 3, pp. 1–19, 2009.
- [Sun01] Sung Yi, Lie Liu, Chian Kerm Sin, Fei Su, Shan Gao, "A study of microwave curing process for underfill used in flip chip packaging. Part 2: 3D FEM simulation of microwave power distribution inside variable frequency microwave oven," *Advances in Electronic Materials and Packaging*, EMAP, Jeju



Island, South Korea, Nov. 2001.

- [Sun11] Sun Yan, Zhao Guotao, Luo Hong, "Smart Building Control Based on Wireless Sensor-Actuator Networks," *Chinese Journal of Electronics*, vol. 20, no.3, 2011.
- [Sun14] R. Sundar, S. Hebbbar, V. Golla, "Implementing Intelligent Traffic Control System for Congestion Control, Ambulance Clearance, and Stolen Vehicle Detection," *IEEE Sensors Journal*, vol. 15, pp. 1109–1113, 2014.

## T

- [Taa96] A. Taaghoul, T. K. Sarkar, "Near-field to near/far-field transformation for arbitrary near-field geometry, utilizing an equivalent magnetic current," *IEEE Trans. Electromagnetic Compatibility*, vol. 38, no. 3, pp. 536 – 542, 1996.
- [Tae07] Tae Jin Park, You Jin Chon, Dong Kyu Park, Seung Ho Hong, "BACnet over ZigBee, A new approach to wireless datalink channel for BACnet," *5th IEEE International Conference on Industrial Informatics*, 2007.
- [Tah12] T. M. Taher, M. J. Misurac, J. L. LoCicero, D. R. Ucci, "Microwave Oven Signal Interference and Mitigation for Wi-Fi Communication Systems," *In Proceedings of 5th IEEE Consumer Communications and Networking Conference*, Las Vegas, NV, USA, pp. 67–68, 10–12 January 2012.
- [Tan15] S. Tanwar, N. Kumar, J. J. P. C. Rodrigues, "A Systematic review on Heterogeneous Routing Protocols for Wireless Sensor Networks," *Journal of Network and Computer Applications*, vol. 53, pp. 39-56, 2015.
- [Tay11] J. E. Taylor, "Wireless telegraphy in relation to interferences and perturbations," *Journal of the Institution of Electrical Engineers*, vol. 47, pp. 119-140, 1911.
- [Ton07] O. K. Tonguz, Hsin-Mu Tsai, C. Saraydar, T. Talty, A. Macdonald, "Intra-Car Wireless Sensor Networks Using RFID: Opportunities and Challenges," *Mobile Networking for Vehicular Environments*, Anchorage, AK, USA, May 11, 2007.
- [Top07] T. Topa, A. Karwowski, "Efficient 2D Interpolation Technique for Evaluation of Equivalence-Principle Sources in MoM-FDTD Method," *Second European Conference on Antennas and Propagation (EuCAP)*, Edinburgh, UK, Nov. 2007.
- [Tsu09] T. Tsuboi, J. Yamada, N. Yamauchi, M. Nakagawa, T. Maruyama, "UWB Radio Propagation for Intra Vehicle Communications," *International Conference on Ultra Modern Telecommunications & Workshops*, St. Petersburg, Russia, October 12-14, 2009.
- [Tub07] M. Tubaishat, S. Yi, S. Hongchi, "Adaptive traffic light control with wireless sensor networks," *In Proceedings of the 4th IEEE Consumer Communications and Networking Conference (CCNC)*, Las Vegas, NV, USA, 11–13 January 2007.
- [Tub08] M. Tubaishat, Q. Qi, Y. Shang, H. Shi, "Wireless sensor-based traffic light control," *In Proceedings of the 5th IEEE Consumer Communications and Networking Conference (CCNC 2008)*, Las Vegas, NV, USA, 10–12 January 2008.
- [Tya15] S. Tyagi, S. Tanwar, S. K. Gupta, N. Kumar, J. J. P. C. Rodrigues, "A Lifetime Extended Multi-levels Heterogeneous Routing Protocol for Wireless Sensor

Networks," *Telecommunication Systems*, vol. 59, no. 1, pp. 43-62, 2015.

## U

- [Unb01] M. Unbehaun, "Scalability of wireless LAN systems in the unlicensed 17 GHz frequency band," in *Proc. IEEE GLOBECOM*, San Antonio, USA, 2001, pp. 3599 – 3603.

## V

- [Val10] J. Vales-Alonso, P. Pablo Lopez-Matencio, F. J. Gonzalez-Castaño, H. Navarro-Hellin, P. J. Baños-Guirao, F. J. Perez- Martinez, R. P. Martinez-Alvarez, D. Gonzalez-Jimenez, F. Gil-Castiñeira; R. Duro-Fernandez, "Ambient Intelligence Systems for Personalized Sport Training," *Sensors*, 10, pp. 2359-2385, 2010.
- [Val13] J. Vales-Alonso, P. Lopez-Matencio, J. Veiga-Gontan, P. Banos Guirao, J. J. Alcaraz, "An effort control system for training elite team-sport athletes," *The 6th International Conference on Human System Interaction*, Sopot, Poland, 2013.

## W

- [Wad13] S. Wada, M. Fukase, Y. Nakanishi, L. Tatsuta, "In search of a usability of Kinect in the training of traditional Japanese "KATA" — Stylized gestures and movements," *Second International Conference on e-Learning and e-Technologies in Education*, Lodz, Poland, 2013.
- [Wal14] M. Walter, D. Shutin, U. C. Fiebig, "Delay-dependent Doppler probability density functions for vehicle-to-vehicle scatter channels," *IEEE Transactions on Antennas and Propagation*, vol. 62, pp. 2238–2249, 2014.
- [Wan10] Wang Hailun, Jiang Chundi, Yu Shiming, "Tire Safety Detecting System Based on ZigBee," *2nd International Workshop on Intelligent Systems and Applications (ISA)*, Wuhan, China, May 22-23, 2010.
- [Wan12] Y. Wang, W.-J. Lu, H.-B. Zhu, "An empirical path-loss model for wireless channels in indoor short-range office environment," *International Journal of Antennas and Propagation*, vol. 2012, Article ID 636349, 7 pages, 2012.
- [Wan16] X. Wang, H. Cheng, Y. Yao, "Addressing-based routing optimization for 6LoWPAN WSN in vehicular scenario," *IEEE Sensors Journal*, vol. 16, pp. 3939–3947, 2016.
- [Wat10] T. Watanabe, N. Michishita, Y. Yamada, "Surface electric field distributions of lightweight phantom composed of wave absorber for simplified SAR measurement," *Asia-Pacific Microwave Conference Proceedings*, pp. 1352-1355, Dec. 2010.
- [Web94] W. T. Webb, R. D. Shenton, "Pan-European Railway Communications: Where PMR and Cellular Meet," *Electronics and Communications Engineering Journal*, pp. 195-202, 1994.

- [Wei08] Weiyun Jiao, Xiaojing Wang, Li Zhao, "Monitoring System of Car-Guardrail Accident based on Wireless Sensor Networks," *8th International Conference on ITS Telecommunications*, Phuket, Thailand, pp. 146 – 149, October 24, 2008.
- [Wei12] Wei-Jiang Zhao, Bin-Fang Wang, En-Xiao Liu, Hark Byeong Park, Hyun Ho Park, Eakhwan Song, Er-Ping Li, "An Effective and Efficient Approach for Radiated Emission Prediction Based on Amplitude-Only Near-Field Measurements," *IEEE Transactions on Electromagnetic Compatibility*, vol. 54, no. 5, pp. 1186-1189, 2012.
- [Wei12b] Wei-Jiang Zhao, Hark Byeong Park, M. Tan, Hyun Ho Park, En-Xiao Liu, Eakhwan Song, Er-Ping Li, "Far-field prediction from amplitude-only near-field measurements using equivalent electric currents," *IEEE International Symposium on Electromagnetic Compatibility (EMC)*, Pittsburgh, PA, USA, 6-10 Aug. 2012.
- [Wen02] Y. Wen, X. Zhang, "Radiation Characteristics of Microwave Ovens," *In Proceedings of 3rd International Symposium on Electromagnetic Compatibility*, Beijing, China, pp. 214–217, 21–24 May 2002.
- [Wen03] Y. Wen, L. Zhang, C. Liu, X. Zhang, "Measurement and Calculation of the Radiation Characteristics of Microwave Ovens," *In Proceedings of IEEE International Symposium on Electromagnetic Compatibility*, Istanbul, Turkey, vol. 1, p. 92, 11-16 May 2003.
- [Wen10] Wenqi Guo, W. M. Healy, Mengchu Zhou, "ZigBee-Wireless Mesh Networks for Building Automation and Control," *International Conference on Networking, Sensing and Control*, 2010.
- [Wes02] J. C. West, Z. Zhao, "Electromagnetic modeling of multipath scattering from breaking water waves with rough faces," *IEEE TGRS*, vol. 40, no. 3, pp. 583-592, Mar. 2002.
- [Wic09] K. Wickramaratna, M. Kubat, K. Premaratne, "Predicting Missing Items in Shopping Carts," *IEEE Transactions On Knowledge And Data Engineering*, vol. 21, no. 7, pp. 985-998, 2009.
- [Won13] A. C. W. Wong, M. Dawkins, G. Devita, N. Kasparidis, A. Katsiamis, O. King, F. Lauria, J. Schiff, A. J. Burdett, "A 1 V 5 mA Multimode IEEE 802.15.6/Bluetooth Low-Energy WBAN Transceiver for Biotelemetry Applications," *IEEE Journ. Solis-State Circ.*, vol. 48(1), pp. 186-198, 2013.
- [WuN12] Wu Ningyuan, Zheng Zengwei, Cai Jianping, Chen Yuanyi, Lv Jin, "Advertisement and shopping guide system for large supermarkets based on wireless sensor network," *in Proc. IEEE CSEA*, Zhangjiajie, China, 2012, pp. 518 – 522.

## X

- [Xia13] Xiao Hong Mao, Yee Hui Lee, See Ho Ting, "Wideband channel modeling within

- a shopping mall in UHF band," in *Proc. ICICS, Tainan*, 2013, pp. 1-3.
- [Xio15] W. Xiong, X. Hu, T. Jiang, "Measurement and characterization of link quality for IEEE 802.15.4-compliant wireless sensor networks in vehicular communications," *IEEE Transactions on Industrial Informatics*, 2015.
- [Xua06] Xuan Zhong, Hoi-Ho Chan, T. J. Rogers, C. P. Rosenberg, El J. Coyle, "The development and eStadium testbeds for research and development of wireless services for large-scale sports venues," *IEEE 2nd International Conference on Testbeds and Research Infrastructures for the Development of Networks and Communities*, Barcelona, Spain, 2006.
- ## Y
- [Yam04] K. Yamazaki, T. Kawamoto, H. Fujinami, T. Shigemitsu, "Equivalent dipole moment method to characterize magnetic fields generated by electric appliances: extension to intermediate frequencies of up to 100 kHz," *IEEE Trans. Electromagnetic Compatibility*, vol. 46, no. 1, pp. 115 - 120, 2004.
- [Yan09] Yan Wei, Xu Jiadong, Li Ping, "Predicting far-field RCS from near-field data based on MOM," *International Conference on Microwave Technology and Computational Electromagnetics (ICMTCE)*, Beijing, China, 3-6 Nov. 2009.
- [Yan10] H. Yan, H. Huo, Y. Xu, M. Gidlund, "Wireless Sensor Network Based E-Health System—Implementation and Experimental Results," *IEEE Trans. Consum. Electron.*, 2010, vo. 56, pp. 2288–2295, 2010.
- [Yan13] K. Yang, A. F. Molisch, T. Ekman, T. Røste, "A deterministic round earth loss model for open-sea radio propagation," in *Proc. of the 77th IEEE VTC Spring*, Dresden, Germany, 2013.
- [Ye15] M. Ye, Y. Wang, C. Dai, X. Wang, "A hybrid genetic algorithm for the minimum exposure path problem of wireless sensor networks based on a numerical functional extreme model," *IEEE Transactions on Vehicular Technology*, 2015.
- [Yic08] J. Yick, B. Mukherjee and D. Ghosal, "Wireless sensor network survey," *Comput. Netw.*, vol. 52, no. 12, pp. 2292–2330, Aug. 2008.
- [Yin00] Ying Wang, S. Safavi-Naeini, S. K. Chaudhuri, "A hybrid technique based on combining ray tracing and FDTD methods for site-specific modeling of indoor radio wave propagation," *IEEE Trans. Antennas and Prop.*, vol. 48, no. 5, pp. 743-754, 2000.
- [Yok06] Y. Yokohata, Y. Yamato, M. Takemoto, E. Tanaka, K. Nishiki, "Context-aware content-provision service for shopping malls based on ubiquitous service-oriented network framework and authentication and access control agent framework," in *Proc IEEE CCNC*, 2006, pp. 1330 – 1331.
- [Yon12] Yongnu Jin, Daehan Kwak, Kyung Sup Kwak, "Performance Analysis of Intra-Vehicle Ultra-Wide Band Propagation in Multi-User Environments," *IEEE 1st International Workshop on Vehicular Communications, Sensing, and Computing (VCSC)*, Seoul, South Korea, June 18, 2012.

- [YuY11] Yu-Yi Chen, Zhen-Jie Qiu, Jun-Chao Lu, Jinn-Ke Jan, "A Secure RFID Deactivation/Activation Mechanism for Customer Service and Consumer Shopping," in *Proc. BWCCA*, Barcelona, Spain, 2011, pp. 405 – 410.

## Z

- [Zam10] M. A. Zamora-Izquierdo, J. Santa, A. F. Gomez-Skarmeta, "An Integral and Networked Home Automation Solution for Indoor Ambient Intelligence," *IEEE Pervasive Computing*, vol. 9, 2010.
- [Zem12] T. Zemen, A. F. Molisch, "Adaptive reduced-rank estimation of non-stationary time-variant channels using subspace selection," *IEEE Transactions on Vehicular Technology*, vol. 61, pp. 4042–4056, 2012.
- [Zha05] Y. Zhao, B. Agee, J. H. Reed, "Simulation and Measurement of Microwave Oven Leakage for 802.11 WLAN Interference Management," In *Proceedings of IEEE International Symposium on Microwave, Antenna, Propagation and EMC Technologies for Wireless Communications Proceedings*, Beijing, China, vol. 2, pp. 1580–1583, 8–12 August 2005.
- [Zhe12] Zhengshan Luo, Hongchao Wang, "Research on intelligent supermarket architecture based on the Internet of Things technology," in *Proc. ICNC*, Chongqing, China, 2012, pp. 1219 – 1223.
- [Zhi09] Zhi Zhang, Zhibo Pang, Jun Chen, Qiang Chen, H. Tenhunen, Li-Rong Zheng, Xiaolang Yan, "Two-Layered Wireless Sensor Networks for Warehouses and Supermarkets," in *Proc. UBIComm*, Sliema, 2009, pp. 220 – 224.
- [Zhi13] Zhijian Yin, Haojie Ning, Y. Inoue, Meimei Han, Tao Liu, "A Novel Wireless Motion Sensor for analyzing Golf Swing," *IEEE Sensors*, Baltimore, MD, USA, 2013.
- [Zho10] B. Zhou, J. Cao, X. Zeng, H. Wu, "Adaptive traffic light control in wireless sensor network-based intelligent transportation system," In *Proceedings of the IEEE 72nd Vehicular Technology Conference Fall (VTC 2010-Fall)*, Ottawa, ON, USA, 6–9 September 2010.
- [Zhu10] M. Zhu, X. Zhao, Y. Zhang, "Study on a sea radio-wave propagation loss model," *Proc. of the International Conference on Communications and Mobile Computing*, 2010.
- [Zua09] A. Zualkernan, A. R. Al-Ali, M. A. Jabbar, I. Zabalawi, A. Wasfy, "InfoPods: Zigbee-Based remote information monitoring devices for Smart-Homes," *IEEE Trans. Consum. Electron.*, vol. 55, pp. 1221–1226, 2009.
- [Zul12] N. S. A. Zulkifli, F. K. C. Harun, N. S. Azahar, "XBee Wireless Sensor Networks for Heart Rate Monitoring in Sport Training," *International Conference on Biomedical Engineering*, Penang, Malaysia, 2012.

# List of Publications

In this section, the list of publications that I authored is presented. I divided the list in three sections: International Indexed Journals, International Conferences and National Conferences.

The list of each section is arranged chronologically, except my main contributions (i.e. those works where I am the first author), which appear at the top of the lists. My name in each paper appears in bold font. This way, I try to show clearer what my main contributions are.

## International Indexed Journals

Main contributions, me as a first author:

- [1] **P. L. Iturri**, J. A. Nazabal, L. Azpilicueta, P. Rodriguez, M. Beruete, C. Fernandez-Valdivielso, F. Falcone, "Impact of High Power Interference Sources in Planning and Deployment of Wireless Sensor Networks and Devices in the 2.4 GHz Frequency Band in Heterogeneous Environments," *Sensors*, vol. 12, issue 11, pp. 15689-15708, 2012.
- [2] **Peio Lopez Iturri**, Erik Aguirre, Leire Azpilicueta, Uxue Gárate and Francisco Falcone, "ZigBee Radio Channel Analysis in a Complex Vehicular Environment," *IEEE Antennas and Propagation Magazine*, vol. 56, no. 4, August 2014.
- [3] **Peio Lopez Iturri**, Leire Azpilicueta, Juan Antonio Nazabal, Carlos Fernández-Valdivielso, Jesús Soret, Francisco Falcone, "Analysis of Energy Consumption Performance towards Optimal Radioplanning of Wireless Sensor Networks in Heterogeneous Indoor Environments", *Radioengineering*, vol. 23, no. 3, September 2014.
- [4] **Peio Lopez-Iturri**, Erik Aguirre, Leire Azpilicueta, José J. Astrain, Jesús Villadangos and Francisco Falcone, "Radio Characterization for ISM 2.4 GHz Wireless Sensor Networks for Judo Monitoring Applications," *Sensors*, vol. 14, pp. 24004-24028, December 2014.
- [5] **Peio López Iturri**, Pablo Rodríguez-Ulibarri, Erik Aguirre, Leire Azpilicueta, Miguel Beruete and Francisco Falcone, "Hybrid Equivalent Source – 3D Ray Launching Simulation Technique for Deterministic Estimation of Radiated Emissions of Electrical Appliances," *Journal of Electromagnetic Waves and Applications*. vol. 30, issue 4, 2016.

- [6] **Peio Lopez-Iturri**, Erik Aguirre, Leire Azpilicueta, Silvia de Miguel-Bilbao, Victoria Ramos and Francisco Falcone, "Estimation of Radiofrequency Power Leakage from Microwave Ovens for Dosimetric Assessment at Non Ionizing Radiation Exposure Levels," *BioMed Research International*, Hindawi Publishing Corporation, Article ID 603260, 2015.
- [7] **Peio Lopez-Iturri**, Fran Casino, Erik Aguirre, Leire Azpilicueta, Francisco Falcone, Agusti Solanas, "Performance Analysis of ZigBee Wireless Networks for AAL through Hybrid Ray Launching and Collaborative Filtering," *Journal of Sensors*, vol. 2016, Article ID 2424101, 2016.
- [8] **Peio Lopez-Iturri**, Leyre Azpilicueta, Erik Aguirre, José Javier Astrain, Eduardo Salinero, Jesús Villadangos, Francisco Falcone, "Implementation of Wireless Sensor Network Architecture for Interactive Shopping Carts to Enable Context Aware Commercial Areas," *IEEE Sensors Journal*, vol. 16, no. 13, July 2016.
- [9] **Peio Lopez-Iturri**, Erik Aguirre, Leyre Azpilicueta, José Javier Astrain, Jesús Villadangos, Francisco Falcone, "Implementation and Analysis of ISM 2.4 GHz Wireless Sensor Network System in Judo Training Venues," *Sensors*, vol. 16, p. 1247, 2016.

#### Rest of contributions:

- [10] J. A. Nazábal, **P. L. Iturri**, L. Azpilicueta, F. Falcone, C. Fernández-Valdivielso, "Performance Analysis of IEEE 802.15.4 Compliant Wireless Devices for Heterogeneous Indoor Home Automation Environments," *International Journal of Antennas and Propagation*, Hindawi Publishing Corporation, Article ID 176383, 2012.
- [11] E. Aguirre, **P. L. Iturri**, L. Azpilicueta, J. Arpón, F. Falcone, "Characterization and Consideration of Topological Impact of Wireless Propagation in a Commercial Aircraft Environment," *IEEE Antennas and Propagation Magazine*, vol. 55, issue 6, pp. 240–258, December 2012.
- [12] E. Aguirre, J. Arpón, L. Azpilicueta, **P. López Iturri**, S. de Miguel, V. Ramos, F. Falcone, "Estimation of Electromagnetic Dosimetric Values from Non-Ionizing Radiofrequency Fields in an Indoor Commercial Airplane Environment", *Electromagnetic Biology and Medicine*, Published online 24 July 2013.
- [13] Erik Aguirre, **Peio Lopez Iturri**, Leire Azpilicueta, Silvia de Miguel-Bilbao, Victoria Ramos and Francisco Falcone, "Analysis of Estimation of Electromagnetic Dosimetric Values from Non-Ionizing Radiofrequency Fields in Conventional Road Vehicle Environments", *Electromagnetic Biology and Medicine*, Published online 21 January 2014.
- [14] Leire Azpilicueta, **Peio Lopez Iturri**, Erik Aguirre, Francisco Falcone, "Radio Channel Characterization for Bluetooth Communication Systems Onboard Commercial Aircrafts," *Microwave and Optical Technology Letters*, vol. 56, no. 11, November 2014.
- [15] Leire Azpilicueta, **Peio Lopez Iturri**, Erik Aguirre, Ignacio Mateo, José Javier Astrain, Jesús Villadangos, Francisco Falcone, "Analysis of Radio Wave Propagation for ISM 2.4GHz Wireless Sensor Networks in Inhomogeneous Vegetation Environments," *Sensors*, 14, 23650-23672, December 2014.

- [16] Silvia de Miguel-Bilbao, Erik Aguirre, **Peio Lopez-Iturri**, Leire Azpilicueta, José Roldán, Victoria Ramos and Francisco Falcone, "Evaluation of Electromagnetic Interference and Exposure Assessment from s-Health Solutions based on Wi-Fi Devices," *BioMed Research International*, Hindawi Publishing Corporation, Article ID 784362, 2014.
- [17] Erik Aguirre, **Peio Lopez-Iturri**, Leire Azpilicueta, José Javier Astráin, Jesús Villadangos and Francisco Falcone, "Analysis of Wireless Sensor Network Topology and Estimation of Optimal Network Deployment by Deterministic Radio Channel Characterization" *Sensors*, 15, 3766-3788, January 2015.
- [18] Hisham Baghdadi, Erik Aguirre, **Peio Lopez**, Leire Azpilicueta, Jose Javier Astrain, Jesús Villadangos and Francisco Falcone, "Characterization of UHF Radio Channels for Wireless Sensor Systems Embedded in Surfboards," *IEEE Antennas and Wireless Propagation Letters*, vol. 14, pp. 1526 – 1529, 2015.
- [19] Leire Azpilicueta, **Peio López Iturri**, Erik Aguirre, José Javier Astráin, Jesús Villadangos, Cristobal Zubiri and Francisco Falcone, "Characterization of Wireless Channel Impact on Wireless Sensor Network Performance in Public Transportation Buses", *IEEE Transactions on Intelligent Transportation Systems*, vol. 16, issue 6, pp. 3280 – 3293, 2015.
- [20] Leire Azpilicueta, Erik Aguirre, **Peio Lopez-Iturri**, Francisco Falcone, "An Accurate UTD Extension to a Ray Launching Algorithm for the Analysis of Complex Indoor Radio Environments," *Journal of Electromagnetic Waves and Applications*, published online 1 Dic. 2015.
- [21] Erik Aguirre, Santiago Led, **Peio Lopez Iturri**, Leire Azpilicueta, Luis Serrano and Francisco Falcone, "Implementation of Context Aware e-Health Environments based on Social Sensor Networks," *Sensors*, 16(3), 2016.
- [22] Leyre Azpilicueta, **Peio López-Iturri**, Erik Aguirre, Carlos Martínez, José Javier Astráin, Jesús Villadangos, Francisco Falcone, "Evaluation of Deployment Challenges of Wireless Sensor Networks at Signalized Intersections," *Sensors*, 16(7), 2016.
- [23] Erik Aguirre, **Peio Lopez-Iturri**, Leyre Azpilicueta, Carmen Rivarés, Jose Javier Astrain, Jesús Villadangos, Francisco Falcone, "Design and Performance Analysis of Wireless Body Area Networks in Complex Indoor e-Health Hospital Environments for Patient Remote Monitoring," *International Journal of Distributed Sensor Networks*, vol. 12(9), 2016.
- [24] Fran Casino, Leire Azpilicueta, **Peio Lopez-Iturri**, Erik Aguirre, Francisco Falcone and Agustí Solanas, "Optimised Wireless Channel Characterization in Large Complex Environments by Hybrid Ray Launching- Collaborative Filtering Approach," *IEEE Antennas and Wireless Propagation Letters*, Early access, 2016.
- [25] Alberto Córdoba, José Javier Astrain, Jesús Villadangos, Francisco Falcone, Leire Azpilicueta, **Peio Lopez-Iturri**, Erik Aguirre, "SesToCross: Semantic Expert System to Manage Road Crossing," *IEEE Transactions on Intelligent Transportation Systems*, Early access, 2016.
- [26] Erik Aguirre, **Peio Lopez-Iturri**, Leyre Azpilicueta, José Javier Astrain, Jesús Villadangos, Daniel Santesteban, Francisco Falcone, "Implementation and Analysis of a Wireless Sensor Network-based Pet Monitoring System for Domestic Scenarios," *Sensor*, vol. 16, pp. 1384, August 2016.



- [27] Erik Aguirre, **Peio Lopez-Iturri**, Leyre Azpilicueta, Aitor Redondo, José Javier Astrain, Jesús Villadangos, Alfonso Bahillo, Asier Perallos, Francisco Falcone, "Design and Implementation of Context Aware Applications with Wireless Sensor Network Support in Urban Train Transportation Environments," *IEEE Sensors Journal*, Early access, 2016.
- [28] Leire Azpilicueta, **Peio Lopez-Iturri**, Erik Aguirre, Arancha León and Francisco Falcone, "Influence of Meshing Adaption in Convergence Performance of Deterministic Ray Launching Estimation in Indoor Scenarios" *Journal of Electromagnetic Waves and Applications*, 2017.
- [29] Leyre Azpilicueta, Jose Javier Astrain, **Peio Lopez-Iturri**, Fausto Granda-Gutierrez, Cesar Vargas-Rosales, Jesus Villadangos, Asier Perallos, Alfonso Bahillo, Francisco Falcone, "Optimization and Design of Wireless Systems for the Implementation of Context Aware Scenarios in Railway Passenger Vehicles," accepted in *IEEE Transactions on Intelligent Transportation Systems*.

## Book Chapters

- [1] **Peio Lopez-Iturri**, Leyre Azpilicueta, Erik Aguirre, Francisco Falcone, "Chapter 13. Wireless performance in dense-transceiver scenarios to enable context-aware scenarios," *The World of Applied Electromagnetics in Appreciation of Magdy Fahmy Iskander* (to be published by Springer).

## International Conference Contributions

Main contributions, me as a first author:

- [1] **Peio López**, Juan Antonio Nazábal, Victor Torres, Carlos Fernández, Francisco Falcone, "Analysis of Topological impact in Wireless Indoor Sensor Networks," (2011 *IEEE AP-S International Symposium on Antennas and Propagation and 2011 USNC/URSI National Radio Science Meeting*).
- [2] **Peio López Iturri**, Juan Antonio Nazábal, Leire Azpilicueta, Carlos Fernández, Francisco Falcone, "Impact and Characterization of the Microwave Oven Power Leakage on 802.15.4 Networks," (2013 *IEEE AP-S International Symposium*).
- [3] **Peio López Iturri**, Juan Antonio Nazábal, Leire Azpilicueta, Carlos Fernández-Valdivielso, Francisco Falcone, "Impact of the microwave oven power leakage on 802.15.4 networks," (2013 *EuCAP International Symposium*).
- [4] **Peio Lopez-Iturri**, Erik Aguirre, Leire Azpilicueta, José J. Astrain, Jesús Villadangos, Francisco Falcone, "Radio Characterization for ISM 2.4 GHz Wireless Sensor Networks for Judo Applications," (In *Proceedings of the 1st Int. Elec. Conf. on Sens. and App.*, 1-16 June 2014; *Sciforum Electronic Conference Series*).
- [5] **Peio Lopez Iturri**, Erik Aguirre, Leire Azpilicueta, Silvia de Miguel-Bilbao, Victoria Ramos, Uxue Garate, Francisco Falcone, "Assessment of Electromagnetic Dosimetric values from Non-Ionizing Radiofrequency Sources in a Conventional Road

- Vehicle," (2014 IEEE International Symposium on Antennas and Propagation and USNC-URSI National Radio Science Meeting).
- [6] **Peio López-Iturri**, Erik Aguirre, Leire Azpilicueta, Carlos Fernández-Valdivielso, Ignacio Matías, Francisco Falcone, "Analysis of Efficient Dense Wireless Sensor Network Deployment in Smart City Environments," (*IEEE Sensors 2014*).
- [7] **Peio Lopez-Iturri**, Silvia de Miguel-Bilbao, Erik Aguirre, Leire Azpilicueta, Victoria Ramos, Francisco Falcone, "Dosimetric Assessment of Radiofrequency Power Leakage from Microwave Ovens in Complex Scenarios," (2015 IEEE International Symposium on Antennas and Propagation and USNC-URSI National Radio Science Meeting).
- [8] **Peio Lopez-Iturri**, Erik Aguirre, Leire Azpilicueta, Francisco Falcone, "Performance Analysis of Heterogeneous Wireless Networks in Complex Indoor Scenarios," (2015 IEEE International Symposium on Antennas and Propagation and USNC-URSI National Radio Science Meeting).
- [9] **Peio Lopez-Iturri**, Erik Aguirre, Leyre Azpilicueta, José J. Astrain, Jesús Villadangos, Francisco Falcone, "Assessment of ISM 2.4 GHz Wireless Sensor Networks Performance in Judo Training Venues," (2nd International Electronic Conference on Sensors and Applications-ECSA 2015).
- [10] **Peio Lopez-Iturri**, Erik Aguirre, Leyre Azpilicueta, Pablo Rodríguez-Ulbarri, Miguel Beruete, Francisco Falcone, "Hybrid Method for Deterministic Estimation of Radiated Emissions of Electrical Appliances," (2016 EuCAP. 10th European Conference on Antennas and Propagation).
- [11] **Peio Lopez-Iturri**, Amaia Ortiz de Lejarazu, Erik Aguirre, Leyre Azpilicueta, Francisco Falcone, "Radiofrequency Interference Analysis for s-Health and Context Aware scenarios in Hospital Environments," (2016 IEEE International Symposium on Antennas and Propagation and USNC-URSI National Radio Science Meeting).
- [12] **Peio López-Iturri**, Erik Aguirre, Francisco Falcone, Leyre Azpilicueta, Fran Casino, Agusti Solanas, "Analysis of Vehicular Connectivity in Smart Health Service Provision Scenarios," (*The 7th International Conference on Information, Intelligence, Systems and Applications - IISA 2016*).
- [13] **Peio Lopez-Iturri**, Santiago Led, Erik Aguirre, Leyre Azpilicueta, Luis Serrano, Francisco Falcone, "Analysis of Bluetooth-based Wireless Sensor Networks Performance in Hospital Environments," (In *Proceedings of the 3th Int. Elec. Conf. on Sens. and App.*, 15-30 Nov. 2016; *Sciforum Electronic Conference Series*).
- [14] **Peio Lopez-Iturri**, Fran Casino, Erik Aguirre, Leyre Azpilicueta, Agusti Solanas, Francisco Falcone, "Hybrid Ray Launching-Collaborative Filtering Approach for Wireless Propagation in Indoor Environments," accepted in (2017 IEEE International Symposium on Antennas and Propagation and USNC-URSI National Radio Science Meeting).
- [15] **Peio Lopez-Iturri**, Erik Aguirre, Leyre Azpilicueta, Jose Javier Astrain, Jesús Villadangos, Francisco Falcone, "Deterministic Radio Propagation Estimations in Judo venues for WSN deployment by 3D Ray Launching Method," accepted in (2017 IEEE International Symposium on Antennas and Propagation and USNC-URSI National Radio Science Meeting).

## Rest of contributions:

- [16] Carmen Rivares, Leire Azpilicueta, **Peio López**, Juan Antonio Nazabal, Francisco Falcone, "Influence of Human Body and Indoor Scenarios in On-Body Wireless Communication Systems," (2013 *IEEE AP-S International Symposium*).
- [17] Erik Aguirre, **Peio Lopez Iturri**, Leire Azpilicueta, Silvia de Miguel, Victoria Ramos, Francisco Falcone, "Dosimetric Assessment for Non-Ionizing ISM 2.4 GHz Wireless Systems in a Commercial Passenger Aircraft," (2014 *EuCAP International Symposium*).
- [18] Leire Azpilicueta, **Peio López Iturri**, Erik Aguirre, Ignacio Mateo, José Javier Astráin, Jesús Villadangos, Francisco Falcone, "Analysis of Radio Wave Propagation for ISM 2.4GHz Wireless Sensor Networks in Inhomogeneous Vegetation Environments," (In *Proceedings of the 1st Int. Elec. Conf. on Sens. and App.*, 1-16 June 2014; *Sciforum Electronic Conference Series*).
- [19] Erik Aguirre, **Peio Lopez-Iturri**, Leire Azpilicueta, José Javier Astrain, Jesús Villadangos, Francisco Falcone, "Analysis of Wireless Sensor Network Topology and Estimation of Optimal Network Deployment by Deterministic Radio Channel Characterization," (In *Proceedings of the 1st Int. Elec. Conf. on Sens. and App.*, 1-16 June 2014; *Sciforum Electronic Conference Series*).
- [20] Erik Aguirre, Maryuri Flores, Leire Azpilicueta, **Peio López-Iturri**, Francisco Falcone, Agusti Solanas, "Implementing Context Aware Scenarios to Enable Smart Health in Complex Urban Environments," (2014 *IEEE International Symposium on Medical and Measurements and Applications MeMeA*).
- [21] Eduardo Salinero, Leire Azpilicueta, Erik Aguirre, **Peio López-Iturri**, José Javier Astráin, Jesús Villadangos, Francisco Falcone, "Channel Characterization in Indoor Wireless Sensor Network Deployment in Commercial Environment," (2014 *IEEE International Symposium on Antennas and Propagation and USNC-URSI National Radio Science Meeting*).
- [22] Arancha León, Leire Azpilicueta, Erik Aguirre, **Peio Lopez Iturri**, Francisco Falcone, "Topological Dependence in the Performance of Deterministic Wireless Channel Estimation," (2014 *IEEE International Symposium on Antennas and Propagation and USNC-URSI National Radio Science Meeting*).
- [23] Leire Azpilicueta, **Peio Lopez Iturri**, Erik Aguirre, Tomás Laborra, Francisco Falcone, "Estimation of Wireless Coverage in Complex Cave Environments for Speleology Applications," (2014 *IEEE International Symposium on Antennas and Propagation and USNC-URSI National Radio Science Meeting*).
- [24] Hisham Baghdadi, Erik Aguirre, **Peio Lopez**, Leire Azpilicueta, Francisco Falcone, "Analysis of radiopropagation of wireless transceivers in surfboards," (2014 *IEEE International Symposium on Antennas and Propagation and USNC-URSI National Radio Science Meeting*).
- [25] Erik Aguirre, **Peio López-Iturri**, Leire Azpilicueta, Francisco Falcone, "Characterization of Wireless Channel Response in In-Vehicle Environments," (2014 *IEEE Mediterranean Microwave Symposium*).
- [26] Erik Aguirre, **Peio Lopez Iturri**, Leire Azpilicueta, Silvia de Miguel-Bilbao, Victoria Ramos, Francisco Falcone, "Deterministic 3D Ray Launching EMF/Human Body

- Interaction Estimation in Complex Scenarios," (2015 COST Action EMF-MED Workshop - EMF Interactions with Excitable Tissues).
- [27] Fran Casino, Leire Azpilicueta, **Peio Lopez-Iturri**, Erik Aguirre, Francisco Falcone, Agusti Solanas, "Hybrid-based Optimization of Wireless Channel Characterization for Health Services in Medical Complex Environments," (*The 6th International Conference on Information, Intelligence, Systems and Applications - IISA 2015*).
- [28] Amaia Ortiz de Lejarazu, **Peio López-Iturri**, Erik Aguirre, Leire Azpilicueta, Francisco Falcone, Fran Casino, Agusti Solanas, "Challenges in the Implementation of Context-Aware Scenarios within Emergency Rooms," (*The 6th International Conference on Information, Intelligence, Systems and Applications - IISA 2015*).
- [29] Aitor Redondo, Leire Azpilicueta, **Peio Lopez-Iturri**, Erik Aguirre, José Javier Astrain, Jesús Villadangos, Francisco Falcone, "Radio Propagation Analysis for Wireless Sensor Network Deployment in Urban Train Transportation Environments," (*4th International Symposium on Sensor Science - I3S 2015*).
- [30] David Abajo, Leire Azpilicueta, Erik Aguirre, **Peio Lopez-Iturri**, José Javier Astrain, Jesús Villadangos, Francisco Falcone, "Implementation of Wireless Sensor Networks for Photovoltaic Energy Farm Applications," (*4th International Symposium on Sensor Science - I3S 2015*).
- [31] Alba Martínez, Erik Aguirre, Leire Azpilicueta, **Peio Lopez-Iturri**, José Javier Astrain, Jesús Villadangos, Francisco Falcone, "Analysis of RFID-based Distributed Urban Parking Systems," (*4th International Symposium on Sensor Science - I3S 2015*).
- [32] Leire Azpilicueta, **Peio López-Iturri**, Erik Aguirre, Francisco Falcone, "Convergence Evaluation of Deterministic 3D Ray Launching Approach in Complex Environments," (*2015 IEEE International Symposium on Antennas and Propagation and USNC-URSI National Radio Science Meeting*).
- [33] Erik Aguirre, Silvia de Miguel-Bilbao, **Peio Lopez-Iturri**, Leire Azpilicueta, José Roldán, Victoria Ramos, Francisco Falcone, "Exposure Assessment from s-Health Solutions Based on WLAN/WBAN Systems," (*2015 IEEE International Symposium on Antennas and Propagation and USNC-URSI National Radio Science Meeting*).
- [34] José Javier Martínez, **Peio Lopez-Iturri**, Erik Aguirre, Leire Azpilicueta, Constantinos Patsakis, Achilleas Papageorgiou, Agusti Solanas, Francisco Falcone, "Analysis of Wireless Sensor Network Performance Embedded in Motorcycle Communication System," (*2015 IEEE International Symposium on Antennas and Propagation and USNC-URSI National Radio Science Meeting*).
- [35] Leire Azpilicueta, Erik Aguirre, Francisco Falcone, **Peio Lopez-Iturri**, Ana Vazquez Alejos, "Radio Channel Characterization of Vehicle-to-Infrastructure Communications at 60GHz," (*2015 International Conference on Electromagnetics in Advanced Applications-ICEAA and IEEE-APS Topical Conference on Antennas and Propagation in Wireless Communications -APWC 2015*).
- [36] Fran Casino, **Peio López-Iturri**, Erik Aguirre, Leire Azpilicueta, Agusti Solanas, Francisco Falcone, "Dense Wireless Sensor Network Design for the Implementation of Smart Health Environments," (*2015 International Conference on Electromagnetics in Advanced Applications-ICEAA and IEEE-APS Topical Conference on Antennas and Propagation in Wireless Communications -APWC 2015*).
- [37] Daniel Santesteban, Erik Aguirre, **Peio Lopez-Iturri**, Leyre Azpilicueta, José Javier Astrain, Jesús Villadangos, Francisco Falcone, "Radio Propagation Analysis for

- ZigBee based Indoor Dog Monitoring System,” (2nd International Electronic Conference on Sensors and Applications-ECSA 2015).
- [38] Carlos Martínez, Leyre Azpilicueta, **Peio López-Iturri**, Erik Aguirre, José Javier Astráin, Jesús Villadangos, Francisco Falcone, “Radio Wave Characterization in Wireless Sensor Network-based Intelligent Transportation Systems for Traffic Light Control Systems,” (2nd International Electronic Conference on Sensors and Applications-ECSA 2015).
- [39] Silvia de Miguel Bilbao, Juan Blas, Erik Aguirre, **Peio López Iturri**, Leyre Azpilicueta, Francisco Falcone, Victoria Ramos, “Study on the Impact of the Body Shadow Effect in Wireless Channels through Dosimetry Measurements,” (2016 EuCAP. 10th European Conference on Antennas and Propagation).
- [40] Leyre Azpilicueta, **Peio López-Iturri**, Erik Aguirre, Francisco Falcone, “Characterisation of Radio Wave Propagation in Complex Indoor Environments with and Accurate Ray Launching and UTD Method,” (2016 EuCAP. 10th European Conference on Antennas and Propagation).
- [41] Leyre Azpilicueta, **Peio López-Iturri**, Erik Aguirre, Francisco Falcone, “Radio Channel Characterization of WBAN Systems to Enable Context Aware Connectivity in Commercial Aircraft,” (2016 IEEE International Symposium on Antennas and Propagation and USNC-URSI National Radio Science Meeting).
- [42] Leyre Azpilicueta, Erik Aguirre, **Peio López-Iturri**, José Javier Astrain, Jesús Villadangos, Alfonso Bahillo, Asier Perallos, Francisco Falcone, “Embedded Wireless Sensor Networks for Context Aware Train Environments,” (2016 IEEE International Symposium on Antennas and Propagation and USNC-URSI National Radio Science Meeting).
- [43] Leyre Azpilicueta, Erik Aguirre, **Peio López-Iturri**, José Javier Astrain, Jesús Villadangos, Francisco Falcone, “Analysis of Energy Consumption Performance for Wireless Sensor Networks in Inhomogeneous Vegetation Environments,” (2016 IEEE International Symposium on Antennas and Propagation and USNC-URSI National Radio Science Meeting).
- [44] Leyre Azpilicueta, Cesar Vargas, **Peio López-Iturri**, Erik Aguirre, Alex Ariznabarreta, Francisco Falcone, “Analysis of Wireless Sensor Network Performance in Urban Infrastructure to Vehicle Scenarios,” (2016 IEEE International Symposium on Antennas and Propagation and USNC-URSI National Radio Science Meeting).
- [45] Erik Aguirre, **Peio Lopez-Iturri**, Leyre Azpilicueta, Aitor Redondo, Francisco Falcone, “Dosimetric Study of Urban Train Transportation Environment,” (2016 IEEE International Symposium on Antennas and Propagation and USNC-URSI National Radio Science Meeting).
- [46] Fran Casino, **Peio López-Iturri**, Erik Aguirre, Leyre Azpilicueta, Francisco Falcone, Agusti Solanas, “Optimal parameter estimation for wireless signal analysis in context-aware scenarios,” (The 7th International Conference on Information, Intelligence, Systems and Applications - IISA 2016).
- [47] Fran Casino, **Peio López-Iturri**, Erik Aguirre, Leyre Azpilicueta, Francisco Falcone, Edgar Batista, Agusti Solanas, “Two-dimensional Collaborative Filtering Approach to Wireless Channel Characterization,” (ISC2 IEEE International Smart Cities Conference – ISC2 2016).

- [48] Fausto Granda, Leyre Azpilicueta, Cesar Vargas-Rosales, **Peio Lopez-Iturri**, Erik Aguirre, José Javier Astrain, Jesús Villadangos, Francisco Falcone, "Characterizations of Radio Propagation Channel in Urban Vehicle to Infrastructure environments to support WSNs," (In *Proceedings of the 3th Int. Elec. Conf. on Sens. and App.*, 15-30 Nov. 2016; Sciforum Electronic Conference Series).
- [49] Leyre Azpilicueta, César Vargas-Rosales, **Peio Lopez-Iturri**, Erik Aguirre, Francisco Falcone, "Characterisation of Radio Wave Propagation in Vehicular Environments through Deterministic Methods," accepted in (2017 *IEEE International Symposium on Antennas and Propagation and USNC-URSI National Radio Science Meeting*).
- [50] Erik Aguirre, **Peio Lopez-Iturri**, Leyre Azpilicueta, Daniel Santesteban, Francisco Falcone, "Study of the Influence of a Dog in Radio Propagation Considering Domestic Environments," accepted in (2017 *IEEE International Symposium on Antennas and Propagation and USNC-URSI National Radio Science Meeting*).
- [51] Leyre Azpilicueta, **Peio López-Iturri**, Erik Aguirre, Carlos Martínez, Francisco Falcone, "Assessment of ISM 2.4GHz Wireless Sensor Networks Performance in Urban Infrastructure Scenarios," accepted in (2017 *IEEE International Symposium on Antennas and Propagation and USNC-URSI National Radio Science Meeting*).

## National Conference Contributions

Main contributions, me as a first author:

- [1] **Peio López**, Juan Antonio Nazábal, Leire Azpilicueta, Guillermo Martínez, Raimundo García, Jesús Soret, José Torres, Julio Martos, Carlos Fernández-Valdivielso, Francisco Falcone, "Análisis del comportamiento de redes de sensores inalámbricos en entornos interiores heterogéneos," (2011 *URSI XXVI National Symposium*).
- [2] **Peio López Iturri**, Juan Antonio Nazábal, Leire Azpilicueta, Carlos Fernández-Valdivielso, Francisco Falcone, "Impacto de la potencia de fuga de hornos microondas en redes 802.15.4," (2012 *URSI XXVII National Symposium*).
- [3] **Peio López**, Leire Azpilicueta, Erik Aguirre, Silvia de Miguel, Victoria Ramos, Francisco Falcone, "Análisis Dosimétrico de las Fugas de Hornos Microondas," (2013 *URSI XXVIII National Symposium*).
- [4] **Peio Lopez-Iturri**, Erik Aguirre, Leire Azpilicueta, Francisco Falcone, "Haririk Gabeko Komunikazio Sistemen Azterketa Ingurune Konplexuetan 3D Ray Launching Metodo Deterministaren bidez," (*Ikertzaile Euskaldunen I. Nazioarteko Kongresua- IkerGazte* 2015).
- [5] **Peio Lopez-Iturri**, Erik Aguirre, Leire Azpilicueta, José Javier Astrain, Jesús Villadangos, Francisco Falcone, "Caracterización de la Banda ISM 2.4 GHz para Aplicaciones de Redes de Sensores Inalámbricas en Entornos de Judo," (2015 *URSI XXX National Symposium*).

- [6] **Peio Lopez-Iturri**, Erik Aguirre, Leire Azpilicueta, José Javier Astrain, Jesús Villadangos, Francisco Falcone, "Sistemas Inalámbricos Heterogéneos como Facilitadores de Entornos Contextuales," (2015 *URSI XXX National Symposium*).
- [7] **Peio Lopez-Iturri**, Leyre Azpilicueta, Erik Aguirre, José Javier Astrain, Jesús Villadangos, Alfonso Bahillo, Asier Perallos, Francisco Falcone, "Caracterización de Redes de Sensores en Entornos Contextuales Ferroviarios," (2016 *URSI XXXI National Symposium*)
- [8] **Peio Lopez-Iturri**, Erik Aguirre, Leyre Azpilicueta, Pablo Rodriguez-Ulibarri, Miguel Beruete, Francisco Falcone, "Gailu Elektrikoek sortutako Erradiazioaren Estimazio Determinista Metodo Híbrido berri baten bidez," (*Ikertzaile Euskaldunen II. Nazioarteko Kongresua- IkerGazte* 2017).

#### Rest of contributions:

- [9] Erik Aguirre, Leire Azpilicueta, **Peio López**, Cristobal Zubiri, José Javier Astráin, Jesús Villadangos, Francisco Falcone, "Caracterización Radioeléctrica de Sistemas Inalámbricos Embarcados en Autobuses Urbanos," (2013 *URSI XXVIII National Symposium*).
- [10] Leire Azpilicueta, **Peio López**, Erik Aguirre, Uxue Gárate, Francisco Falcone, "Análisis del Canal Radioeléctrico en un Entorno Vehicular Complejo," (2013 *URSI XXVIII National Symposium*).
- [11] Eduardo Salinero, Leire Azpilicueta, **Peio López Iturri**, Erik Aguirre, Francisco Falcone, "Caracterización del Canal Radioeléctrico en Grandes Superficies Comerciales," (2014 *URSI XXIX National Symposium*).
- [12] Tomas Laborra, Erik Aguirre, **Peio Lopez**, Leire Azpilicueta, José Javier Astráin, Jesús Villadangos, Francisco Falcone, "Sistema de Comunicación en Tiempo Real Basado en WSN para Aplicaciones Espeleológicas," (2014 *URSI XXIX National Symposium*).
- [13] Hisham Baghdadi, Erik Aguirre, **Peio Lopez**, Leire Azpilicueta, José Javier Astráin, Jesús Villadangos, Francisco Falcone, "Caracterización Radioeléctrica en Entorno Acuático para Sistemas Inalámbricos Embebidos en Tablas de Surf," (2014 *URSI XXIX National Symposium*).
- [14] Erik Aguirre, **Peio Lopez-Iturri**, Leire Azpilicueta, Francisco Falcone, "Ingurune komplexuen azterketa dosimetricoa 3D Ray Launching Simulazio metodoaren bidez eta giza gorputzaren eredia erabiliz," (*Ikertzaile Euskaldunen I. Nazioarteko Kongresua-IkerGazte* 2015).
- [15] Leire Azpilicueta, **Peio López-Iturri**, Erik Aguirre, José Javier Astráin, Jesús Villadangos, Francisco Falcone, "Análisis de la Propagación Electromagnética de Redes de Sensores Inalámbricos en Entornos con Vegetación," (2015 *URSI XXX National Symposium*).
- [16] Erik Aguirre, Alba Martínez, Leire Azpilicueta, **Peio López-Iturri**, Francisco Falcone, "Estudio y planificación radio de sistema de gestión automática de áreas ZER/ZEL basada en tecnología RFID," (2015 *URSI XXX National Symposium*).
- [17] Leyre Azpilicueta, Fran Casino, **Peio Lopez-Iturri**, Erik Aguirre, Agusti Solanas, Francisco Falcone, "Análisis de Técnicas Híbridas para la Estimación de

Comportamiento de Redes de Sensores en Entornos Complejos," (2016 URSI XXXI National Symposium).

## Other Merits and Awards

- ECSA Best Paper Award: "Analysis of Wireless Sensor Network Topology and Estimation of Optimal Network Deployment by Deterministic Radio Channel Characterization" (*1st International Electronic Conference on Sensors and Applications*, 1-16 June, 2014). <http://sciforum.net/conference/ecsa-1/page/14>.
- IISA Best Paper Award: "Hybrid-based Optimization of Wireless Channel Characterization for Health Services in Medical Complex Environments" (*The 6th International Conference on Information, Intelligence, Systems and Applications - IISA 2015*).
- Assistant Editor of *Microwave Processing* journal, ISSN: 2353-6446.
- Reviewer for:
  - *IEEE Transactions on Intelligent Transportation Systems*. ISSN: 1524-9050.
  - *IEEE Antennas and Wireless Propagation Letters*. ISSN: 1536-1225.
  - *International Journal of Antennas and Propagation*. ISSN: 1687-5869 (Print).
  - *International Journal of Distributed Sensor Networks*. ISSN: 1550-1329 (Print).
  - *Mathematical and Computational Applications*. ISSN: 2297-8747.
  - *14th IEEE Mediterranean Microwave Symposium* (December 12-14 2014, Marrakech, Morocco).
  - *7th International Conference on Information, Intelligence, Systems and Applications, IISA 2016* (13-15 July, 2016, Chalkidiki, Greece).
  - *British Journal of Medicine and Medical Research*. ISSN: 2231-0614.
  - *Physical Science International Journal*. ISSN: 2348-0130.